UNIVERSITY OF SOUTHAMPTON

DEPARTMENT OF AERONAUTICS AND ASTRONAUTICS

PROPULSION SIMULATION IN A MAGNETIC SUSPENSION WIND TUNNEL WITH SPECIAL REFERENCE TO FORCE MEASUREMENT

by

Keith Stuart Garbutt

A Thesis Submitted for the Degree of

Doctor of Philosophy

October 1992

UNIVERSITY OF SOUTHAMPTON

ABSTRACT

FACULTY OF ENGINEERING AND APPLIED SCIENCE

DEPARTMENT OF AERONAUTICS AND ASTRONAUTICS

Doctor of Philosophy

PROPULSION SIMULATION IN A MAGNETIC SUSPENSION WIND TUNNEL WITH SPECIAL REFERENCE TO FORCE MEASUREMENT

by Keith Stuart Garbutt

The primary aim of this research was to demonstrate the feasibility of simulating an engine exhaust flow in a wind tunnel, using a model levitated by a Magnetic Suspension and Balance System (MSBS). The project formed part of a continuing effort to prove the viability of the MSBS as an aid to wind tunnel testing. It is important that propulsion simulation can be performed in a future commercial MSBS wind tunnel facility. The MSBS eliminates support interference, which often affects the regions of a flight vehicle also influenced by the engine exhaust. During exhaust simulation in an MSBS there is no physical connection to the model through which exhaust gas can be supplied, and the model must incorporate a gas generator.

Two techniques for gas generation on-board a suspended model are considered in this thesis. A compressed gas thruster is shown to be unsuitable for exhaust simulation at this scale, because the thrust profile produced varies strongly with time and is incompatible with the control and data analysis requirements. The issue of acceptability of thrust profiles is addressed. It is concluded that the Southampton MSBS hardware, rather than the control software, was the limiting factor during this project in deciding what constituted an acceptable thrust profile. Solid propellant rocket thrusters were also investigated, and a rocket motor was developed which allowed a successful demonstration of propulsion simulation testing in an MSBS.

A deficiency in the ability to measure the forces influencing a suspended model was highlighted by the propulsion simulation research. A study showed that the concept of an external balance for measuring the forces produced by the MSBS electromagnets was both under-exploited, and suitable for development with the Southampton facility. This thesis describes the design and production of a three-component balance. The balance was used initially to improve the ability of the control system to generate independent force and moment components on a model, and later in a test series investigating high angle of attack aerodynamics. This was the first such test series performed in an MSBS wind tunnel.

CONTENTS

LIST OF TABLES

ACKNOWLEDGEMENTS

I welcome this opportunity to express my most sincere thanks to all those who have provided help and support during this research.

I was thirteen months old when Mike Goodyer, now Professor of Experimental Aerodynamics in this Department, submitted his PhD thesis on the subject of magnetic suspension systems. The fact that he is still at the forefront of this field is a tribute to his intelligence and dedication. As my supervisor during this research program, his ideas and guidance have been of exceptional value.

Under the control of Mike Bartlett and Colin Bielby, the staff of the Mechanical Workshop have produced high quality components with skill and good humour. Special thanks are due to Tim Judd - a real craftsman.

The Electronics Workshop staff have been consistently receptive and helpful. Many thanks to Rob Stainsbridge, always willing to get involved in problems, and to use his insight to provide quality solutions.

No magnetic suspension project at Southampton would be possible without the contribution of Dennis Odgers. With his endless supply of components and his perpetual patience, he is a valuable resource.

Little did I know three years ago, that by the time I completed this research I would be a happily married man. Thanks Clare!

Throughout my education I have enjoyed unwavering personal and financial support from my parents. With their backing I have been able to seize and enjoy the many opportunities arising during my time at Southampton, and their contribution is greatly appreciated.

LIST OF SYMBOLS AND ABBREVIATIONS

a	linear acceleration (m/s^2)
A	nozzle throat area, Axial force (N)
ADC	Analogue to Digital Converter
B	magnetic flux density (T)
c	output from control block, Coupling coefficient
C	force or moment coefficient
CFD	Computational Fluid Dynamics
CPU	Central Processing Unit
d	diameter (m)
D	aerodynamic drag (N), differential function, control system demand
DAC	Digital to Analogue Converter
DDF	Demand Distribution Factor
DFM	Direct Force Measurement
f	frequency (Hz)
F	Force (N)
g	gravitational acceleration
G	control system loop Gain
H	(strictly $\mu_0 H$) magnetic field strength (T), Heave force (N)
i	current (A)
k, K	constants
kB	Kilobyte
l	length (m)
L	aerodynamic lift (N), characteristic length (m), inductance (H)
m	mass (kg)
$\dot{m}$	mass flow rate (kg/s)
M	Magnetisation (T), Mach number
MB	Megabyte
MFF	Magnetising Field Factor
MSBS	Magnetic Suspension and Balance System
n	damping ratio, a number
NPR	Nozzle Pressure Ratio
p	pressure (N/m^2)

P	Pitching moment (Nm)
PACS	Photodiode Array Control System
PC	Personal Computer
PDP11	Digital Equipment Corp. computer system
Pr	Prandtl number
PRCR	Post-Run Current Replication
q	dynamic pressure (N/m^2)
R	Gas constant (kJ/kgK), Resistance (Ω)
Re	Reynolds number
S	Strouhal number
SBIR	Small Business Innovation and Research
STOL	Short Take-off and Landing
T	Time constant (s), Temperature (K)
Th	Thrust (N)
u	input to control block
v	Velocity (m/s)
V	Volume (m^3), Voltage (V)
VDU	Visual Display Unit
x,y,z	general axis system identified by subscript
α	angle of attack (°)
γ	ratio of specific heats of a gas
η	effectiveness of magnets in producing a force or moment (N/A)
θ	angle of pitch, nose apex angle (°)
μ_0	permeability of free space (H/m)
ρ	density (kg/m^3)
τ	inductive time constant (s)
ϕ	angle of roll (°)
φ	angle of yaw (°)

Subscripts

I-IV	specific electromagnet group
0	stream (stagnation)
const	having constant value
d	value demanded by a control system
DFM	DFM axis system
EM	due to the action of the electromagnet array
Ext	due to external forces
f	force
i	general electromagnet group
j	jet

limit	indicating an electromagnet at maximum operating current
m	moment, measured value
max	maximum electromagnet current (about 20 A)
N	Normal force
no-lim	indicating an electromagnet within limits of operating current
p	prediction
r	reference value
s	position sensing axis system
t	at time t
T	Tangential force
true	true value
var	of variable value
α	at this angle of attack
∞	stream (static)

Computer program names

MAGEN	Magnetising field generator
MAGEN2	Modified version of above
PCMSBS	PC-based control system for the MSBS

1. INTRODUCTION

Wind tunnel testing is a fundamental research technique in aeronautics. The aim of wind tunnel tests is generally to infer from observation of a fluid flowing about a scale model of a vehicle, component or structure, how the flow will behave around the full size device in service. To promote the accuracy and validity of the results obtained from these tests, designers and users of wind tunnels have found it necessary to address a number of failings inherent in the practice, whose effects can cause a discrepancy between test results and those obtained at full scale. These failings are related to testing at reduced scale, interference from the test section walls, the influence of the model support on the fluid flow, boundary layer effects and turbulence to name but a few.

Despite these complications, wind tunnel testing of scale models remains the most reliable and practical method available for accurately predicting the properties of a fluid flow around a vehicle, component or structure. Theoretical methods and Computational Fluid Dynamics (CFD) have not yet advanced to the stage where wind tunnel tests are no longer required, if only to verify the calculated results. Significant investment continues to increase the diversity and capability of the wind tunnel test facilities available to engineers.

New types of wind tunnel have been developed in response to some of the problems outlined above. Scale effects are measured by Reynolds number, which includes the ratio of density to viscosity of the flow medium. The cryogenic wind tunnel concept exploits the increase in this ratio exhibited by gases at very low temperatures, and permits the testing of a small model at full scale Reynolds number. Adaptive walls in the wind tunnel test section can be contoured to control the shape of local streamlines. Wall interference can be reduced by this practice. Magnetic suspension of wind tunnel models has been developed to eliminate the effects of the model support, manifested as geometrical changes at the model-support interface, changes in the flowfield due to the presence of the support, and as restrictions placed by the support on the available range of model positions and attitudes.

1.1 REVIEW OF MAGNETIC SUSPENSION DEVELOPMENT

The concept of magnetic suspension for wind tunnel models was probably rather ahead of its time when the first system was reported by ONERA in 1957[1]. Evidently, the

technology existed to build a magnetic suspension system comprising of a magnetic model, an array of electromagnets for suspension and control, position sensing equipment and a controller. However, although it was possible to demonstrate suspension and control of a model in five degrees of freedom, and to gather some simple aerodynamic data, it was neither feasible nor practical to build a larger system capable of fully exploiting the versatility and potential offered by this technique.

Researchers discovered that the power consumption of a large Magnetic Suspension and Balance System (MSBS) would be considerable, and that measurement of several aerodynamic force components acting simultaneously on a suspended model was extremely complex and time consuming, except in very simple cases. Equipment used to detect the position of the model proved to be delicate and unreliable, and the analogue control systems were not easily adapted to new conditions. These problems are perhaps responsible for the decline in magnetic suspension research that followed the initial boom of the 1960s, which saw 11 additional systems constructed at 9 institutions in Europe and the United States.

Since that period NASA Langley Research Centre (LRC) has become the focus for MSBS activity, acquiring and updating disused systems from two US organisations, and funding further research abroad, notably at the University of Southampton. LRC has also coordinated the production of a regularly updated bibliography of publications related to magnetic suspension[2]. Until recently a specialist newsletter[3] aimed at promoting the exchange of information between different parties active in this area was also supported by LRC. Research into magnetic suspension has continued at a reduced level at LRC, and at Southampton and Oxford Universities in the UK. More recently the National Aeronautical Laboratory (NAL) in Japan, and the Moscow Aviation Institute (MAI) have developed their own MSBS systems for wind tunnel research.

Technological advances and the results of a sustained research effort have now removed many of the objections to the construction of a large magnetic suspension facility - generally viewed as the logical next step in the evolution of this technique. Superconducting magnets would reduce the power consumption of such a facility. New and updated methods for force measurement - one alternative is investigated in this thesis - promise uncomplicated evaluation of the full set of six force and moment components. Digital position sensing hardware is now available, offering increased precision and reliability over previous equipment. Finally, computerised control of magnetic suspension systems has unlocked their potential for suspension over large attitude ranges, with oscillations available for dynamic testing, simplified interchange

between models, rapid data processing, and also the incorporation of redundancy, improving control system reliability to a level above that of the most vulnerable component.

A number of design studies have been funded to assess the technical issues and economics related to the construction of a large MSBS[4,5]. The most recent (ref 5) estimates that the cost of a production MSBS with a 2.4 m test section fell from $88 million to $19 million (1990 prices) between 1981 and 1989, due to technological advances and refinements in the proposed design.

It is ironic that two wind tunnel technologies which were both initially investigated as potential methods for reducing the size of a production MSBS, have been developed from conception through to commercial application during the gestation period of the magnetic suspension approach. A commercial MSBS would probably incorporate these techniques: cryogenic wind tunnel testing and adaptive test section walls. The cooling of a cryogenic tunnel could be combined with the use of 'warm' superconducting electromagnets operating at liquid nitrogen temperatures. Adaptive walls remove the need for the plenum chamber necessary to enclose a conventional slotted test section. They also allow for a slightly smaller test section relative to the size of the model. An adaptive walled MSBS wind tunnel would therefore have a reduced spacing between the electromagnet poles and the model core, and consequently smaller magnets and a lower power consumption.

The present state of magnetic suspension research is that seven systems are operational, with one under construction. These are summarized in Table 1 below, while a description of the earlier systems can be found in ref 6. The short-term outlook for a number of these facilities is poor, with funding and policy problems at NASA Langley putting the future of their two systems in doubt. The uncertain economic situation in the former Soviet Union will hinder further progress at MAI. Plans for a new MSBS for use with a hypersonic wind tunnel at the Defense Research Agency (DRA) Farnborough, were shelved after the rejection of all construction bids. Finally, there are no immediate plans for further MSBS research at Southampton after the completion of this project.

In contrast, NAL in Japan has received funding for a second, larger MSBS which is presently under construction. This could perhaps be interpreted as another example of Western research being commercially exploited elsewhere. Advances in the US and Europe include a project underway at LRC to demonstrate a five degree of freedom MSBS with a novel, planar electromagnet array[7], and continuing research into the hypersonic aerodynamics of cones and spheres at Oxford University.

Table 1: Presently Active Magnetic Suspension and Balance Systems
Reproduced from ref 3, previous capabilities in parentheses

Organisation	Degrees of freedom	Test section size (mm)	Mach number	Year of construction
University of Southampton	5 (6)	178 octagonal (152 × 203)	0-0.2 (0.9)	1962
AEDC/LRC (USA)	5	272 × 319	0-0.5 (8.0)	1965
MIT/LRC (USA)	5 (6)	152 octagonal	0-0.5	1969
Oxford University	3	120 × 120	hypersonic	1975
MAI/TsAGI (CIS)	5	400 × 600	subsonic	1983
MAI (CIS)	6	300 × 400	subsonic	1989
NAL (Japan)	5 (6)	100 × 100	subsonic	1987
NAL (Japan)	6	600 × 600	subsonic	under construction

1.2 SCOPE OF THIS RESEARCH

The research program described in this thesis was funded indirectly by LRC through two policy directives, combining further development of magnetic suspension technology with an initiative to encourage small business activity in high technology areas.

Under the Small Business Innovation Research (SBIR) program, NASA Langley funded Physical Sciences Inc. (PSI) of Andover, Massachusetts to investigate techniques for propulsion simulation in magnetic suspension wind tunnels. Propulsion simulation - replication of the effects of engine inlet and exhaust flows on the flowfield around a wind tunnel model - has particular relevance to wind tunnel testing with an MSBS, as some of the flow regions subject to support interference are also those typically influenced by the propulsion system.

PSI subcontracted the University of Southampton to perform proof of concept tests in the 178 mm Southampton MSBS, on a model equipped with a development exhaust flow simulator. This work, and an investigation into an alternative exhaust simulation technique, is documented in the first part of the thesis, Chapters 3 to 7. The use of steel propulsion

simulation models, rather than those with the permanent magnets cores more usually employed at Southampton, necessitated the development of a technique for the magnetisation of steel models over a large angle of attack range. This development merits separate discussion, and is presented before the results of the propulsion simulation investigation in Chapter 5.

The propulsion simulation research highlighted the inability of the Southampton MSBS to adequately perform the 'balance' part of its function, and accurately measure the loads acting on a model in suspension. A review of force measurement practice suggested that a technique first investigated in the 1960's had not been developed to its full potential, and would benefit from the application of new technology. Subsequent development of a three-component form of this method for force measurement gave the Southampton MSBS a much improved balance capability. The three-component balance was used first to enhance an aspect of the MSBS control system, and then for force measurement during a unique aerodynamic investigation. Development and application of the improved force measurement technique are described in the second part of this thesis, Chapters 8 to 11.

Finally, modifications to the MSBS control system during this research program are discussed. The most significant development was the integration of a new control computer, which allowed the control software to be implemented in a higher level language, improving the accessibility of the system. Control system development is the subject of Chapter 12.

2. MAGNETIC SUSPENSION FUNDAMENTALS

This chapter aims to introduce the fundamental principles of an MSBS, to enable the non-specialist reader to view the research program in context. Relevant technologies, methods and issues will be introduced, and the scope of present and future applications discussed.

2.1 COMPONENTS OF AN MSBS

An MSBS for wind tunnel use is classified as a 'large-gap' magnetic suspension system: the air-gap between the electromagnet poles and the suspended model is of a similar order of magnitude to the system scale. The other principal use of large-gap magnetic suspension is in magnetically-levitated (mag-lev) trains. These applications are in contrast to the 'small-gap' of a magnetic bearing or vibration isolation system. Large-gap and small-gap magnetic suspension principles are compared in ref 8.

Wind tunnel magnetic suspension systems have been produced in a variety of configurations, but a few key components are common to each:

Model Core

The object to be suspended must be magnetised and commonly consists of a magnetic core surrounded by an aerodynamic fairing of the required shape. The core can be a permanent magnet, or a ferromagnetic alloy which is magnetised by the electromagnet array during suspension. A typical aircraft or missile model is conveniently constructed with a cylindrical core magnetised along the fuselage axis. The most promising core technology suitable for use with a future large MSBS is a superconducting solenoidal coil, which would provide much stronger magnetisation than can be achieved with conventional cores. A simple coil can be suspended and controlled in five degrees of freedom, but for control of roll attitude, some asymmetry in its design is required as outlined in Section 2.3. A superconducting core demonstrator has been built and tested at Southampton[9]. Use of a model with a strongly magnetised core allows the size, cost and power requirement of the suspension electromagnets to be reduced.

Electromagnet Array

A number of non-collinear electromagnets are required, that number being equal to or greater than the number of degrees of freedom to be actively controlled. To encourage uniform fields within the test section, the trend appears to be towards diametrically

opposing pairs of electromagnets, with the result that the total number of magnets for a simple arrangement becomes equal to twice the number of degrees of freedom controlled.

Power Supplies

Precise control of the electromagnet currents allows stable control of a suspended model, and bipolar operation is often required. Rapid current changes, overcoming the resistance caused by high electromagnet inductance, may be necessary to counter transient external forces. Generally the current in each electromagnet is regulated by a dedicated current source. An alternative is the distribution of current from one power supply to a combination of magnets, in an attempt to control just a single degree of freedom with each source. This approach was used in the design of the 152 mm MSBS at the Massachusetts Institute of Technology (MIT)[10], and has been shown to limit the capability of the system to reach the maximum continuous current acceptable to each magnet. It is likely that any future MSBS will control each electromagnet with an individual power supply, and will manage demand coupling using the control computer.

Position Sensors

The function of a position sensing sub-system in an MSBS is to enable the controller to react to changes in model position and attitude. Optical position sensors have found widespread application during the development of magnetic suspension systems for wind tunnels. The present generation of position sensors, which detect shadows cast by the model, are not regarded as the optimum solution for a large MSBS[8]. The preferred technique would appear to be camera-based tracking of targets on a model. Electromagnetic and X-ray shadow position sensing systems have been demonstrated[11,12] but these techniques presented new problems of complex signal processing and safety respectively.

Controller

Present MSBS geometries exhibit open-loop instability, and active control is required to achieve stable suspension. Control systems employing feedback of model position have been exclusively used for magnetic suspension systems to date. Early systems were regulated by analogue controllers, but the flexibility of digital systems has ensured that computerised control will be employed for any future large-gap MSBS.

Axis systems

A number of orthogonal axis systems can be employed during the discussion of MSBS subjects. The notation is that generally used for flight vehicles, and is illustrated in Figure 2.1a. Several axis systems are referred to in this thesis, and will be defined here.

• **Wind Tunnel Axes** are aligned so that the x-axis coincides with the centreline of the wind tunnel test section. The z-axis conventionally points vertically downward, as shown in Figure 2.1b.

• **Model Axes** are often used when control issues are discussed. These axes are defined relative to the model, as shown in Figure 2.1c. The model position and attitude can be described in terms of the displacement between the wind tunnel and model axes. In particular the pitch angle between the two axis systems defines the angle of incidence α (also referred to as the angle of attack) between the model and the airflow.

• **Position Sensing Axes** in the Southampton MSBS are centred on the datum for the high angle of attack position sensing system, which is inclined at 45 degrees to the stream direction (Figure 2.1d). All position measurements are initially made relative to this axis system.

• **Resultant Axes** are defined as being based on the instantaneous direction of the resultant aerodynamic force acting on the model. Generally this implies that they are inclined to the wind tunnel axes, by an angle governed by the model's lift to drag ratio *L/D* in a particular attitude. This axis system is illustrated in Figure 2.1e.

It is often necessary to perform transformations of perpendicular vectors between the axis systems described. In most cases this transformation is a simple pitch rotation, with no translation. For the situation shown in Figure 2.2, to transform vectors from an axis system *a*, inclined at a pitch angle θ_a to the freestream, to an axis system *b*, inclined at θ_b, the functions

$$X_b = X_a \cos(\theta_b - \theta_a) - Z_a \sin(\theta_b - \theta_a)$$

$$Z_b = Z_a \cos(\theta_b - \theta_a) + X_a \sin(\theta_b - \theta_a)$$

give the moduli of the transformed vectors.

2.2 FORCE AND MOMENT GENERATION AND MODEL MAGNETISATION

The properties of the magnetic fields generated by an electromagnet array can be used by an MSBS control system to influence a suspended model in a number of ways. A uniform field, such as that produced between two poles of opposite sign, can have two effects on a magnetic element depending on its orientation. If the element is aligned with the field, no

resultant force or moment is experienced. However, a ferro-magnetic element would be magnetised, as shown in Figure 2.3. In contrast, a magnetised element at incidence to a uniform field experiences a restoring moment, tending to align it with the field vector.

Forces are exerted on the element by field gradients. In Figure 2.4, the field strength changes rapidly between the two similar poles, and a force is experienced by the element as indicated. The magnitude of the force component diminishes as the element is angled away from its line of action.

The force F experienced by a magnetic element in a magnetic field can be expressed (from ref 13) as

$$F = \mu_0 \int_V M.\nabla H \, dV$$

The local force is thus proportional to both the field gradient ∇H and the degree of magnetisation M. For a typical MSBS electromagnet separated from the model by a large air gap, the field produced at the model is proportional to the applied current. Model magnetisation can often be assumed constant, and force is therefore proportional to current.

2.3 MSBS FEATURES AND APPLICATIONS

Support interference

With many aircraft and missiles sold before a full scale prototype has been tested, accurate predictions of range and performance are essential, and increasing precision is demanded of wind tunnel test results. Support interference during these tests remains a problem, and has been the subject of extensive research. A bibliography compiled by NASA[14,15] lists 176 works published since 1945 dealing with this phenomenon. As illustrated in Figure 2.5, aerodynamic support interference can be experienced by a number of different mechanisms, including

- Distortion of model geometry
- Disturbance to the airflow over the model
- Interference with the wake

Ease of testing

In addition to the elimination of support interference, a wind tunnel equipped with an MSBS offers several operational advantages. The model can be moved with ease for

testing at different (potentially unlimited) attitudes. It is straightforward to oscillate the model for dynamic testing, without the complications of mechanical complexity and distortion typical of a model support used for dynamic tests. Changing to a different model is simply a matter of loading the relevant data files. These features should contribute towards increased productivity in a commercial wind tunnel equipped with an MSBS, compared to a conventional facility.

Stores separation

The findings of a survey of the US aerospace industry[16], gives examples of specific tests which were found to be difficult to accomplish in conventional wind tunnels, but would have been easily performed in a large MSBS. Some of these tests concerned stores separation. The simultaneous and independent support of models of an aircraft and a store in a conventional wind tunnel is extremely complex. Magnetic suspension of the store with mechanical support of the aircraft would allow detailed studies of the forces experienced during different phases of the separation. Scale drop tests of stores are sometimes performed to investigate dynamic effects, but it is difficult to achieve the correct separation rate. In an MSBS the store can be driven away from the aircraft at a correctly scaled velocity[17]. Proof of concept stores separation trials using the 152 mm MSBS at NASA Langley are described in ref 18.

Roll control

Control of the roll attitude of a magnetically suspended model, although satisfactorily demonstrated, presents more difficulties than that of the other degrees of freedom, and has been viewed as an area of weakness with regard to the capabilities of a large MSBS. Roll control necessitates the provision of a lateral component of model magnetisation. A recent study[5] has examined techniques for improving the configuration of permanent magnets mounted in the wings of an aircraft model, and the possible use of additional electromagnets.

Coupling

It is conventional that for multiple degree of freedom control, each is treated separately by the controller. The behaviour of each component can thus be characterised, and appropriate control algorithms can be employed. A demand for control to a particular degree of freedom may effect others if an incorrect distribution of demand to the magnets is employed. This cross-coupling is a feature of several aspects of magnetic suspension systems. Coupling of the position measures can occur, whereby motion in a single degree of freedom causes a change in the measured value of another. The control system must

correctly decouple the position measures and calculate the true model position and attitude relative to a convenient axis system.

Force measurement

Accurate force and moment measurement is vital in aerodynamic testing. Most MSBS force measurement schemes relate the loads acting on the model in a particular condition to the instantaneous electromagnet currents. A coupling problem similar to that just described exists in force measurement, if the force is deduced from the magnet currents. Given the high precision with which measurements of current can be made, this is a potentially attractive technique. Complications arise during the application of multiple forces and moments, under conditions where the electromagnet current changes could be in response to one of several force components. It then becomes difficult to resolve the force components from the coupled current changes, without extensive and laborious pre-calibration of the system. The force measurement scheme developed during this project goes some way towards alleviating this problem.

Telemetry

The origins of aerodynamic loads are sometimes studied by examining the local static pressure at points on the surface of a wind tunnel model. In a development of work with model-mounted radio transmitters at Farnborough in the 1960s, researchers at NASA Langley have developed a technique for infra-red telemetry of pressures measured by a transducer on-board a suspended model, to an external data acquisition system[19]. They aim to extend this technique to telemetry of force measurements, taken from a compact strain gauge balance located between the model core and its outer shell. This would give an instantaneous reading of the aerodynamic force and moment components acting during a wind tunnel test. There would be no need to measure and subsequently process the electromagnet currents.

High angle of attack

The aerodynamics of high incidence are particularly susceptible to support interference, so it is important that a production MSBS has a high angle of attack capability. A recent research program conducted at Southampton[20], culminated in the demonstration of suspension at incidences from below zero to beyond 90 degrees. To achieve this it was necessary to modify the electromagnet array and to develop a new control philosophy, as described later.

2.4 PREVIOUS WORK AT SOUTHAMPTON

MSBS research at the University of Southampton began in 1959, with the first system commissioned in 1964. Early studies explored the potential of dynamic testing[21,22]. Subsequent development gave the Southampton MSBS a capability to regulate roll angle, conferring full six degree of freedom control for the first time[23]. The Magnus force acting on rapidly spinning models of artillery shells was investigated[24]. The magnetic suspension system was integrated with a prototype cryogenic wind tunnel, to demonstrate the compatibility of the two technologies[25]. More recent work has concentrated on design issues relevant to a large MSBS, including further development of roll control techniques[6], force calibration methods[26], superconducting model cores[9], and extreme attitude suspension[20]. The project documented in this thesis has continued the trend of using the small Southampton MSBS for proof of concept studies aimed at removing technical objections to a larger system.

2.5 CURRENT STATUS OF THE SOUTHAMPTON MSBS

The present configuration of the Southampton MSBS owes much to the work of Britcher[6] and Parker[20], although some components date back to the original 1960s system. The work presented herein did not involve major alterations to the MSBS hardware, the most significant change being the replacement of the control computer as described in Section 12.3. The key MSBS components introduced in Section 2.1 above will now be reconsidered in the context of the system at Southampton:

Models

Recent work conducted at Southampton has concentrated almost exclusively on suspension of models with permanent magnet cores. The five component optical position sensing system presently in use places some restrictions on model geometry, and an axisymmetric shape is often used. Passive roll control can be achieved by using a non-circular cylindrical core, which will tend to adopt a preferred roll attitude. This allows the suspension of simple winged models if required.

Electromagnets

Ten electromagnets are presently used for suspension and control, distributed about the test section as shown in Figure 2.6. For control purposes, the magnets are divided into four symmetrical groups, as shown in Figure 2.7. These groups will be referred to throughout this text. The skewed arrangement of the lateral magnets was incorporated by

Parker, to allow the generation of sideforce and yawing moment on a model during suspension at very high angles of attack. All magnets are copper-wound, with a thermally imposed steady current limit of around 20 A. The lateral and vertical groups have laminated iron cores to increase the magnetic flux and hence the force generating capability of these magnets.

Power Supplies

Power is obtained from 440 V, 3-phase mains, converted to 100 V DC by a transformer and regulator assembly. Magnets are driven by individual power controllers, loosely referred to as power supplies throughout this thesis. These devices are DC servo-motor controllers manufactured by CSR Contraves, and are documented in ref 27. Their mode of operation is pulse-width modulation: the output is switched between -95 and +95 V at around 5 kHz, and the width of each pulse is adjusted so as to give the required mean current. Regeneration of reactive power keeps the power consumption of these controllers low, making them well suited to use with an MSBS. The high inductance of the electromagnets does however have an adverse effect on their operation, as described in Section 12.5.2.

Position Sensors

Optical position sensing is employed, using a digital system based on detection of shadows cast by the model onto five self-scanning photodiode arrays. Each array consists of a linear matrix of 1024 individual photodiodes, with a total length of 25 mm. The arrays are illuminated by collimated laser light sheets, so that motion of a model edge is projected at full scale onto the sensor, and the distance between the model and the sensor has a minimal effect on sensor illumination. A shadow edge is detected as a transition from saturated to unsaturated photodiodes, and its position returned as a count of the number photodiodes illuminated. The photodiodes are generally referred to as pixels, and the information from an array as a pixel count. The relationship between model motion and the pixel count for each degree of freedom is position-dependent. As an example, for the case of a model suspended at 45 degrees of incidence (the position sensing datum attitude), the response to displacements in model/sensing axes is:

- **Heave displacement**, 91000 pixels/m: Varies with cosine of pitch displacement from datum.

- **Lateral displacement**, 91000 pixels/m: Essentially constant for present range of positions and attitudes.

• **Axial displacement**, 39400 pixels/m: Also dependent on cosine of pitch displacement.

• **Pitch angle**, 40.1 pixels/degree: Complex relationship (refer to ref 20), sensitivity approximately double at extremes of pitch range.

• **Yaw angle**, 40.1 pixels/degree: Sensitivity also increases with pitch displacement.

The arrangement of the photodiode arrays allows for suspension of axisymmetric models over a large angle of attack range, with smaller displacements available in heave, lateral and axial motion, and in yaw angle. Roll angle is not presently controlled, although a facility does exist to include roll sensing if necessary for a future project. Further details regarding the position sensing system may be found in ref 20.

Controller

The control software in use at the start of this work was that developed by Parker. Control was implemented on a DEC PDP11/84 mini-computer, which was shared with the Adaptive-Wall Wind Tunnel Group. A lack of processing speed with this computer made it necessary to use the DEC assembly level language, MACRO-11, for coding of the control routines, although a version of FORTRAN was available for writing non time-critical support software. During the project the PDP11 was replaced with a personal computer (PC), as described in Section 12.4.

Dual phase-advance control algorithms remain in use, as initially implemented by Britcher[6]. These algorithms were first used by the analogue control system as implemented between 1964 and 1980. The present controller can be regarded as a digital simulation of the original analogue version, and its action can still be represented by

$$\frac{c}{u} = \left(\frac{1+nTD}{1+TD}\right)^2 \qquad \ldots 2.1$$

where n controls the damping, and T the time period of the system. These terms will be discussed in more detail where relevant.

The dual-phase advance controller is analogous to a simple proportional plus differential block, and is thus incapable of reducing steady state position errors to zero. A separate error integrator is used to achieve precise positioning of the suspended model. The innovative feature of Parker's control system was the use of Demand Distribution Factors (DDFs) to achieve a high angle of attack capability. These pre-calculated parameters are functions of angle of attack. They enable the controller to distribute a demand for motion

in a particular degree of freedom to a combination of electromagnets, in such a way that only the required degree of freedom is influenced. The effectiveness of the various magnets at influencing the model vary with its orientation, so DDFs are strongly attitude-dependent. Previous control systems assigned demand more simply; demands for control of heave for instance, were sent only to electromagnets above or below the model. The inflexibility of this approach limited suspension to a small attitude range. The distributed demand strategy is likely to be widely implemented on future systems.

To maintain suspension of a model, the controller first interrogates the position sensing system as to the location of the model shadow edges on the five photodiode arrays. This information is decoded to yield the model location in five degrees of freedom. Position errors are calculated, and fed into the control block. The resulting demands to control each degree of freedom are converted using DDFs into commands to the individual electromagnets. The magnet commands for control of the five degrees of freedom are then summed. The totals are converted to analogue control signals, and output to the power supplies to complete the control loop.

The control loop rate is 242 Hz, a fairly arbitrary figure, but convenient for integration of the control and position sensing systems. Electromagnet currents are monitored with shunts, and the shunt voltages measured with a 12-bit ADC. The small memory of the PDP11 restricted the storage of run-data to a limit of around 125 control loops. The new computer has a much larger memory for storage of control software, control data and run-data.

Axis systems

The high angle of attack controller is presently implemented in model axes: position errors and commands for motion to reduce those errors are evaluated in an axis system which has the model as its datum. Sensing system axes have also been employed to suspend a model over a large incidence range[20], and little difference in performance was found between the two control strategies.

Wind Tunnel

An open return, low speed wind tunnel is presently available for use with the MSBS, having a maximum Mach number of around 0.2. Prior to this project, some aerodynamic testing had been performed using this tunnel[28], but no experiments had been carried out which utilised the unique high angle of attack capability of the Southampton MSBS.

3. INTRODUCTION TO PROPULSION SIMULATION

This chapter will outline the origins and justification of the propulsion simulation research. The principles of engine exhaust simulation will be explained, and a summary presented of the simulation techniques available to users of conventional wind tunnel facilities.

3.1 THE NEED TO REPRESENT PROPULSION SYSTEMS IN WIND TUNNEL TESTS

For a wind tunnel test of a model of an aircraft or flight vehicle to accurately represent the full-scale case, the effects of the propulsion system on the surrounding flowfield must be included. A model of a rocket-powered vehicle therefore needs to include exhaust simulation to be truly representative, while replication of an air-breathing engine should additionally incorporate an inlet flow.

Propulsion simulation assumes particular importance during certain types of test. Correct simulation of the propulsion system is critical to the general problem of airframe/propulsion system integration. For a fighter aircraft configuration with engines installed inside the fuselage, afterbody drag can make up a significant proportion of the total drag. Changes in the properties of the exhaust flow can significantly alter this drag component. Peters and Kennedy[29] determine the effect on afterbody drag coefficient of several parameters. At a Mach number of 0.6, the afterbody drag coefficient of a boattail model falls by 50 % as the Nozzle Pressure Ratio (NPR) is increased. Afterbody drag coefficients based on cross-sectional area observed at this Mach number fall within the range 0.02-0.12. This information will be used in Section 4.2 to estimate the force measurement accuracy requirement for propulsion simulation experiments.

Rear fuselage engine exhausts can influence the flow over a large region of the afterbody, and alter the aircraft's stability or the effectiveness of its control surfaces. Development of thrust reversers, or vectored thrust for V/STOL or improved manoeuvrability, is clearly dependent on the correct simulation of a given propulsion system. Some examples of propulsion aerodynamics are illustrated in Figure 3.1.

3.2 PROPULSION SYSTEM AERODYNAMICS

The interaction between the propulsion system, the external flow and the airframe is often assessed in a conventional wind tunnel facility by separate consideration of the inlet and exhaust flows. This simplification can be most easily justified for the case of a fuselage mounted engine, where the inlet and exhaust are relatively remote.

The aerodynamics of an engine inlet are dependent on the inlet flow, which in turn is influenced by the engine operating condition. Rising internal pressure in an inlet of increasing cross-section can yield a contribution to thrust. The entire surface flowfield over a pod containing an externally mounted engine can be affected by spillage from the inlet. The majority of inlet tests are conducted at a Reynolds number significantly below the flight value. This leads to an incorrectly scaled, enlarged boundary layer. In an attempt to minimise the effects of test scale, inlet geometries may be altered so as to reduce the ingestion of low-energy boundary layer[30]. A major concern during inlet investigations appears to be resolution of the different drag components. Transonic inlet drag is particularly susceptible to variations in mass flow rate. This flow regime is also that in which aircraft thrust minus drag is typically at a minimum, so transonic inlet testing assumes special importance.

An exhaust flow can influence the external stream by several mechanisms. The displacement effect of a propulsive jet can reduce the afterbody profile drag coefficient by encouraging recompression of the external flow[31]. The boundary between the jet and external flows is subject to shear forces because of the velocity differences. This results in mixing and entrainment which can affect the pressure distributions on local airframe surfaces. Where a jet is exhausted in the region of a surface, two further interaction mechanisms may occur. Interaction at a large angle can cause impingement: the direct application of a force by momentum transfer. A shallower interaction angle can cause the jet to attach to the surface, forming a high energy boundary layer. These interactions are typical of vectored thrust or ground effect operations[32].

Engine installations in external pods require closer examination of the combined effects of inlet and exhaust flows, but tend to be less subject to propulsion system interaction with the airframe. Recent stealth aircraft designs exhibit a high level of airframe and propulsion system integration, and have presumably been subjected to thorough propulsion simulation testing during their development.

3.3 IMPORTANT PARAMETERS FOR SIMULATION

Simulation of propulsion effects in ground test facilities is based on the consideration of a number of similarity parameters. Traditionally, simulation of inlet flows has concentrated on achieving a correctly scaled mass flow rate, while exhausts are often characterised by NPR. The ratio of specific heats of the jet γ_j is also an important parameter[33].

The importance of other jet properties such as temperature, pressure, Mach number and Reynolds number depends on the particular propulsion simulation test to be attempted. Nozzle afterbody drag and thrust reverser effects have been shown to be strongly dependent on jet temperature.

It has not previously been possible to perform completely representative propulsion simulation in a conventional wind tunnel. The scale of the apparatus has prevented testing at the correct stream and jet Reynolds number, and the correct values of other parameters cannot generally be attained simultaneously. The test engineer is forced to compromise, selecting a small number of parameters to be correctly scaled for each investigation.

The availability of full scale Reynolds number in wind tunnel tests, brought about by the exploitation of the cryogenic wind tunnel concept, has encouraged researchers to investigate the possibility of complete propulsion simulation. Asai[34] defines a complete set of propulsion simulation similarity parameters as

- Simulation of external (freestream) flow: M_0, Re_0, γ_0, Pr_0
- Simulation of internal (jet) flow: M_j, Re_j, γ_j, Pr_j
- Simulation of jet / stream interaction: p_j/p_0, T_j/T_0, v_j/v_0, L_j/L_0

He goes on to show that a mixture of nitrogen and methane, at ambient temperature or slightly above, can give a very complete exhaust simulation when vented into a moderately pressurised cryogenic wind tunnel. The propulsion simulation parameters listed above are not ranked in any order of preference, but can be used to assess the suitability of the more commonly used propulsion simulation techniques.

Asai introduces a similarity polygon as an aid to the assessment, allowing a qualitative comparison of propulsion simulation techniques. Each vertex on the polygon represents a similarity parameter, and a regular shape depicts their full scale values. For propulsion simulation, the radial position of each vertex is scaled according to the parameter values

achieved with a given method. The degree of distortion of the similarity polygon produced for each method gives an indication of its validity as a propulsion simulation technique.

3.4 PROPULSION SIMULATION TECHNIQUES

In addition to achieving similarity with a real flow, simulation techniques must be assessed in terms of cost, complexity and safety. An additional consideration is the possibility of errors in the test results caused by contamination of the tunnel working fluid by the exhaust gases.

3.4.1 Inlet simulation

As described above, simulations of the inlet and exhaust flows of an air-breathing propulsion system are often performed in separate tests. It is practical to conduct the majority of inlet tests at a correctly scaled mass flow rate[35]. A simple flow-through model may be used, but an enlarged exit is required to achieve the correct mass flow rate, and the geometrical alteration can cause a disturbance to the external flow which propagates back upstream.

3.4.2 Exhaust simulation

This thesis concentrates on exhaust simulation, as exhaust tests are more subject to support interference, and are therefore more relevant to an MSBS. Only exhaust simulation was required of the University under the terms of the contract to simulate a propulsion system in the Southampton MSBS.

Dry Air and cold gases

The most common exhaust simulation method in wind tunnel tests is the use of compressed dry air at ambient temperature. Generally the full scale nozzle pressure ratio is duplicated, but it is not possible to simultaneously achieve a realistic jet velocity. The temperature ratio will evidently be incorrect using this technique. The major advantages of dry air exhaust simulation are that it is simple and cheap, and that the exhaust gases do not contaminate the wind tunnel.

Other gases used for ambient temperature jet simulation have included helium, which has a high gas constant, allowing the correct value of some temperature related parameters to be achieved. However, helium has the disadvantage of a high ratio of specific heats. Cold carbon dioxide has been used in wind tunnel propulsion simulation, to achieve the ratio of

specific heats of the combustion products of hydrogen and air, typical of the exhaust of a liquid propellant rocket[36].

Gas mixtures can be used to combine the favourable properties of a number of gases. Peters and Kennedy[29] used graduated gas mixtures to isolate the effects of some jet parameters on the success of an exhaust simulation. Ratio of specific heats was found to have an affect on jet plume shape. The gas constant and temperature of the jet tended to influence the degree of entrainment. The use of gas mixtures was developed by Asai for use in a cryogenic wind tunnel, as described above.

Hot Jet

For tests where temperature effects are important, heated air can be used as the jet fluid. A ratio of specific heats similar to that of turbojet or ramjet exhaust can be achieved by using air heated to ramjet exhaust temperature (1800 K)[36]. Asai's use of compressed gas mixtures at ambient temperature for propulsion simulation in a cryogenic wind tunnel can be regarded as a hot jet technique, as the jet is at an elevated temperature relative to the freestream, and a realistic temperature ratio is attained.

A number of more complex hot jet simulation techniques have been developed for conventional wind tunnels, for cases where hot air is not sufficiently representative of the engine exhaust. The hot jet can be obtained by catalytic decomposition of hydrogen peroxide (H_2O_2)[36], or by a variety of combustion methods. Pindzola[37] reviewed a number of early techniques attempting simulation of turbojet and rocket exhausts. Combustion of hydrogen and air gives exhaust properties similar to those of an afterburning turbojet. Simulation of the very high temperatures of a rocket exhaust may require a rocket powered propulsion simulator. Solid rockets can also provide a useful simulation of turbojet exhaust.

Hot jet techniques share the disadvantages of cost, complexity of model design, and potential safety hazards. Compatibility with the wind tunnel facility may also be a problem.

Turbo-Simulators

Several propulsion simulation techniques have been developed using turbo-machinery. These range from miniature turbojet engines located within a wind tunnel model to externally driven compressors and turbines, which allow simultaneous and independent control of the inlet and exhaust flows. An external turbojet can be used to provide real turbojet exhaust with the correct properties and composition. The use of such an engine to

also control the inlet flow is hampered by a problem inherent with the use of any external turbo-machinery to regulate propulsive flows. The restricted diameter of pipes from the model to the machinery leads to a very high power requirement[33], especially for testing at transonic speeds. This problem can be alleviated by using a half-span model, illustrated in Figure 3.2.

3.4.3 Summary

Typical similarity polygons for the propulsion simulation techniques described above are shown in Figure 3.3. The cold air jet (Figure 3.3a) fails to match the flight values of Reynolds number, and of the temperature and velocity ratios. Use of a hot jet with an H_2O_2 thruster (Figure 3.3b) improves the matching of temperature and velocity ratios, at the expanse of jet Prandtl number. A hot jet simulation using a rocket as the gas generator would be represented by a similarity polygon of a comparable shape to that of the H_2O_2 thruster, but with a high temperature ratio. The idealised turbo-simulator of Figure 3.3c matches all parameters except the stream and jet Reynolds numbers.

Asai's compressed gas technique for use in a cryogenic wind tunnel provides the best match with the full scale conditions, and would give a regular similarity polygon. The other methods each include parameters which are far removed from their full scale value. For simulation of propulsion systems in a non-cryogenic wind tunnel facility, the test engineer would need to make corrections to the test data in order to account for the imperfect representation of inlet or exhaust flows.

3.5 PROPULSION SIMULATION FOR AN MSBS

Base flows are an area of aerodynamics particularly subject to support interference in conventional wind tunnel testing, and it follows that a commercial MSBS would periodically be utilised for investigations into base flows. The influence of the propulsion system on base flows for flight vehicles leads to the conclusion that a commercial wind tunnel equipped with an MSBS should be capable of performing propulsion simulation tests. Given the complexities outlined above of achieving adequate propulsion simulation even in a conventional wind tunnel, performing these tests with a magnetically suspended model presents a particular challenge. The overriding design consideration, as no support exists through which to supply or remove representative inlet and nozzle flows, becomes the need to incorporate a gas generator into the levitated model.

The requirement for propulsion simulation in an MSBS was recognised among the findings of the *Study of Needs for a Magnetic Suspension System Operating With a Transonic Wind Tunnel*[16]. Research into propulsion simulation was subsequently supported by NASA, under their Small Business Innovation and Research (SBIR) initiative. NASA Langley Research Centre contracted Physical Sciences Inc. (PSI) of Andover, Massachusetts to investigate propulsion simulation techniques compatible with an MSBS. Phase I of the contract was a feasibility study, examining potential methods for exhaust simulation, and identifying important design issues. The contract was then extended to Phase II, during which PSI aimed to confirm experimentally the results of the feasibility study, and to demonstrate propulsion simulation in an existing MSBS.

The University of Southampton was subcontracted to perform the proof of concept trials in its MSBS facility, and this work formed the basis of the propulsion simulation research reported here. The candidate techniques and details of the propulsion simulation experiments are described in the following chapters.

4. PREPARATION FOR PROPULSION SIMULATION

The options for propulsion simulation in an MSBS are explained, along with the background to the selection by PSI of a compressed gas thruster for development as a technology demonstrator. The performance requirement for an exhaust simulator in the Southampton MSBS is examined. A number of modifications to the system were necessary to allow propulsion simulation testing, and these are described.

4.1 PROPULSION SIMULATION TECHNIQUES FOR AN MSBS

During Phase I of their contract with NASA Langley Research Centre, to evaluate exhaust simulation techniques for use in a wind tunnel equipped with MSBS, PSI identified four potential gas generation methods for producing a propulsive jet. These were

- Compressed gas cylinders
- Liquid propellant rockets
- Solid propellant rockets
- Laser assisted techniques

A brief description of each is appropriate:

Compressed Gas Cylinders

A model could be designed to incorporate a storage tank for compressed gas, or to accommodate a one-shot sealed container. Cylinders containing liquified gas under pressure are commercially available in a variety of sizes and containing different gases. A thruster using such a cylinder as the gas generator would contrive to release the contents in a controlled manner. The aim would be to release a steady stream of vapour, producing a jet of constant thrust while the cylinder emptied.

Of the gases readily available in cylinders, carbon dioxide and ammonia were considered the most suitable candidates. They have an advantageous physical property in that they are easy to liquify at room temperature. A larger mass of propellant can thus be stored in a cylinder of a given volume. Problems to be solved with a compressed gas thruster include flow regulation, and prevention of excessive cooling of the gas container. The latter can be viewed as a need to supply latent heat of vaporisation to the propellant.

Liquid Propellant Rockets

Gas generation by catalytic decomposition of H_2O_2 (hydrogen peroxide) to form steam and oxygen is sometimes used for propulsion simulation in conventional wind tunnel facilities. This method has the advantages of producing a hot exhaust plume of controllable pressure and temperature (around 1000 K), but it is mechanically complex and expensive. The ratio of specific heats of the exhaust is fixed at 1.27, compared to 1.34 for a typical turbojet exhaust, or 1.23 for rocket exhaust. The major disadvantages are related to safety. Skin contact with hydrogen peroxide is dangerous. Furthermore, the generation of oxygen gas in the exhaust creates an explosion hazard.

Solid Propellant Rockets

Small solid propellant rocket motors are a mature technology. They have a wide range of applications, from aircraft ejection seats to meteorological sounding vehicles. Solid propellant rockets are capable of producing a particle-free exhaust, and the thrust profile can be precisely controlled by varying the propellant geometry. Jet temperature can reach 2500 K. The similarities between the thermodynamic properties of a rocket exhaust plume and those of a jet engine exhaust, have encouraged previous experimentation with solid rockets for wind tunnel propulsion simulation as described in ref 37. The disadvantages of solid rockets are related to safety, cost, and the lack of an ability to interrupt the motor run between ignition and burn-out.

Laser Assisted Methods

A high energy laser beam could be used to supply heat to a thruster. Several options for laser assisted propulsion simulation were put forward by PSI. The simplest method proposed was for laser ablation of a solid, whereby the laser heats a suitable material, which then vaporises to generate a propulsive stream. An alternative proposal uses a specially shaped nozzle to focus a laser beam. Air in the nozzle is heated until it breaks down forming a detonation wave and so produces thrust. Rapid pulsing of the laser is employed to produce a succession of thrust impulses. This technique uses no fuel, and has the potential to allow inlet as well as exhaust simulation, although the properties of the exhaust were not rigorously considered by PSI. The two laser assisted schemes are described in detail in ref 32. The major disadvantage with both techniques is the laser power requirement, initially estimated at around 2 kW per Newton of thrust, with the estimate later exceeding 10 kW per Newton for the ablative thruster.

4.2 THRUSTER PERFORMANCE REQUIREMENT

The performance requirement for the proposed thruster is defined by considering the case of propulsion simulation for a typical fighter aircraft (F/A-18, two F404 engines). Defining nozzle pressure ratio as the most important parameter to be accurately simulated, and assuming that a scale model will be used, the mass flow and thrust requirements for the thruster can be derived.

A simplified solution presented in ref 32 leads to

$$\frac{\dot{m}}{A} = \frac{p_\infty}{\sqrt{RT_0}} \left(\frac{p_j}{p_\infty}\right) \sqrt{\gamma} \left(\frac{2}{\gamma+1}\right)^{\left(\frac{\gamma+1}{2(\gamma-1)}\right)} \qquad \ldots 4.1$$

Substituting flight values of NPR (3.0 - 4.0), ratio of specific heats (1.34), and assuming operation at sea level for compatibility with an MSBS at atmospheric pressure (p_∞ = 101.3 kNm^{-2}), the above reduces to

$$2.05\times10^5 \leq \frac{\dot{m}}{A}\sqrt{RT_0} \leq 2.73\times10^5 \quad \frac{N}{m^2 s}(kg\,kJ)^{1/2}$$

This term will be referred to as the *mass flow parameter*. In order to match the units of the mass flow parameter to those commonly used for the gas constant R, it is necessary to divide by gravitational acceleration giving

$$2.09\times10^4 \leq \frac{\dot{m}}{A}\sqrt{RT_0} \leq 2.78\times10^4 \quad \frac{kg}{m^2 s}(kg/kJ)^{1/2}$$

The thrust per unit nozzle throat area is given by

$$\frac{Th}{A} = \sqrt{\frac{2}{\gamma-1}}\ \gamma \left(\frac{2}{\gamma+1}\right)^{\frac{\gamma+1}{2(\gamma-1)}} p_\infty \left(\frac{p_j}{p_\infty}\right) \sqrt{1-\left(\frac{p_j}{p_\infty}\right)^{\frac{1-\gamma}{\gamma}}} \qquad \ldots 4.2$$

which reduces to

$$2.84\times10^5 \leq \frac{Th}{A} \leq 4.18\times10^5 \quad N/m^2$$

The properties of some real engine exhausts, including the derived parameters for mass flow rate and thrust for an NPR of 4.0, are presented in the following table:

Table 2: Typical Properties of Engine Exhausts

Property	Turbojet Engine	Ramjet Engine	Rocket Engine
Jet Temperature (K)	1000	1800	3200
Gas Constant (kJ/kgK)	0.285	0.317	0.377
Ratio of Specific Heats	1.34	1.27	1.23
Nozzle Pressure Ratio	4.0	5.6 (M = 2.0)	200[a]
Jet Reynolds no. (m^{-1})	14.6×10^6	$\sim23\times10^6$	$\sim50\times10^6$
Mass flow parameter ($kg/m^2s(kJkg)^{1/2}$)	2.78×10^4	1.57×10^4	3.83×10^5
Thrust / Area (N/m^2)	4.18×10^5	1.14×10^5	2.03×10^6

The small scale of the Southampton MSBS dictated that the process of designing a propulsion simulator was mainly concerned with miniaturisation. The largest possible model scale would therefore be used. The octagonal MSBS test section measures 178 mm across its flats. Taking 178 mm as representative of the largest permissible model dimension, this corresponds to a scale close to 1/100 for the F/A-18. Two F404 engines are installed, but the simulation of a single engine will be considered for simplicity. The 1/100 scale nozzle throat diameter is approximately 4.4 mm. The mass flow and thrust requirements therefore become

$$\dot{m}\sqrt{RT_0} \approx 0.42\,\frac{kg}{s}(kJ/kg)^{1/2} \quad , \quad Th \approx 6.4\,N$$

The mass flow parameter must be applied to a specific gas to be meaningful. For carbon dioxide, which was favoured by PSI throughout the selection of a compressed gas thruster propellant, the ambient temperature mass flow requirement becomes

$$\dot{m} \approx 0.057\ kg/s$$

For steady suspension during a thrust impulse, the MSBS would be required to apply a restraining force equal to the thrust. Although the exact force capability of the Southampton MSBS with a propulsion simulator would depend on the magnetic properties of the particular model, it was estimated based on recent experience that a 6.4 N restraining force would be close to the maximum achievable.

[a]Space Shuttle main engine

In Section 3.1 the change in the afterbody drag of a body with a boattail, due to the presence of an exhaust plume was described. A reduction in afterbody drag coefficient from 0.1 to 0.05 will be taken as representative of this effect. Testing a propulsion simulator model of diameter 25 mm in the Southampton MSBS, a thruster-*off* afterbody drag of around 0.14 N would be expected at the maximum tunnel Mach number of 0.2. The change in afterbody drag with the thruster firing would therefore be 0.07 N. To resolve this change in the presence of a 6.4 N thrust impulse would require a force measurement accuracy exceeding 1.1 %. Precise evaluation of the drag change would demand a more accurate force measurement. This information will be used in the assessment of force measurement schemes later in the thesis.

4.3 DESIGN CONSIDERATIONS

A number of issues were identified by PSI, to be addressed first in the selection of a propulsion simulation technique, and subsequently in the design of a thruster-equipped MSBS model:

- **Compactness** of the thruster is desirable for compatibility with the present generation of small MSBS wind tunnels.

- **High Density Propellants** maximise the thruster run time for a given mass flow rate.

- **Lightweight** design reduces the size of the magnetic core to be integrated into a simulator, for the generation of suspension forces.

- **Remote Activation** enables the thruster to be fired with a minimal disturbance to the flowfield and the magnetic field.

- **Thrust Level** should have a maximum value within the capability of the MSBS.

- **Thrust Profile** should be compatible with the MSBS control system. The duration of a period of stable thrust should be long enough for data acquisition after the model becomes steady.

- **Safety** is promoted if the propellant material is non-toxic and non-corrosive, with a minimum of hot particulates in the exhaust.

This is not an comprehensive list of criteria relevant to the design of a wind tunnel propulsion simulator, but was considered by PSI to be an adequate starting point for the proof of concept studies in an MSBS. A rigorous list would additionally include a full characterisation of the exhaust properties and the jet geometry, and would consider the influence of the external shape of the model.

A compressed gas thruster was selected by PSI for proof of concept propulsion simulation trials in two MSBS facilities: Southampton and LRC. The decision to develop the compressed gas thruster was based on the perceived simplicity of this gas generation technique. Carbon dioxide was chosen as the propellant gas. It is cheaper and more easily available in bottles than ammonia. Carbon dioxide presents less of safety hazard than ammonia, which is an irritant.

A thruster was proposed containing a small disposable CO_2 bottle, the contents of which could be exhausted via a nozzle. The major difference between the proposed design and that eventually tested was that the conceptual thruster incorporated a solenoid valve to regulate the flow of exhaust gas. At this scale no fast-acting solenoid valve was commercially available, and PSI were forced to omit a control valve from the final design of the small CO_2 thruster. It was however feasible to incorporate a solenoid valve for exhaust flow regulation into the design of the larger thruster, intended for testing in the 0.33 m MSBS at LRC. The implications of employing a design with no control valve are examined in Section 6.1.

4.4 MODIFICATIONS TO THE SOUTHAMPTON MSBS TO ALLOW PROPULSION SIMULATION

4.4.1 Axial position sensing geometry

The major hardware change made to the Southampton MSBS to allow propulsion simulation experiments, was the reconfiguration of the axial position sensing equipment. The initial configuration was that designed by Parker[20], to enable axial position sensing over a large angle of attack range and is shown in Figure 4.1. A laser light sheet of approximately 30 × 7 mm, originating at the downstream end of the test section and directed along the wind tunnel axis, was deflected at an angle of 45 degrees over the tail of a suspended model, and then onto a photodiode array. With this configuration, a model with a magnetic core length of around 180 mm could be rotated about the centre of its core, from below zero incidence to beyond 90 degrees.

It was clear that the efflux from a suspended propulsion simulator, exhausted along the wind tunnel centreline, would interfere with the axial laser sheet. Furthermore it seemed likely that a broader region of the test section downstream of the model could be subject to clouding by the exhaust gas. Two features of Parker's design, axial position sensing by scanning across the model tail, and a laser origin downstream of the model, were therefore ruled out.

The range of alternative axial scanning geometries was severely limited by the lack of space and the restricted light access paths around the Southampton MSBS test section. One geometry was identified which allowed scanning across the nose of a model of a suitable size, and also retained a high angle of attack capability. This geometry was selected for axial position sensing during the propulsion simulation tests.

Two alternative orientations of the laser sheet relative to the model were considered, the selection being dependent on the nose geometry of the propulsion simulators. As shown in Figure 4.2, a laser sheet aligned along the model axis can be used to indicate the axial position of a blunt-nosed model. A conical nose could be monitored using a transverse light sheet, the width of the image giving an indication of axial position. The former approach was considered to be preferable, being similar to the tail sensing previously employed, and less subject to coupling with model motion in other degrees of freedom. PSI agreed to supply a propulsion simulator having a hemispherical nose shape.

The layout for nose scanning is shown in Figure 4.3. The axial position laser is mounted to the right of the MSBS, angled so as to allow direct passage of its beam to a mirror located beneath the upstream end of the test section, behind the forward axial electromagnet. This mirror directs the beam upward and backward across the test section, to a second mirror located between the upper electromagnets. The beam is returned, offset laterally to avoid a second contact with the model nose. A third mirror collects the beam and directs it onto the axial photodiode array, located as before on a platform mounted to the left hand side of the MSBS.

It was necessary to increase the angle of incidence of the beam as it crossed the test section, from 45 to 50 degrees. This angle was required to allow positioning of the mirrors in the available locations, and to permit suspension of a model of typical propulsion simulator dimensions centrally within the electromagnet array. The software used to generate position sensing data for use by the control system was modified to account for this change.

The design of components for the new optical alignment was governed by considerations of space. Elliptical mirrors were used, because alignment of the light sheet along the major axis of an elliptical mirror, allowed larger angles of deflection in the confined spaces available than with a similar rectangular mirror. A low-profile, compact mirror mount was designed, allowing rotation of the mirrors about 3 axes. The laser and optics for generation of a light sheet were transferred from the original axial position sensing system.

New windows were installed in the wind tunnel test section, to allow passage of the realigned laser light sheets. As is conventional, the new windows are standard optical components, with a coating designed to reduce the reflection of helium-neon laser light.

In the Southampton MSBS, the model is traditionally hand-launched from the upstream end of the test section. The operator's hand necessarily obscures the nose-scanning axial laser sheet during such a launch. A keyboard command was incorporated into the high angle of attack control system to toggle axial control *on* or *off*. With nose scanning operational, models are launched into four degree of freedom control, with manual restraint of axial motion. The operator then moves his hand so as to lightly grip the sides of the model nose, simultaneously allowing passage of the axial sensing beam. The model is moved into a suitable axial position, and axial control is then enabled with a key press. With five degrees of freedom controlled, the model is then released.

4.4.2 Control system modifications

The major modification to the control system necessary to allow propulsion simulation testing to take place was the introduction of magnetisation for iron models. The use of iron as the magnetic material for propulsion simulator models marked a departure from recent practice at Southampton, where models with permanent magnet cores had been preferred for some time. Magnetisation of iron models with the high angle of attack controller involved the development of a new strategy, and is described in the following chapter.

An improvement in the quality of control was achieved by including a software correction for a power supply response error. This error arose because the response of the power controllers used with the Southampton MSBS is degraded by the high inductance of the electromagnets, which is above the rated value of the power controllers. The technique used to limit the effects of this problem is described in Section 12.2.

To improve the capability of the system to record run data during the first propulsion simulation experiments, a second computer was incorporated to act as a data logger

(Section 12.3.2). This computer was later also used for control of the magnetic suspension system (Section 12.4).

A pressure transducer was installed on the inlet of the MSBS wind tunnel, to allow the control computer to record test section dynamic pressure. The controller was later connected to the wind tunnel speed regulator, to close the tunnel speed control loop and allow automatic control of tunnel Mach number. Tunnel speed monitoring and control are more fully described in Section 12.4.2.

Further changes to the control system are described where appropriate in the chapters which deal with the simulation techniques investigated. The optimisation of control system parameters for the new models is outlined in Section 12.5.1.

4.4.3 Representative model

The first large iron model to be suspended was a dummy propulsion simulator, designed to be representative of the compressed gas model designed by PSI in properties such as size, total mass and unmagnetised payload mass. A schematic is presented in Figure 4.4, and the representative model is shown together with the compressed gas thruster and a development solid rocket thruster in Plate 1. The representative model was used to confirm the correct operation of the nose scanning axial position sensor described above, to allow the selection of control parameters for this new class of model, and to determine the axial force capability of the MSBS acting on a typical propulsion simulator.

Provision was made to assess the effects of the centre of gravity shift caused by the exhaustion of on-board propellant. The representative model has an internal component of the same weight as the carbon dioxide carried by the compressed gas thruster (16 g). This weight was installed and removed to simulate the effects of releasing the propellant, and traversed along the central axis of the model to move the centre of gravity. However, its weight was so small compared to that of the model, that no significant effects were observed.

5. MAGNETISATION OF FERRO-MAGNETIC MODELS

This chapter describes the development of a novel technique for the magnetisation of ferrous models. The new capability was made necessary by the decision to construct the propulsion simulator models from steel, given the difficulty of machining permanent magnet alloys. The feature of this method is that the magnetisation vector is now rotated to match the instantaneous angle of attack of the model. This is the first use of an adaptive magnetisation procedure, and allows the suspension of iron models over the full angle of attack range available with the Southampton MSBS.

5.1 MODEL CORES

A typical model for use in a wind tunnel equipped with an MSBS consists of a magnetised core surrounded by a non-magnetic aerodynamic fairing. The core is acted upon by the MSBS electromagnets to provide suspension and control forces. The fairing represents the shape of the test vehicle, and transmits aerodynamic forces to the core when the wind tunnel is in operation. Use of this two-part design represents a compromise between the weight penalty of suspending the fairing as a load, and the saving in design and manufacture achieved by using a simple core, which can subsequently be re-used in other models.

Strength of magnetisation of the model core is of great importance in the design of an MSBS. Forces to suspend the model and control it under the influence of propulsive or aerodynamic loads can be provided by a smaller and cheaper electromagnet array, if the model is strongly magnetised. Three generic core options are available; permanent magnets, soft iron and solenoids.

Permanent magnet cores

Recent work with the University of Southampton MSBS has concentrated almost exclusively on permanent-magnet models. Core materials have been selected using a number of criteria including the residual level of magnetisation, ability to avoid demagnetisation, cost and mechanical properties. Materials have included Alnico V[38] and Platinax. These alloys are prone to gradual demagnetisation under typical MSBS operating conditions, and must be periodically re-magnetised. The facilities at Southampton permit the re-magnetisation of these cores.

Uncertainty over the instantaneous level of magnetisation can complicate the measurement of forces acting on a model[39]. A calibration to determine the relationship between externally applied forces and electromagnet currents is invalidated by any change in the state of model magnetisation. New materials such as samarium-cobalt and neodymium-iron-boron have recently been used as model cores to reduce this problem. These alloys exhibit excellent resistance to demagnetisation and have a high residual magnetisation of approximately 1.0 - 1.2 T.

Permanent magnet alloys with the exception of Platinax tend to share brittleness as a physical property. For ease of manufacture they are generally formed into elemental geometries, and are typically supplied as cylinders or discs. If roll control of an MSBS model is to be attempted, a non-axisymmetric core shape is required, which is generally produced by grinding flats onto a cylindrical core. An alternative is to provide auxiliary magnet elements in the model.

Iron cores

A soft-iron core in an MSBS model does not retain its magnetisation to any significant extent, and must be subjected to a constant magnetising field whilst in suspension. The magnetising field is different to that used for suspension in that field intensity magnetises a core aligned with the field, whilst field gradients generate electromagnetic force. Moments are produced by uniform fields which are not aligned with the core, as described in Section 2.2. Uniform magnetic fields are also referred to as magnetising fields in this text. For an iron element the relationship between the magnetising field and the degree of magnetisation is non-linear.

Several factors combine to make soft-iron attractive as a core material under certain circumstances:

- **Cost:** Soft iron in the form of mild or electrical steel is much cheaper and more readily available than permanent magnet alloys.

- **Strength of magnetisation:** Steel can be magnetised to around 2 T, compared to a maximum not much greater than 1 T for permanent magnets[40]. However, a trade-off exists given the limited availability of current in the electromagnets of an MSBS, between the benefits of a strongly magnetised iron model, and the need to provide a magnetising field.

• **Ease of machining:** The brittleness of most permanent magnet alloys is in contrast to the ease with which steels can be machined. A steel model can therefore be produced with complex internal and external geometries. All of the ferrous metal present can be magnetised to contribute to suspension and control. The proportion of excess material to be suspended as load is reduced. Ease of machining was the decisive factor in the decision to use steel cores for the propulsion simulators.

Solenoids

A solenoid with a current flowing can be used as a magnetic element in an MSBS model. Although an auxiliary solenoid powered by an on-board battery has been used to enable roll control of a permanent magnet cored model[22], the primary use of solenoid cores is envisaged to be the use of a superconducting solenoid as the main magnetic component. A demonstration superconducting core, developed at the University of Southampton[9], consisted of a cryostat containing a superconducting coil immersed in liquid helium. The rate of evaporation of the helium determined the life span of the core, and hence the wind tunnel run-time available before stopping to recharge the cryostat.

Superconducting solenoids can achieve very high levels of magnetisation, with operation at 6.5 T predicted for the next generation of high temperature (liquid nitrogen coolant) superconducting materials, suitable for use in an MSBS model[41]. The strong magnetisation would lead to significant savings in electromagnet array size and cost, especially in the proposed design for a large MSBS[5]. The disadvantages of this type of core are primarily cost and complexity, in addition to the inconvenience of periodic recharging. Accepting that superconducting cores are very appealing for use in a future large MSBS, the present generation of small development magnetic suspension wind tunnels are unlikely to use superconducting models except as technology demonstrators. They were not therefore a practical option for propulsion simulation.

5.2 MAGNETISATION TECHNIQUES

Magnetisation of an iron-cored model has been achieved prior to this research using one of two alternative techniques:

Free magnetisation

Model magnetisation can be a natural consequence of suspension. An asymmetric electromagnet array (this category includes most of the systems constructed to date) can be

configured in such a way that the magnets which support the weight of the model also provide magnetisation. Figure 5.1 shows such an array, and is representative of the Southampton MSBS before Britcher's work commenced in 1978. Each end of the core is attracted by an opposingly signed pole, the result being 'automatic' magnetisation. A disadvantage is that the degree of magnetisation of the core is both unknown and variable, depending on model position and external forces. Suspension of an iron model over a large angle of attack range using this magnetisation technique would be complex and has not been attempted.

Forced magnetisation

The alternative approach to magnetisation employed to date has been the provision of an extra pair of coils to provide magnetisation, in addition to those employed for levitation of the model. This approach is typified by the 152 mm MSBS constructed at MIT[10] (now at NASA Langley), which has a pair of 'axial' coils specifically for model magnetisation. An exact and quantifiable magnetising field is provided, but the state of magnetisation of the model depends on its angle of attack, and the angle of attack range is limited to those attitudes where the magnetising coils remain effective.

5.3 MAGNETISATION OF PROPULSION SIMULATORS

An iron model was the obvious choice for a suspended propulsion simulator, given the expected complexity of internal design of this type of model. As a consequence, it was necessary to develop a technique for the provision of a magnetising field in the Southampton MSBS. This would be the first use of iron models with the present symmetrical electromagnet array and high angle of attack controller. Use of the symmetrical array would not give 'automatic' magnetisation as described above, so an active magnetisation technique was required. At low angles of attack this could conceivably be provided by the axial, air-cored solenoids, in a similar manner to the ex-MIT system. Thus the electromagnet array could be employed to perform the magnetisation and suspension functions concurrently.

Given the length of the propulsion simulator proposed by PSI: 203 mm to be suspended in the octagonal test section measuring 178 mm across flats, it was accepted that suspension at high angles of attack would be impossible, and even at moderate angles blockage of the test section would complicate the interpretation any wind tunnel results. However, restriction of the angle of attack range to that achievable with a static axial magnetising field was regarded as being a retrograde step. Consideration was therefore given to the

development of a capability to magnetise a model over the full angle of attack range for this system, presently -9° to 99°.

5.4 MAGNETISATION TO HIGH ANGLES OF ATTACK

The ten electromagnets surrounding the test section of the Southampton MSBS are notionally divided into four groups as described in Section 2.5 and shown in Figure 2.7. It was evident that magnetisation by these groups could be combined to provide a variety of magnetising fields, covering a wide angle of attack range.

This is a similar strategy to the combination of the group effects used by the high angle of attack controller. At each attitude, the group effects can be combined so as to produce decoupled force components in model axes, in 5 degrees of freedom. This allows the controller to position and restrain the model as required. Clearly, use of the magnets to perform the suspension and magnetisation rôles simultaneously could lead to conflicts, given the limited current available to the coils.

The technique used for magnetisation is to regard each group as capable of providing a magnetising vector. The direction of each group vector is determined by the fixed geometry of the electromagnet array, with magnitude proportional to group current. To produce a magnetising field rather than a control force, the magnets of a group are driven so as to generate opposite poles at the test section, producing a field in the area between the poles. The magnetisation of a ferro-magnetic element subject to a field is described in Section 2.2. The magnetising vectors available from the four groups can subsequently be combined to produce fields of diverse magnitude and direction.

A specific aim was defined as the generation of a magnetising field of constant magnitude, able to be rotated by the control system to match the model's instantaneous angle of attack. To achieve this aim the magnetising capability of each group would need to be derived, and a suitable technique developed for combining these capabilities to produce a magnetising field of a chosen intensity, at any angle over the full attitude range.

5.5 USE OF 'FORCE' TO DETERMINE MAGNETISING CAPABILITY

The program FORCE was developed by Britcher[6] from routines originally produced at MIT, and can be used to predict the interactions between a variety of configurations of

model and air-cored electromagnets. Coils and model core are interpreted as a number of linear and volumetric elements respectively, and the total forces and moments are calculated by summing the interactions between the elements. If no model is specified, FORCE can estimate the field strengths and gradients generated by the electromagnet array at selected points in space.

Results obtained from FORCE as applied to the Southampton MSBS are inexact, the main source of error being the lack of a routine to model the effects of iron cores on the performance of those electromagnets so equipped. However, calibration constants relating the software output to experimental data have been derived by Parker[20] using the results of work by Eskins published in ref 39. These constants have been updated during the current research and are given in the following table, for loads applied to a model in the x - z plane at zero incidence:

Table 3: Comparison of predicted force capability with measured results

Force or Moment Component	Measured Data (N or Nm)	FORCE Prediction (N or Nm)	Error Ratio
Heave Force	4.89	2.258	2.16
Axial Force	1.60	2.250	0.71
Pitching Moment	0.373	0.173	2.16

The pattern of these results is related to the presence of iron cores in some of the electromagnets. Magnets with iron cores are used to control heave and pitch at zero incidence. FORCE predicts lower control forces than those measured, as less effective air-cored magnets are assumed. The predicted axial control force more closely matches the true result, as axial force is generated only by the air-cored magnets of group IV at zero incidence. These results demonstrate the need to perform a calibration before using FORCE to model the MSBS hardware. A more complete discussion of the sources of error related to the use of FORCE can be found in ref 6.

FORCE was used to determine the distribution of field strength over the x - z plane of the test section - this being the plane generally occupied by the model axis when using the high angle of attack controller. Each group in turn was made to generate a simulated magnetising field. The predicted field strengths and directions thus obtained are shown in Figures 5.2 - 5.5, and exhibit significant variation in these properties over the area of

study. The results for groups I and II have similar characteristics due to their symmetry, and these groups will henceforth be considered together.

For groups I and II the field strength has a large variation over the test section. This variation can be attributed to the proximity of the group I and II magnet poles to the area of study. The field direction is more variable than for the other groups, as a result of the orientation of the member coils which do not point directly at each other across the test section (Figure 2.6). The coils of groups III and IV face each other directly in the x - z plane, and the field direction for these groups is more uniform.

Group III, which consists of the four lateral electromagnets, generates a peak in field strength in the centre of the test section. The poles of these four magnets face each other as shown in Figure 2.6. This arrangement gives a reduction in field strength near to the magnet poles. Group IV generates the most uniform field because the axial magnets are arranged roughly as a Helmholtz pair.

It was necessary to allocate a single magnetising field vector to each group, based on the results obtained using FORCE. As a starting point, the field strengths assigned were taken as those calculated for the centroid of the test section. Given that field strength varies with position as described above, it would have been desirable to use a direct force measurement technique such as that described in Section 5.9. However the high angle of attack magnetisation based on these preliminary values was subsequently successful, and no change to this simplified assignment has yet been attempted.

For groups III and IV, the angle of attack for the magnetisation vectors was taken as that at the centroid. The direction of the magnetising field generated by these groups is consistent over much of the x - z plane, because of the favourable pointing of the group members described above.

For groups I (and group II), the pointing asymmetry leads to greater changes in the angle of attack of the magnetising field with position. The angle changes from 132 (48) degrees at the centroid, to almost 90 (90) degrees near the poles of the magnets, as shown in Figure 5.2b (5.3b). Considering the length of the models to be suspended, an intermediate figure of 130 (50) degrees was selected as the first approximation to magnetisation angle. Successful magnetisation was subsequently achieved. The magnetising vectors used are presented here, where field strength is related to a current flowing in all of the group electromagnets:

Table 4: Assignment of magnetisation vectors to the electromagnet groups

Magnet Group	Magnetising Field Strength (T/A)	Incidence of Magnetising Vector (degrees)
I	7.2×10^{-4}	130
II	7.2×10^{-4}	50
III	9.5×10^{-4}	33
IV	10.0×10^{-4}	0

FORCE was later used to make a more sophisticated estimate of the appropriate magnetising field direction, as will now be described. An iron element tends to align itself with a field (Section 2.2), and so the 'average' direction of a complex magnetising field acting on a given model, could be taken as that at which no pitching moment is experienced. FORCE predictably indicated that for a magnetising field generated by group I or II, the angle for no pitching moment was dependent on model geometry. Assuming a typical permanent magnet model of 145 mm length and 9 mm diameter, the no-moment angle was 132 (48) degrees: the same as the field orientation at the centroid. For a typical propulsion simulator of dimensions 203 mm length and 13 mm diameter, the angle became 120 (60) degrees. The assignment of magnetisation vectors should therefore relate to the model with which they are to be used.

Assignment of magnetising field vectors is demonstrably a complicated issue, with magnitude and direction uncertain in some cases. However, minor errors are not thought to have had a dramatic effect on high angle of attack magnetisation, or on the testing of propulsion simulators. Incorrect assignment of the direction of each vector can be tolerated since the magnetising field component acting in the true direction is cosine dependent. Thus a ten degree pointing error will only result in a 1.5 % drop in the contribution to magnetisation from the group concerned.

Magnitude errors will affect only the assumed value of magnetising field strength. The value employed for propulsion simulation tests was determined experimentally as described in Section 5.8, and force calibrations were carried out at this level of magnetisation. Errors in its measurement would not affect the outcome of the tests.

5.6 COMBINATION OF MAGNETISING FIELD VECTORS

A typical magnetisation response of an iron element subject to a magnetising field is shown in Figure 5.6. According to ref 40, the field strength required to achieve saturation is 0.013 T. It should be noted that this value corresponds to the saturation of an iron element of an easily magnetised geometry, such as a long cylinder. More compact shapes are less easily magnetised, and it was anticipated that the field strength required for saturation of an iron propulsion simulator would significantly exceed the quoted figure. It seemed likely that a compromise would be necessary in the efficient use of the electromagnet array, between magnetisation of the model and generation of forces and moments.

The equations for the generation of a magnetising field of strength B at incidence α in the Southampton MSBS are the following:

$$\sum_{i=1}^{i=4} MFF_i B_i \cos(\alpha-\alpha_i) = B_\alpha \qquad \ldots 5.1$$

$$\sum_{i=1}^{i=4} MFF_i B_i \sin(\alpha-\alpha_i) = 0 \qquad \ldots 5.2$$

where the subscript i denotes the electromagnet group, and α_i is the incidence of the group magnetisation vector. The values MFF_i indicate the magnetisation contributed by each group and are defined as the Magnetising Field Factors (MFFs). The magnetising current in Amperes in each group is made equal to its MFF.

With four variables and two unknowns, the solution to these equations is over-defined and an infinite number of solutions exist for the MFFs at each angle of attack. To find the most suitable combination of vectors a grid search technique was employed in a new computer program: MAGEN (MAgnetising field GENerator). The contributions from two of the electromagnet groups were cycled through a range of values. Equations 5.1 and 5.2 were then used to calculate the MFFs for the remaining groups to produce a selected total field strength and direction.

A suitable scoring system was required to assess the suitability of each of the possible solutions generated. The selected approach was to favour those solutions making most efficient use of the electromagnets according to the following measures:

- **Minimum total system current:** This approach favours solutions having a small sum of MFFs.

- **Minimum highest group current:** Here the lowest maximum MFF is recorded.

These two strategies are regularly used in MSBS development, and examples of their application can be found in refs 8 and 20. The former test tends to reduce the total power consumption, the latter to reduce the risk of overloading individual magnets. A combined score can be calculated, but the 'minimum highest group current' test was chosen for generation of the first magnetising field vectors, as it became evident during suspension trials with an iron model that overloading of some groups was occurring.

The high angle of attack control system was modified to incorporate the generation of magnetising fields. To reduce the use of computer memory, MFFs were derived and stored for generation of magnetising fields at ten degree intervals. During suspension, linear interpolation is employed to estimate the correct MFFs at intermediate angles. This approach is routinely used by the MSBS control system to reduce the memory requirement for attitude-dependent data.

Selection of MFFs is linked to the instantaneous pitch angle. A keyboard selectable field-factor was incorporated into the control software to allow on-line scaling of the magnetising field during initial trials. The resulting MFF for each group is summed with the current demanded by the controller for suspension and control. The total demand is then output to the electromagnets.

5.7 SUSPENSION OF IRON MODELS

The first iron model to be suspended was a 130 mm bar of diameter 16 mm. The length was chosen for compatibility with the tail-scanning axial position sensor. Nose scanning for the longer propulsion simulation models (Section 4.4.1) had not yet been implemented. A relatively small model diameter was chosen to increase its slenderness for easy magnetisation. This also reduced the model weight, and hence its capability to cause damage should a loss of control occur. Parker's PIXEL software[20] was employed as usual to generate position sensing data for the new model.

Conflict between the suspension and magnetisation rôles being performed simultaneously by the electromagnet array was immediately evident. The current demanded of some magnets exceeded the maximum available 20 A. To alleviate this problem, the burden of model magnetisation was shifted away from groups containing overloaded magnets, to those with spare capacity.

The conflict could likewise have been resolved by changing the Demand Distribution Factors (DDFs), used to determine the groups used to provide suspension and control forces, or by combined optimisation of both sets of parameters. However, at this stage only the MFFs were adjusted, to minimise the number of changes under way during the development, and therefore the number of possible errors.

Redistribution of magnetising field generation was performed by a modified version of the MAGEN software - MAGEN2. This version allows selection of a reduced MFF for an overloaded magnet group, and the grid search then provides a number of options for the remaining magnetising field factors. A suitable option is chosen by the user based on recent results.

On some occasions the MFFs selected with MAGEN2 caused control difficulties. Typically the problem was linked to a large shift in the burden of magnetisation among the magnet groups over a small angle of attack interval. It was assumed that inaccuracies in the generation of the MFFs, perhaps coupled with the power supply calibration problems (Section 12.2), were leading to unexpected changes of magnetisation linked to pitch motion of the model. Temporary decoupling of magnetisation from angle of attack at the problem attitudes gave an improvement in control, supporting this hypothesis. The problem was rectified by more careful selection of MFFs, avoiding choices which would lead to a high rate of change of MFF with angle of attack.

This problem is similar to that encountered by Parker[20], during his development of the high angle of attack controller. Rapidly changing the pitch-dependent demands for the generation of control forces, also led to poor quality of control.

Initially suspension of the iron bar model was attempted with a magnetising field of 1.25×10^{-2} T at the test section origin, but this proved inadequate. The model was not sufficiently magnetised for the suspension magnets to exert the required control forces upon it. The magnetising field was gradually increased, and a value of 1.8×10^{-2} T was used during subsequent development work. The magnetising field most suitable for propulsion simulation was found by experiment (Section 5.8.2).

Empirical adjustments to magnetising field strength and distribution have allowed the derivation of usable MFFs, and successful suspension of an iron bar model over the 108 degree angle of attack range available with the Southampton MSBS.

5.8 SUSPENSION OF PROPULSION SIMULATORS

A model representative in size, weight and magnetic properties of a propulsion simulator, was initially suspended employing the same magnetising field strength used with the iron bar model. MAGEN2 was used as described above to redistribute the magnetising burden as required to allow suspension between −5 and 25 degrees of incidence.

The major problem encountered during propulsion simulation experiments was a difficulty in providing an adequate axial force to resist the propulsive impulse. Three aspects of model magnetisation were addressed in attempts to improve the axial force capability:

5.8.1 Redistribution for axial force

The maximum axial force that could be tolerated by the suspended propulsion simulators was determined by a series of static calibrations. As the applied axial force was increased, one or more electromagnets would reach their maximum current. Increasing the applied force beyond this point would eventually cause loss of control of the model.

The precise point at which control was lost was difficult to predict. With ten electromagnets a certain amount of redundancy exists for the generation of control forces, even with one or more magnets at maximum current. Loss of control was assumed to occur when this redundancy was exhausted.

To some extent it was possible to use MAGEN2 to shift the burden of magnetisation away from the limiting magnets, allowing an increase in axial force capability. The limit to this technique was reached when magnets from three groups approached their maximum currents simultaneously. At this point, shifting magnetisation to the fourth group could not provide a magnetising field returning a valid solution to Equations 5.1 and 5.2.

5.8.2 Optimisation of magnetising field strength for axial force

The problem of how best to balance the application of the magnetising field with the provision of an axial force was solved using an experimental technique with the model suspended at zero incidence. In this attitude only the axial electromagnets (group IV) are presently used to provide axial force. They must also contribute to magnetisation, as it is not possible to adequately magnetise an iron model at zero angle of attack without some use of the axial magnets.

When an axial force is applied to the model in suspension, the control software sends a demand for increased current to the axial magnets. The current flowing in the two

members of this group then consists of a force element having the same polarity in both magnets, and a magnetising element having opposing polarities. The difference in the axial currents is thus equal to twice the magnetising field factor for group IV, as the MFF is added to the current demand to one magnet and subtracted from the other. This difference in currents tends to cause one magnet to reach its limit under the application of an increasing axial load, while the other still has spare capacity.

Further application of axial load at this stage would result in an increase in current in the unlimited magnet, while the other remained at maximum current. A drop in the magnetising field *strength* would result from the decrease in the difference in current between the axial magnets, although the force-producing field *gradient* would increase in proportion to the total axial current.

The changes in axial force resulting from changes to field strength and gradient can be derived from a standard expression for electromagnetic force, which was introduced in Section 2.2:

$$F_a = \mu_0 V M \nabla_a H$$

$$\therefore F_a + \delta F_a = \mu_0 V (M + \delta M)(\nabla_a H + \delta \nabla_a H), \quad \delta F_a = \mu_0 V \left(M \delta \nabla_a H + \nabla_a H \delta M\right)$$

Assuming that one of the two axial magnets is at its limit

$$\nabla_a H = k_1(i_{\text{lim}} + i_{no\text{-lim}}) \quad \therefore \quad \delta \nabla_a H = k_1 \delta i_{no\text{-lim}}$$

The non-linearity of the magnetising field/magnetisation relationship has been illustrated, but for a small change it is assumed that

$$M = k_2 + k_3(i_{\text{lim}} - \delta i_{no\text{-lim}}) \quad \therefore \quad \delta M = -k_3 \delta i_{no\text{-lim}}$$

The effect on axial force can be expressed as

$$\delta F_a = \mu_0 V \left(M k_1 \delta i_{no\text{-lim}} - \nabla_a H k_3 \delta i_{no\text{-lim}}\right) \doteq \delta_1 - \delta_2$$

If $\delta_1 > \delta_2$, so that the benefit to axial force from increased field strength outweighs the loss due to reduced magnetisation, then the lower magnetisation represents an improvement, and should be used henceforth. In experimental terms, with one axial current at its limit, an increasing axial force can be tolerated up to a point where the force response reaches zero and axial control of the model is almost lost. At this point $\delta_1 = \delta_2$ and no further increase in axial force is possible. The level of magnetisation derived for this point is regarded as the optimum under these circumstances. Further increase in the non-limited axial current would result in a reduction in force, and an almost certain loss of axial control.

This technique can only yield a useful result if the magnetisation level at the start of the test is above the optimum. If at the starting point $\delta_1 < \delta_2$, no application of axial force can be tolerated, beyond that applied when the first current limit is reached.

As the axial force is increased and a significant decrease in the magnetising field occurs, it is no longer valid to assume that the magnetising field / magnetisation relationship is linear. A different section of the magnetisation curve for iron comes into effect, changing the magnitude of δ_2.

A secondary effect of reducing the level of magnetisation is the increase in the suspension currents in some members of the other magnet groups. A less magnetised model requires the influence of a stronger vertical field gradient to overcome its weight. This effect can lead to a loss of control if a suspension magnet reaches its current limit.

In practice, the optimum level of magnetisation was found by recording electromagnet current data, during the application of an increasing axial force to the model in suspension at zero incidence. As the force was increased, one axial magnet would reach its current limit. Further axial force would then be applied until control of the model was just lost. At this condition, it was assumed that $\delta_1 = \delta_2$, and that the optimum level of magnetisation was acting. This level was calculated from the electromagnet currents, and used thereafter.

The optimum level of magnetisation at zero incidence was found to be 1.6×10^{-2} T. This level was also used at 10 and 20 degrees angle of attack, after further experiments had shown satisfactory performance at these attitudes.

5.8.3 Preservation of the magnetising field during a thrust impulse

One result of a magnet reaching its maximum current under the influence of a large axial force, is a reduction in the total magnetising field strength as described above. This can lead to a loss of suspension as well as of axial control.

The thrust peak generated by the carbon dioxide thruster was of very short duration, typically less than one second (Section 6.1.1). It was possible to withstand a transient axial force greater than the steady state maximum. In these circumstances the model would accelerate briefly in the axial direction until the thrust level fell below the restraining force limit. At this point the model could generally be bought back under control, as long as it had remained within the field of view of the axial position sensor. However in circumstances where a decrease in model magnetisation resulted in a reduction in lift capability, it was rarely possible to maintain suspension of the model.

To improve the chances of withstanding a high thrust peak, the control software was modified to ensure that the magnetising field was preserved even during demands for axial force outside the practical limit. This was achieved by capping the output from the axial magnet which did not reach its maximum current. By capping the output using

$$i_{IV} \leq i_{max} - 2 \times MFF_{IV,\alpha}$$

the difference between the two axial currents required for adequate magnetisation during a demand for axial load was guaranteed. Following the optimisation of the magnetisation level described above, the capping also ensured that maximum axial force was applied to the model at the point where one axial magnet reached its limit. During the propulsion simulation experiments it was only necessary to cap the currents of group IV, but this procedure could be extended to the other groups if required.

5.9 COMBINED OPTIMISATION OF FORCE GENERATION AND MAGNETISATION

During the development of a high angle of attack magnetisation strategy, a conflict arose as expected between use of the current-carrying capacity of the electromagnet array for magnetisation and for suspension. The response was to shift the burden of magnetisation to avoid conflict wherever possible. The parameters governing the generation of control forces and moments were not changed for the reasons given in Section 5.7. A more satisfactory approach may have been to develop an integrated technique for the combination of the two tasks, but this was not feasible during the time available.

For a combined optimisation, data on the degree of magnetisation of an individual model in response to the application of a range of magnetising fields would be required. No means of obtaining this information was available during the propulsion simulation study, but the subsequent development of the DFM rig described later has made a future investigation possible in this area. The procedure could involve an iron-cored model supported in the rig and subjected to a known steady field. A variety of magnetising fields could simultaneously be applied, and the resulting force exerted on the model measured by the rig.

The effects on the magnetised iron core caused by each magnet group could be found for different incidences, in a similar manner to the effectiveness investigation described in Chapter 10. The question would then be one of how best to use this information to derive compatible DDFs and MFFs.

This could be achieved by developing a new grid search technique to investigate the magnetisation and suspension aspects together. Although the two sets of parameters DDFs and MFFs are not interdependent, a combined scoring system could be developed to emphasise combinations which minimise total power consumption or peak magnet currents. Experience with the Southampton MSBS, which is current-limited in common with most systems, suggests that a package emphasising avoidance of magnet overloads would be the best alternative.

6. PROPULSION SIMULATION USING THE COMPRESSED GAS THRUSTER

The compressed gas thruster was devised by PSI for proof of concept propulsion simulation trials in the Southampton MSBS. This chapter describes its design and development, and the tests subsequently performed. The contract with PSI also required analysis of test data, and attempts to evaluate the forces acting on the thruster during firings in suspension are discussed. Conclusions are drawn relating to shortcomings in the original design. Possible modifications relevant to the design of a second generation compressed gas thruster are suggested.

6.1 DESCRIPTION OF THE COMPRESSED GAS THRUSTER

The CO_2 thruster supplied was broadly in line with the original concept presented in ref 32. A schematic of the final design is shown in Figure 6.1, and the model itself with a gas bottle alongside is shown in Plate 1. The major components of the thruster are a steel body inside which a disposable gas bottle containing 16 g of carbon dioxide can be installed. The bottles used have a thin membrane and a screw fitting at one end. An explosive squib is used to drive a hollow pin through the membrane. Propellant gas is then released through the pin to a convergent nozzle in the model tail. At a model scale compatible with the Southampton MSBS it was not possible to incorporate an active control valve for regulation of nozzle pressure ratio (NPR), as initially intended. NPR was therefore free to vary during a run, dependent on the condition of the propellant gas released.

Electronics and a battery in the nose are used to control firing of the squib, in response to the illumination of a nose-mounted sensor using a low power laser. A window covers the sensor, and a filter is fitted to allow the passage of helium-neon laser light at 632.8 nm. The filter is used to prevent accidental firing due to excessive background light.

6.1.1 Thrust profile characteristics

In the design study for the small scale carbon dioxide propulsion simulator[32], PSI envisaged a compressed gas thruster producing a step thrust profile of two to three seconds duration. A CO_2 thruster with such a profile would have been suitable for propulsion simulation in the Southampton MSBS. A typical profile from the actual thruster

is shown in Figure 6.2. A peak corresponding to puncturing the gas bottle is followed by an almost exponential decay in thrust over a period of around one second.

The critical factor leading to this discrepancy between the predicted and actual thruster performance, was the assumption that the propulsion simulator model had enough thermal mass to maintain the temperature of the carbon dioxide bottle and contents during a firing. The observed thrust decay is a result of rapid cooling of the thruster as the carbon dioxide absorbs heat for vaporisation and expansion from the model structure. This cooling reduces the vapour pressure and consequently the rate of CO_2 vaporisation. It was not uncommon for freezing of the carbon dioxide to occur, causing particles of solid phase propellant to be ejected in the exhaust.

Sensitivity of the thruster performance to temperature is demonstrated by a comparison of the results of bench tests performed before shipping, with those obtained after its delivery. In the relatively warm (20 °C) laboratory at PSI in Andover MA, peak thrust was measured to be 11.5 N (2.5 mm nozzle). The cooler atmosphere of the MSBS laboratory (March, 13 °C) at the University of Southampton reduced the average peak thrust to 9.0 N.

The behaviour of the compressed gas thruster is also dependent on model attitude. In the vertical, nose-down orientation initially used for bench tests, the bottle membrane is uppermost, and only gaseous carbon dioxide is released through the firing pin. However, most tests in suspension were performed with the model horizontal, at zero angle of attack. In this attitude mixed-phase carbon dioxide is released, with an unpredictable effect on thrust profile.

Tests of the suspended model at incidence with the nose raised by up to twenty degrees were attempted. In this attitude it was assumed that mainly liquid CO_2 was released from the bottle. Bench testing of the thruster in a nose-up attitude was not possible with the static test stand described in Section 6.3 below. Given the erratic performance of the carbon dioxide thruster, and the realisation that accurate measurement of the forces acting in suspension would not be possible, no attempt was made to obtain a static thrust profile for nose-up attitudes.

6.1.2 Firing and membrane puncture

The mechanism of puncture of the gas bottle membrane proved to have a critical effect on the subsequent release of propellant. A more detailed description of the design and operation of the firing system is therefore appropriate.

PSI originally expected the sharpened membrane-puncturing pin to be driven out of the gas bottle by the high pressure of the carbon dioxide, which reached 58 bar at 21 °C. The push-out did not occur reliably in practice, so a hollow pin was developed, with O-rings fitted at the base giving a tight fit in the pin holder to prevent its ejection. The new pin was drilled with a central bore, and a small diameter lateral hole to vent the gas (Figure 6.3).

Using this firing strategy, the rate of release of carbon dioxide following insertion of the pin was dependent on a number of factors. The most important of these was the state of the pin head in terms of sharpness and geometry, which determined the size and shape of the hole produced in the bottle membrane. A ragged hole allowed the release of gas around the pin as well as through its central bore. On occasion the pin failed to fully pierce the membrane, creating a small hole and giving a very slow release of gas. The diameter of the central bore at the pin head was affected by deformation caused by the impact with the membrane. In addition, the depth to which the pin penetrated the bottle varied. This parameter was dependent on pin head shape, squib performance, and on pin stiffness due to O-ring degradation or the build-up of combustion products near the squib.

The dependence of the rate of CO_2 release on these factors led to inconsistencies in the thrust profile obtained from the compressed gas propulsion simulator. Combined with the temperature related problems described in Section 6.1.1 above, the resulting unreliable performance of this thruster caused severe control problems. The small-scale CO_2 thruster was judged as being poorly suited to MSBS propulsion simulation.

6.1.3 Further design aspects relating to the PSI model

During the development of the compressed gas propulsion simulator, recommendations were made to PSI relating to a number of aspects of its design. In the initial proposal, components such as the nose were to be constructed of plastic to reduce the weight of the model. It was suggested that the electrical steel alloy used for construction of the body also be used for these other parts. They would then be magnetised during suspension, and be able to contribute to the generation of electromagnetic control forces.

Position sensing of the axial location of models in the Southampton MSBS is traditionally achieved by monitoring the shadow cast in a light sheet directed over the tail of a suspended model. This technique was not suitable for propulsion simulators given the presence of an exhaust plume at this location, and nose scanning was seen as an attractive alternative. For this purpose a blunt nose geometry was selected as discussed in Section 4.4.1.

In two areas, requests from Southampton for design changes to the carbon dioxide thruster model were not incorporated by PSI. The hemispherical tail configuration is not representative of that in the region of a typical engine exhaust. A boattail rear fuselage was suggested, as a boattail shape is commonly used at an engine exhaust in the design of flight vehicles. The effects of different exhaust parameters on the behaviour of plumes emitted from a boattail have been thoroughly investigated[29]. At this stage in the research it was expected that a measurement of the change in drag coefficient of the propulsion simulator due to the presence of the exhaust plume would be feasible. The incorporation of a rear fuselage boattail would have allowed a direct comparison of this result with the published data.

A second area of concern in the design of the carbon dioxide thruster was the need for passive roll control. Firing of the thruster was to be achieved by directing a laser through a small aperture near the model nose. The test section of the Southampton MSBS is surrounded by electromagnets and position sensing equipment, limiting visual access to a suspended model. Some form of roll control was required to ensure that the firing aperture could be correctly oriented relative to an available light path for the laser.

Active control of roll attitude was neither feasible nor necessary. The present MSBS control system does not include control of roll, and development to this level of sophistication was not justifiable for the simple roll positioning requirement. Passive control was suggested whereby the model is caused to have a preferred roll attitude, by the deliberate provision of asymmetry in its magnetic or mass distributions.

No provision for roll control of the carbon dioxide propulsion simulator was made by PSI. To ensure correct roll attitude during the trials at Southampton, it was necessary to attach a mass to the outside of the model. The position of the external mass was adjusted as required to ensure visibility of the firing aperture through the test section window for each trial.

This rather *ad-hoc* roll control arrangement was not accurate enough to allow permanent alignment of the firing laser. It was necessary to manually direct the laser toward the firing aperture for each test, and the ignition timing was therefore made unpredictable. This factor ruled out the use of a predictive control strategy, whereby anticipation of the moment of firing could aid control of the suspended model during a thrust impulse. Such strategies had been suggested during Phase I of the SBIR contract awarded to PSI by NASA.

6.2 A FUTURE IMPROVED CARBON DIOXIDE THRUSTER

At a larger scale than that of the compressed gas thruster tested at Southampton, it should be possible to incorporate an active solenoid valve to control the release of propellant gas, using feedback of the nozzle pressure ratio to give a steady thrust profile despite cooling of the model structure.

For small temperature changes it can be argued that thrust Th is independent of exhaust temperature T.

$$Th = \dot{m}v = \rho A v^2$$

and the temperature dependence of these terms cancels since

$$\rho \propto \frac{p}{T}, \qquad v^2 \propto M^2 T$$

so to a first order approximation

$$Th \propto p$$

A pressure feedback system should therefore be able to regulate the thrust of a larger compressed gas propulsion simulator. The assumption of independence of thrust from temperature ceases to be valid when a larger temperature change is considered. Secondary effects such as changes in nozzle diameter and flow discharge coefficient would affect the thrust level. It is also recognised that in the case of a supersonic jet the expression for thrust is more complex than that employed here. Further research, perhaps investigating the feasibility of additional feedback of propellant temperature, is necessary to determine whether a large scale, constant thrust compressed gas thruster is viable.

PSI demonstrated an intermediate approach in a large scale carbon dioxide propulsion simulator[42], with a capacity of 200 g of CO_2. This device used heating elements to prevent excessive cooling of the equipment. These elements were electrically heated to around 75 °C before each run, and transferred sufficient energy to the carbon dioxide to prevent formation of the solid phase. The thrust profile, shown in Figure 6.4, includes a period of nominally steady thrust, but this level was still subject to a slight decay as the exhaust temperature dropped during the run.

For the small scale thruster, inconsistent performance caused by the unpredictable interaction between the firing pin and the gas bottle membrane, could be eliminated in a future design by pre-puncturing the membrane with a larger, robust fitting. This fitting would be sealed to the neck of the gas bottle to ensure that gas was only able to escape through its bore. The rate of propellant flow could be regulated by a constriction in a

permanent component, rather than an easily-damaged pin. Firing could be achieved by operation of a simple *on-off* valve, activated electrically or by firing a squib.

If an optically-triggered firing system was again included, roll control could be incorporated by the provision of asymmetry or by the inclusion of a capability to rotate the firing window and sensor relative to the model fuselage. An alternative would be to mount the window at the tip of the nose, and direct the firing laser along the wind tunnel axis. The precise control of thruster firing enabled by the provision of passive roll control would allow the use of a predictive control strategy (Section 12.5) to improve the reaction of the MSBS control system to a sudden thrust impulse.

6.3 THRUSTER BENCH TEST FACILITY

A bench test facility was required to allow measurement of the thrust profiles produced by the propulsion simulators. A simple test stand was constructed, incorporating one of the force transducers later used in the DFM rig (Chapter 8 onwards). A schematic of the test stand is shown in Figure 6.5. The model nose is held in a cup-shaped retainer. Three lateral support pins are provided to hold the thruster in a vertical position. They also allow precise adjustment of its alignment. The pins are generally set to allow a small amount of lateral motion, to reduce the effects of friction on the measured thrust.

The stand was intended for bench tests of a vertical model, but the attitude-dependence of the CO_2 thruster performance introduced above made it necessary to also test in a horizontal attitude. To allow horizontal tests the model was suspended from a pair of cotton slings, adjusted so as to guide the nose correctly into the retainer as illustrated in Figure 6.5. A static firing of the compressed gas thruster in a horizontal attitude is shown Plate 2.

Thrust data was recorded using the MSBS PC. A technique was developed to allow efficient data acquisition despite uncertainty over the timing of each firing. The PC software was able to recognise the start of a thrust impulse and begin data acquisition at that time. A buffer was used to continuously store a small quantity of data until the recording period began. This allowed a comparison to be made of the zero-thrust data from before and after the firing, to confirm the consistent behaviour of the test equipment. For tests of the carbon dioxide thruster in the nose-down orientation, a 16 g difference between the start and end readings would be expected, due to the release of the propellant

gas. The calibration of the thrust test stand was easily confirmed by loading it with laboratory weights.

6.4 BENCH TESTS AND OPERATIONAL EXPERIENCE WITH THE CO_2 THRUSTER

Bench tests of the carbon dioxide thruster showed a high peak thrust and poor repeatability. The peaky profile was attributed to excessive cooling of the CO_2 cartridge as discussed in Section 6.1.1. The inconsistency exhibited between runs seemed to be caused by the changing condition of the firing pin, and detail differences in puncturing the gas bottle membrane in successive tests.

To bring the peak thrust down to a level where a firing in suspension could reasonably be attempted, the nozzle was gradually enlarged from 2.5 mm to 7.5 mm. This reduced the average peak thrust to around 4 N. Thrust profiles obtained with different nozzle diameters are shown in Figure 6.6.

Operation of the thruster presented no undue problems, but was labour intensive. The short life span of some of its components, notably the firing pin, which had a service life of about six tests, made it necessary to perform a bench test between each firing in suspension. Reloading the model took around five minutes, and involved replacing the explosive squib, resetting the pin and changing the CO_2 cartridge. The reloading process was more complex for the carbon dioxide model than for the rocket thrusters described in the following chapter.

Accidental firing of the carbon dioxide propulsion simulator occurred on two occasions. In one instance background light set off the thruster when the He-Ne filter was removed to check an electrical connection. The second accidental firing was caused by light from a photographic flash, which evidently had sufficient intensity in the 632.8 nm range accepted by the filter to cause ignition.

6.5 SUSPENSION AND FORCE CALIBRATION

Initial suspension of the carbon dioxide thruster at zero angle of attack was easily achieved, as work with the representative propulsion simulator described in Section 4.4.3 had enabled the prior derivation of suitable control parameters for this class of model. The

angle of attack range was subsequently expanded to allow suspension between incidences of -9° and 25°.

The lower angle is the minimum addressed by the present controller. The upper limit on angle of attack reflects the power limitations of the electromagnet array. Parker[20] identified angles of attack around 30 degrees as being subject to a high power requirement for suspension with the present electromagnet configuration. At these attitudes the lateral magnets (group III) become ineffective in producing lift force, which must therefore be provided by groups I and II. It was not possible to balance the power demands for suspension and magnetisation above 25 degrees of incidence. Attempts to reconcile these often conflicting demands are discussed in Section 5.7.

At 25 degrees angle of attack it was only just possible to suspend the model, with all magnet groups operating near their maximum current. At angles close to this limit, the electromagnet currents for steady suspension remained high, with a minimal capability remaining to react to external forces. No firing of the thruster was therefore attempted at angles of attack greater than 20 degrees.

Axial force capability was maximised by redistributing the task of generating the magnetising field, to magnet groups not heavily used for axial control. A maximum force of 4.9 N could be resisted at zero incidence. This fell to around 4.0 N at twenty degrees.

At zero incidence, only the axial magnets (group IV) are presently used to provide the axial force component. A calibration of axial force against group IV current is presented in Figure 6.7. The graph shows good linearity and agreement between the loading and unloading phases. The onset of distortion at extreme loads is the result of an axial magnet reaching its maximum current. It was necessary to perform a more comprehensive force calibration at other angles of attack, as described in Section 6.7 below.

6.6 CARBON DIOXIDE THRUSTER TEST SERIES

Once it had been shown that the capability of the MSBS to apply static axial force to the compressed gas propulsion simulator exceeded the level of the expected thrust peak, firing of the thruster in suspension was attempted. The thrust peak tended to cause a large transient axial motion of the model. A large peak would often cause the model to move out of range of the axial position sensor. This event usually caused a loss of control. If the

initial disturbance did not exceed the allowable limits, it was generally possible to regain control of the thruster.

A number of strategies were employed in an attempt to increase the success rate of suspended thruster trials, related to axial force generation and magnetisation (Section 5.8), and to control system optimisation (Section 12.5.1). When these strategies were correctly used with the carbon dioxide thruster, the success rate - measured as the proportion of trials where the model was retained in suspension - reached around 75 %. The most effective way to improve the chances of retaining suspension was the reduction of the overall thrust level, by increasing the nozzle diameter. This measure could not protect against occasional very high thrust levels caused by worn or damaged thruster components.

Following initial trials at zero incidence and wind *off*, the test envelope was extended to include wind *on* tests with tunnel speeds of Mach 0.05 and 0.1, and angles of attack of 10 and 20 degrees for each tunnel speed (0, 0.05, 0.1), giving a total of nine test conditions. An additional increase in nozzle diameter to 9 mm was required, to further reduce the thrust level given the reduced axial force capability at incidence.

During the trials of the compressed gas thruster in suspension, the MSBS was controlled by the PDP11/84 computer, while data acquisition was performed by the PC. This arrangement of computer hardware is discussed in Section 12.3.2. Uncertainty concerning the response of the MSBS controller to the unpredictable thrust impulse, made it difficult to use the response to trigger the start of data acquisition. It was therefore necessary to record a relatively long period of run data, and to attempt to fire the thruster at some time during this period. Typically 20 seconds of run data were recorded to capture a 1-2 second firing event. The inefficiency of this practice was recognised, but the use of the PC as a data logger had effectively removed any computer memory constraints, and the unwanted data could be discarded later as required.

6.7 DATA ANALYSIS

The ultimate aim of the wind tunnel tests conducted using the suspended CO_2 thruster was to measure the difference in drag coefficient caused by the presence of an exhaust plume. To make this measurement during a thruster firing, it was expected that the values of three parameters would be evaluated:

1. **Instantaneous thrust:** Probably inferred from bench tests of the thruster.

2. **Instantaneous total external force:** This measurement comprises of thrust and drag, and for tests at incidence also includes lift and pitching moment.

3. **No-thrust instantaneous total external force:** Aerodynamic forces acting with no exhaust plume present.

Thruster *on* drag could then be found as the difference between parameters (1) and (2), and compared to the thruster *off* drag found in (3). As described in Section 4.2, the change in afterbody drag due to the presence of the exhaust plume was expected to be around 1 % of the measured thrust, this factor determining the requirement for accuracy of force measurement.

6.7.1 Data analysis by three degree of freedom pre-calibration

An attempt was made to calibrate the MSBS for three degrees of freedom with the carbon dioxide model. This calibration would be categorised as a Direct Calculation technique in Section 8.2. The aim was to use the results of a static calibration of system current variation with lift, drag, and pitching moment, to allow simultaneous extraction of these force components from run-data obtained during thruster trials in suspension.

This approach is based on the assumption that a generalised force or moment component F_i, applied to a suspended model having a constant level of magnetisation, has an effect on the current in an electromagnet i_j given by

$$\delta i_j = k_{ij}\, \delta F_i$$

where i = 1-6 for six degrees of freedom
j = 1-10 for the ten electromagnets
and k_{ij} is a constant of proportionality specific to each degree of freedom i and magnet j.

The general solution for the total change in system current caused by the application of a complete set of forces and moments becomes

$$\delta \boldsymbol{i} = \boldsymbol{K}\, \delta \boldsymbol{F} \qquad \ldots 6.1$$

where

$$\delta i = [\delta i_1 \;\; \delta i_2 \;\; \ldots \;\; \delta i_{10}] \qquad K = \begin{bmatrix} k_{1,1} & \cdots & k_{1,6} \\ \vdots & \ddots & \vdots \\ k_{10,1} & \cdots & k_{10,6} \end{bmatrix} \qquad \delta F = \begin{bmatrix} \delta F_1 \\ \delta F_2 \\ \vdots \\ \delta F_6 \end{bmatrix}$$

Having obtained the calibration constants k_{ij} as required, it should then be possible to deduce the force matrix responsible for an observed change in system current using

$$\delta F = K^{-1} \delta i$$

The propulsion simulation tests involved suspension of an axisymmetric model at low incidence. Roll is not controlled, and rolling moment is not considered. The primary aerodynamic forces acting in this case are lift, drag and pitching moment. It was assumed for the purposes of this analysis that the lateral force and moment components, sideforce and yawing moment, were negligible. The possibility of the presence of unexpected lateral loads corrupting the measured forces was reduced, when the analysis ceased to consider the lateral electromagnet currents as described below.

Static calibrations were performed at the three test attitudes of 0, 10 and 20 degrees of incidence, to measure the system current response to application of the three components under investigation. The loading geometry is shown in Figure 6.8. A mixed axis system was employed for the force components. Axial force was applied in line with the model axis, and thus yielded calibration results in model axes. Heave force was conveniently applied by loading the suspended model with equal weights at points *A* and *B* in the figure. This gave a heave calibration in wind tunnel axes. Measured axial force was thus coincident with propulsive thrust, and heave force with lift. The effect of pitching moment was deduced by consideration of two similar heave loading states. The difference in system current, observed when an applied load was moved from the nose *A* to the tail *B* of the model, could be attributed to pitching moment in either axis system.

The only consequence of calibrating in a mixed-axis system was that the results calculated were themselves in mixed-axes. Equation 6.1 is not fundamentally limited to orthogonal axis systems.

6.7.2 Simplified solution

With only three unknown force components, the ten simultaneous equations implicit in Equation 6.1 represent a considerable over-solution, and a simplified approach was developed. By limiting the calibration to just three electromagnet currents, a solution was possible via a much simplified matrix inversion. The data analysis effort required to derive

the calibration constants was similarly reduced. Furthermore some of the currents, especially those in the lateral electromagnets, were little affected by application of forces in the x - z plane. Their removal did not detract from the solution, and reduced the effect on the analysis of any lateral force or moment present. The most attractive option was the selection of three electromagnets showing large current responses to the three force and moment components under investigation.

The governing equation then becomes

$$\begin{bmatrix} \delta i_a & \delta i_b & \delta i_c \end{bmatrix} = \begin{bmatrix} k_{Ha} & k_{Aa} & k_{Pa} \\ k_{Hb} & k_{Ab} & k_{Pb} \\ k_{Hc} & k_{Ac} & k_{Pc} \end{bmatrix} \begin{bmatrix} \delta F_H \\ \delta F_A \\ \delta F_P \end{bmatrix}$$

where F_H, F_A, F_P are the components of heave force, axial force and pitching moment respectively, and δi_{a-c} are the current changes in the three selected electromagnets. The forward lower (I), aft lower (II), and aft axial (IV) electromagnets were chosen for their large current variations during the static loading tests described above, and because they represented all of the non-lateral magnet groups. Similar changes in the currents of members of a particular group would be expected in response to a force component, as the control system drives the group members together. Recording currents from members of the same group would not generally give the same insight into the control forces acting, as recording currents from members of different groups.

6.7.3 Analysis of motion transients

A new computer program, TRANSIENT was developed to deduce the forces and moments acting on the model, from the observed changes in system current and model position. The aim was to extract continuous values of heave force, axial force and pitching moment from data recorded during a thruster firing. As the model did not remain stationary during the thruster trials, it was necessary to account for its inertia and acceleration in the analysis.

The equation of motion for a suspended propulsion simulator was initially assumed to be

$$F_{EM} + F_{Ext} = ma + kv \qquad \ldots 6.2$$

and this equation was solved by TRANSIENT for the three degrees of freedom under consideration in turn.

The term kv represents natural damping of the model motion, perhaps caused by eddy currents. Analysis of model motion following a force impulse showed negligible damping

of this type, all damping being attributable to the control system. The damping term was subsequently discarded from further analysis.

A second order approximation is used to estimate the instantaneous velocity and acceleration of the model from the position signals recorded:

$$v_t = \frac{x_{t+1} - x_{t-1}}{2\Delta t}, \qquad a_t = \frac{v_{t+1} - v_{t-1}}{2\Delta t}$$

where x_t, v_t, and a_t represent position, velocity and acceleration at time t. Once TRANSIENT has calculated the inertial forces, a matrix inversion is performed to solve Equation 6.2 for each of the three degrees of freedom under investigation, thus finding the externally acting force components. This process is repeated for all data points recorded during a thruster firing.

The results obtained from the analysis of data using TRANSIENT were generally disappointing. The axial force extracted from a wind-*off* thruster firing should have matched a typical thrust profile. However, the profile obtained was badly corrupted, as shown in Figure 6.9, and the magnitude of the thrust error tended to follow the axial motion of the model. A number of position-dependent factors were thought to have combined to denigrate the results. Some of these factors were identified, and modifications made in attempts to reduce their effects.

Coupling of position measures

Position inputs to TRANSIENT were initially simple position measures as obtained by combination of the five position sensor outputs, which were then decoded to metres and radians. As described in Section 2.3, coupling exists between some of these measures.

The motion analysis was extended to include consideration of the coupling of heave and pitch motion to measurement of axial position. The position measures were decoupled by the ANALYZE software (Section 12.3.3), prior to the storage of selected data for transient analysis.

Change of magnetisation

A constant level of magnetisation was promoted by the use of restricted current levels for certain electromagnets (Section 5.8.3). However, the analysis of tests performed before the development of this feature, or where it was incorrectly applied, needed to take account of the change in the level of magnetisation.

The data required to include this feature in the analysis was generated experimentally. A static calibration was performed whereby the applied load was kept constant, and the level of magnetisation varied. The effect of magnetising field strength on axial calibration coefficient is shown in Figure 6.10. A linear relationship was assumed to apply over the relatively small range of magnetisation values considered. Calibration coefficients were subsequently made variable in TRANSIENT according to this relationship, where changes in the magnetising field were detected.

Change of zero-force current

The current level for steady suspension varies in the electromagnets according to model position. TRANSIENT calculates forces by considering the difference between the system current observed at an instant during a motion transient, and that recorded for steady state conditions. Motion of the model changes the steady state 'zero-force' current.

In an attempt to account for this source of error, the change in zero-force current in the axial magnets with axial position was assessed, this being the dominant manifestation of the effect for the propulsion simulation tests. A plot of group IV current with steady axial position is shown in Figure 6.11. TRANSIENT was modified to include a linear approximation to this relationship.

Change of calibration constants

Force calibration constants were also shown to be dependent on position, but the dependency was small and was not included in the analysis software. A future, more accurate analysis of this type would need to consider the inclusion of position-dependent changes to the calibration constants.

The package of measures outlined gave a mild improvement in the force and moment data acquired with TRANSIENT. The thrust profile of Figure 6.12 bears a greater resemblance to a profile recorded during a bench test than does the result previously attained Figure 6.9, but overall the result remains unsatisfactory, and an erroneous dependence of the measured thrust on axial position is still evident.

Position-dependent effects were thought to be responsible for the poor results, rather than the governing equations used to interpret the behaviour of the MSBS. Previous research[39] has suggested that linear force/current relationships derived from combined calibrations in several degrees of freedom can give good results, provided the calibrations are not invalidated by a change of conditions such as a model motion. The requirement for

measuring forces to an accuracy better than 1 % of the thrust level (Section 6.7) has clearly not been met.

6.8 RESULTS OF COMPRESSED GAS PROPULSION SIMULATION

Some typical results obtained from a wind tunnel test of the compressed gas propulsion simulator are presented in Figure 6.13, showing the three force and moment components calculated for a test at 10 degrees of incidence and a tunnel speed of Mach 0.1. The measured axial force, which should match the thrust profile generated during this test, has a similar shape to that shown in Figure 6.12, with an erroneous trough corresponding to the primary axial motion response to the thrust impulse. Small values of heave force and pitching moment are recorded, but it is unlikely that these data accurately reflect the aerodynamic loads resulting from the presence of the exhaust plume, as similar traces were obtained during wind-*off* trials.

It became clear that given the available apparatus, two of the parameters introduced in Section 6.7 above, whose evaluation would allow measurement of a change in thruster drag coefficient, could not be accurately assessed. The thrust level of (1) was uncertain and variable for this model, while as described above, attempts to extract three force and moment components simultaneously were not successful if the model moved away from the datum position. This prevented accurate assessment of parameter (2). Parameter (3) could be found with more confidence.

A comparison of the extracted thrust profile with an axial position trace was shown in Figure 6.12. The apparent position-dependence of thrust indicates that TRANSIENT is failing to take account of all of the relevant position-dependent factors. To fully characterise the effects identified for subsequent modelling in an analysis routine, extensive pre-calibration would be required, observing the changes to magnetisation, calibration constant and zero-force current due to force or moment application in each of the five degrees of freedom controlled. Coupling for combined motion in several degrees of freedom could further complicate the issue. This process would need to be repeated for each new model. Such a calibration effort would be difficult to justify in terms of the force measurement results obtained.

Further investigations into the subject of position-dependence of the analysis were not deemed worthwhile. Time restrictions would have prevented a rigorous assessment of the numerous position-dependent parameters. It would have been possible only to continue to

incorporate linear approximations into the software to the essentially non-linear relationships found. Furthermore the performance of the compressed gas propulsion simulator was considered to be so far removed from that of a device acceptable for use in production wind tunnel testing, as to draw into question the benefit of the further development of strategies to cope with its unpredictable and peaky thrust profile.

The complexity of the pre-calibration process described demonstrates the advantages of a propulsion simulation test free from any accompanying model motion. A more favourable thrust profile, allowing a period of data acquisition with the model stationary during the thruster firing, would eliminate the need to consider and model any position dependent parameters. Thrust profiles suitable for MSBS propulsion simulators are discussed in Section 12.5.2.

Disappointing results from the analysis of motion transients prompted a review of force measurement practices employed with MSBS facilities. This led directly to the development of the DFM technique described in the second part of this thesis.

Time restrictions prevented a return to this subject, to perform an improved transient analysis using the DFM rig. Were this approach to be attempted in the future, the electromagnetic forces acting on the model could be found using the rig for a number of discreet points during the motion transient, or during a slow motorised translation through the motion transient, with a coupled application of the appropriate electromagnet currents. The magnetic forces could then be combined with the inertial forces to give an improved estimate of motor thrust and the aerodynamic force components. There would be no need to model the coupling of position measures, or any of the other factors described in Section 6.7.3 above.

Despite the lack of accuracy in measuring force components, the compressed gas tests were still successful from the viewpoint of proof of concept, as propulsion simulation was achieved in an MSBS for the first time, and over a range of test conditions. The success was achieved despite using a thruster particularly unsuitable for the task. Even at the small scale of the Southampton MSBS, a workable propulsion simulation technique has been developed using small rocket thrusters, and this topic is described in the next chapter. At a larger scale, a compressed gas thruster has been demonstrated with improved performance (Section 6.2), and this technique may still be an option for propulsion simulation in a future commercial MSBS.

6.9 SATISFACTION OF PERFORMANCE AND DESIGN CRITERIA

The performance requirement for the CO_2 thruster (Section 4.2) specified the flow characteristics necessary for an accurate scale simulation of an illustrative propulsion system. A nozzle diameter of 4.4 mm was required. The nozzle on the compressed gas exhaust simulator was enlarged in stages from 2.5 to 10.1 mm to reduce the thrust level for control purposes. The nozzle diameter tested which was nearest to the requirement was 5.0 mm, and this case, for which the thrust profile was shown in Figure 6.6, will be further evaluated:

- **Nozzle diameter:** The required value could have been achieved, results for a similar nozzle diameter are considered.

- **Thrust:** 6.4 N was specified, and this value was achieved at the start of the profile in Figure 6.6, before cooling of the thruster reduced the rate of propellant vaporisation.

- **Mass flow rate:** 0.016 kg of propellant was consumed during a one second run, so the average mass flow rate is 0.016 kg/s, compared to the requirement for 0.057 kg/s. However, as the initial thrust reached the target value, it is inferred from Equation 4.1 that the specified mass flow rate was similarly achieved at this time.

- **Nozzle pressure ratio:** From Equation 4.2, the thrust per unit nozzle area is dependent on NPR, so it is assumed that the required NPR of 4.0 was achieved at the start of the thruster firing.

In summary, the scale exhaust simulation appears to have been momentarily achieved, before cooling of the thruster affected its performance. As anticipated in Section 4.2, the design thrust of 6.4 N exceeded that maximum 5 N control force which the MSBS could exert on the propulsion simulation model. However, the difference between these forces is not large, and the provision of more magnetic material in the model, or a relaxation of the magnet current limits, would allow successful propulsion simulation tests at the design point, if the thrust profile had a more suitable form. A more suitable thrust profile would also benefit attempts to improve the force measurement accuracy. An accuracy better than 1 % would allow an investigation into base drag coefficient changes caused by the presence of the exhaust plume.

Referring to the design parameters initially specified by PSI, and introduced in Section 4.3, the design of the compressed gas thruster can be summarised as follows, awarding each criteria an approximate score from *1 = poor*, to *5 = excellent*:

Table 5: Evaluation of compressed gas thruster design

Design Parameter	Comment	Rating
Compactness	Compact propellant but requires support equipment.	3
High Density Propellant	Volume of CO_2 is small compared to model, but run-time remains short.	3
Lightweight	Thruster has high weight, but steel components can contribute to magnetic force.	3
Remote Activation	Good light activated method, spoiled by lack of roll control.	4
Thrust Level	Initially far too high, reduced by enlarged nozzle but unreliable.	2
Thrust Profile	Very poorly suited to testing in an MSBS, no steady thrust for data acquisition.	1
Safety	Propellant is safe, but explosive squib requires careful handling, model should have external switch.	2

An equivalent table describing the performance of the rocket thruster is presented in Section 7.7.

A similarity polygon depicting the overall success of a cold jet for exhaust simulation in a conventional wind tunnel is shown in Figure 3.3a, and was discussed in Section 3.4.3. The significance of the failure of this technique to match the stream and jet Reynolds numbers and temperature ratio with the flight condition, would need to be evaluated in the context of a specific test.

The compressed gas thruster for MSBS propulsion simulation has been shown to be capable of achieving the scale exhaust parameters. If a future design could demonstrate

improved control of the thrust profile, this technique would not be fundamentally any worse than the cold air exhaust simulators often used in conventional wind tunnel facilities.

7. PROPULSION SIMULATION WITH SOLID ROCKET THRUSTERS

Solid rocket thrusters were developed in parallel with compressed gas devices for propulsion simulation in the Southampton MSBS. This chapter describes the evolution of a solid rocket motor suitable for testing in suspension, and concludes that solid rockets are preferable to compressed gas thrusters for MSBS propulsion simulation at this scale.

7.1 INTRODUCTION

The use of solid rocket thrusters to generate an exhaust plume in an MSBS was first considered by PSI in their initial proposal to NASA for the propulsion simulation contract[32]. Rockets were later rejected in favour of a compressed gas exhaust simulation technique, primarily on grounds of safety and cost. A further objection was expressed regarding the particulate nature of the exhaust from some solid rockets, and possible contamination of the MSBS and wind tunnel hardware.

At Southampton some doubt was expressed over the strength of the cost and safety objections, particularly given the availability of small solid propellant motors from hobby shops, for use in model rockets and aircraft. These motors cost less than £2 each (1991), and are considered safe enough for use by supervised children. The proposed compressed gas thruster from PSI raised its own safety issues, regarding the use of an explosive squib to puncture the CO_2 bottle. Furthermore, exhaust debris would not be a significant problem in an open return wind tunnel such as that presently in use with the Southampton MSBS, although its presence would detract from the realism of the exhaust simulation.

During the development of the Southampton MSBS for propulsion simulation testing, it became clear that the compressed gas simulator would be delivered behind schedule. During the resulting slack period, experiments with solid rockets were performed to evaluate their potential, and to gain experience in propulsion simulation techniques. Following delivery and testing of the carbon dioxide thruster, an improved rocket motor was developed which appeared to offer the best combination of attributes for exhaust simulation in a small MSBS.

7.2 COMMERCIALLY AVAILABLE SOLID ROCKETS

Two types of solid rocket were readily available. The first, manufactured by Estes Inc of Penrose, Colorado, use a resin-bonded black powder propellant, packaged in cardboard cylinders of 17 mm or 24 mm diameter, having a length of 70 mm. Each motor is fitted with a clay nozzle. Estes motors have a two-phase thrust profile, whereby an early peak is followed by a steady thrust region. Peak thrust varies between 8 N and 32 N for the different motors available, with a total duration of 0.4-1.7 seconds. The thrust impulse is followed after a time delay by an impulse acting in the reverse direction, designed to deploy a recovery device. Estes motors are intended solely for use in model rockets. The variant considered in this chapter has a specific impulse of 80.4 s.

The second motor is sold under the brand name Jet-X in the form of propellant pellets, the primary constituent being guanidine nitrate. The pellets are combusted inside a reusable metal case, and the exhaust gases released through a simple orifice. A low level of thrust is produced for up to twenty seconds. Jet-X motors are intended for use with free-flight model aircraft. The thrust level produced is around 0.2 N - an order of magnitude below that expected from the compressed gas thruster.

Jet-X was quickly rejected as a potential propulsion simulation technique. The low speed and highly particulate composition of the exhaust plume would have made it unrepresentative of any typical engine efflux. Real and simulated exhaust characteristics are discussed in Section 4.2.

7.3 USE OF ESTES MODEL ROCKETS

A typical thrust profile for an Estes rocket motor is shown in Figure 7.1. The thrust peak occurring between 0.2 and 0.4 seconds is a consequence of the ignition technique employed, and is useful when the motors are used with model rockets. The high initial thrust rapidly accelerates the model, ensuring that it reaches a stable flying speed before leaving the launch pad. A range of total impulses are available, from 0.5 to 20 Ns. The propellant is common between types, with quantity and nozzle geometry altered to obtain a range of performance specifications.

Electrical igniters are normally used with these motors. To ensure reliable ignition, a hole in the propellant is provided in proximity to the rocket nozzle, through which the igniter is inserted (Figure 7.2). Following ignition, the igniter debris is ejected through the nozzle.

The thrust peak is a consequence of the increasing area of burning propellant during core burning, before the transition to end burning, as illustrated in Figure 7.3. Motor thrust is related to the instantaneous surface area of burning propellant, and this area reaches a maximum after around 0.2 seconds. After the transition, end burning dominates, providing a steady thrust until the remaining propellant is consumed.

For successful propulsion simulation in an MSBS, an initial aim was the provision of a sustained steady thrust. This would aid the acquisition of data with the motor firing and the model still, following the damping of any motion transients caused by the initial application of thrust. Estes motors were not compatible with this long-term aim, as it was anticipated from design calculations that the thrust peak could cause control difficulties due to its magnitude and sudden application. The thrust peak combined with the short run duration could make it difficult to stabilise the model and take data before the motor expired.

However, Estes motors gave a useful approximation to the peaky thrust profile obtained by PSI from the compressed gas propulsion simulator. Their use allowed successful development of applicable control and data reduction techniques, well in advance of delivery of the carbon dioxide thruster. Attempts were thus made to cope with peaky thrust profiles, even though the need to do so was not anticipated during the formulation of the contract with PSI, nor written into it.

7.3.1 Propulsion simulation with Estes rockets

A steel model was constructed having similar dimensions to those expected of the carbon dioxide propulsion simulator. This model is shown with a rocket motor in Plate 1. Electrical igniters were used, with current from an external source supplied to the model via two thin umbilical wires. No attempt was made to incorporate an on-board ignition power source for these preliminary tests.

The peak thrust level of all of the Estes motors available exceeded the predicted 5 N restraining capability of the Southampton MSBS with a typical propulsion simulator model. A motor was selected with a peak thrust of 13 N, and a long steady thrust region of around 1.2 seconds at 6 N following this peak. To reduce these thrust levels, the motor was exhausted into a settling chamber, and then through a convergent nozzle. A nozzle diameter of 6 mm was used to obtain the thrust profile of Figure 7.1, with a peak of around 7.5 N, and a steady 1 N thrust level.

The solid rocket model was suspended in the MSBS and a static calibration carried out, showing that a maximum axial force of 5.2 N could be exerted on the model at zero incidence. The axial force capability of the control system was thus between the peak and steady thrust levels of the rocket thruster. An account of the method used to magnetise iron models and the steps taken to maximise the axial force capability of the MSBS is presented in Chapter 5. Attempts were then made to control the model in suspension whilst firing a rocket.

7.3.2 Experimental set-up

The standard MSBS test section was not used during these experiments with solid rocket thrusters. The standard test section has coated glass windows installed to allow optical position sensing, and these could have been damaged by misdirected rocket exhaust if control of the model was lost during a firing. An alternative test section was fabricated from a length of 150 mm diameter plastic tubing, protecting both the model and MSBS hardware from possible damage following a loss of control. Slots were cut into the tubing to enable the passage of the laser light sheets used for position sensing. No attempt was made to use this test section for wind-*on* testing.

During tests with Estes rockets, the MSBS control system was still implemented on the PDP11/84 computer. Data acquisition was performed by the PC, storing a complete record of model position and electromagnet currents over an interval of 20 seconds. Power for electrical ignition was provided by a 6 V, 5 A bench power supply, which was manually activated to fire the rocket motor, soon after the start of the data storage period.

Estes electrical igniters contain a small coil coated in a flammable material. With application of sufficient current, the coil heats up to the ignition temperature of the coating, which flares and in turn ignites the rocket propellant. This process is reliable and permits remote operation of the rocket, but the timing is not precise and a variable delay of up to one second is experienced before ignition occurs. Application of an advanced control strategy as suggested in ref 32, employing foreknowledge of the timing of a thrust impulse to initiate a restraining force on an MSBS model just as the motor fired, would therefore be difficult with this type of electrical ignition. A similar conclusion was drawn with regard to firing the compressed gas thruster (Section 6.1).

7.3.3 Propulsion simulation experience

All firings in this test series were conducted at zero incidence. The response of the MSBS control system during a solid rocket propulsion simulation trial will be considered later in this chapter. The first attempt at firing a solid rocket thruster from on-board the suspended

steel model was successful, with the model retained in suspension. Initially the tests had a success rate of around fifty percent. The success rate subsequently increased as a number of factors causing suspension or control difficulties were identified and addressed:

Laser flicker

For convenience, firing of the thruster was at first controlled by switching on the ignition power supply at its mains socket. This socket was in a mains loop which also supplied power to the MSBS lasers. A power surge to the supply at switch-on occasionally caused a flicker in laser output, resulting in unpredictable transient model motion just as the rocket was fired. The laser flicker was identified from recorded run-data, and a switch was then incorporated into the igniter circuit. This allowed the power supply to be pre-energised without a model in suspension, and no further control problems were caused by ignition power drain.

Igniter smoke

On a number of occasions, smoke from the igniter drifted across the path of one of the position sensing laser light sheets, with sufficient density to cause an error in position detection. As with the laser flicker problem, this caused a model excursion from which recovery was not always achieved. No problems were observed due to rocket exhaust obscuring any of the optical pathways, as the exhaust was always ejected with sufficient velocity to clear any smoke from the test section.

Igniter smoke was removed by running the MSBS wind tunnel at idling speed during subsequent solid rocket trials. The plastic test section was not sealed into the wind tunnel diffuser, but the fan was able to induce sufficient test section flow to draw smoke away from the critical areas.

Loss of magnetisation

In response to a large rocket thrust and the ensuing model motion, the controller would sometimes demand a restoring force larger than that available. This would cause one or more of the dedicated electromagnet power supplies to reach maximum current. Further axial motion of the model in response to the inadequate restraint was often acceptable, limited by the length of the axial position sensor. The major problem caused by an overloaded magnet was a reduction of model magnetisation.

Magnetisation is dependent on the difference in instantaneous current between members of an electromagnet group, and an overload would reduce that difference. Reduction of magnetisation decreased the suspension forces acting on the model, often causing loss of

control before the axial excursion became dangerously large. To preserve the level of magnetisation, software limits were imposed on the currents of certain magnets, as described in Section 5.8.3.

7.4 SOLID ROCKET DEVELOPMENT

Estes solid rockets provided an ideal opportunity to perform propulsion simulation tests in the Southampton MSBS prior to the delivery of the compressed gas thruster from PSI. An added advantage was that the peaky thrust profile of the Estes rockets allowed early development of control strategies to cope with a sudden application of thrust. This allowed rapid progress to be made with the CO_2 model once it arrived.

Following the first test series, solid rockets were developed to a form more suitable for long term use for propulsion simulation with an MSBS. This development was in conjunction with a local specialist company, Rocket Services[a], who advised on design changes and produced a new type of rocket motor. Later in the research program, following tests of the compressed gas simulator and the DFM rig described elsewhere in this thesis, the new solid rockets were bench tested and fired in suspension.

7.4.1 Improved solid rockets

The aim of the new motor design was to produce a thrust profile with an extended steady region and no thrust peaks. Assuming that a cylindrical propellant charge would yield a steady thrust once end burning was established, the regions of the thrust profile requiring special attention were thus ignition and burn-out.

Evidence from thrust traces obtained during the development process suggested that for this propellant, the rate at which ignition spread over the surface was fast compared to the rate of progress of the burning surface through its bulk. This observation was confirmed by Rocket Services. The new rocket design has a plain propellant surface for ignition, to avoid the Estes-type thrust peak caused by a transition from core to end burning (Section 7.3).

A fuse igniter was used, inserted through the nozzle of a new model, described below. The fuse was itself ignited outside of the model. The first firings of the new motors were conducted with the fuse in contact with the propellant. This practice resulted in localised

[a]Rocket Services, PO Box 342, Wareham, Dorset BH20 7HR, UK.

ignition and a starting thrust peak as shown in Figure 7.4. Thereafter a shorter fuse was used, which flared in front of the propellant surface and gave reliable and uniform ignition with no thrust peak (Figure 7.6). Estes electrical igniters were employed for ignition of the fuse outside the model, permitting remote firing with the model in suspension. Once the propellant ignited, fuse debris was ejected through the nozzle. The electrical igniter and its wires then fell away, leaving the model in unrestrained suspension without the need for a complex internal firing system. A drawback was that use of a fuse accentuated the timing problem described in Section 7.3.2. The delay between applying power to the igniter and ignition of the rocket motor varied from 1-3 seconds.

The upstream end of the propellant charge - the last part to burn - was initially exposed, and tests showed an end peak in the thrust profile. An example of this occurrence is shown in Figure 7.4. This peak was attributed to an uneven breakthrough of the upstream surface followed by a flashover and ignition of all of the exposed propellant (Figure 7.5a). A layer of epoxy adhesive applied to this surface (Figure 7.5b) prevented the flashover, and promoted a controlled finish to the thrust profile of the new motors, as illustrated in Figure 7.6.

Thrust rise time for the improved rocket motor was typically around 50-60 ms. This range marginally exceeded the 45 ms suggested in Section 12.5.2 as a minimum rise time for a thruster suitable for use in the Southampton MSBS with feedback control. The acceptable limit was estimated by considering the maximum rate of change of electromagnet current possible with the present power supplies. As the rise time obtained was above the minimum, good control during rocket ignition was expected, with reduced axial motion of the model caused by the initial thrust.

The observed rise time reflected the spread of ignition over the exposed propellant surface, and the time to generate sufficient exhaust to pressurise the settling chamber in the new model. A slower thrust increase could have been attained by a more sophisticated motor design, perhaps incorporating a conical propellant geometry to gradually increase the surface area during end burning, or by increasing the volume of the settling chamber.

As in the Estes design, the new solid rocket motors have a cardboard casing around the propellant charge. The casing adheres to the propellant, inhibiting uncontrolled surface burning. A similar propellant as that contained in Estes motors is used, but the simplified design of the new motors allows sufficient propellant for a two second run to be contained in a tube approximately half the length of an Estes motor.

7.4.2 Model for improved rocket motors

A steel model compatible with the new solid rockets was fabricated, and is shown in the schematic of Figure 7.7. A settling chamber was provided to match the internal diameter of the motor casing, encouraging a smooth internal flow of exhaust gas. This chamber also provided a location for pressure monitoring upstream of the nozzle. Externally the model has a boattail, as this shape is often used in the region of engine exhausts.

A feature of the new solid rocket motor is its compactness. The volume occupied by the propulsion system in the new model is small compared to that of the compressed gas propulsion simulator (Figure 6.1). More space remains for magnetic material, increasing the forces that can be generated on the model by a given electromagnet array. Alternatively the internal volume could be used to carry instrumentation, such as a pressure measurement system as described below, or the model made smaller, to reduce blockage of the wind tunnel test section.

The nozzle is detachable to allow different geometries to be tested; presently a simple convergent nozzle is used. The nozzle exit area used in the first tests was smaller compared to the base area of the model than is usual in full scale applications, to maintain thrust level with the convergent nozzle.

An attempt was made to predict the thrust of the new rocket motors, as installed in the new model. Standard nozzle flow and thermodynamic relationships were invoked, and applied to published information relating to the performance of the similar Estes motors[43].

The predicted thrust level was significantly higher than that attained during bench tests. The loss of exhaust energy observed with the redesigned motors was attributed to heat transfer to the steel structure of the new model. Heat loss to the cardboard body and ceramic nozzle of an Estes motor would occur at a much lower rate. Rather than attempt to develop a more complex mathematical model of the behaviour of an internal rocket exhaust flow with heat transfer to the walls, thrust level was thereafter adjusted empirically by gradual adjustments to the nozzle geometry.

7.5 PRESSURE MONITORING

To allow a comparison of rocket thrusters with other propulsion simulation techniques and full scale exhaust flows, it was necessary to fully characterise the rocket exhaust. Parameters such as ratio of specific heats of the exhaust, and density of the propellant

(used to estimate mass flow rate from thrust duration) were taken directly from data published by Estes[43], given the commonality of propellants. The remaining characteristic which had to be measured directly was exhaust stagnation pressure. For the new rocket motor, stagnation pressure would depend on the design of the nozzle.

Two techniques were used to measure stagnation pressure during bench tests of the new solid rocket system: a pitot probe positioned in the exhaust plume close to the nozzle, and a static tapping in the settling chamber downstream of the motor. The layouts for the two techniques are shown in Figure 7.8. For both types of test the pressure was measured using a transducer driven by a bench power supply, with data acquisition via a spare ADC channel.

The central, potential core of the exhaust plume, in which entrainment would be minimal and the stagnation pressure still approximately equal to that in the nozzle, was assumed to persist for 4-5 nozzle diameters downstream of the orifice[44]. To minimise the influence upstream, the probe was itself positioned 1-2 diameters clear of the orifice.

With a nozzle diameter of only 4 mm, accurate positioning of the probe was required. Some pressure data was affected by an incorrectly positioned probe, or by the probe being deflected by the force of the exhaust jet. Plate 3 shows a static firing with stagnation pressure measurement, in which the probe is poorly aligned and the exhaust plume is deflected. A further problem encountered was damage to the pitot probe caused by the temperature of the rocket exhaust, around 2000 K for a typical solid rocket[37]. The probe, of stainless steel construction, was ablated to an uneven end shape or blocked on several occasions.

The static tapping, use of which offered few complications in practice, became the preferred pressure measurement point. However, it was important to ensure that forces arising from the connection to the pressure transducer did not interfere unduly with thrust measurement during the bench tests. This was achieved by using a 400 mm flexible connecting tube to the transducer, which was loosely supported on a pivot. The data presented in Figures 7.9 and 7.10, showing good correlation between measured values of exhaust stagnation pressure and of thrust for the two techniques, suggests that drag from the static tapping connection was minimal.

7.5.1 Pressure measurement results

Some variation was recorded in the nominally steady thrust period (Figures 7.9 and 7.10). This could be due to inconsistent propellant density, irregular burning or the passage of

combustion debris through the nozzle. This variation was not further investigated due to lack of time. On some occasions a gradual increase of thrust was recorded. This was thought to be a result of partial clogging of the nozzle with combustion debris, which tended to build up on the internal surfaces of the steel model. This was in contrast to the characteristics of the Estes rocket motors. Bench tests of the Estes motors showed a gradual decrease in the 'steady' thrust, as the clay nozzle was ablated and increased in diameter (Figure 7.1).

The stagnation pressure data in Figure 7.9 lags slightly behind thrust at the start of the run. In Figure 7.10 the static pressure appears to follow the thrust more faithfully, but as described below and shown in Figure 7.11, a lag was also recorded during this test. The lag could be due to the volume of gas contained in the tube between the pressure transducer and the pressure tapping. Restricted gas flow through the tapping to pressurise or decompress the connecting tube would limit the response time of the pressure measurement system. This effect had no significant bearing on the propulsion simulation tests, and was not considered further.

Figure 7.9 has a finishing thrust peak, for the reasons described above in Section 7.4.1. The stagnation probe became partially blocked by exhaust debris towards the end of this test, and the pressure trace falls early and fails to correctly follow the peak.

In Figure 7.10 the pressure trace measured at the internal static tapping follows the thrust profile more closely than the stagnation pressure of Figure 7.9. The static tapping yields a higher pressure, whereas the thrust levels in the two diagrams are in good agreement. These observations suggest that the stagnation probe was not correctly positioned in the potential core of the exhaust jet. As described above, it was difficult to maintain the correct position of the probe during a motor firing.

Figure 7.11 shows chamber static pressure plotted against thrust for the rocket bench test of Figure 7.10. The hysteresis loop during the start and finish transients is a reflection of the pressure measurement lagging behind that of thrust, as described above. The data for full thrust, in the upper right hand corner of the figure, suggests that thrust can be estimated from motor static pressure upstream of the nozzle. A least squares fit indicates a gradient of 2.05 N/Bar for this data. This result supports the suggestion in Section 6.2 of a linear *thrust/pressure* relationship, and has implications for possible future propulsion simulation research.

As an alternative to the development of a thruster with a highly reliable and repeatable thrust profile, a propulsion simulator could be developed whereby pressure telemetry from the model yields an instantaneous thrust measurement. An infra-red pressure telemetry system has been developed for the NASA Langley 330 mm MSBS[19], as a refinement of the radio telemetry techniques used at Farnborough in the 1960s. Pressure measurement could prove to be an attractive method for acquiring the precise thrust data necessary for 'production' propulsion simulation research.

7.6 TESTS IN SUSPENSION

A static calibration with the new model in suspension at zero incidence, showed that the MSBS could exert a maximum axial restraining force upon it of 4 N. As bench tests indicated a thrust of just over 2 N with the 4 mm diameter nozzle, and the thrust rise time appeared to be greater than the 45 ms electromagnet response time (Section 12.5.2), no problems were expected in firing the new rocket motors in suspension.

Several motor firings were performed on-board a suspended model. One such firing is shown in Plate 4. By this stage of the research the MSBS control system and data logging tasks were both being performed by the Personal Computer (PC). Ten seconds of position and current data were recorded for each test, with data obtained at the control loop rate of 242 Hz. Initially the rockets were tested with the model in free suspension. Subsequently, settling chamber static pressure was monitored via the flexible hose to the pressure transducer.

A typical axial position response to the 'top hat' thrust profile is shown in Figure 7.12. The start and finish of the rocket firing provoke a similar but opposite transient response in axial position, as the control system compensates for the changing conditions. Once the starting response is damped out by the controller, the desired condition of a stationary model with the thruster firing is achieved between 1.5 and 2.25 seconds. Attainment of this stable condition eliminates the need to perform the involved analysis of motion transients described in Section 6.7, which was required with the compressed gas thruster.

Data analysis for this test series was performed using the DFM rig (Chapter 8 onwards). The ten seconds of run data were first processed by averaging each tenth of a second into one data point. Data prior to ignition and after the response to flame-out were discarded. This left a reasonable number of data points to be analyzed.

External heave force, axial force, and pitching moment experienced by the model at each data point, were measured by the DFM rig using the procedures described in Section 9.3. These force components represent the summation of the instantaneous aerodynamic loads, motor thrust and model weight. As the tests were conducted wind-*off* at zero incidence, it was expected that motor thrust alone would be measured, as external axial force.

Force data from the firing illustrated in Figure 7.12 is shown in Figure 7.13. The axial force recorded between 1.5 and 2.25 seconds is around 2.25 N, in good agreement with the levels of motor thrust measured during bench tests (Figures 7.9 and 7.10). Much smaller variations in heave force and pitching moment were recorded. Figure 7.14, a closer look at these data, shows no significant trend in pitching moment during the run. However a slight negative (upward) heave force develops before the burn-out at 2.25 seconds. This force is attributed to the consumption of the 0.12 N of propellant contained in the solid rocket motors. A force measurement resolution of 5 % of the motor thrust has therefore been demonstrated. In Section 4.2, the accuracy requirement was defined as 1.1 % or below.

Figure 7.15 shows data from a suspended rocket firing with pressure measurement. Again a thrust of 2.25 N is recorded towards the end of the firing, where the model is steady. The gradual rise in static pressure is thought to be related to blockage of the nozzle with exhaust debris. Figure 7.16 shows the relationship between static pressure and measured thrust for this run. The gradient of the least squares fit to this data is lower than expected. The DFM rig may have been incorrectly calibrated, or the suspected nozzle blockage could be responsible for this anomaly. Use of the DFM rig to measure the forces has also increased the scatter of this data compared to the equivalent bench test (Figure 7.11).

These results represent the first use of the DFM rig with an iron model. During the force measurement, a coil heating problem was encountered caused by the high electromagnet currents for suspension of the rocket model, and the length of time taken to process the data: To maximise the capability of the Southampton MSBS to generate axial force on the propulsion simulator models, the burden of generating the magnetising field is shifted away from the magnets used to produce axial force, to those also used for suspension (Section 5.8.1). These magnets therefore operate at a continuously high current when the thruster models are suspended. The electromagnets are not actively cooled, and continuous operation at high current leads to heating over a period of a few minutes.

Analysis of the fifty or more data points recorded for each test takes significantly longer than the test itself; around thirty seconds per data point following the procedure of Section

9.3.4. During the analysis of propulsion simulation data, several magnets heated up to the extent that a pause for system cooling was required after evaluation of each set of run data. Several hours were required for the magnets to return to room temperature, so the data reduction process was disrupted.

A number of approaches could reduce the heating problem in the future. These approaches include employing a more rigorous selection of data points to be analyzed, reducing the number of points further by averaging over an interval greater than one tenth of a second, or modifying the analysis procedure to reduce the time taken per data point.

7.7 SATISFACTION OF PERFORMANCE AND DESIGN CRITERIA

The solid propellant rocket motors described in this chapter were not intended to achieve an accurate scale simulation of a specific engine exhaust. The aim of their development was to demonstrate propulsion simulation in an MSBS, using a device with characteristics more suited to the application than those of the compressed gas thruster produced by PSI. However, a comparison will be made between the performance of the rocket thrusters and the criteria outlined in Section 4.2, to assess the requirements for a future solid rocket device.

- **Nozzle diameter:** A nozzle having a diameter of 4 mm was selected empirically to give a suitable level of thrust. This diameter is coincidentally close to the 4.6 mm requirement.

- **Thrust:** An average thrust of around 2.25 N was observed during tests of the new rocket motors. This value falls well short of the 6.7 N requirement. Thrust could be increased by using a more powerful propellent, or by altering the propellant geometry to increase the instantaneous area of combustion.

- **Mass flow rate:** Substituting rocket exhaust properties into the equations of Section 4.2 yields a mass flow requirement of 0.012 kg/s. The new motors consume 12.5 g of propellant in approximately 2.2 seconds, giving a mass flow rate of 0.0057 kg/s.

- **Nozzle pressure ratio:** From the measurements of static pressure upstream of the nozzle, the nozzle pressure ratio for the new engines was around 2.25. Increasing NPR to the required level of 4.0 would be compatible with the necessary increases

in thrust and mass flow rate. These figures correspond to jet Mach numbers of 1.11 and 1.41 respectively for full expansion in a convergent-divergent nozzle.

As the technology of solid propellant rockets is well advanced, the development of a motor with scaled exhaust characteristics and a thrust profile suitable for MSBS testing, would not be expected to be troublesome. It has been shown that force measurement approaching the level of accuracy required to resolve changes in base drag coefficient due to the exhaust plume, is promoted by an acceptable thrust profile.

Referring to the design parameters initially specified for the compressed gas thruster, which were introduced in Section 4.3, the performance of the solid rocket thruster is summarised below to allow a comparison with the compressed gas exhaust simulator, again awarding each criteria an approximate score from *1 = poor*, to *5 = excellent.*

Table 6: Evaluation of the solid rocket thruster design

Design Parameter	Comment	Rating
Compactness	Thruster is extremely compact	5
High Density Propellant	Good run duration for propellant volume	5
Lightweight	Solid propellant requires no support equipment, total mass minimal	5
Remote Activation	Fuse ignition effective but needs trailing wires, timing poor	3
Thrust Level	Can be reliably tailored to requirement, good consistency between runs	4
Thrust Profile	Step profile can easily be attained, ramps require complex propellant design	4
Safety	High temperature exhaust, cannot interrupt run, but motors safe to handle	3

An equivalent table describing the performance of the compressed gas thruster was presented in Section 6.9.

The similarity polygons discussed in Section 3.3 illustrated the advantages of a hot jet exhaust simulation over a conventional cold jet technique. Use of a solid propellant rocket as the simulator introduces an unusual problem, in that the jet has a higher temperature than that of a conventional engine. This factor would need to be considered in the context of a specific test, before a decision was made as to which propulsion simulation technique to use. It has however been shown that in practical terms, a solid rocket is preferable to a compressed gas thruster, for propulsion simulation in an MSBS at small scales.

7.8 FUTURE DEVELOPMENT

Solid rocket thrusters have proved successful for demonstrating propulsion simulation in a small MSBS. There remain a number of aspects of their performance which need to be addressed, before a conclusion can be drawn as to the suitability of this simulation technique for use in a larger facility.

Safety

The safety issue would become much more pressing at larger scales. Protection of the MSBS facility and personnel in the event of an accident or loss of control involving a larger solid rocket would be paramount.

Thrust Profile

A longer rise time would reduce model motion in response to ignition of the thruster. This could be achieved by shaping the propellant charge, or by graduating its properties.

Smoke reduction

A propellant should be selected to reduce the debris present in the exhaust, especially for use in a closed circuit wind tunnel.

Repeatability

A purpose-built rocket may achieve sufficient repeatability of thrust profile to enable the target wind tunnel tests - measuring base drag changes as described in Section 4.2 - to be performed without the provision of additional instrumentation. An alternative technique would be the use of on-board chamber pressure measurement, to give an indication of instantaneous thrust.

8. FORCE MEASUREMENT IN AN MSBS

The propulsion simulation research demonstrated the difficulty of measuring forces and moments acting on a magnetically suspended wind tunnel model. In particular the limitations of a conventional pre-calibration technique were exposed, for the case where model position is not constant during an experiment. These findings prompted a review of force measurement practice, and led directly to the work described in the following chapters.

8.1 INTRODUCTION TO FORCE MEASUREMENT

For a Magnetic Suspension and Balance System (MSBS) to be effective as an aid to wind tunnel testing, it is vitally important that it is able to adequately perform its 'balance' function. Previous experience of force measurement in an MSBS has demonstrated that accurate assessment of aerodynamic loads is straightforward for simple cases, such as the measurement of a single force component applied to a centrally suspended model. The accurate evaluation of multiple forces and moments with a model suspended in an arbitrary position, can be particularly complex and time consuming.

For conventional wind tunnel testing, different force measurement methods are appropriate for different classes of experiment. A balance used during an investigation to find the static lift and drag coefficients of a flight vehicle will not be suitable for dynamic testing to evaluate its stability derivatives. As magnetic suspension technology matures, it is likely that a similar situation will develop. Considerable effort has been already been invested in research into force measurement techniques for an MSBS. A number of methods have been developed, applicable to one or more of the force measurement situations encountered. A summary of techniques for force measurement in an MSBS follows.

8.2 REVIEW OF FORCE CALIBRATION AND MEASUREMENT TECHNIQUES

The most recent study to be performed at Southampton which was devoted exclusively to MSBS force calibration was by Eskins[39]. He identified five categories of force measurement process:

Static calibration

The most common and intuitively obvious technique, a static calibration is performed by applying known loads to a model in suspension, and recording the variation in electromagnet current required to maintain its position. Relationships between force and current can be derived, and subsequently used to analyze wind tunnel data, deducing the force components which must be acting to produce the observed changes in current.

Static calibrations are notoriously time consuming to perform in all but the most simple cases. The force/current relationships have been shown to exhibit a high degree of position-dependence, so a separate calibration is required for each test attitude. Despite these disadvantages, static calibration remains the benchmark against which other methods are judged.

Dynamic calibration

This technique has been developed at Southampton[26,38,39], and is elegant in its simplicity. A suspended model is caused to oscillate sinusoidally in a chosen degree of freedom, while position traces and magnet currents are recorded. The force or moment required to cause the accelerations observed during an oscillation can be deduced from the model's inertial characteristics, and the force/current relationship derived in a similar manner to that used in a static calibration. Dynamic calibration is however limited to small current excursions about steady-state suspension values, and is regarded as having limited application.

To date dynamic calibration has met with only partial success, and has never been shown to give acceptably close agreement with the results of a static calibration. A high degree of accuracy is required in the measurement of model position and electromagnet current. Impure motion, and imperfections in the electromagnet array complicate the calculations, as does the dependence of magnet effectiveness on model position. The non-linear relationship between demand voltage and output current for the Southampton MSBS power supplies (Section 12.2), is thought to have degraded the dynamic calibration results obtained so far with this facility, by corrupting the motion sinusoid.

Direct measurement with an external balance

An external balance allows a direct measurement of the forces exerted by the electromagnet array, and so avoids the difficulties associated with trying to relate magnet currents to force components by the calibration methods described. The model is physically supported in position within the MSBS, by a device capable of measuring the forces and moments acting when the magnets are energised.

The force/current relationships are therefore easily deduced, and the technique lends itself to automation to speed up acquisition of the full matrix of electromagnet effects. A disadvantage is the need to calibrate the balance itself, so that its output can be correctly interpreted. However, this calibration need only be performed once for each balance, and can be achieved outside the MSBS, without using expensive wind tunnel time.

The external balance method may be regarded as merely shifting the burden of calibration from MSBS to balance. However, careful design can make the balance calibration straightforward, perhaps by the use of techniques for the design of conventional wind tunnel balances. Furthermore, the calculations required to convert electromagnet currents to aerodynamic force components can be made redundant, if the balance is used to measure directly those components acting when the currents recorded during an actual wind tunnel test are replicated.

Direct measurement with an internal balance

Direct measurement of the forces acting under test conditions is taken a stage further by use of an internal balance, as proposed in ref 45. A compact, six-component strain gauge balance could be installed between a model core and its aerodynamic shell. The balance would give an instantaneous reading of the force components resulting from the action of an airflow on the shell, communicated to a data acquisition system by a remote telemetry technique.

The technology of compact strain gauge balances and telemetry from models in an MSBS has been demonstrated, but application of an internal balance is limited by restrictions of space inside an MSBS model. Volume that could be occupied by magnetic material is instead used for extra payload, and the model is therefore more difficult to suspend and control. Use of an internal balance is however a promising force measurement concept for a future large MSBS.

Direct Calculation

Theoretical relationships are used in this technique to calculate the forces and moments experienced by a magnetic model core under the influence of a number of electromagnets. Magnet currents and model position are recorded during a wind tunnel test, and subsequently processed to deduce the aerodynamic force components. The success of this method depends on accurate modelling of the electromagnet and model system. Ultimately a practical calibration must be performed using one of the above techniques, to validate the calculated results.

8.3 FORCE MEASUREMENT SUMMARY

With the exception of the internal balance, all of the force measurement techniques described rely on the accurate measurement and recording of currents flowing in the MSBS electromagnets. Current measurement presents no fundamental problems, and is arguably more convenient and practical than force measurement with a conventional wind tunnel balance. Known magnet currents can be processed to calculate the electromagnetic forces and moments instantaneously applied to a suspended model. Aerodynamic forces can then be deduced by considering the balance of the total array of forces acting on the model.

A static model which is not a propulsion simulator experiences only magnetic, gravitational and aerodynamic forces, which by definition must be in balance for the model to remain stationary. The electromagnetic forces can be considered as balancing those due to gravity and airflow. The total aerodynamic force is therefore equal to the change in electromagnetic force between the wind *on* and wind *off* cases.

If the model is accelerating then inertial forces must also be considered. A further complication in the case of propulsion simulation in an MSBS is the presence of a thrust vector, and a change in model weight as the propellant is consumed.

The processing of the measured magnet currents to find the electromagnetic force exerted on a model core is the key step for these force measurement techniques. Theoretical methods can be used to estimate the effectiveness of different combinations of magnets in producing forces and moments, but a practical calibration must always be performed at some stage to check the accuracy of the calculations. This methodology is analogous to the use in aerodynamics of practical wind tunnel tests to validate the performance of Computational Fluid Dynamics (CFD) techniques.

A static calibration is a simple, reliable procedure when performed for a single force component, assuming that only the appropriate degree of freedom will be loaded during the wind tunnel test. A decoupled system using clearly identified magnets to control each force component further simplifies this process, as only a limited number of magnet currents need be recorded. Under multiple loads however, a rapid increase occurs in the calibration workload and in subsequent calculations to resolve the different force components.

For example, to fully pre-calibrate the Southampton MSBS at a (coarse) pitch spacing of 5 degrees, assuming minor excursions in the other degrees of freedom, it would be necessary to measure the effect of each magnet group at each attitude, and the variation of that effect with a disturbance in each of the five degrees of freedom presently controlled. This conservative example includes

- 23 pitch attitudes,
- 4 electromagnet groups,
- 11 positions per pitch attitude (central position plus a positive and negative disturbance in the 5 degrees of freedom),
- A total of 1012 separate tests to be performed.

Typically, an MSBS control system considers each degree of freedom separately. The instantaneous controller demand to a given degree of freedom should therefore be proportional to the appropriate opposing external force, and this relationship could conceivably be used to measure the aerodynamic force components. However, this method would rely on the controller generating pure, decoupled forces and moments, a condition that could only be verified by a check against known applied loads - a static calibration.

An important difference between the calibration of the internal and external force balances, and the other methods which calibrate against the electromagnet array, is that the former can be performed away from the MSBS, while the latter consume expensive wind tunnel time. This factor must be considered during future studies into the appropriate force measurement techniques for a commercial MSBS.

8.4 SOUTHAMPTON MSBS FORCE MEASUREMENT SHORTFALL

The high angle of attack capability of the Southampton MSBS makes static calibration an unsuitable force measurement technique. The combination of aerodynamic force and moment components generated on a body at incidence to an airflow, and the distribution by the controller of force component demands amongst all ten electromagnets, makes a complete static calibration prohibitively complex. At the beginning of this research program, no practical method existed for using the high angle of attack MSBS to generate useful aerodynamic data. The unique potential of this facility to investigate high alpha aerodynamics free from support interference remained unrealised.

8.4.1 Selection of remedial action

A review of previous force calibration research was conducted, and suggested that the use of an external force balance was an under-exploited method of force measurement. The techniques described in Section 8.2 above were assessed as follows:

- **Static calibration** is impractical for complex combined force and moment loading at high angles as described.

- **Dynamic calibration** has potential for future development, but can be complex, has limited application, and has not yet been demonstrated to a sufficient degree of accuracy. Further dynamic calibration work at Southampton may be appropriate now that the power supply non-linearity has been addressed (Section 12.2).

- The **external balance** method promises compatibility with high angle of attack testing, and at the small scale of the Southampton MSBS. Measurement of aerodynamic forces by installing the model and balance in the wind tunnel, and duplicating currents recorded in a wind tunnel test is an attractive technique.

- The level of technology required for an **internal balance** rules out this method for a low-cost development project, especially at the small physical scale of the Southampton MSBS.

- **Direct calculation** of forces and fields based on electromagnetic theory is used in some instances at Southampton. Britcher's FORCE program[6] is an example, but a calibration against practical results is still required (Section 5.5).

Direct Force Measurement (DFM) with an external force balance was therefore proposed as a potential solution to the Southampton MSBS force measurement shortfall. A feasibility study was performed, concentrating on the method of converting force to a suitable quantity for computerised data acquisition.

Previous research into external balances has been of limited scope, the major example being the construction of a force balance for use with an MSBS by Vlajinac[46]. He designed a rig to support a model via gas bearings, with air as the bearing fluid. Force and moment components in six degrees of freedom were deduced from air pressure measured inside the bearings. A static calibration of the rig was required to relate bearing pressure to applied load. The pneumatic calibration rig appears to have performed well, exhibiting good linearity between load and pressure change. Some interaction between the degrees of

freedom was detected and quantified, but its presence did not appear to detract from the overall accuracy of force measurement with this rig.

Since the research by Vlajinac, miniature force transducers have become obtainable, giving electrical output in response to an applied load. At the time of this investigation, two categories of force transducer were readily available: piezoelectric devices, and strain gauge load cells.

Piezoelectric force transducers produce a charge when loaded, and each device requires a charge-amplifier to convert the output into a voltage suitable for transmission to a data acquisition module. Charge leakage causes the steady output level to fall with time, but it is possible to reduce the leakage to an extremely low level, allowing quasi-static measurement of force. An advantage of this class of device is its ability to accurately measure force over a very wide range, typically 4 or 5 decades.

Conventional wind tunnel balances using piezoelectric force measurement have been demonstrated[47], although this is still an immature technology. The mode of operation of piezoelectric transducers makes them best suited to measurement of fluctuating or periodic forces, and their application has tended to be concentrated in this area.

Strain gauge force transducers are available in compact units, either as buttons for measurement of compressive forces, or in a threaded configuration that also allows measurement of tensile force. An internal strain gauge network responds to load with a very small deflection, and the output is a steady voltage proportional to the load. The only signal processing requirement is voltage amplification. Strain gauge force transducers are easily damaged if overloaded, so a unit with the correct load range must be chosen for each application, to give the best resolution whilst retaining a reasonable safety margin.

Unit cost was the decisive factor which led to selection of strain gauge transducers for the new balance. Piezoelectric transducers, each with a dedicated charge amplifier, were available for around £800 (1991), double the £400 cost of a strain gauge force transducer. To confirm the compatibility of strain gauge devices with an MSBS, a sample was placed in the test section, and subjected to a variety of magnetic fields. The output showed no dependence on field strength, although electrical noise was increased by operation of the electromagnet array. This result supported the findings of ref 45.

Three transducers were purchased from Entran Ltd[48] with a working range of +/- 22 N, and a safe force limit of +/- 44 N. This range was judged to accommodate the likely range

of force measurement requirements with the Southampton MSBS, while retaining a safety margin to protect against damage of the transducers by overload. The decision to purchase three transducers is explained in Section 8.7 below.

8.5 DESIGN OF A DIRECT FORCE MEASUREMENT (DFM) RIG

A DFM rig for use in a commercial MSBS was conceived as a starting point for the design of the new equipment, with the emphasis on Post-Run Current Replication (PRCR) test techniques. Design features of a commercial rig might include:

- **Measurement of the full complement of six degrees of freedom:** A commercial balance should be capable of measuring three force and three moment components.

- **Precise position adjustment in six degrees of freedom:** Given the dependence of electromagnet effectiveness on model position, the position during the PRCR analysis must be matched to that adopted during the wind tunnel test. The available range of position adjustment should match the capabilities and expected application of the particular MSBS facility.

- **Motorised position adjustment six degrees of freedom:** If position adjustment is motorised, force measurement can become highly automated and time-efficient. Wind tunnel test procedures would not be restricted by the capabilities of the rig, as they were during the aerodynamic investigation described in Chapter 11, where tests were performed with the model in a constant attitude to simplify the force measurement procedure.

- **Compatibility the with MSBS position sensing system:** This capability would allow accurate positioning of the model in the test section, by comparing the position measurements during calibration with those obtained while the model was in suspension for the wind tunnel test.

- **Compatibility with models of various shapes:** A versatile rig should be able to hold all models used in the MSBS. The alternative is just to hold the magnetic core, but this would remove the option of using the MSBS position sensors for correctly matching the test attitude. However, pre-calibration of a single core for use in a number of models might be efficient in terms of tunnel time for a commercial MSBS.

• **Rig compatible with rest of MSBS hardware:** It should be possible to rapidly install the rig in the MSBS wind tunnel test section. The presence of the rig should not affect the operation of the MSBS, for example by means of strong ferro-magnetism or eddy currents. These effects would complicate the extraction of the forces acting on the model core. It is therefore important to use non-magnetic materials throughout, and to reduce the potential for eddy current generation by avoiding major conductive loops in the rig.

• **Minimum coupling in measurement of force components:** The aim of the design should be to ensure that applied force components only invoke a response from the appropriate transducers. Calibration of the rig then becomes unnecessary, and the individual transducers can be calibrated in isolation.

• **Minimum deflection under load:** The application of magnetic force to the model should not cause a significant position error, given the position-dependence of electromagnet effectiveness. The need to correct model position after energising the electromagnet array would prolong the test procedure.

• **Balance fulfils design criteria applicable to any wind tunnel balance:** In ref 49 a number of general performance requirements applicable to the design of a wind tunnel balance are outlined. In summary, the criteria are

Accuracy: the indicated load is equal to the applied load.
Sensitivity: small changes in load can be detected.
Period: the balance returns a steady reading soon after the load is applied.
Stability: the balance returns to a constant position after displacement, promoting repeatability in the readings.
Damping: kinetic energy associated with the balance following the application of load is rapidly dissipated.

8.6 TEST TECHNIQUES FOR A LARGE DFM RIG

The emphasis of this study is on PRCR test techniques, whereby wind *on* magnet currents are recreated with the DFM rig and model installed in the test section. The electromagnetic forces acting on the model are then measured directly. This method is appropriate for a limited aerodynamic study such as that described in Chapter 11, where a relatively small number of force measurements are to be made.

Testing in a commercial MSBS would be more meticulous, with larger numbers of data points and repeat tests. The time required to perform PRCR force measurement for all of the data points could become prohibitive. In this case it would be more efficient to use the DFM rig to obtain the full calibration matrix for the model to be tested. The traditional pre-calibration could be rapidly performed with a motorised DFM rig. A computational method would then be used to deduce aerodynamic force from electromagnet currents, without the need for further tunnel time.

An extension of this test philosophy is to fully pre-calibrate the system for a small number of model cores, which are then used in various aerodynamic shells for wind tunnel tests. Knowing the force/current relationships for the core would eliminate the need for a separate calibration for each new model. Given the position dependence of force calibration, an accurate measurement of the location of the core relative to the outer shell would be required. The core position could then be deduced from that of the shell, whose location would be measured by the MSBS position sensing system. This position measurement imitates standard practice with internal strain gauge balances in conventional wind tunnel models.

8.7 LIMITED DESIGN FOR PROOF-OF-CONCEPT STUDY

A full DFM system similar to that outlined above was not appropriate for the technology demonstrator proposed for use with the Southampton MSBS. A less ambitious design was envisaged. A number of design criteria differed from those outlined above:

For simplicity and economy, only three force and moment components would be measured, using three force transducers. The components chosen were those typically addressed by a three component balance: lift, drag and pitching moment.

Positioning adjustment would be required in five degrees of freedom only, as axisymmetric models are presently suspended in the Southampton MSBS, and roll attitude is generally irrelevant. The available angle of attack range would be matched to the -10 to 100 degrees capability, with small adjustments possible in the other degrees of freedom.

The model holder would be designed to grip only the expected axisymmetric models. The capability to grip models of various diameters would be incorporated.

All position adjustment would be manual, as the cost and complexity of a motorised system could not be justified at this stage.

The absolute accuracy of the force transducers is quoted as 1 % of the full scale measurement, equivalent to 0.22 N. This is a conservative estimate, and the manufacturers stress that the accuracy would be improved by an *in situ* calibration. The 12-bit ADC system used with the Southampton MSBS gives a force measurement resolution of 0.005 N with these transducers. It should be noted that the choice of force transducer for this proof-of-concept external balance was governed primarily by cost and availability rather than by performance.

In Section 4.2 it was stated that to successfully perform the target propulsion simulation experiment, it would be necessary to detect a change in base drag approximately equal to 1 % of the thrust of an exhaust simulator model. Given the transducer characteristics, it appears that the DFM rig is capable of this level of accuracy, but this application was not attempted during the research.

The accuracy of a conventional wind tunnel balance would typically be expected to approach one force 'count' - the third decimal place of force coefficient - equivalent to an accuracy of 0.1 % for an example force coefficient of unity. This level of precision is not far removed from that potentially achievable with the development DFM rig, and it is assumed that a more advanced design could meet the force measurement requirements of a commercial wind tunnel balance.

8.8 DESIGN ASPECTS

A schematic of the DFM rig produced is shown in Figure 8.1. A photograph is presented as plate 5. The structural materials are primarily aluminium and brass. Steel springs are used in a number of locations as they were most readily available, but these could be replaced with phosphor-bronze springs if required. An assessment of the effects of using steel springs on the operation of the rig is presented in Section 9.2.1.

The model holder grips an axisymmetric model in two jaws, and is sufficiently compact to fit between the two inclined crossing pairs of laser light sheets used for position sensing. Plate 6 shows the rig installed in the MSBS wind tunnel test section. Laser light can be seen impinging on the ogive cylinder model held in position by the rig. The model holder is supported by a sub-frame which interfaces to the main rig assembly via the three force

transducers, labelled *A*, *B* and *C* in the schematic. The five components of position adjustment are distributed for simplicity of design between the model holder, sub-frame and main assembly as follows:

- Model holder: full yaw angle, gross lateral position, gross axial position
- Sub-frame: full pitch angle, full vertical position, fine lateral position
- Main assembly: fine axial position

A consequence of this distribution is that the final adjustments of all translations are in wind tunnel axes, while the two rotations are adjusted in model axes. The present MSBS control system uses model axes only, so a routine was added to the DFM support software to convert the translation measures to wind tunnel axes, as described in Section 9.3.1. Having the measures and adjustments in the same axis system simplifies the process of matching the model position to that recorded during suspension.

The layout of the transducers was partially dictated by the need for compatibility with the position sensing system. From the schematic (Figure 8.1) it is clear that the sum of the outputs from transducers *A* and *B* measures a vertical force component, while their difference is proportional to pitching moment. Transducer *C* measures horizontal force. Pitching moment *P* is given by

$$P = (F_a - F_b)\, l_{ab}$$

where l_{ab} is the x-wise spacing of the transducers. A small spacing increases the difference in force output from the transducers for a given pitching moment, increasing the measurement resolution. The limit to reducing the spacing is dictated by the need for increasing the accuracy of measuring the spacing, and the absolute force limits of the transducers. For all measurements of pitching moment in this thesis, the pitching moment reference is the centre of the model holder - generally coincident with the 50 % of body length position for an axisymmetric model.

If only the x - z plane force and moment components are to be measured, the transducers must all lie on the x - z plane. This plane is largely occupied in the vicinity of the model by the axial position sensing laser light sheet. The light sheet has two possible locations depending on whether tail scanning (conventional models) or nose scanning (propulsion simulators) is in operation. To ensure compatibility with both types of test, it was necessary to use a large axial spacing between the vertical transducers *A* and *B*. The resolution of pitching moment measurement was consequently reduced.

For greatest accuracy, the transducer manufacturer recommends elimination of any off-axis loading components during operation of the transducer. An additional consideration is that the transducers are easily damaged by application of torque about the load axis. To reduce off-axis loading and the application of torque, an ideal transducer mount would be a universal joint, allowing free motion about three axes.

A trade-off was required in the design of the mounts for the three-component DFM rig. A small amount of off-axis loading was accepted, to reduce force measurement errors caused by friction from the lateral motion restraints. The arrangement of transducers adopted prevents motion of the model, holder and sub-frame in the degrees of freedom addressed by the force balance. Control of the remaining degrees of freedom is provided by a number of adjustable stops, whose action is illustrated in Figure 8.2. To allow the stops to remain clear of the sub-frame, thus reducing friction errors in force measurement, a single axis transducer mount is used as shown in Figure 8.3, rather than a full universal joint.

This mount can transmit a bending moment to the transducer, in response to lateral forces, yawing moments or rolling moments applied to the model. Steady off-axis loads are eliminated by adjustment of a laterally adjustable weight. Nylon nuts are used to take up the slack between the transducer and its mount. This gives the mount and transducer system a degree of flexibility. When subjected to a moderate off-axis load, the flexibility allows displacement of the sub-frame until it comes into contact with the lateral stops.

By using this arrangement, small off-axis loads are tolerated, but the restraints prevent possible damage of the transducers caused by excessive off-axis loads.

A robust interface between the DFM rig and the MSBS hardware was required to give repeatable location of the rig in the test section, reducing the need for adjustment of model position each time the rig was installed. A three point attachment is used. At the upstream end of the test section the DFM rig attaches to a pair of fixtures on the MSBS framework. There is no access to the downstream end of the test section with the wind tunnel assembled, so a passive locator for the downstream end of the DFM rig was preferred. This is provided by plastic feet which locate the rig relative to the floor and sides of the test section. The feet allow the rig to slide into the test section without causing damage.

A metal fixture subject to a varying magnetic field will experience eddy currents. To reduce eddy currents in the DFM rig, insulation was incorporated between the rig and the MSBS, and a large loop in the sub-frame was broken by insulation at a joint. These

precautionary measures were taken before the rig was tested, and no investigation into their effect has been performed.

8.8.1 Support electronics

The force transducers require a 15 V supply, and are quoted as producing 56 mV per Newton of applied force. A support unit, referred to as the Load Cell Amplifier, was designed and built in the Electronics Workshop to regulate the input voltage, and amplify the output to a level suitable for the MSBS data acquisition system. Operational amplifiers are used with a pre-set gain of 25. Six channels are provided to enable the use of this equipment with future, more sophisticated DFM rigs. An audible alarm is incorporated, which sounds if a force of more than 25 N is applied to one of the transducers. To take advantage of this protection, the load cell amplifier should be activated whenever the DFM rig is handled.

8.8.2 Support software

Software to complement the DFM rig was designed to perform a number of tasks:

- Interpret recorded wind tunnel data.
- Aid position matching with a graphical display.
- Drive the electromagnets to match the currents recorded with wind *on*.
- Record and interpret signals from the force transducers.
- Perform automated force measurement sequences for a number of different types of test.
- Read test data from disc and write decoded force measurements to data files.

A new C program, DFMSOFT, was developed to manage force measurement with the DFM rig. Details of its function are described as appropriate in the following chapters.

9. DEVELOPMENT OF DIRECT FORCE MEASUREMENT TECHNIQUES

This chapter describes the development and testing of the Direct Force Measurement (DFM) apparatus. Possible sources of error in force measurement are investigated and quantified. A test procedure is derived, based on operational experience gained during the commissioning of the new equipment.

9.1 COMMISSIONING THE DFM EQUIPMENT

No fundamental problems were found in the design of the DFM rig, but a number of minor modifications improved its performance. The force measurement support software DFMSOFT was developed to display a graphical image, to aid position adjustment of the model in the rig to match a position recorded during suspension. A graphical image is preferred to a numerical display of model position for easy interpretation by the operator, and because of the distance (presently around 4 m) between the DFM rig controls and the PC monitor. The display is shown in Plate 7. Position matching is achieved by adjusting the model position to reduce the size of the error bar for each degree of freedom. A colour change indicates a position match within the limits defined below in Section 9.2.3. Bars are also used to indicate the load experienced by each force transducer.

Despite steady outputs from the Load Cell Amplifier (Section 8.8.1), the values of force as measured by the MSBS data acquisition system showed significant drift over a short time, typically just a few seconds. This problem was traced to poor electrical contacts between the ADC card and the rest of the equipment. Forces are generally measured as the difference between the transducer outputs at two significant data points such as wind *on* and wind *off*, and drift was occurring between taking these two readings. After improving the electrical connections, the effect of any remaining drift was reduced by altering the test procedures so as to minimise the time interval between pairs of transducer readings.

The force transducers had a calibration matching the manufacturer's specification. However, voltage gain in the Load Cell Amplifier is manually adjustable and is therefore inexact. The combined effect of the amplification and the analogue to digital conversion of each transducer signal was unknown. For these reasons it was necessary to perform a static calibration for each transducer as installed in the data acquisition system. The

transducers were mounted in turn in the thrust test stand (Section 6.3), and loaded with laboratory weights to enable the derivation of individual calibration constants.

9.2 INVESTIGATION OF ASPECTS OF DFM PERFORMANCE

9.2.1 Use of Steel Springs

A number of steel springs are used in the DFM rig. Steel springs were chosen for convenience as they were readily available during the manufacture of the apparatus. Some simple calculations were performed to estimate the possible effects of the use of steel springs on force measurements.

The volume of steel contained in the springs was estimated. The total volume of all springs presently used in the DFM rig was found to be around one percent of the magnetic core volume of the ogive cylinder model, which was used for most of the DFM tests described in this thesis. The spring steel was not expected to be strongly magnetised during force measurement tests, as the symmetry of the Southampton MSBS electromagnet array leads to low magnetising fields during suspension of permanent magnet models. The error in force measurement due to the spring steel was therefore estimated to be rather less than one percent. Given the overall accuracy expected of the force measurements, the added errors due to the use of steel springs were considered acceptable, and no attempt has yet been made to obtain replacement springs in a non-magnetic material.

9.2.2 Effect of rig presence on magnetic fields

A test was performed to ascertain whether the presence of the DFM rig influenced the magnetic fields generated in the test section for a given system current. A change would affect the electromagnetic forces acting on the model core, and so reduce the accuracy of force measurements. Field changes could result from the generation of eddy currents in the rig, or from the use of steel elements in its construction.

The rig was installed in the MSBS test section with the model holder clamp jaws removed. This allowed space for suspension of a model without removing the rig from the test section. System current was recorded, and compared with that required to suspend the model in the same position without the presence of the DFM rig.

The first test was performed with poor quality of control due to an optical alignment problem. Electromagnet currents for suspension with the rig installed varied by up to 0.2 A from those recorded with the test section empty. For a repeat test with the model

steady, the observed variation in suspension currents caused by presence of the rig fell to 0 - 0.06 A. Force measurement for the repeat test showed a difference of below 1 mN in heave and axial forces, and below 0.1 mNm in pitching moment, between the two states.

Current variations during unsteady control of the model were assumed to have generated eddy currents in the rig during the first test. The associated magnetic field changes altered the average suspension currents. Improved control with reduced current variation yielded better agreement. The difference in transducer output attributed above to the presence of the DFM rig does not represent an absolute error in force and moment values. During analysis of wind tunnel test data steady average suspension currents are duplicated before taking a transducer reading. It is assumed that the use of average currents during DFM analysis eliminates the generation of eddy currents. Force values are generally measured as the difference between transducer readings at two suspension states, so any steady force error caused by the presence of the rig would be expected to cancel out. It was concluded that presence of the DFM rig was not a significant source of force measurement error during this research.

9.2.3 Investigation of position matching

The success of force measurement using a Post Run Current Replication (PRCR) technique is partially dependent on the accurate positioning of a model using the DFM rig, to match a position recorded during suspension. The effectiveness of the electromagnet groups is known to be position-dependent, but this dependence had not been suitably quantified. An investigation into the effect of errors in position matching on magnet effectiveness was performed, in order to allow the definition of an acceptable position error for future DFM experiments.

Effectiveness was measured for the four electromagnet groups, in producing heave and axial forces on the ogive cylinder model, with various model position errors introduced into the five controlled degrees of freedom. The procedure for measuring magnet group effectiveness is described in the following chapter. Pitching moment effectiveness was not considered in this simple investigation. The initial measurement took place at zero angle of attack, and was subsequently repeated at 45 and 90 degrees of incidence. For each degree of freedom, group effectiveness was measured for position errors from -100 to +100 pixels. The relationship between MSBS position sensing units and metres/degrees is summarized in Section 2.5, from which it can be deduced that the simulated position errors corresponded to displacements of up to 3.6 mm and 2.5 degrees.

To simplify the experimental procedure, the position errors were introduced in rig axes. As described in the previous chapter, this is a mixed axis system. The measurements of electromagnet group effectiveness were made in model axes.

The results of the position error investigations in the three test attitudes are shown in Figures 9.1a-e. The graphs show the absolute error in magnet group effectiveness in producing heave *H*, and axial *A* forces on the ogive cylinder model, caused by a 10 pixel position error in the specified degree of freedom. Two conclusions are drawn from these results:

- The position errors caused changes in magnet effectiveness, but the changes in were all below 1 % of the maximum effectiveness for that group.

- Pitch attitude errors produce a greater change in magnet effectiveness than errors in the other degrees of freedom.

Prior to this investigation, a position error of +/- 10 pixels in each degree of freedom was arbitrarily defined as acceptable during DFM tests. The errors in the assumed values of magnet effectiveness associated with this tolerance were acceptably low compared to the overall accuracy expected of the tests (Section 8.7), so no change was made to the DFM test procedure as a result of the position error investigation.

9.2.4 Assessment of coupling between degrees of freedom

A static calibration of the DFM rig was performed to assess the coupling in force measurement between the different degrees of freedom. Knowledge of the level of coupling was required to aid interpretation of the rig output during DFM tests.

Laboratory weights and a number of pulleys were used to load all six degrees of freedom, whilst monitoring the rig output of apparent heave force, axial force and pitching moment. The results of the static calibration are shown in the following table:

Table 7: Coupling between the loads applied to the DFM rig and those measured

Applied load	Lift coupling (%)	Drag coupling (%)	Pitching moment coupling (%)
Lift force (N)	**99.1**	-.34	*-.37*
Drag force (N)	.98	**93.6**	*-.17*
Lateral force (N)	-.86	-1.00	*.89*
Pitching moment (Nm)	*1.33*	*3.1*	**98.4**
Yawing moment (Nm)	*1.78*	*.27*	3.2
Rolling moment (Nm)	*-197*	*102*	-3.5

It should be recognised that the couplings between forces and moments (shown in italics) were measured in units of N/Nm or Nm/N, and are not strictly comparable with the couplings between forces or moments alone.

Application of those force and moments to be measured by the three-component balance gave results below the desired 100 % coupling. This shortfall was attributed to friction in the rig. As the calibration was performed outside of the MSBS, it was not possible to use the methods of Section 9.3.3 below, applying electromagnetic forces to overcome the friction. Calibrations performed by loading a suspended model yielded improved results.

It is evident from the table that rolling moments caused the greatest coupling to the instrumented degrees of freedom. The sensitivity of each force transducer to rolling moment was dependent on its rotational position: It was possible to change - but not to eliminate - the roll sensitivity of the rig by rotating the transducers in their holders. This effect is a result of accepting undesirable off-axis transducer loads, to allow a reduction in friction caused by the lateral motion restraints (Section 8.8), and would not be a problem for a six-component balance.

Axisymmetric models were used throughout this research, so it was expected that no rolling moment would be applied to the rig at low incidence. At high angles of attack, yawing moments in model axes are transmitted to the rig as rolling moments in rig axes. Lateral force and yawing moment would be experienced during wind tunnel tests of an axisymmetric body at high incidence, caused by periodic vortex shedding as discussed in Chapter 11. However, these loads would be cyclic with an expected mean value of zero, so it was assumed that the coupling to the measured force components would be minimal.

Having recognised the presence of cross-coupling between loads applied to the DFM rig, no attempt was made to decouple subsequent force and moment measurements. The level of coupling among the components to be measured by the rig was acceptably low, considering its anticipated applications. The coupling was dependent on the set-up of the rig, which changed frequently during its development. Repeat calibrations would have been prohibitively time consuming. Finally, the major coupling was due to lateral forces and moments, which could not be measured by the rig to allow a decoupling to be performed.

9.3 DFM TESTING AND TEST TECHNIQUES

9.3.1 Data manipulation

For the measurement of steady aerodynamic force components acting on a suspended model, an average current is recorded at the test condition for each electromagnet. Presently, data is recorded over a period of one second, and an average taken of the 242 values. Electromagnet currents recorded during suspension exhibit periodic and random variation. The periodic component results from control system responses to cyclic model motion, and is swamped by the random, noise-related component if the quality of suspension is good, and the model appears to the eye to be still.

The one second recording period is long enough to include several cycles of model motion at the natural frequency of around 10 Hz, should such a motion be present. Some of the complex combined roll and lateral oscillations, observed during wind tunnel testing of an ogive cylinder at moderate incidence as described in Chapter 11, had lower frequencies close to 1 Hz. The effects of these oscillations were not therefore adequately smoothed by the one second recording period, but the irregular nature of the oscillations discouraged the use of a longer averaging period, as this would have invalidated the concept of an average aerodynamic force. In addition to reducing random and cyclic errors from the test data, the use of steady, average currents during force measurements reduced the possibility of eddy current generation within the DFM rig (Section 9.2.2).

Position measures are recorded and averaged in a similar manner to electromagnet currents. Presently the photodiode array counts are decoded into degree of freedom measures prior to storage, as the manual adjustment of model position in the rig is performed on a degree of freedom basis. These position measures are in sensing system axes, whereas the DFM rig operates primarily in wind tunnel axes. As a result, adjustment of heave position at the DFM rig initially caused a coupled response to axial position as

measured by the MSBS position sensors, and vice versa. The software used to manage force measurement, DFMSOFT, was extended to allow decoupled adjustment of the heave and axial components. This decoupling was more complex than a standard axis transformation, because these two measures are already coupled in sensing system axes, by an amount dependent on angle of attack as shown in Figure 9.2. Furthermore, the position sensing geometry means that different units are used to measure these components. This geometry leads to

$$H_{DFM} = \sin\theta_s \left(H_s + c_{AH} A_s(\tan(\theta_s - \alpha) - 1)\right)$$

$$A_{DFM} = \sin\theta_s \left(H_s + c_{AH} A_s(\tan(\theta_s - \alpha) + 1)\right)$$

where the subscripts *DFM* and *s* denote rig and sensing system axes respectively, α is the angle of attack of the model, and θ_s is the inclination of the position sensing system - 45 degrees for the Southampton MSBS as presently configured. c_{AH} is a coefficient for correlating the units of pixel measurement for heave and axial position.

9.3.2 Electromagnet currents

A simple feedback loop is used to ensure that the electromagnet currents applied during a force measurement match those recorded during a wind tunnel test as closely as possible. The observed non-linearity in the relationship between demanded current and that output by the power supplies (Section 12.2), makes this approach necessary. Changes in the power supply calibration with system warm-up and over longer periods of time, rule out the use of the calibration software described in Section 12.2.5, to achieve a precise match without resorting to current feedback.

During current matching, demands to the electromagnets are adjusted by a proportional feedback loop until the measured currents match those recorded within acceptable limits, at which point the output currents are frozen. The present definition of an acceptable current match is a total absolute error over the ten electromagnets below 0.5 A. The maximum observed group effectiveness with the ogive cylinder model was 165 mN/A for group II (2 magnets) in heave force, and 10.5 mNm/A in pitching moment. This corresponds to a potential error of 41 mN in force, or 2.6 mNm in moment measurement, which was judged acceptable during the research. For a commercial DFM system, a more precise match of each electromagnet current may be more appropriate.

The zero system current point was not used as a reference for force measurements, as small force differences would then have to be resolved from the difference between two transducer outputs, one representing the weight of the model on the rig, the other the suspended model plus an external force. For accurate measurement of small aerodynamic

forces, steady suspension of the model with wind *off* was the preferred zero point. Forces and moments acting at a given data point were calculated from the difference in transducer output due to changing the electromagnet currents from the data point - wind *on* -values, to the zero point - wind *off* - values.

Rather than using the feedback method described above to find the zero point current during analysis of each data point, current demands for the zero point were stored at the start of a test series and retrieved as necessary thereafter. This enabled the time interval between taking transducer readings at the data point and at the zero point to be reduced, minimising errors due to ADC drift (Section 9.1). A necessary assumption was that power supply calibration changes during each test were negligible. A separate reading of the transducers at each zero point was required, due to changing zero-force transducer outputs, which are discussed below.

One instance in which the use of a zero-current reference may be appropriate is during the measurement of forces acting on models with soft-iron cores. During DFM analysis of data obtained with an iron propulsion simulator model (Section 7.6), it was necessary to maintain high currents for several minutes, during which time the most heavily used electromagnets became rather hot. The zero force point for an iron propulsion simulator tends to include several high currents, as the burden of model magnetisation is shifted to those magnets not needed for control of the thrust impulse (Section 5.8.1). These magnets become heavily used during steady suspension. Significant time is spent at the reference point during DFM analysis, and the use of a low-current reference in this case would reduce magnet heating, and hence the cooling time required between analyses.

9.3.3 Mechanical effects

Much of the DFM test procedure is concerned with reduction of the effects of friction and mechanical backlash within the rig on the measured forces, with two operations performed at each data point specifically to achieve this aim.

Mechanical backlash can cause a variation in transducer output for zero magnetic force. The zero-force output is governed by the last application of magnetic force experienced, as this determines the final position of the rig components. In an attempt to reduce the effect of the changing zero force point, a 'take up slack' operation is performed for each data point, to move the components to a position where no further change in zero force output will occur under the application of forces in the data point direction. The 'take up slack' involves driving the electromagnets suddenly to approximate data point currents for a brief

period, before returning the currents to zero and commencing the current matching process described above.

Before reading the force transducers at each data or zero point, a current oscillation is performed. A decaying sinusoidal component is added to the steady currents, to overcome static friction and 'relax' the rig into the desired data point state. Presently, a 10 Hz component is faded from a commanded 10 A to zero over around 3 seconds. The actual maximum variation of magnet current is limited to around 2 A by the inductance of the electromagnets, which restricts the rate of change of current (Section 12.5.2). The oscillation process is the DFM equivalent of tapping a barometer, and has many parallels in engineering where the property that a coefficient of dynamic friction often has a lower value than the equivalent static coefficient is applied.

The benefits of the two operations described are illustrated by Figure 9.3. This graph shows the pitching moment for a wind tunnel test of the ogive cylinder model at thirty degrees of incidence, for which the data was re-analyzed with and without the two operations described above. The 'take up slack' operation smooths the data, by reducing random errors in the zero-force measurement. Use of the current oscillation increases the measured pitching moment, by overcoming frictional resistance to the slight motion of the rig components, necessary for force to be transmitted to the transducers.

Some flexibility existed in the rig, and changes in the model position were observed under load. Initial position matching is performed with the electromagnets de-energised, and in some cases model position changed sufficiently with application of the zero point currents that an adjustment was necessary. It was however generally possible to set the model position so that the two significant points for each force measurement - the data point and the zero point - both corresponded to a model position within the limits of position matching acceptability derived in Section 9.2.3 above.

9.3.4 Summary of test procedure

As presently implemented, Direct Force Measurement (DFM) analysis of wind tunnel data is carried out according to the following procedure:

Wind tunnel tests are performed with the model suspended in a single position, and tunnel speed regulated. Data is recorded first with the model in suspension with wind *off*, and subsequently at a number of wind speeds. The speed profile usually consists of several steps up to a maximum speed, followed by repeat points for decreasing speed, and finally a repeat zero-force point. The data for each point consists of the average taken over one

second of ten electromagnet currents, five position measures and tunnel Mach number. After each run this data is stored in a disc file.

To analyze wind tunnel data, the model is mounted in the DFM rig, which is then installed in the MSBS wind tunnel test section. Force measurement is controlled by DFMSOFT, which loads the wind tunnel run-data and informs the operator of the state of the position match. Model position is manually adjusted until a satisfactory match is achieved, after which the magnets are driven until the zero point currents are duplicated, and the power supply demands required to achieve an adequate match of the zero point currents are recorded.

Each data point is analyzed by first performing a 'take up slack', using approximate data point currents. Magnet currents are then accurately matched to the data point values. Currents are oscillated to reduce frictional effects, and the force transducers are read. Following the reading the magnet currents are smoothly slewed to the zero point currents, and a second oscillation is applied. Zero point forces are read, and the difference calculated between the two sets of transducer readings. Force differences are decoded to find lift drag and pitching moment, values of which are then stored for subsequent interpretation. When all data points have been analyzed, a disc file consisting of the forces and moments measured for each tunnel Mach number is created.

Once this test procedure had been developed, and confidence gained in operation of the new equipment, the DFM rig was employed for research into two areas. The first, an examination of the ability of the MSBS control system to generate decoupled force components, is presented in the next chapter. This is followed by a chapter containing an account of an investigation into the aerodynamics of an ogive cylinder at high angles of attack, free from support interference.

10. GENERATION OF FORCE COMPONENTS USING THE ELECTROMAGNET ARRAY

This chapter describes the use of the DFM equipment to improve the generation of forces and moments by the MSBS. The new equipment allowed the effectiveness of the electromagnet array in influencing a model to be measured, whereas previous research relied on estimates of its effectiveness. The results are used to improve the ability of the controller to generate decoupled forces and moments. Methods for optimising force and moment generation are discussed, and applied to a specific wind tunnel test.

10.1 INTRODUCTION

The control system designed by Parker[20], with its unique high angle of attack capability, regulates the position of a model suspended in the Southampton MSBS by separate consideration of the five degrees of freedom controlled. The ability of the control system to generate pure decoupled force and moment components on the model, in each degree of freedom and at any angle of attack, by combining the influence of the available electromagnets, is fundamental to its success.

Generation of force components is dependent on the correct assignment of a number of Demand Distribution Factors (DDFs). These factors determine the ratios by which a demand, say for pure heave motion of the model, is shared amongst the four groups into which the electromagnet array is notionally divided (Figure 2.7). The DDFs are selected so that only the required force or moment component is generated, with minimum coupling to the other degrees of freedom.

The extent to which a magnet group is effective in contributing to provision of force or moment in a specific degree of freedom depends on the position and attitude of the model. For the high angle of attack controller, it is assumed that the small motions available in bodily translation and yaw angle have a negligible effect on group effectiveness. The DDFs are therefore adjusted only in response to changes in pitch angle. Furthermore, as only the lateral electromagnets (group III) possess the capability to generate side force and yawing moment given these motion restrictions, DDFs in the lateral degrees of freedom are made constant. Consequently, the only DDFs required to vary are those governing the generation of force components acting in the x - z plane; namely heave force, axial force, and pitching moment.

Parker derived his DDFs from a study of the effectiveness of the four magnet groups in generating forces and moments at different angles of attack. He then developed a technique for combining the effects to produce the required pure force components without coupling. As no facility was available for making true measurements of group effectiveness, Parker's values were estimated using Britcher's FORCE software[6], described in Section 5.5.

Construction of the Direct Force Measurement (DFM) rig described in the preceding chapters, provided the first opportunity to verify the estimates of magnet group effectiveness, and hence the subsequently derived demand distribution factors. It was anticipated that improvements in the quality of control achieved by the assignment of improved DDFs might benefit the high angle of attack wind tunnel tests to be performed following this investigation. Further aims included the accumulation of operational experience with the DFM rig, and the development of experimental and data analysis techniques.

10.2 DETERMINATION OF GROUP EFFECTIVENESS

Measurements of electromagnet group effectiveness were performed with the DFM rig on the model later used in the high angle of attack wind tunnel test series. This model is shown in Figure 10.1. It is a 145 mm long ogive cylinder having a diameter of 18 mm. The core consists of discs of neodymium-iron-boron permanent magnet alloy, of total length of 100 mm and diameter 12.5 mm. The aerodynamic shell is of aluminium construction. The ratio of the ogive nose radius to the model radius is 5:1.

Effectiveness was measured at 10 degree intervals over the complete pitch range available to the control system; from -10° to 100° angle of attack. The test interval was chosen to match the operation of the high angle of attack controller as recently implemented on the PC. This software presently stores DDF data at 10 degree intervals. Linear interpolation is used to estimate the DDFs for intermediate angles. The spacing interval is a throwback to the limited availability of memory on the previous control computer, and could now be reduced.

The DFM rig, with the model in place, was installed in the MSBS test section. The high angle of attack position sensing system was used to ensure correct positioning of the model. Position signals previously recorded from suspension of the model in the test

attitude were compared to those obtained with it mechanically held in place. The tolerance to which a match in position was required is discussed in Section 9.2.3.

At each attitude the four magnet groups were separately cycled through a range of currents, and the forces exerted on the model recorded. Each group can be driven so as to produce either force or moment components on the model. These actions are described in Section 2.2. Separate tests were thus necessary to determined the effectiveness of each group in production of x - z forces, and in generation of pitching moment.

Testing was automated to the extent that occasional changes to pitch attitude were the only action required of the operator. An experimental procedure was developed to increase the consistency of the data, as described in Section 9.3.4.

10.3 REDUCTION OF DATA

Data analysis was performed using a specially developed software package: REDUCE. Group effectiveness was calculated as the gradient of the *force / current* or *moment / current* curves. REDUCE was developed to allow an examination of the graph for each set of test data. Rogue points could be identified and discarded at this stage, before a least squares fit was used to find the gradient - the effectiveness of the magnet group - for each test.

The effectiveness of each group in the generation of x - z forces and of pitching moment, as measured using the DFM rig, is presented in Figures 10.2-10.4. These results are in wind tunnel axes, and show the force or moment produced per unit current, where the current flows in all members of the electromagnet group. The effectiveness of groups I and II is equal at incidences of 0° and 90°, due to the symmetry of the electromagnet array. Group IV is the most effective in producing an axial force at low incidence. The difficulty in suspending propulsion simulator models at moderate incidence (Section 6.5) is a result of the lift force effectiveness of group III passing through zero close to 30° angle of attack.

To allow a comparison of group effectiveness with the results obtained by Parker using FORCE, the data was scaled to convert effectiveness measured in Newtons / Ampere, into the force produced by the group at maximum current (20 A for each electromagnet in the group). The converted data is presented for comparison with the FORCE predictions in Figures 10.5-10.8.

It should be noted that Parker's effectiveness predictions assume a model core of length 102 mm and diameter 19 mm, with a magnetisation of 1.0 T. The effectiveness measured by the DFM rig is that applying to a core of 100 mm length, having a diameter of 12.5 mm and a magnetisation of approximately 1.2 T. Some discrepancies are inevitable, but a general comparison of the results can still be made.

The overall correlation between the predicted and measured effectiveness is good. For groups I and II, the application of simple scaling factors would bring the results into close agreement. However, the same scaling factor does not apply to each curve, and this disagreement is the source of errors in the generation of force components by the high angle of attack control system, to be described later. The largest error is in the prediction of the ability of the axial magnets (group IV) to generate a force component in the stream direction. This error may originate from the incorrect derivation by Parker of the correction ratio for the axial magnets, to be applied to output from FORCE. This issue is discussed in Section 5.5. Sources of error inherent in FORCE are outlined in ref 6.

Coupling between the production of forces and of moments would ideally be zero, but some coupling was detected during this magnet effectiveness investigation. The coupling might be the result of imperfections in the test technique or the equipment. The coupling effect was generally small compared to the primary force or moment measured. An example is given in Figure 10.9, which shows a small pitching moment detected during a test of group I effectiveness at zero incidence. A number of possible sources of coupling existed during the tests:

An example of an imperfection in test technique was coupling resulting from errors in positioning the model; only in the centre of the test section will the symmetry of the Southampton MSBS allow independent generation of decoupled forces and moments for each electromagnet group. Inaccuracy of current measurement could have contributed to the coupling detected. The DFM equipment represented a further source of error. Inexact calibration of the force transducers or internal friction could have caused the apparent measurement of coupling where perhaps none existed. Asymmetry in the electromagnet array could cause coupling between force and moment generation. It was therefore uncertain whether the detected coupling was caused by hardware anomalies, or whether it was a reflection of limitations in the force measurement procedure.

10.4 DERIVATION OF NEW DDFs

Having measured the effectiveness of the electromagnet array, it was possible to derive a set of demand distribution factors capable of producing truly decoupled force components on a suspended model. The technique employed was similar to that developed by Parker. The equations in this chapter use the symbol η to denote electromagnet group effectiveness in generating force and moment components. ηf represents effectiveness when the group is driven to produce force, and ηm the effectiveness when moment generation is commanded. Each effectiveness measure has two subscripts. The first indicates the identity of the electromagnet group, where i is a general group. The degrees of freedom influenced by the group are indicated by the second subscript as follows: *dof*, a general degree of freedom; N, normal force; T, tangential force; and P, pitching moment.

From ref 20, for a set of DDFs to generate a decoupled force component F in the degree of freedom *dof*, they must satisfy

$$\sum_i \left(DDF_{i,dof}\ \eta f_{i,dof}\right) D_{dof}\ G_{dof} = F_{dof} \qquad \ldots\ 10.1$$

for the force component, and

$$\sum_i \left(DDF_{i,dof}\ \eta f_{i,T}\right) D_{dof}\ G_{dof} = 0 \qquad \ldots\ 10.2$$

to ensure that no tangential force component is produced. D is the control system demand for force based on position error, and G is the overall loop gain implemented in the controller for this degree of freedom and model attitude.

This formulation involves two equations and four unknown DDFs. An infinite number of solutions exist. Following Parker's methodology, a grid search program DDF_SEARCH was developed to investigate possible solutions to Equations 10.1 and 10.2. A scoring system was applied to the data, with the highest-scoring result perceived as offering the best available DDF combination.

The generation of moments was considered by Parker to be independent of force generation. For a perfect MSBS having a symmetrical electromagnet distribution and a centrally suspended model this would be true. Two approaches were applied to the derivation of DDFs for the generation of control moments, and are discussed later.

10.4.1 Magnitudes of DDFs and gains

From the equations above, the control force generated per unit demand is given by

$$\frac{F_{dof}}{D_{dof}} = \sum_i \left(DDF_{i,dof}\, \eta f_{i,dof}\right) G_{dof} \qquad \ldots 10.3$$

Parker identifies the desirability of separating the roles of DDF and loop gain in the controller. His intention is to use loop gain to determine the force per control system demand, whilst DDFs only control the distribution of force component generation among the electromagnet groups. He uses

$$\sum_i DDF_{i,dof} = k \qquad \ldots 10.4$$

in his solution, in an attempt to achieve a decoupling, where k is a constant value for each degree of freedom, and the value 4.0 is arbitrarily chosen for convenience. This solution neglects to consider the variability of group effectiveness. The result is that force per controller demand becomes dependent on both angle of attack, and the particular combination of DDFs chosen during a grid search. For the effect of loop gain to be truly independent of DDFs, we need

$$\sum_i \left(DDF_{i,dof}\, \eta f_{i,dof}\right) = k$$

This formulation achieves the required separation of the rôles of loop gain and DDF, and should therefore be used in the DDF selection process.

As a result of the approach adopted by Parker, the values of force per unit demand used in the high angle of attack controller varied with angle of attack. To allow a direct substitution of new DDFs for old during the investigation into magnet effectiveness, it was necessary to match the existing variation in force per unit demand. The match was achieved by including a routine to evaluate force per control system demand for Parker's DDFs at each angle of attack in the DDF_SEARCH software. These values then became the required force per demand during the grid search.

Changes in the magnitude of the overall force vector produced by Equation 10.4, reduce the smoothness of the DDFs derived. To illustrate this point, Figures 10.10a-d show two sets of demand distribution data. The first DDFs are those presently employed in the Southampton MSBS, and change more rapidly with angle of attack than the second set, selected to produce a constant magnitude force vector of 250 mN in response to a unit demand at any angle of attack. Parker[20] found that large changes in DDF degraded the quality of control. Implementation of the constant-demand DDFs could be achieved by an appropriate scaling of the loop gains for each angle of attack. Scaling the loop gain by

$$G_{new} = G_{old}\, \frac{(F_{dof}/D_{dof})_{const}}{(F_{dof}/D_{dof})_{var}}$$

would ensure that the overall force per unit demand at each angle of attack was unaffected by the change to constant-demand DDFs. Lack of time has so far prevented such a modification. Further possible control software development is discussed in Section 12.5.7.

10.4.2 Scoring system

The scoring system used during this investigation to make a selection from the possible DDF combinations was developed from that used by Parker. During the grid search for the most suitable DDFs to use at a particular attitude, Parker looked for those DDFs capable of producing the largest force component. Maximum force is reached when the first electromagnet reaches its maximum current. As the current in a group in response to a demand for generation of a control force is given by

$$i_i = DDF_{i,dof}\, D_{i,dof}\, G_{dof}$$

it follows that

$$D_{MAX} \propto \frac{i_{i,MAX}}{DDF_{MAX}}$$

where i_{MAX} is approximately 20 A for all ten electromagnets of the Southampton MSBS. Maximum force is thus inversely proportional to the largest DDF of each trial set, so Parker's grid search effectively sought to minimise the value of the largest DDF.

This test tends to favour solutions where several DDFs have a moderate value, rather than concentrating on the use of the magnet group which is most effective in generating the required force or moment. The total system current therefore tends to be high, and the ability to concurrently generate other force and moment components, or to magnetise an iron model, is reduced. A test was therefore developed which aimed to shift the emphasis of the control strategy toward more 'efficient' use of the electromagnets.

From Equation 10.3, the total MSBS electromagnet current resulting from a force demand in component *dof* can be expressed as

$$i_{MSBS,dof} \propto \sum_i \left(DDF_{i,dof}\right) D_{dof}$$

A test seeking to reduce system current should therefore minimise the sum of DDFs for each force component. A test was derived which sought to combine the attributes of low system current and high force capability, by reducing the value of the ratio

$$\frac{\sum_i DDF_{i,dof}}{DDF_{MAX,dof}}$$

To illustrate the effects of the change in DDF selection criteria, Figures 10.11a and 10.11b show the range of force capability and force generation efficiency for the heave and axial force components over the available angle of attack range, for DDFs generated using the old and new techniques. Efficiency in this instance is measured as the force produced per unit electromagnet current. The differences between the two sets of results are not large, at some angles the same DDFs are selected using either selection criteria. However, the trade-off between peak force generation and power consumption is illustrated.

10.4.3 Derivation of DDFs with a three component solution

Initially a solution to Equation 10.1 was attempted using three equations and a single parameter grid search to find the four unknown DDFs. In addition to generating the required pure force component, this technique endeavoured to eliminate the coupling between the production of forces and of moments described in Section 10.3 above. For example, generating a pure normal force without an associated tangential force or moment, would require a simultaneous solution of

$$\sum_i \left(DDF_{N,i}\ \eta f_{N,i}\right) = F_{N,dof} \qquad \ldots\ 10.5$$

$$\sum_i \left(DDF_{i,N}\ \eta f_{i,T}\right) = \sum_i \left(DDF_{i,N}\ \eta f_{i,P}\right) = 0 \qquad \ldots\ 10.6$$

The equations for the generation of the tangential force component can be obtained by transposing T and N in the above. The three component solution for pitching moment generation is based on

$$\sum_i \left(DDF_{i,P}\ \eta m_{i,P}\right) = P_{dof} \qquad \ldots\ 10.7$$

$$\sum_i \left(DDF_{i,P}\ \eta m_{i,N}\right) = \sum_i \left(DDF_{i,P}\ \eta m_{i,T}\right) = 0 \qquad \ldots\ 10.8$$

Given three equations and four unknowns for each case, the grid search for the best DDF solution required the examination of only one sequence of results. These were generated by DDF_SEARCH, which cycled a single DDF through a range of possible values, solving Equations 10.5 and 10.6 for a force, or Equations 10.7 and 10.8 for a moment at each point. The best of the candidate sets of DDFs were selected using the new scoring system.

DDF selections based on the three degree of freedom grid search were not successful. The attempt to eliminate coupling between forces and moments led to the generation of unusable DDFs, in that electromagnet groups were commanded to work in strong opposition in an attempt to balance out a small coupling while still satisfying the equations. The inconsistency of the coupling results, their insignificance in comparison to

the primary forces, and uncertainty as to whether real couplings or DFM rig errors were being detected (Section 10.3), led to the rejection of this technique.

10.4.4 Derivation of DDFs with a two component solution

Thereafter, the coupling between the generation of forces and moments was assumed to be negligible. Specifically it was assumed that

$$\eta f_{i,P} = \eta m_{i,N} = \eta m_{i,T} = 0$$

This separated the selection of DDFs for x - z plane forces, and for pitching moment. The selection process now resembled that employed by Parker, whereby heave and axial DDFs were found using a two-component grid search technique, and pitching moment DDFs by direct assignment.

Demand distribution factors for the x - z plane were chosen using DDF_SEARCH, modified to perform a two-parameter grid search. Selection of DDFs was based on the scoring system described above, designed to favour those DDFs giving a high force capability combined with efficient use of the electromagnet array. Force per unit demand was matched to the existing values as discussed. This matching allowed a direct substitution of new DDFs for old in the control software, and hence a straightforward comparison of their operation.

The effectiveness of the four electromagnet groups in producing pitching moment was described in Section 10.3 and shown in Figure 10.4. Parker discusses strategies for the assignment of demand distribution factors for the generation of pitching moment in the following manner:

Maximum pitching moment is obtained if all groups are always used, regardless of their effectiveness. The most efficient use of the limited current capability of the electromagnet array is achieved if only the most effective group is employed. An alternative is to scale the demand to a particular group in proportion to its ability to generate pitching moment. This procedure represents a compromise between maximum moment capability and efficient use of the electromagnets. A proportional distribution is thus consistent with the strategy of Section 10.4.2, used to generate force components in the x - z plane, and was consequently chosen for generation of the new pitch DDFs.

Parker restricted the generation of pitching moment to the vertical electromagnets - groups I and II - for simplicity, and in response to uncertainty over the accuracy of the estimates of group effectiveness obtained using FORCE. Having measured the true group effectiveness, and to relieve the vertical magnets in view of their extensive role in

suspension, the generation of pitching moment was now extended to the other magnet groups.

The selection of DDFs for pitching moment, if it is assumed that driving the electromagnets to produce a moment leads to no coupled generation of force components, does not require a computerised grid search. The assignment

$$\sum_i \left(DDF_{i,P}\ \eta m_{i,P}\right) = P_{dof} \qquad \ldots\ 10.9$$

is made for each angle of attack, where P_{dof} is the required pitching moment per unit demand. To allow simple substitution of the new pitch DDFs, this value was matched to that already in use at different angles of attack, following the method of Section 10.4.1. Pitch DDFs were assigned in direct proportion to effectiveness:

$$\frac{DDF_{i,P}}{\eta m_{i,P}} = k$$

Substituting this relationship into Equation 10.9 gives

$$DDF_{i,P} = \frac{\eta m_{i,P}\ P_{dof}}{\sum_i (\eta m_{i,P})^2}$$

The high angle of attack controller was modified to allow pitching moment generation using all four electromagnet groups. The new pitch DDFs, shown in Figure 10.12, were implemented without complication.

10.5 OPTIMISATION FOR A SPECIFIC CASE

Parker observed that a selection of DDFs based on, for instance, the provision of maximum force components, is limited in that the maxima for the two perpendicular forces cannot be achieved simultaneously. During a demand for a combination of the components, the maximum force available will be that in which the sum of the demands just causes one of the electromagnets to reach its maximum current. The circumstances in which this limit is reached depend on the combination of the two components requested, and on the concurrent use of the electromagnet array to control other degrees of freedom.

The discussion continues with the premise that further optimisation of DDFs is pointless without knowledge of the particular test conditions to which the data is to be applied. An agile fighter aircraft is presented as an example, where an ideal set of DDFs would maximise MSBS force capability in the direction of the resultant aerodynamic force. This

direction is related to the lift to drag ratio, as illustrated in Figure 2.1e, and is therefore angle of attack dependent. Model weight is regarded as secondary in magnitude to aerodynamic force, and is neglected.

Parker suggests two techniques for optimisation in this case. The first involves a lengthened grid search which begins by finding demand distribution factors for the normal force component for a particular attitude. The force capability in the direction of the aerodynamic resultant is then calculated for various trial values of tangential DDF. The maximum resultant force is then compared to that estimated for other trial DDF combinations.

The second technique employs a control system operating in an axis system based on the direction of the resultant aerodynamic force. Magnet effects are transformed into these axes and a regular DDF search performed. The maximum force in the resultant direction is found. Generation of tangential forces does not detract from the ability to generate the normal (aerodynamic resultant) component, since the tangential forces experienced will be small by definition. A complication of this solution is the use of model-dependent control system axes.

An improvement to this idea would be the transformation of the resultant axes DDFs back into model axes. The full process of DDF selection would thus involve an initial transformation of magnet effects into the axes of the aerodynamic resultant, an independent optimisation of normal and tangential force as discussed in Section 10.4.2, and a final transformation of the new DDFs back into control system axes.

This methodology was used to optimise the DDFs for the case of the ogive cylinder model (which is not a propulsion simulator), tested over a large angle of attack range as described in the following chapter. In this instance it was not sensible to discount the effect of model weight, given the relatively small aerodynamic forces generated at the low Mach numbers available in the Southampton MSBS wind tunnel.

The resultant force acting on the model is the vector sum of lift, drag and model weight. Weight is constant, so once the lift and drag coefficients are known, the direction and magnitude of the resultant can be calculated for any tunnel speed. Maximum controllable speed is defined as that at which provision of a restraining force just causes an electromagnet to reach its limiting current.

Optimisation of DDFs with tunnel speed as a new factor was achieved by including speed as an additional variable in the existing grid search software DDF_SEARCH. For each imaginary speed increase, the direction of the resultant force was calculated from the model weight and its measured lift to drag ratio, and the effectiveness of the electromagnets transformed into resultant axes. DDFs were conventionally derived, and the notional tunnel speed increased until no solution could be found within the limitations of electromagnet current.

This approach can be visualised as a search within a maximum force envelope, surrounding the suspended model for a given angle of attack, as shown in Figure 10.13. The envelope illustrates the maximum magnetic force available to control or restrain the model in any direction. Here the x - z plane - that under investigation in this instance - is shown. The DDF search for maximum tunnel speed involves finding the point at which a vector in the lift + drag direction, offset by the model weight vector, just touches the maximum force boundary.

10.5.1 Use of aerodynamically optimised DDFs

Having derived a set of DDFs intended to maximise force capability for the ogive cylinder model, an attempt was made to use the new values to expand the test envelope described in the following chapter.

It became clear that in the region from 70 to 100 degrees angle of attack, where the new DDFs were expected to yield increased maximum test speeds, stability limits rather than maximum electromagnet currents were defining the maximum achievable tunnel speed, and no real benefit could be demonstrated from the optimised values. As will be described in Section 11.5.4, in these regions of the test envelope, the ogive cylinder experiences vortex shedding at a frequency similar to the control loop rate, and the frequency matching was seen to cause control problems. Evidently, the maximum force envelope calculated for static aerodynamic loads was not applicable under strongly dynamic conditions.

Only a theoretical demonstration of the advantages of aerodynamically optimised DDFs is therefore possible. An indication of their potential is shown in Figure 10.14. This graph shows the predicted maximum wind tunnel test speed in the Southampton MSBS for the ogive cylinder over a large angle of attack range, assuming steady loads. The maximum test speed is calculated as that at which the first electromagnet group just experiences its limiting current, when a force is commanded to counter the appropriate aerodynamic and gravitational effects on the model.

At low incidence the maximum tunnel Mach number is not sufficient to make use of the increased force capability. At moderate incidence the resultant of lift, drag and weight is approximately aligned with the heave vector in model axes. The conventional DDF selection maximises this force component, and little benefit is gained from the optimised DDFs. At high angles of attack, the force-optimised DDFs promise a modest increase in test Mach number under steady loads.

10.6 EXPERIENCE WITH THE NEW DDFS

No problems were encountered in substituting the DDFs based on measured magnet effectiveness, for those found from computer estimates. An immediate improvement in the control of the ogive cylinder was apparent in that suspension was now possible from -9° to 99° angle of attack, compared with -7° to 97° using the old DDFs. The new maxima reflect the limits of the control software, which is programmed to allow control between −10 and 100 degrees of incidence. Suspension at the absolute extreme angles is prevented by the possibility of a disturbance taking the model beyond the limit of controllable pitch. Further expansion of the angle of attack range could be achieved by making minor modifications to the control and position sensing software. Ultimately the extremes of incidence would be limited by the viewing range of the position sensing system, and the inability of the present electromagnet array to generate sideforce at incidences close to −60° and 120°.

It was possible to quantify control improvements gained by the use of the new DDFs, by measuring the coupling between supposedly perpendicular control forces in the x - z plane. With the model and DFM rig installed in the MSBS test section, demands for heave and axial force at different angles of attack were sent to the electromagnet array, and the actual forces generated were measured. Coupling was calculated as the ratio of any detected coupling force to the primary force, and is shown in Figures 10.15a and 10.15b for the old and new DDFs respectively. A coupled force up to 60 % of the magnitude of the primary force was detected at some incidences using the old DDFs. The source of these errors lies in the incorrect assumptions of electromagnet effectiveness introduced in Section 10.3 above. It was possible to predict the level of coupling using the old DDFs and the measured effectiveness of the electromagnet array. The good agreement between the predicted and measured coupling illustrates consistency in the results obtained using the DFM rig.

Errors in the use of the rig caused the small couplings of Figure 10.15b, obtained using the new DDFs. Possible sources of error include transducer calibrations and rig friction. It was possible to reduce the coupling by performing repeat tests, in which effectiveness measurements, DDF generation and coupling assessment were performed in quick succession. This procedure was used to generate the data of Figure 10.15c, which shows coupling between force components reduced to a maximum of 6 % from the original 60 %. This figure also illustrates the degree of accuracy to which the primary force components are generated. The *force ratio* is the ratio of the force component demanded to that measured. The maximum error is again close to 6 %, this value perhaps being indicative of the overall level of accuracy achieved with the DFM equipment.

The assertion by Britcher[8] that a typical MSBS tends to be force-limited rather than moment-limited is supported by recent experience with the Southampton system. During the course of this research, numerous instances of a force limit were encountered, but on no occasion was a control problem attributed to a limited capability for the generation of moments.

Having improved the quality of control of the ogive cylinder model, and gained further experience in using the DFM rig to the measure forces and moments acting upon it, it was now possible to apply the new balance capabilities of the Southampton MSBS to an aerodynamic investigation. The behaviour of low-speed flow around the ogive cylinder model was studied, free of support interference, and over a large angle of attack range. This work is presented in the next chapter.

11. HIGH ANGLE OF ATTACK WIND TUNNEL TESTS WITH AN OGIVE CYLINDER

The new capability provided by the DFM apparatus, to measure the aerodynamic forces acting on a suspended model at any angle of attack, is proven during a series of wind tunnel tests. The low-speed aerodynamics of an ogive cylinder are introduced, and the results of wind tunnel tests performed with such a model are compared to published data. The effect of surface roughness on effective Reynolds number is demonstrated.

11.1 INTRODUCTION

Investigation of the flow around a two-dimensional circular cylinder in crossflow is a classic area of study in aerodynamics. An ogive cylinder at high angles of attack is a very similar equivalent case in three dimensions, and a substantial research effort has also been devoted to this flow regime.

The circular cylinder at low speed in crossflow has many parallels in aircraft design. Some, such as bracing wires or permanently exposed undercarriage struts, are of decreased relevance today. However in some instances, such as the case of an aircraft fuselage during a spin, the assessment of forces during crossflow over a cylinder remains vitally important.

The tactical benefits of high manoeuvrability for missiles and fighter aircraft are universally acknowledged. The advent of digital flight control systems able to allow flight at incidences beyond the stall has led to a resurgence of interest in the behaviour of a cylinder-nose combination at a high angle of attack to an airflow. Flight vehicles tend to be limited in maximum sustainable g-loading, and at lower speeds a high normal force coefficient is required to achieve the maximum normal acceleration. The need for high angles of attack is therefore greatest during subsonic flight.

Research into this area of aerodynamics has addressed a number of issues. These include the causes and consequences of the different flow regimes that are observed, the effects of test conditions such as model geometry, surface condition, Reynolds number and Mach number, and the influence of the model support apparatus on the results obtained. A summary of results to date is presented below.

A suitable case for aerodynamic investigation was required to develop and demonstrate the capabilities of the Direct Force Measurement (DFM) rig introduced in the previous chapters. Tests on an ogive cylinder model were attractive for a number of reasons:

- An ogive cylinder model was available.

- The model was suitable for testing over a large angle of attack range, and would allow the first use of this capability in an MSBS to generate useful wind tunnel data.

- Without active roll control, testing of a non-axisymmetric model would present control problems.

- The case of an ogive cylinder is often cited as an example of a wind tunnel test subject to support interference, as justification for proposed further MSBS development[16].

- The proposed tests would ably demonstrate the improvements made during this research program to the control system, data acquisition capacity, wind tunnel hardware and force measurement capability.

It was decided to test the ogive cylinder model over a wide range of tunnel speeds and incidences, using the DFM rig to derive lift, drag and pitching moment from the data recorded.

11.2 SUBSONIC FLOW OVER AN INCLINED OGIVE CYLINDER

The flow over an ogive cylinder undergoes a number of changes with angle of attack, and is also influenced by other parameters, as will be described.

11.2.1 Low incidence: Typically 0-30 degrees

At zero incidence, laminar flow can be expected over an ogive nose, with a transition to a turbulent boundary layer occurring at some point along the body. At moderate incidence the flow soon separates from the body. The detached shear layers roll up to form a pair of stable vortices, which originate downstream of the nose and persist into the wake. These vortices initially have a symmetric arrangement, and contribute vortex lift to the

aerodynamic forces acting on the ogive cylinder. Figure 11.1a shows a vortex arrangement of this type. For convenience a pointed nose geometry is illustrated.

11.2.2 Moderate incidence: Typically 30-50 degrees

Beyond an angle of attack known as the *onset angle*, which depends on model geometry and the flow conditions, the vortices shift to an asymmetric arrangement, which is first observed at the downstream end of the body. One vortex moves closer to the model, and both move closer to the x - z centre-line (Figure 11.1b). Increasing the angle of attack beyond the onset angle causes the origin of the asymmetry to gradually move up the body towards the nose.

The uneven pressure distribution around the model resulting from the new asymmetric flow regime results in a lateral aerodynamic force, so onset angle can be determined by monitoring the first manifestation of sideforce as angle of attack is increased. The polarity of the sideforce depends on the orientation of the vortex arrangement.

It is generally accepted that the choice of which alternative asymmetric vortex arrangement occurs is determined by imperfections in the model nose shape, which may be of microscopic dimension[50]. Roll orientation of the nose therefore determines the trailing vortex arrangement, even when the flow over the nose itself appears symmetric. Moir[51] elegantly demonstrates this effect by using an ogive cylinder model which allows rotation of the nose relative to the body. As the nose-body combination is rolled through 360 degrees, changes in the vortex asymmetry cause variation of sideforce with a characteristic signature as shown in Figure 11.2. Repeating the experiment with the nose displaced by a given angle causes the sideforce signature to be similarly displaced.

Moir assumes that small disturbances are produced in the apparently symmetric flow over the nose, and persist downstream to cause subsequent asymmetric flow over the body. Modi and Stewart[51] show that a rapidly spinning nose tip can reduce sideforce by 25-71 percent, with the direction of tip rotation determining the polarity of the residual sideforce. Spin rates of around 2000 rpm are used. In their experiment, sideforce became independent of roll attitude, and was experienced even at very low incidence as a tip Magnus force.

Degani[52] reviews a number of publications, showing that at angles of attack above the onset angle, the flow asymmetry at first varies continuously with roll attitude. At crossover points the vortex configuration becomes almost symmetric. A maximum asymmetry exists for a particular model configuration. Computational work using Navier-Stokes equations

suggests that the flow is initially symmetric but convectively unstable, the implication of this instability being that any disturbance in the flow causes a rapid growth in asymmetry downstream.

Canning and Nielsen[53] investigated the relationship between sideforce and the other force components. Normal force coefficient is seen to vary by up to 30 percent during a 360° roll manoeuvre, and generally increases with the magnitude of the sideforce. Axial force tends to diminish slightly with increasing sideforce.

11.2.3 High moderate incidence: Typically 50-65 degrees

As described by Moir[51], increasing the angle of attack beyond the onset angle leads to greater separation between the body and the trailing vortex pair. Eventually a second vortex system forms in the resulting gap, sourced at points referred to as foci further downstream along the body. If the body has sufficient length, more vortices develop at progressively higher angles of attack. Eventually a series of vortex pairs exist, of alternate orientation, and the total sideforce experienced is determined by their overall effect.

Degani[52] identified a higher angle of attack region, where continuous variation of sideforce with nose roll attitude ceases. The trailing vortex system developed a bistable nature, flipping between two opposite asymmetric states as roll attitude was changed. The sideforce signature then approached an irregular square wave.

Degani and Zilliac[54] investigated unsteadiness in the wake of an ogive cylinder using hot wire anemometry, pressure transducers and flow visualisation. Power spectra of the unsteadiness frequencies were produced for a large angle of attack range. In the range associated with the bistable flow regime, an unsteadiness was observed having a Strouhal number approximately double that of von Kármán vortex shedding. Degani et al[55] suggest that the phenomena of vortex flipping and higher frequency unsteadiness are linked to the appearance of foci in the surface flow patterns, and subsequent *vortex interaction* between the pairs of trailing vortices.

11.2.4 High incidence: Typically 65-90 degrees

Any further increase in the angle of attack leads to instability in the wake, which subsequently exhibits the classic von Kármán periodic vortex shedding of a cylinder in crossflow. Vortex shedding rapidly becomes the dominant feature of the flow, and the vortex interaction effect diminishes. The mean sideforce during vortex shedding is almost zero. As the angle of attack approaches 90 degrees, so the flow approximates that around a two-dimensional circular cylinder.

Strouhal number S is used to characterise periodic wake phenomena. For a circular cylinder of diameter d in a crossflow ($\alpha = 90°$) of velocity v, which is shedding vortices at frequency f, it is generally accepted from experimental results that

$$S_{90} = \frac{fd}{v} \approx 0.21 \qquad \ldots 11.1$$

At incidences approaching 90 degrees, the crossflow velocity component varies with the sine of the angle of attack. It has been confirmed that for an axisymmetric body at an incidence where vortex shedding is observed

$$S_{\alpha} \approx S_{90} \sin\alpha \qquad \ldots 11.2$$

Champigny[56] uses this relationship in an attempt to explain the spacing of stable vortex pairs at lower incidence. The spacing is measured by examining the surface pressure distribution along the body of an inclined ogive cylinder. He postulates that the arrangement of vortex pairs is similar to a stable von Kármán vortex street. The period T of vortex shedding is given by

$$T = \frac{1}{f} \approx \frac{d}{S_{90} v \sin\alpha}$$

during which time the flow component along the ogive cylinder axis travels a distance x given by

$$x = T v \cos\alpha$$

The vortex spacing appears to be related to model diameter and

$$\frac{x}{d} \approx \frac{1}{S_{90} \tan\alpha}$$

Champigny shows that this relationship gives a fair match with the observed spacing of vortex foci.

11.2.5 Effect of nose shape and fineness ratio

Nose shape has been shown to have a number of effects on the flow over an axisymmetric body at incidence. The relationship between surface features on the nose and the orientation of trailing vortices has been discussed above. Canning and Nielsen[53] demonstrated that it was possible to control the generation of sideforce by deliberately adding a dominant feature to the nose, to overwhelm the effects of nose micro-imperfections on the trailing vortex asymmetry.

Moir[51] considers the effect of nose shape, particularly of apex angle, on sideforce onset incidence. The common assertion is that onset of sideforce occurs as the angle of attack reaches the nose apex angle

$$\alpha_{onset} = \theta_{apex}$$

and this equality is found to hold for bodies with a low fineness ratio - the ratio of length to diameter - below approximately 5. With low fineness ratio, the model geometry approaches that of an isolated nose, and flow asymmetry does not generally develop below an angle of attack equal to the apex angle.

For a model with a longer body, flow asymmetry is observed at the tail at low incidence, extending towards the nose with increasing incidence. At an angle of attack approximately equal to the nose apex angle, the asymmetry reaches the nose. Apex angle therefore influences the rate of forward propagation of flow asymmetry with increasing angle of attack.

An ogive cylinder with a high fineness ratio approaches the case of a blunt cylinder at incidence, as described by Sarpkaya[57] who suggests that the onset angle for a blunt cylinder is related to fineness ratio by

$$\alpha_{onset} = \tan^{-1}\left(\frac{4d}{l}\right)$$

Moir concludes that for a general ogive cylinder, development of flow asymmetry and sideforce is influenced by both nose shape (including geometry and surface condition) and fineness ratio.

11.2.6 Effect of Mach number

Flow asymmetry and sideforce are experienced by an inclined ogive cylinder primarily at low Mach numbers. These phenomena decrease at Mach numbers greater than 0.4 - the critical Mach number - falling almost to zero in a sonic flow. Normal force coefficients rise sharply with Mach number at moderate incidence[53]. The effect is reduced at very high angles of attack[58].

11.2.7 Effect of Reynolds number

The effect of Reynolds number on the drag of a two-dimensional circular cylinder in crossflow is well documented. In the absence of Mach number effects, transition from laminar to turbulent flow around a smooth cylinder occurs between Reynolds numbers of 0.2 and 2 million[59], with the critical Reynolds number having a value between 0.2 and 0.5 million, depending on surface condition and wind tunnel turbulence. In transient Reynolds number flows, drag coefficient drops to a minimum, before recovering at supercritical Reynolds numbers.

Champigny[56] investigated the effects of Reynolds number based on diameter, on the normal force coefficient (C_N) of an ogive cylinder over a large angle of attack range. He found that at low angles, up to about 25 degrees of incidence, C_N was unaffected by flow Reynolds number. At higher angles, the C_N curves for the different Reynolds numbers diverge, with high force coefficients obtained for both low and high Reynolds numbers, but low coefficients for transitional flows. At these angles the relationship between force coefficient and Reynolds number is similar to that for a cylinder in crossflow, but retains its dependence on angle of attack. Champigny's results are reproduced in Figure 11.3.

The effect of Reynolds number on sideforce onset angle was explored by Moir, whose preliminary results suggest that onset angle is increased for subcritical flows. Sideforce coefficient appears to be reduced at transition Reynolds numbers.

11.2.8 Effects of surface roughness and flow turbulence

Increased roughness and turbulence both appear to cause the flow to simulate a higher stream Reynolds number. Where the wake configuration is sensitive to details of nose geometry, changes due to polishing or handling a model can have a major effect on its characteristics. Surface flow visualisation using an oil-based mixture can also cause a change in the flow[55]. The coating appears to increase the effective surface roughness when applied to a smooth model.

11.2.9 Support interference

A number of authors have investigated the technique for reducing the drag of a circular cylinder in crossflow of using a 'splitter plate'[60]. This is a thin strip of material aligned with the cylinder axis, and positioned just downstream as shown in Figure 11.4a. The plate disrupts the interaction between shear layers shed from either side of the cylinder, and affects the size and Strouhal number of the wake. The size and position of the plate influences the wake behaviour, and drag reductions of around 30 percent are possible for flows at subcritical Reynolds numbers.

The case of a circular cylinder with a splitter plate downstream is analogous to a wind tunnel test of an ogive cylinder at high angles of attack, where the model support is a strut as illustrated. A suitable analogy for the alternative physical support technique using a sting, might be that it increases the effective fineness ratio of the model, and could modify the flow behaviour described in Section 11.2.5 above. The similarity between a sting installation and an increased fineness ratio is demonstrated by Figure 11.4b.

Investigations into support interference on ogive cylinder tests[53,58] conclude that a sting support is the least disruptive option. The vortex configuration just downstream of the cylinder at incidence is the dominant feature of the flow, and the disruption caused there by a strut has a major effect on the values of force coefficient measured.

Canning and Nielsen[53] attempted to quantify the interference of the two support methods by measuring the force changes caused by the proximity of a dummy strut or sting to an ogive cylinder. At high angles of attack these measurements were themselves affected by interference, as the wakes of the strut and sting coincided. The difficulty in eliminating support interference for this type of test is often cited in support of further development of magnetic suspension systems for wind tunnel research.

11.3 WIND TUNNEL TESTS

The ogive cylinder model used in these tests is described in Section 10.2 and illustrated in Figure 10.1. Control of the MSBS had already been implemented on the PC at this stage of the research program, allowing automated control of wind speed and giving a number of other new test capabilities detailed in Section 12.4.2.

The chosen test procedure was to vary the tunnel speed in steps over a suitable speed range, with the model suspended at constant incidence. The constant incidence approach was taken to promote rapid data reduction using the DFM rig, because with tunnel speed the only variable it was not necessary to manually adjust model position in the rig between data points. As suspension of the model is not presently possible concurrently with data storage to disc, it was necessary to stop the tunnel and retrieve the model between tests at each angle of attack. The use of a separate disc file for each test simplified the handling of data during data reduction.

Tests were conducted over an incidence range of -5 to 95 degrees. An incidence spacing of 5 degrees was chosen, representing a compromise between experimental workload and continuity of results. Two data acquisition techniques were available: continuous storage of data over a total period of up to 25 seconds, or the recording of a large number of data points, each obtained by averaging continuous data over a pre-selected time period.

Storage of data recorded at a number of points was the preferred option for the high angle of attack wind tunnel tests. Discreet, rather than continuous data, is compatible with the DFM analysis procedure presently implemented. A one second averaging period was

selected to smooth any random system noise, without seeking to disguise the irregular force fluctuations associated with the complex, low frequency periodic motion observed at some incidences. Sixteen items of information were stored: ten electromagnet currents, five position measures and wind tunnel speed.

11.4 DATA ANALYSIS

The DFM rig was successfully used to reduce the wind tunnel test data and yielded lift, drag and pitching moment for each data point. In some cases the drift in transducer output described in Section 9.1 led to erroneous results, and repeat reductions were performed to ensure that force data from the different tests was truly comparable.

Another potential source of error was due to the use of the DFM rig to measure x - z plane forces in the presence of a strong lateral force component. The issue of coupling between measured forces is discussed in Section 9.2.4. Furthermore, as described in Section 11.2.2 the magnitude of the sideforce affects that of the heave and axial force components. At moderate incidence, sideforce was observed to vary in an irregular fashion with a period greater that during which data was recorded. Scattering in the measured forces would therefore be expected, as the data would represent a random average of a non-integer number of oscillations. The data recording interval was not increased to encompass a large number of sideforce cycles, as the irregularity of the oscillation would invalidate the concept of an average force.

Measured values of lift, drag and pitching moment were processed to find the force coefficients, and later to find the coefficients in model axes, using a modified version of the REDUCE data analysis program described in Section 10.3.

11.5 RESULTS OF HIGH ALPHA TESTING

11.5.1 Low incidence: 0-25 degrees

At low angles of attack it was possible to suspend and control the model without difficulty over the available speed range. With automatic speed control, the range of tunnel Mach numbers was 0.02 to 0.185.

Forces and moments measured using the DFM rig for a typical low incidence wind tunnel test are shown in Figure 11.5a. The good agreement between values recorded for

increasing and decreasing Mach number increases confidence in the validity of this data. In Figure 11.5b these values have been converted into coefficient form, based on the frontal area of the model at zero incidence. The increased scatter of the data at low speed could be due to errors in speed measurement, which would be magnified by the $1/v^2$ function used to derive the coefficients.

11.5.2 Moderate incidence: 30-45 degrees

Lateral force was first observed at 30 degrees. At this attitude and thereafter, a roll to sideforce coupling was observed which dominated testing at moderate angles of attack.

An axisymmetric model with a cylindrical core is unrestrained in roll in the Southampton MSBS, and tends to adopt a preferred roll attitude at each angle of attack which is governed by imperfections in its distribution of mass and magnetic material. Following a disturbance, such as launching the model or changing its position in suspension, any roll displacement causes a roll oscillation, damped very lightly by eddy currents in the model and by skin friction. At moderate angles of attack, the range of roll attitudes included in an oscillation could cause rapid changes in the aerodynamic sideforce experienced by the model. It was assumed that the mechanism discussed in Section 11.2.2 above was responsible, where the trailing vortex configuration is dependent on model attitude. A change in sideforce tended to result in transient lateral motion, quickly suppressed as the controller reacted to the new conditions.

Often the lateral response would excite further roll motion. An irregular cycle of lateral motion connected with a sustained roll oscillation was generally the result. In some instances roll was excited to the extent that the model would begin to spin. The rapidly fluctuating lateral forces acting on the model during a spin made control difficult, and it was often necessary to shut down the tunnel at this stage to prevent a loss of suspension. Spin rate never reached a sufficiently high value that the sideforce could be regarded as a steady Magnus force, as observed by Modi and Stewart for a spinning nose tip (Section 11.2.2). Attempts to avoid residual roll motion by careful launching and positioning of the model were only partially successful, because other factors also acted to cause this motion.

Changes in the preferred roll attitude of the model were observed with tunnel speed, and sudden speed changes were seen to cause a roll oscillation. It is assumed that the centre of gravity, aerodynamic centre and magnetic centre were neither coincident nor all situated on the model axis. Changes in the aerodynamic forces and average electromagnet currents at different tunnel speeds could therefore affect the steady roll attitude of the model. As a result roll position and consequently sideforce were subject to change during a test, and

the changes could excite the irregular motion described above, or cause a rapid spin-up in roll.

11.5.3 High moderate incidence: 50-65 degrees

Control difficulties due to the changing sideforce, and the increasing aerodynamic forces experienced by the model at higher incidence, reduced the maximum safe tunnel speed as angle of attack increased further. At 45 degrees the maximum Mach number was around 0.1. Between 50 and 70 degrees of incidence more severe buffeting was observed, and initially it was not possible to subject the model to tunnel speeds above Mach 0.06 without risking a loss of suspension. This change in behaviour was attributed to a transition from the smoothly varying wake asymmetry experienced at low moderate incidence, to the bistable flipping of the trailing vortex arrangement, described in Section 11.2.3 above.

An improvement in lateral performance was achieved by changing the control laws used to regulate slip and yaw motion. The control algorithms for these two degrees of freedom were modified from dual phase advance to multiple phase advance, following an investigation by Futter[61]. He found that an improvement in suspension stiffness could be achieved by this change. Multiple phase advance control was not extended to the other controlled degrees of freedom because of the computing overhead. The changes made to the controller are described in Section 12.5.4.

Some further benefit in lateral control was obtained by changing the axial position (in model axes) of the suspended model for some tests at high moderate incidence. Commanding a positive axial displacement of up to 10 mm brought the forward part of the magnetic core centrally between the forward lateral electromagnets. The mechanism by which this change yielded an improvement in lateral control is probably related to increased effectiveness of the lateral magnets in producing sideforce on the relocated core. A change in the relative effectiveness of the forward and aft lateral magnets with position may also have been a factor. Closer proximity of the model nose to the top wall of the test section, as a result of the axial position change, is not thought to have affected the aerodynamic forces experienced for a given tunnel speed. Degani and Zilliac investigated this possibility in their study of flow unsteadiness[54], but found no evidence that the proximity of a tunnel wall to the nose influenced the sideforce on an ogive cylinder.

The improved lateral stiffness achieved by these two approaches reduced the side motion of the model. This allowed satisfactory suspension in the high moderate incidence range at Mach numbers up to 0.1. Variations of forces and coefficients from a test at an incidence

of 50° are shown in Figures 11.6a and 11.6b. This test was conducted with an axial displacement but without the improved control laws, and the maximum Mach number was consequently restricted to 0.07.

11.5.4 High incidence: 70-95 degrees

At angles of attack increasing beyond 70 degrees the ogive cylinder model appeared to be subject to periodic vortex shedding of the type described in Section 11.2.4 above, resulting in high frequency lateral motion. From Equations 11.1 and 11.2 above, it is possible to estimate the vortex shedding frequency for a given tunnel speed and angle of attack. Frequencies similar to the control loop rate of 242 Hz were expected at angles of attack above 70 degrees, for tunnel speeds of Mach 0.06 - 0.065.

A simple lateral motion resonance would not be expected under these unusual circumstances as the natural frequency of the model-controller system is around 10 Hz, but the similarity of frequencies still seemed to cause poor control in this speed range. Multiple phase advance algorithms were subsequently employed to improve the quality of lateral control at high angles of attack, allowing the speed range to be extended beyond this difficult region.

The maximum tunnel speed in this incidence range was partially determined by the maximum operating current of the electromagnets. High currents were required to restrain the suspended model, under the action of the large aerodynamic forces generated at high angles of attack and high tunnel speeds. Further control problems were encountered at Mach numbers approaching 0.12, which were attributed to vortex shedding at twice the control loop rate. The combination of large aerodynamic forces and model oscillations limited the maximum tunnel speed to around Mach 0.11 for angles of attack from 70 to 95 degrees. Force and moment data obtained at 70 degrees is shown in Figures 11.7a and 11.7b.

The trends in force and moment coefficient for the full angle of attack range are shown in Figure 11.8. Up to 60 degrees of incidence, lift and drag have similar magnitudes. At higher angles lift decreases and large drag forces are experienced. The emphasis of the published data appears to be on the force components rather than on pitching moment. The observed trend in pitching moment coefficient is shown in Figure 11.8, but will not be considered further.

11.5.5 Effect of nose shape and fineness ratio

Changes in the steady roll attitude under certain conditions were observed between runs. It was assumed that the nose features responsible for sideforce generation were altered by handling the model, and the occasional impacts with the wind tunnel following a loss of suspension. The impacts may also have caused a change in the position of the magnetic core, and hence the positions of the gravitational and magnetic centres.

Changes in the preferred roll attitude of the model prevented repeat testing in some instances. Under conditions where the model showed a tendency to spin, the maximum tunnel speed for spin stability at a given angle of attack changed on a daily basis.

11.5.6 Effect of Mach number

The values of Mach number achievable in the Southampton MSBS wind tunnel are sufficiently low to prevent the onset of Mach number effects during experiments conducted in this facility. The critical Mach number for a cylinder in crossflow[59] is approximately 0.4. The maximum tunnel Mach number available was 0.185.

11.5.7 Effect of Reynolds number

Force coefficients were seen to be dependent on tunnel speed, indicating a Reynolds number dependence. A trend of decreasing force coefficient with tunnel speed is evident in Figure 11.6b, for an incidence of 50°. Expansion of the Reynolds number range upwards was not feasible, given the low maximum tunnel speed and limited model size compatible with the Southampton MSBS. This observation prompted attempts to influence the flow regime by changing the surface roughness of the model, as described below.

11.5.8 Effect of surface roughness and flow turbulence

Two phenomena were observed which were possibly related to the surface condition of the model; an apparent Reynolds number influence on force coefficients despite the subcritical test Reynolds number, and the effect of nose imperfections on the generation of sideforce. To further investigate the effect of surface roughness, the model was smoothed by careful machining, and the application of a lacquer coat. Surface smoothing made little difference to the aerodynamic characteristics of the model, and no significant changes in the measured force coefficients were observed.

The investigation of the effect of surface condition on the flow was extended by application of 0.6 mm grit to the surface of the model, over 65 mm of the nose and body. Further wind tunnel testing revealed a drop in drag at angles of attack greater than 50 degrees. This gave a good correlation with the results obtained by Champigny, who

observed a reduction in critical Reynolds number for an ogive cylinder at with a roughened surface. Results obtained with the gritted model are shown in Figure 11.9. Drag coefficient was raised slightly at low incidence due to increased skin friction following the application of grit to the model. A reduction in lift coefficient was observed between 50 and 70 degrees of incidence.

The level of turbulence in the MSBS wind tunnel has not been measured. Some turbulence beyond that typical of this type of facility would however be expected for these tests, caused by wear and tear to the upstream lip of the test section, and imperfect alignment of the inlet. Such turbulence could have contributed to the manifestation of Reynolds number effects, at lower stream Reynolds numbers that those at which such effects would normally be expected.

11.5.9 Support interference

There was no support interference during these tests. It can however be assumed that inaccuracies from sources such as tunnel blockage, which was approximately 1 % at zero incidence and 10 % at 90 degrees, reduce confidence in the absolute values of force coefficient measured. Given the presence of further sources of error including the effect of sideforce on the operation of the DFM rig, and the changing condition of the model, no attempt was made to correct the results for blockage.

11.5.10 Other results

Data obtained for a Mach number of 0.1 over the full angle of attack range was presented in Figure 11.8. This speed was chosen as the maximum at which data was available for all attitudes (except 95°, M = 0.09), and corresponds to a Reynolds number based on model diameter of 0.41×10^5.

The results obtained from MSBS wind tunnel testing are compared to published data in Figure 11.10. Values of normal force coefficient were calculated for this graph from the lift and drag coefficients already discussed. At low and moderate incidence the MSBS results agree well with those obtained by Champigny[56] for a Reynolds number of 0.28×10^6. A comparison with published data at the test Reynolds number was not possible, as the maximum Reynolds numbers available in the Southampton MSBS wind tunnel fall well below the lowest values typically used for testing in conventional facilities. The fall in normal force coefficient above 50° would appear from Figure 11.3 to be associated with a higher Reynolds number. This observation supports the assertion made in Section 11.5.8 above, that surface roughness and tunnel turbulence caused high Reynolds number behaviour.

The disparity in Reynolds number prevents the drawing of firm conclusions from a comparison of the MSBS results with those of Dietz and Altstatt[58]. However, at very high angles of attack the values of normal force coefficient obtained lie between those for a sting-supported ogive cylinder and those for a strut-supported model. Canning and Nielsen's results[53] show the minimum normal force coefficient obtained from tests at different roll angles. The Reynolds number is closer to the critical value than in the other tests, and the normal forces are lower in agreement with Figure 11.3.

The test envelope for the complete angle of attack range is shown in Figure 11.11. The predictions of maximum feasible test speed based on the force capability of the MSBS (Section 10.5) are also shown, reproduced from Figure 10.14. The trends in these data show good agreement. It seems likely that the shortfall between the predicted and achieved test Mach numbers is due to the simultaneous generation of lateral forces at high angles of attack, in response to vortex shedding. Sideforce generation would cause certain magnets to reach maximum current at a tunnel speed below that at which the limit would be reached under the application of steady loads in the x - z plane.

11.6 FURTHER WIND TUNNEL TESTS

The data presented shows good agreement with the results of previous investigations into the low speed aerodynamics of an inclined ogive cylinder. A number of extensions to the preliminary testing performed during this research programme are now possible at Southampton, as will now be described:

Roll control of an axisymmetric model would be advantageous in the acquisition of precise measurements in the degrees of freedom available to the present DFM rig. Given the partial dependence of normal force on sideforce[53], the method of Canning and Nielsen could be followed, whereby the normal force coefficient recorded is the minimum value obtained from a number of measurements at different roll attitudes.

Modifying the DFM rig to measure sideforce and yawing moment would allow a complete characterisation of ogive cylinder aerodynamics. Techniques for sideforce reduction such as those investigated by Modi and Stewart[50], could be demonstrated. A further obvious extension to the present work would be a study of the support interference on aerodynamic forces. This area could be investigated by measuring the force changes caused by the proximity of a dummy sting or strut to a suspended model.

A number of the authors cited encountered operational difficulties in conventional wind tunnels, caused by the oscillatory sideforce resulting from vortex shedding during tests on an ogive cylinder. The difficulties of extending this study into an MSBS have been described. Advanced control techniques for coping with the sudden lateral forces could be investigated. If the control problems at the extremes of the present test envelope could be alleviated, the emphasis would be shifted to withstanding large steady aerodynamic forces. The optimisation technique of Section 10.5, developed to maximise the ability of the MSBS to respond to large aerodynamic forces could then be used.

12. MSBS CONTROL SYSTEM DEVELOPMENT

The control system for the Southampton MSBS has been substantially developed during this research. A software correction to a behavioral anomaly exhibited by the power supplies was implemented. Control and data reduction techniques for the propulsion simulation experiments were developed. A new control computer was purchased and integrated into the system. Alternative control algorithms were evaluated. The work in these areas is described in this chapter, which concludes with a critique of system reliability.

12.1 INTRODUCTION: CONTROL SYSTEM CIRCA 1989

At the beginning of this research program, the control system for the Southampton MSBS was implemented on a Digital Equipment Corp. (DEC) PDP11/84 mini-computer, itself an upgrade of an older PDP11/34. The operating system used was DEC RT-11, and the MSBS control software in use was that developed by Parker[20], to achieve suspension over a large angle of attack range for the first time.

Significant progress in MSBS development had been achieved at Southampton using this first generation digital control system, but a number of shortcomings were apparent:

Programming languages

The control software was written in MACRO-11 assembler. This low level language was employed to achieve rapid software execution. Some MACRO routines were taken directly from the original digital implementation of the MSBS controller, performed by Britcher[6] in 1980. An alternative language, RT-11 FORTRAN, was available for writing support and analysis software, but the lack of an optimising compiler left this language deficient in speed. The use of an assembly level language for the controller, especially an uncommon DEC variant, made it difficult for non-experts to understand and improve the system, and prevented any easy transfer or exchange of software with interested parties.

Memory

One megabyte (MB) of memory was available on the PDP11, of which only the first 64 kilobytes (kB) were directly addressable. The higher memory could be addressed using overlays, but the time penalty associated with this practice prevented the use of overlays with the high angle of attack controller. The lowest 64 kB of memory was therefore all

that was available for both the suspension software and the storage of run-data. The complexity of the high angle of attack control software made it larger than previous control programs, and just 4 kB of memory remained for data storage.

Processing speed

During the development of the PACS position sensing hardware, Parker found it convenient to reduce the control loop rate from Britcher's 256 Hz to 242 Hz. On the PDP11/84, the high angle of attack control software could be run at an unrestricted loop rate 317 Hz, showing that some scope remained for increasing the sophistication of the controller. However, the computing overhead associated with the provision of a magnetising field (Chapter 5), and the calibration of the power supplies (Section 12.2), reduced the spare processing capacity essentially to nil.

Commands and communications

A serial line connected the PDP11 to the MSBS control terminal. The slow rate of data transfer available with this line severely restricted communication between the controller and the operator. Commands such as those for model motion were limited to an esoteric system of combined single letter and number codes, with no protection against incorrect input values. No reports of system status were available, and in the event of a software problem no error messages were transmitted.

Data presentation

No computer graphics facility for the presentation of run-data was available, although the PDP11 computing facility did include a plotter.

12.2 CALIBRATION OF THE POWER SUPPLIES

One advance made to the control system before its transfer to the Personal Computer (PC) (Section 12.4), was the inclusion of a software calibration designed to improve the behaviour of the MSBS power controllers.

12.2.1 Introduction and background

Power supplied to the electromagnets of the Southampton MSBS is obtained from 4 transformers driven by 440 V, 3-phase mains. Each transformer drives a regulator and rectifier assembly, providing a nominal 95 V, DC output to two or three electromagnets. Further details of this sub-system can be found in ref 62.

Regulation of power in the ten electromagnets is provided by ten dedicated DC servo controllers. The controllers provide a continuous output of up to 20 A, in response to an analogue command voltage from the MSBS control system. They are also capable of a producing a short-term 45 A peak, The controller gain is adjustable, and is presently set so that a command varying between -5 and +5 V, causes the electromagnet current to be driven from -20 to +20 A. The servo controllers are designed to supply current to industrial motors, and are often and hereafter referred to as power supplies.

The power supplies are generally well-suited to operation with an MSBS. Their regenerative switching-mode operation reduces power consumption, and the 4 kHz switching frequency is high enough to remove any bandwidth limitations. The response of an electromagnet current to a control demand is limited by the inductive time constant of the electromagnets, combined with the power supply characteristics. This issue is addressed in Section 12.5.2.

An irregularity in the power supply performance at low currents was first identified by Britcher[62], before being characterised by Thomas[63]. The relationship between static demand voltage and current output is linear as required over most of the operational envelope, but deteriorates into a number of line segments between about -1 and +1 A, as illustrated in Figure 12.1. The cause of this problem was unknown, but it has affected MSBS research at Southampton since these power supplies were commissioned during the major refurbishment of 1980.

Eskins' force calibration work[39] made extensive use of current oscillations in the non-linear region, and the disappointing results obtained were partially attributed to the imperfect power supply characteristic. The lateral magnets generally operate at low current during suspension of a permanent magnet model, and close to zero current the line segment structure effectively reduces the power supply gain. Parker noted that unexpectedly high control loop gains were required for lateral control of a suspended model, to compensate for the low power supply gains.

12.2.2 Investigation of power supply response

An investigation into the power supply DC responses was carried out to establish the cause of the calibration anomalies, and to characterise them to the extent that a suitable correction could be selected and implemented. Initially it was confirmed that the current measuring sub-system was in order, and that the output responses were being correctly measured.

An appraisal of the response of each electromagnet and power supply combination showed a variety of line segment characteristics. A series of individually tailored corrections was therefore required rather than a single, globally applied measure.

One of the power supplies was connected to a purely resistive load instead of an electromagnet, and gave the correct response throughout its performance range. It was concluded that the high inductance of the MSBS electromagnets was disrupting the normal behaviour of the power supplies, which are rated for a load inductance of 1 mH. The magnets have inductances of approximately 60 mH for the vertical and lateral units, and 135 mH for the axial electromagnets.

Such a fundamental difference between the design and operating conditions of the power supplies suggested that a simple hardware modification would not cure the problem, although the subject has not been raised with the manufacturer. This course of action was not felt to be justified, as a software measure to improve the power supply response had already been suggested, which was expected to be practical, successful and inexpensive.

12.2.3 Calibration techniques

Two software techniques for correcting the power supply response were suggested by Thomas[63]. The most straightforward suggestion was the implementation of a look-up table for each controller. This solution would involve an initial calibration experiment, seeking to determine the demand voltage required to yield each possible output current. The calibration results would be stored in a look-up table for each channel. During suspension, calls from the controller for a given current would be referred to the relevant look-up table, to find the command necessary to achieve that current.

Using the 12-bit digital to analogue converter (DAC) presently employed, 4096 output levels are available, and this would be the number of lines required in each look-up table. The pre-calibration technique would entail only a small processing overhead, but the application of look-up tables to all ten electromagnets would entail a significant memory overhead. The memory penalty would be regarded as particularly severe on a memory-limited computer such as the PDP11.

An alternative technique was proposed, exploiting the line segment structure of the response curve. Prior knowledge of the properties of each line would enable the controller to calculate the correct demand for a given output current. Storage of a gradient, an offset and a range delimiter for a typical five-line characteristic would require just fifteen items of data per magnet. This memory saving would be at the expense of increasing the

processing overhead required to calculate the correct demands during suspension. Given the availability of a certain amount of spare processing capacity, compared to the stringent memory limitations, this latter technique was clearly the most suitable for implementation with the PDP11-based MSBS control system.

12.2.4 Implementation on the PDP11

The line segment attributes of the ten magnet and controller combinations were determined. It became apparent that these attributes drifted with time, especially as the system warmed up. Periodic re-calibration was therefore necessary, and to reduce the workload an automatic calibration procedure was developed.

During the calibration each magnet in turn was slowly cycled through its operational range. At each demand voltage, the current output was measured, and a test applied to determine whether the response was consistent with the line segment presently under consideration, or represented the first member of a new segment.

The line segment gradient and offset were found by performing a running least squares fit on the data as it was collected. This enabled a prediction of the current output at subsequent points to be made. If the measured current matched the prediction to within a given tolerance, the point was judged to be on the present line, and its properties were added to the least squares accumulators. Failing the test, the point would be judged to be part of a new line and the accumulators reset.

The line-match test was chosen empirically to give a reasonable number of line segments - around 5 per magnet. An acceptable error between the predicted current i_p and that measured i_m was defined as

$$|i_p - i_m| \leq k_1 + k_2 i_p , \qquad k_1 = 0.25\,A , \qquad k_2 = 0.02$$

The inclusion of a proportional element in the test aimed to enhance its accuracy in the low-current region. Line segment calibration was shown to significantly improve the power supply response, as demonstrated by Figure 12.2.

The high angle of attack control software was modified by the inclusion of a routine to perform the output calibration. This reduced the free-running loop rate from 317 Hz to 295 Hz. Several instances were found whereby quality of suspension was improved by use of the calibration, generally by eliminating a low-frequency cyclic motion, in a degree of freedom controlled by magnets operating at low current. Conversely, an outdated calibration could reduce the model steadiness and induce an oscillation. Following its

development, the line segment power supply calibration procedure remained in use until the PDP11 computer was replaced for control of the MSBS.

12.2.5 Implementation on the PC

Memory was no longer a limiting factor for the MSBS control system following its transfer to the PC, with 4 MB of directly addressable memory. Look-up tables therefore became the preferred power supply calibration technique, and were easily implemented.

A measurement of calibration quality was developed, whereby the absolute difference between the demand and output currents was summed, as the magnets were driven through a specified region of the current envelope. Current measurement was improved by taking an average of several current readings for each demand, as single readings were affected by random noise on the ADC signals. The total current error per magnet over the range -5 A to +5 A was reduced by up to 90 %.

The need for multiple reading of currents slowed the calibration to around 3 minutes per magnet. As the power supply response was only a significant problem near zero current, and to speed up the calibration process, the software correction was confined to a reduced range of currents. This limited calibration remains the preferred option.

A calibration range of -5 to +5 Amperes was chosen to fully enclose the non-linear region. Between these currents the system is calibrated as usual. The full look-up table is still used, but outside the calibration range the contents are made equal to the demands, and the look-up process therefore has no effect on the demands for electromagnet current. To prevent a discontinuity at the boundaries of the calibrated region, data within 1 A of the transition is linearly factored so as to fade smoothly from calibrated to unmodified values.

The benefits of the look-up table calibration are similar to those described above for the line segment technique. Power supply calibration now operates as standard with the Southampton MSBS, and may enable research into areas such as dynamic force calibration (Section 8.2) to continue with greater success than was previously achieved.

12.3 COMPUTING REQUIREMENTS FOR PROPULSION SIMULATION

As finally configured, Parker's high angle of attack controller left sufficient memory on the PDP11 for storage of two thousand integer items of run-data. For an adequate record of conditions in the MSBS at a given instant it is necessary to record the following:

- Position measures: 5
- Electromagnet currents: 10
- Tunnel speed: 1
- Timing flag: 1 (not always required)

For sixteen items of recorded data, 125 data points could therefore be recorded on the PDP11. Run-data is available at 242 Hz with the present control loop rate, so a complete record of just over 0.5 seconds of suspension could be recorded. Data need not of course be logged at the control frequency, but for satisfactory recording of a propulsion simulator firing lasting 1-2 seconds at most, a rapid data acquisition rate is preferred.

The data storage facility provided by the PDP11 was clearly inadequate for the purpose of fulfilling the contractual data acquisition and analysis requirements of the propulsion simulation contract. Furthermore, any increase in the scope of the control software, such as the development necessary to allow magnetisation of iron models, would have reduced and possibly eliminated the limited data storage capacity described. Additional memory could have been made available by limiting the scope of the control software, removing features such as the high angle of attack capability. As the long term aim of the MSBS research at Southampton is to develop MSBS technology, the option of reducing the control system capability was rejected as a retrograde step.

Further aspects of the capability of the PDP11 were unsatisfactory, as described in Section 12.1 above. An improvement to the control and data storage hardware was undoubtedly required, and possible courses of action were investigated.

12.3.1 Purchase of new computer hardware

An upgrade of the PDP11 was not an option, as the 11/84 was the last of this family of computers. Dedicated data buffers were available, but offered no cost saving over the purchase of a Personal Computer (PC), with sufficient memory to meet the likely requirements of the MSBS. A further benefit of a PC solution was that a machine initially employed for data acquisition, could eventually be used to replace the PDP11 as MSBS controller.

The purchase of a PC was selected as the preferred response to the processing and memory limitations of the Southampton MSBS. It was first necessary to consider the processing speed requirement for a suitable PC. To achieve a significant improvement over the PDP11, the PC would need to be capable of running MSBS control software both

faster and in a higher level language. The C language developed by Kernighan and Ritchie[64], was selected for its flexibility, speed of execution and widespread application.

For comparative purposes, benchmark software was developed to run in MACRO-11 Assembler on the PDP11, and in C on an IBM compatible personal computer. The benchmark included integer and floating point arithmetic, data manipulation and looping, to be representative of typical MSBS control software. It was found that a PC with an Intel 80386 central processing unit (CPU), operating at 25 MHz with an Intel 80387 math co-processor, could run the benchmark faster than the PDP11. This specification was adopted as the minimum standard for the new computer.

A PC was selected and purchased from Viglen[65]. Its performance moderately exceeds the above standard as a memory cache is installed. The cache allows rapid access to frequently used data, and so speeds up software execution. The benchmark run-time benefit over the PDP11 is 25 %. High resolution graphics allow for effective data presentation. A standard 48-line programmable interface card was also purchased, to allow communication between the PC and the remaining MSBS hardware.

A significant advantage of using an IBM compatible PC in conjunction with a portable language such as C, is the ease with which future upgrades will be possible. A further performance improvement might involve use of an 80386 processor running at a higher clock speed, an upgrade to an 80486 CPU, or transfer of the software to an alternative operating system. The former option is the most straightforward, and could be accomplished simply by replacing a number of cards in the PC.

12.3.2 Use of the PC as a data logger

During the compressed gas propulsion simulation tests (Section 6.6), the PC was used for data acquisition and presentation, while the PDP11 continued to control model suspension. This distributed processing format, implemented here simply as part of a control transition, is an attractive option for an MSBS-type application.

Distributed processing applied to an MSBS allows the manipulation and display of run-data in conjunction with data storage and retrieval operations, whilst simultaneously maintaining the suspension of a model. This flexibility would be difficult to achieve with a single computer, and the combination of functions described was not viable for the PC-based controller.

As a data logger, the PC took a passive rôle, reading data flowing from the MSBS to the PDP11 without affecting their normal interaction. The communications were configured as shown in Figure 12.3, with the PC having access to a parallel line. A *data ready* signal was used to trigger each reading of the PC interface card. Up to 25 seconds of complete run-data could be recorded, a total of around 100,000 words. A propulsion simulation event would last only a fraction of this time, but unreliable triggering of the compressed gas simulator made it attractive to be able to record for a longer period (Section 6.6).

12.3.3 Analysis of run-data

Analysis software was required to allow the manipulation and presentation of run-data obtained with the PC in its rôle as data logger.

The data logger was programmed to intercept all of the information flowing between the MSBS and PDP11, and this information was recorded as a simple stream. The information in the stream was ordered, and it was possible to synchronise the analysis with the stream by detecting the magnet current data, which is encoded with a channel label.

A software package ANALYZE was developed to satisfy the data processing requirement. Its operation is based on a visual replay of the data storage period. Electromagnet currents are displayed as colour bars, arranged to mimic their presentation as an array of gauges on the MSBS power supply cabinet. Position sensing information is presented to show model shadows in relation to the photodiode arrays. Timing and tunnel speed are represented by additional bars. The replay display is shown in Plate 8.

During the replay, start and end points of events can be marked, as delimiters for the graphical presentation available as the second phase of the analysis. A graph menu then allows selection of the following display options:

- Electromagnet current vs time (10 possible magnet selections)
- Position measure vs time (5 selections)
- Photodiode array reading vs time (5)
- Electromagnet group current vs time (4)
- Tunnel speed vs time
- Magnetising field strength vs time
- Data for TRANSIENT analysis (Section 6.7.3)

Following the selection, the graphs are presented as specified. A hardcopy can be obtained from the printer, or the graph data recorded in a disc file. The software then returns to the replay for further analysis.

12.4 PC-BASED CONTROL SYSTEM

Development of a PC-based controller for the Southampton MSBS was not originally intended to form part of this research program. Having purchased the PC and integrated it into the system as a data logger, the PDP11 was to remain the control computer for the time being.

The transfer of the control system was forced when the PDP11 maintenance contract was terminated due to its rising cost - equivalent to the purchase price of one PC per annum. Further propulsion simulation research, and in particular the development of software for use with the direct force measurement (DFM) rig (Chapters 8-9), which was under construction at the time of this decision, could not be justified using the PDP11, given the risk that it might fail and not be repaired.

An immediate transfer of control of the MSBS to the PC was instigated, addressing the two major areas described in the following sections.

12.4.1 Hardware interface

Bilateral communication between the MSBS and the PDP11 was achieved using a 16 bit i/o card. To ensure reliable communication over the large distance (20 m) between the computer and the MSBS data acquisition hardware, each bit was transmitted through a sheathed twisted pair cable, using push-pull line drivers. Handshake lines were used to indicate readiness to receive, or the presence of new data. For a full description of this communication system, the reader is referred to ref 62.

The data logger intercepted these communications as shown in Figure 12.3. Individual bits were read by comparing the 'high' line of each twisted pair cable with an earth line, via a simple connection to the PC's own i/o card.

With the PDP11 no longer active, line drivers controlled by the PC were required to allow continued use of the existing communications protocol. The cable length was now reduced to around 2 m, but line drivers were retained to preserve the capability to make the control

computer more remote from the MSBS, if required in the future. This strategy also avoided the need to modify the existing data acquisition hardware.

A hardware interface[66] was consequently designed and constructed by the Department's Electronics Workshop. It contains line drivers and receivers to allow the PC to mimic the communications protocol previously employed between the MSBS and PDP11. Integration of the interface was achieved without upset, and no problems have yet been encountered with its use.

12.4.2 Control software

The primary aim of the PC controller development was to achieve independence from the PDP11. Secondary aims included the following:

- Retain all of the features of the high angle of attack controller
- No ambitious software development at this time
- Reorganise the software for clarity where possible
- Create a framework for future software development
- Address the remaining problems identified in Section 12.1

A package of C software known collectively as PCMSBS was produced. The major files are libraries of functions related to a particular aspect of magnetic suspension: position sensing, control, communication with the electromagnet array and so forth. The main program consists of a sequence of calls to the necessary functions. The organisation of PCMSBS is shown in Figure 12.4. Some sections of the code simply replicate those developed by Britcher and Parker[6,20]. A number of new features are also included, and these are now described:

Screen messages and communication with the operator

The man-machine interface was significantly improved by enabling the control software to send detailed messages to the PC screen, whilst retaining a model in suspension. Writing large numbers of characters to the screen is a slow operation, but writing one character per program loop is possible without a prohibitive speed penalty.

A message control routine was developed whereby messages generated in response to a system condition, or to an interrogation by the operator, are sent to a buffer. They are then released and sent to the screen at a rate of one character per control loop; 242 characters per second. The delay is almost invisible to the operator. The message facility created a number of other opportunities for advances in the PC-based control system.

Menu commands

A multi-level menu system has been implemented to promote a logical sequence of commands for requests for model motion and oscillation. The menu structure includes screening against illegal inputs, such as commands for model motion beyond the permissible limits. Several control features are controlled by toggles. The command structure is illustrated in Figure 12.5.

Warnings

The message facility allows the controller to send warnings to the operator. The most important warning is of imminently approaching electromagnet current limits. Others messages warn against overloading the control algorithms, and filling the data storage array.

Interrogation

The MSBS operator can use keyboard commands to interrogate the software as to the value of selected parameters during suspension. Presently, the values of tunnel Mach number and pressure transducer voltage can be requested.

Memory

A number of data storage options are available. Run-data can be stored continuously (every program loop), or intermittently (every *n*th program loop), up to around 100,000 words. Alternatively, run-time averaging is available whereby selected parameters are recorded over a specified time interval, averaged, and then stored. This technique greatly reduces the data storage requirement for wind tunnel tests where static data is required, such as those intended for analysis using the DFM rig.

Power supply calibration

Power supply calibration with the PC controller is achieved using look-up tables rather than the line-segment matching technique developed for the PDP11, and was discussed in Section 12.2.

Tunnel speed control

A pressure transducer was recently added to the MSBS wind tunnel, to allow real-time monitoring of tunnel speed during the tests with the compressed gas propulsion simulator. The transducer is installed to measure the dynamic pressure q_{ref} just upstream of the test section, but a calibration constant is available as a result of work by Newcomb[28], which relates this measurement to that applicable in the test section q_{true}, using

$$q_{true} = 1.017\, q_{ref}$$

The transducer was connected to a previously unused channel of the ADC, and it was a simple matter to close the control loop, employing a spare DAC channel to regulate tunnel speed. Fan speed for the MSBS wind tunnel is governed by an analogue control voltage V which gives maximum speed for a 10 V input. The DAC can supply a potential difference between -5 and +5 V, so an additional 5 V supply is used to bias the output to 0-10 V.

Mach number M is controlled using the algorithm

$$V_{t+1} = V_t + 0.0015\, e$$

where

$$e = \frac{M_d - M_t}{M_d}$$

This algorithm was empirically deduced, the error factor being adjusted until a satisfactory performance was achieved. Satisfactory performance is loosely defined as that where tunnel speed exhibits a balance between rapid response to a changed demand, and reduced overshoot as the new speed is reached. A complete tunnel speed control block diagram is shown in Figure 12.6. Following a demand for a speed change, a message is generated when a satisfactory match with the new speed is reached. Tunnel speed control using the above algorithm is stable and responsive. Figure 12.7 shows the variation in recorded tunnel Mach number for a constant speed demand during a wind tunnel test. It is assumed that the high frequency variation in the signal is due to electrical noise, and that tunnel speed was adequately maintained during the test.

Control algorithms

Dual phase advance control remains the preferred technique for suspension of a model, but other control algorithms have been implemented on occasion, as described in Section 12.5.4 below.

Look-up tables and interpolation

The original high angle of attack controller made extensive use of look-up tables for assignment of parameters dependent on angle of attack. Constants relating to position sensing and control of a particular model were pre-calculated for a number of attitudes over the angle of attack range, to save processing time during suspension.

The memory limitation of the PDP11 forced the look-up tables to be generated at a coarse pitch interval: a ten degree spacing was employed. Linear interpolation was used to estimate the parameter values for intermediate pitch attitudes. The greater memory

available to the PC controller has allowed an expansion of the look-up tables. Presently a one degree spacing is employed. Interpolation yielded no apparent control benefit at this small pitch spacing, and is presently disabled. Further investigation may be necessary to determine a suitable balance between the control advantages of sub-degree look-up table spacing, the use of interpolation to calculate parameters for intermediate attitudes, and the computing cost in terms of memory and processing overhead.

Magnetisation

The generation of magnetising fields is achieved in a similar fashion to the original implementation on the PDP11 described in Chapter 5.

Parameter factoring

Selected control system parameters can be adjusted via keyboard commands while a model is in suspension. This feature allows empirical fine-tuning of the parameters to achieve the best quality of control, and enables an immediate assessment of the effects of changing their values.

Launching

The operation of launching models into suspension is still performed manually, and can be a difficult operation for less experienced personnel. To make launching easier using the PC controller, changes have been made to the assessment of model presence, and the rejection of erroneous position sensing information.

The test of model presence used by Parker to activate the electromagnet array during a launch was the detection of an image on one or more of the four main photodiode arrays. The axial channel was excluded from this test because of the possibility of obscuring the axial sensor during launch or retrieval of a model. During a launch, an image on one photodiode array could be generated before the model was in a suitable position to be controlled, and the interpretation of position based on such limited information was unpredictable. This approach was justified at that time by the need to attempt to retain control of a model even during an excursion which resulted in a loss of detection from one or more sensors. In this situation it would not be acceptable to interpret the model as not present and then to deactivate the electromagnets.

An alternative using two tests is now in use. During launch, the model is not deemed to be present until it is within the field of view of all four main position sensors. From such a position, the model is easily taken into control. Thereafter, the test of model presence reverts to detection of just one image, and retains the advantages described.

Erroneous position sensor data is occasionally generated due to system noise, and is discussed in ref 20. A software 'clamp' is used to detect and reject data showing an unexpectedly large deviation from the previous reading. Large position changes are inevitable during a launch, so the clamp is initially disabled, and becomes operational one second after the model is detected. This measure, in parallel with the model detection change described above, has made model launching significantly easier, especially for less experienced personnel.

12.5 CONTROL ISSUES AND CONTROL ALGORITHMS

The dual phase advance control algorithms presently used by the Southampton MSBS are little changed from the original digital controller developed by Fortescue and Bouchalis[67]. They can be regarded as a digital simulation of the analogue control system used prior to 1980.

Following that initial investigation, which defined the requirements for a digital controller, and successfully demonstrated digital control of two degrees of freedom, development of the control system was continued during several undergraduate projects. Britcher[6] then extended digital control to the remaining degrees of freedom.

During his development of the high angle of attack control system, Parker[20] noted that the algorithms were perhaps outdated, but saw no reason to attempt a modification, as their performance was judged to be adequate.

Suspension of a propulsion simulator as it experienced a thrust impulse was recognised as presenting a control challenge. Gradual changes in thrust level were not expected to cause difficulty, as restraint of the model could be managed under pseudo-steady conditions. However, rapid thrust changes would test the response times of the control system and the electromagnet array.

The dual phase advance control strategy uses feedback of model position and attitude to determine the electromagnet commands necessary to maintain suspension. The response of a digital feedback control system is determined by the control loop rate, and by the gain ratios employed to evaluate the response to a deviation. For a truly immediate response, the use of feedforward was considered.

Feedforward strategies would involve prior knowledge of the exact moment of thruster firing. One suggestion entailed the application of an axial restraining force just before firing. The argument was that rearward acceleration of the model in response to the axial force would almost immediately be countered by the thrust impulse, and the overall axial motion would be reduced. The failure by PSI to provide for passive roll control of the compressed gas propulsion simulator (Section 6.1.3), resulted in the use of a thruster firing technique that did not allow precise timing. The ideas for novel control practices were consequently abandoned.

Given the restriction to feedback control, an investigation into alternatives to dual phase advance algorithms for the MSBS controller could not be justified. No specific problems were identified with their use, no replacement algorithms had yet been suggested, and the PDP11 computer lacked the capability to support a more complex control technique. Now that the PC-based control system is operational there is scope for further development of the controller, although the MSBS hardware, rather than the control software, has been identified as the limiting factor in responding to a sudden force impulse (Section 12.5.2).

12.5.1 Control of propulsion simulators

Models

All of the propulsion simulator models were based in size and weight on the compressed gas thruster developed by PSI. The first solid rocket powered models were made to this specification to enable their use in proof of concept trials prior to compressed gas testing. Later rocket thrusters were also produced along these lines to permit a comparison of their performance with the earlier models.

A generic propulsion simulator class of model was consequently recognised - being axisymmetric of diameter 22-28 mm and length 200 mm, having steel construction and a mass in the region of 0.6 kg. These models were limited to suspension at angles of attack below 25 degrees (Section 6.5). Force calibrations indicated that the maximum axial force that could be applied to suspended propulsion simulators by the electromagnet array was approximately 5 N.

Axial control

At low incidence the axial electromagnets (group IV), are most effective at producing axial force on a suspended model. For this reason they are favoured in the assignment of

axial demand distribution and consequently provide most of the restraint in response to the thrust impulse produced by a propulsion simulator.

These magnets are of different construction and have different properties from the eight iron-cored central electromagnets. Notably the inductive time constant L/R for the axial magnets is 59 ms, compared to 75 ms for the others. The time constant is reflected in the rate of change of magnet current, and hence the application of force to the model in suspension. The algorithms developed for axial control at high angles of attack using the iron-cored electromagnets, do not therefore give the best response at low incidence using the axials.

This issue was highlighted by the low damping of axial motion observed during the initial suspension of propulsion simulators at low angles of attack. As the MSBS control software does not yet make the control algorithms attitude dependent, it was necessary to derive a set of control parameters specifically for propulsion simulation tests at low incidence. This investigation was initially performed using the model designed to be representative of a propulsion simulator (Section 4.4.3).

An empirical technique was used to adjust the dual phase advance algorithms, with the aim of improving the quality of control prior to firing thrusters in suspension. This process can loosely be referred to as an optimisation. Good quality of control is generally regarded as a combination of model steadiness, high gains ('stiffness') and rapid (critical) damping of disturbances.

The dual phase advance algorithms include three constants that were altered for each degree of freedom and at each attitude, in the search for improved control:

- **Loop gain** is the ratio of the final output (demand for control force) from the controller to the input (position error) in each degree of freedom.

- **Damping ratio** is controlled by the value of n in Equation 2.1 - the dual phase advance block - and governs the rate at which a disturbance is reduced to zero.

- **Time constant** is represented by T in Equation 2.1 and determines the natural damped frequency of the degree of freedom.

The optimisation process was performed iteratively. Each parameter in turn was cycled through a range of values. At each value the model was disturbed with a pre-programmed

impulse in the degree of freedom under investigation. The time histories of the responses were recorded and examined. The parameter was then set to the value corresponding with the 'best' observed response, and remained at this new value during subsequent tests of the other parameters.

The pattern of model behaviour was similar for all parameter types. Too high a value would give a rapid model response, but with unsteadiness and possible instability. Too low a value would result in a sluggish response. Generally two or three cycles of testing each parameter in turn were performed for each degree of freedom.

Following the control optimisation, firing of a thruster on board a suspended model was attempted. The first trials were with Estes rockets (Section 7.3). A moderate success rate was achieved and techniques were developed which were of benefit during later tests of the compressed gas exhaust simulator.

12.5.2 Acceptable thrust profile

The major problems encountered in testing the compressed gas propulsion simulator were control related, and were identified as being due to the unfavourable thrust profile generated by the CO_2 thruster. Consideration of the causes of the control difficulties led to a reflection on what might constitute an 'acceptable' thrust profile, for propulsion simulation in an MSBS equipped with a feedback control system.

Suitability of a thrust profile for use in an MSBS is determined by a number of factors including:

- Rise time of the thrust profile as it increases to the steady thrust level
- Response of the control software to model motion caused by the thrust
- Hardware response to demands from the controller
- Magnitude of the peak thrust level
- Duration of period of thrust at peak level

An analysis of these factors is necessary if the acceptable thrust profile is to be defined, and will be related to experience with the compressed gas simulator. The above factors will be considered in turn:

Rise time

The thrust rise time can be regarded as a bonus for the control system, allowing time for the response to the start of the thrust impulse to be initiated before the peak thrust is

reached. A thrust level greater than the instantaneous magnetic restraining force will accelerate the model. A peak thrust exceeding the maximum available restraint will inevitably result in model motion. Some model motion is acceptable if the distance travelled does not become critical before the thrust level begins to fall and the model can be brought to rest.

With the compressed gas thruster, the thrust profile was presented as a *fait accompli*. The sudden rush of CO_2, released in the form of gas and other phases when the gas bottle was punctured, led to an almost instantaneous thrust peak. A rise time as such was not always discernible, given the relatively slow 140 Hz sampling rate used during bench tests of this thruster. A negligible rise time - a step change in thrust - will hereafter be assumed for the compressed gas thruster.

Software response

Following the firing, the control system reacts when it detects model motion. A delay of at least one control loop from the moment of firing is inevitable, as the control sequence begins with position sensing and finishes with a demand for force. No sub-loop rate responses are possible. Following the initial delay, the magnitude of the demand for restraining force is related to the size of the detected motion, and the values of the control system parameters.

In the analysis to follow, the best case software will be assumed, whereby the maximum restraining force is instantly demanded in response to a model motion.

Hardware response

Hardware response is governed by the characteristics of the power supplies and the electromagnets. The mode of operation of the Southampton MSBS power controllers is complex, involving a 4 kHz switching frequency and the use of internal current feedback. A notional simplification for assessing the response time is possible, assuming that the maximum potential of 95 V can be instantly applied across the relevant magnets, and is maintained until the required current is achieved.

For a model at low incidence, it is appropriate to consider the axial electromagnets, with inductance 135 mH and resistance 2.3 Ω. The peak current (V/R) is therefore 41.3 A. The response of an LR circuit to the application of voltage is given by

$$L\frac{di}{dt} + Ri = V$$

with a time constant

$$\tau = \frac{L}{R}$$

τ being 59 ms for the axial magnets.

Applying the full 95 V is in response to a demand for current change, an axial magnet starting from 0.0 A could therefore be expected to reach 26 A (*1/e* or 63 % of the peak current) in 59 ms. A typical current response can be regarded as a segment of the response to a larger current change of this type.

A simple test was performed to measure the hardware response time, under conditions applicable to propulsion simulation testing. Figure 12.8a shows an axial magnet current trace in response to a firing at time $t = 0$ of the compressed gas thruster in suspension. Figure 12.8b shows the response over the same current range in response to a step change in power supply demand at $t = 0$. The current response time in both cases is approximately 45 ms. The shape of the response segments is almost linear, and a ramp approximation to the current response will be assumed hereafter.

The similarity between the rate of current change in response to model motion, and that in response to a demand step, indicates that electromagnet inductance is the limiting factor in the control system response. The power supply and electromagnet hardware, rather than the control software, determines the response to a sudden model motion in the Southampton MSBS. No benefit can therefore be expected from the use of more advanced control algorithms.

An acceptable thrust rise time for a propulsion simulator can be defined as one exceeding the electromagnet response time. If this condition is satisfied, the controller ought to be able to be designed so as to apply an increasing restraining force of a similar magnitude to the instantaneous thrust, and axial motion of the model should be dramatically reduced.

In the thrust profile analysis below, the hardware response segment will be approximated by a linear ramp between the relevant currents over 45 ms.

Magnitude of peak thrust

A peak thrust below the axial force capability of the MSBS is acceptable if the thrust rise time is not so short as to cause excessive axial travel. A peak thrust above the maximum restraining force could possibly be tolerated for a short time, again depending on the amount of axial motion.

The magnitude of the thrust peak from the compressed gas thruster was demonstrably variable (Section 6.1.1), so a range of possible values will now be considered in the analysis.

Duration of peak thrust

Problems inherent in the reduction of data from propulsion simulation tests, where the thrust profile does not include a period of steady thrust, have been described in Section 6.7.3. It is assumed that a usable MSBS propulsion simulator would generate steady thrust for a period at least long enough to allow data collection with the model steady.

The compressed gas thruster was unacceptable in that it produced an instantaneous thrust peak followed by an exponential decay. However, the analysis will assume an improved thruster of this type, capable of maintaining the (variable) peak thrust level at least until the model is brought back under control.

Analysis

An illustrative analysis of the response of an MSBS to a variable thrust profile will be made. In this case a step profile of varying magnitude will be considered. The analysis attempts to predict whether the application of thrust will cause sufficient axial motion, for the model to move out of the viewing range of the position sensors.

It is assumed that application of a step thrust Th to a model of mass m is followed immediately by the application of a restraining force, which ramps up to a maximum value of F during a time interval T_r. For the Southampton MSBS and a generic compressed gas propulsion simulator, the relevant values are:

Th	=	variable
m	=	0.6 kg
F	=	5 N
T_r	=	45 ms

This framework can be used to derive an expression for the distance l, traversed by the model before it is halted by the applied restraining force. Two motion phases are considered. In the first phase, the model accelerates under the influence of its thrust, while the electromagnetic force increases linearly. It is assumed that an average force $F/2$ acts during this period. In the second phase the model is brought to rest by the restraining force. Summing the expressions for distance travelled during these phases:

$$l = \frac{T_r^2}{2m}(Th - F/2)\left(1 - \frac{(Th - F/2)}{(Th - F)}\right)$$

This function yields the maximum axial travel of a model as a function of the magnitude of peak thrust, and was used to calculate the data shown in Figure 12.9. As the level of the peak thrust approaches the maximum restraining force, the axial travel increases rapidly.

The axial position sensor of the Southampton MSBS is configured in such a way that at low incidence, around 12 mm of travel by a suspended model can be tolerated before the sensor is obscured. Figure 12.9 suggests that this travel would be produced by a peak thrust of about 4.2 N. The range of thrust peaks observed during tests of the compressed gas thruster included many which exceeded this level. The analysis accounts for the high failure rate of the tests in suspension.

Thrust profile summary

Referring back to the factors introduced above, the discussion can be summarised:

- Thrust rise time should exceed the time to achieve maximum restraint.
- Simple algorithms can achieve an excellent control software response.
- Hardware limits govern the response of the Southampton MSBS.
- A peak thrust greater than the maximum restraint is rarely acceptable.
- The thrust peak duration should allow for control and data acquisition.

12.5.3 Control of the second generation rocket thruster

The favourable thrust profile of the improved rocket thruster allowed firings in suspension to proceed, free from control problems. The thrust profile, and a typical axial motion response of the model, have been described and illustrated in Sections 7.4-7.6 and Figure 7.6. Control difficulties were minimal as the thrust rise time of the new rocket motors, measured at 50-60 ms, exceeded the 45 ms response time of the axial electromagnets. The controller was therefore able to match the restraining force to the applied thrust more closely than was possible with the compressed gas thruster. Axial travel of the model in response to the thrust impulse was consequently reduced.

12.5.4 Modified control algorithms

An opportunity arose to experiment with modified control algorithms, as a result of an honours project undertaken by Futter[61], which addressed two new control techniques.

Futter attempted a single degree of freedom simulation of the Southampton MSBS, which was used to assess the performance of the new schemes:

The more modest investigation looked into possible advantages of extending the dual phase advance algorithms to multiple phase advance. A phase advance control block is regarded as a lead-lag network, and compensates for the phase lag introduced by the inductance of the electromagnets, so increasing the system stability. The analogue controller used at Southampton before 1980 used two such blocks, to generate around 90 degrees of phase lead close to the resonant frequency of the system. The first digital controller duplicated this process, and has not been modified since its implementation. It was expected that increasing the number of phase advance blocks would yield a further benefit to stability.

Multiple phase advance control was found to yield an increase of up to 600 % in suspension stiffness using the simulation. As the number of phase advance blocks was increased, the extra gain in stiffness rapidly decreased. When the improvement was weighed against the increased processing requirement of the higher order controllers, a five-phase controller appeared to represent a good compromise.

This result supports the findings of Goodyer[22], who evaluated the performance of a number of phase advance schemes. The performance criteria used in this case was the ratio of the control system gain at infinite frequency G_∞, to the DC gain G_0. A lower gain ratio indicates better rejection of high frequency components, and is desirable for an MSBS controller where the natural frequency of the system is only a few Hertz. The decline in the benefit of an increased number of phase advance blocks is illustrated in the following table, which summarises Goodyer's results:

Table 8: Theoretical performance of phase advance controllers (from ref 22)

Number of phase advances	Gain ratio G_∞/G_0
2	34.0
5	24.4
Infinite	23.1

The second area addressed was the use of a state space control technique, as first attempted by Thomas[63]. State space control is attractive for use in the MSBS as it uses

discrete time, and is therefore inherently more suitable for a digital implementation. In addition, this technique can potentially improve the quality of control - measured in this instance as *control force / position error*, or 'stiffness', to a level beyond that achievable with a phase advance controller.

State space control was implemented using four states: model position, velocity, acceleration and rate of change of acceleration. Optimal control theory was applied to minimise an error function, as the state space controller responded to a simulated position disturbance. Further details of this approach can be found in ref 61.

12.5.5 Implementation of multiple phase advance controller

An advantage of the PC control software was demonstrated by the ease with which it was possible to expand the dual phase advance algorithms to 5-phases. Whereas the previously implemented control coding used two separate phase advance modules in sequence, a looping structure is now employed. Expansion to an *n*-phase advance algorithm merely requires insertion of *n* into the loop declaration.

Futter's simulation was shown to be an incomplete representation of the Southampton MSBS. The phase advance parameters proposed by Futter as a result of his simulation trials did not correspond to those eventually found to be suitable. The observed trend was for the proposed values to be too high, causing instability when suspension was attempted. Possible causes of the instability are related to the shortcomings of a real system; electrical noise, digital quantisation errors and mechanical imperfections. These factors act to destabilise the system, and require a 'softer' control algorithm for satisfactory performance. Future simulations will need to more accurately reflect the real MSBS if they are to be of use.

An empirical technique similar to that described in Section 12.5.1 was used to find more acceptable values for the phase advance parameters. The ratios of proposed to acceptable values of the parameters were similar for all five degrees of freedom. Recognition of this trend speeded the search for acceptable values.

Despite the speed advantage of the PC over the PDP11, it was not initially possible to implement 5-phase control for all of the degrees of freedom simultaneously, whilst maintaining the customary control loop rate. It was necessary to temporarily disable a number of non-essential software features, to bring the software back up to speed, and permit a demonstration of multiple phase advance control of five degrees of freedom.

Use of multiple phase advance control algorithms yielded an immediate benefit in the quality of control, notably in suspension stiffness. This was found to be of particular value during the high angle of attack wind tunnel test series described in Section 11.5. Control problems were initially experienced due to the large and unsteady lateral forces acting on the ogive cylinder test model at moderate to high incidence. Multiple phase advance control of the sideslip and yaw channels improved lateral control and permitted expansion of the test envelope.

Stiffness can be subjectively judged by manual manipulation of a suspended model, but to quantify the changes a more precise technique is needed. The deflection per unit load could be measured for each degree of freedom by applying external forces to the model in the manner of a static calibration (Section 8.2). This test would have to be performed with the error integrators disabled, as their action tends to eliminate steady state position errors.

As an alternative to a practical evaluation, the benefit to suspension stiffness of multiple phase advance control was quantified by examining the controller output in response to a simulated position error. This gives a direct measure of suspension stiffness. The test was applied only to the lateral degrees of freedom - sideslip and yaw - as only these channels were routinely subject to multiple phase advance control. It was found that the multiple phase advance strategy increased the stiffness of the sideslip channel by a factor of 1.66, and that of the yaw channel by a factor of 1.62.

12.5.6 Implementation of state space controller

Futter's state space controller was also incorporated into the PC control software. A limited application was attempted, applying state space control only to the vertical heave channel at zero incidence. Futter's control parameters caused instability, but *ad-hoc* adjustments were sufficient to allow low quality suspension using the state space algorithms. The effects of each parameter change were less clearly defined than with a phase advance system, so empirical improvement of the quality of control was difficult.

12.5.7 Future development of the controller

Futter demonstrated diminishing but real control improvements with a greater number of phase advance modules. The logical limit of this control avenue is an infinite-phase advance technique, first proposed by Goodyer[22]. The mathematics of this proposal should be further investigated.

It appears that intuitive adjustment of the control system parameters to improve the quality of suspension, as practised at Southampton since the start of research into magnetic

suspension, is not sufficient to optimise a state space controller. Future progress with state space control may therefore be dependent on the development of an adequate computer simulation of the Southampton MSBS.

12.6 RELIABILITY OF THE MSBS

The reliability of the Southampton MSBS during this research was generally good, but some of the equipment is beginning to show signs of aging. The two position sensing lasers both faded during the course of this research program. One has been replaced, the other will need replacing soon. The quality of the optical components is degrading. This may be due to the high dust levels in the MSBS laboratory, and fumes from the engine test cells below. A number of electronics cards in the data acquisition system have deteriorating contacts, and significant time can be lost unless the operator is familiar with the foibles of the system. A small number of power supply faults have occurred. In each case a fuse or an output transistor had failed, and a simple repair was possible.

A sensible course of action at this stage would appear to be the training of a member of the permanent technical staff of the Department of Aeronautics and Astronautics to assume some responsibility for the MSBS. This would alleviate the onset of a 'skills shortage' with the departure of each temporary researcher.

13. DISCUSSION

In summarising the research programme, this section will address the implications of the results both for continuing development in research facilities such as the Southampton MSBS, and for a future large magnetic suspension system for production wind tunnel testing.

13.1 PROPULSION SIMULATION

Simulation of an engine exhaust in an MSBS appears to present no fundamental difficulties. Minor hardware and software modifications were required to allow propulsion simulation experiments in the MSBS facility at Southampton. No contamination problems were encountered due to the presence of exhaust gases, as an open return wind tunnel was used. In a closed loop MSBS wind tunnel, it is assumed that corrections of the type made during propulsion simulation in a conventional facility would be applied.

Control difficulties were experienced with the carbon dioxide propulsion simulator supplied by PSI, which were attributed to a thrust profile outside the original specification, and incompatible with the Southampton MSBS. The hardware limitation of the maximum rate of change of electromagnet current was the determining factor in assessing the suitability of propulsion simulator thrust profiles. The control software had a secondary effect on the success of these tests. The necessary condition for good control of a propulsion simulator appears to be that the thruster has a rate of thrust increase below the rate at which the restraining force can be applied.

Testing with an exhaust simulator having a thrust profile incorporating a region of steady thrust was found to simplify the data analysis process for propulsion simulation testing. During the period of steady thrust, with the model stationary, it was possible to make a static measurement of the sum of the external forces acting. Reduction of data from an exhaust simulation incorporating an unsteady thrust profile necessitated the analysis of motion and current transients. Transient analysis was complicated by changes in the force calibration algorithms associated with model motion.

At this scale, propulsion simulation achieved by the release of compressed gas compared unfavourably to that performed using solid propellant rockets. The availability of a small solenoid valve to regulate the gas flow could have improved the thrust profile of the CO_2

propulsion simulator. However, objections to the use of a cold jet remain, based on the temperature dependence of some exhaust characteristics.

Assessment of the effect of an exhaust flow on the drag coefficient of a propulsion simulator requires accurate knowledge of the thrust level. It was not feasible to make this measurement during the research program. If a simulator designed for use in a large MSBS exhibited an inconsistent thrust profile, then telemetry of a suitable thrust chamber gas conditions should allow its instantaneous thrust to be monitored. An alternative use of pressure measurement could be in a feedback loop to a thrust control system on-board the model, to enable the thrust to be regulated as required.

Assuming that a production MSBS would operate with a cryogenic wind tunnel, a carbon dioxide propulsion simulator would require on-board heating to prevent freezing of the propellant. The effects of solid CO_2 in the thruster exhaust would need to be considered. A solid rocket propulsion simulation technique would present fewer operational problems. Exhaust cooling might be required, to prevent the exhaust-to-flow temperature ratio from reaching a value too high to be representative of a real propulsion system.

13.2 FORCE MEASUREMENT WITH AN EXTERNAL BALANCE

A review of MSBS force measurement techniques was conducted, prompted by the difficulties encountered in measuring force during the propulsion simulation experiments. The lack of a viable means to employ the unique high angle of attack capability of the Southampton MSBS to generate useful aerodynamic data also highlighted the need to improve force measurement.

The concept of an external balance, holding a model in place in an MSBS while directly measuring the forces exerted by the electromagnet array, was found to be both under-exploited, and suitable for implementation at Southampton. A simple three-component balance was constructed, using three force transducers to measure lift force, drag force and pitching moment. Test procedures were developed to minimise errors in force measurement.

A balance of this type has a number of applications. Two approaches to wind tunnel testing are possible. The selection between them would probably aim to minimise the projected occupancy of an expensive commercial MSBS facility. During tests involving a relatively small number of readings with each model core, a Post-Run Current Replication

(PRCR) force measurement technique appears to be the most suitable. Electromagnet currents recorded during the tests are later replicated with the balance and model installed in the MSBS. The MSBS position sensors can be used to ensure that the test position is duplicated. The magnets act upon the model as they did when the wind tunnel was in operation, allowing a direct measurement of the aerodynamic forces experienced. With this technique the uncertainty over the level of magnetisation of iron models which is inherent in pre-calibration techniques is removed.

For multiple tests using a common model core, a conventional complete pre-calibration of applied force against magnet current might be used. The need for individual force measurements following a test series would be eliminated at the expense of a single, more complex pre-calibration. The motorised external balance envisaged for a large MSBS could make the pre-calibration relatively rapid. Calibration results would be used to calculate the aerodynamic forces acting during subsequent wind tunnel tests. This technique is comparable to the use of wind tunnel tests to verify the results obtained by computational fluid dynamics, or other theoretical methods.

An external balance can also be used in the assessment of the effectiveness of an electromagnet array in producing force and moment components on a model. This information can be used to improve the performance of the control system. The three-component balance was used successfully to improve the performance of the Southampton MSBS controller. Coupling between the generation of the heave force and axial force components was reduced. Improved control allowed an extension of the angle of attack range. The principles here demonstrated may be extended to all degrees of freedom.

An ability to measure the forces and moments acting on an ogive cylinder during low speed wind tunnel tests was demonstrated. This was the first time that wind tunnel tests over a large angle of attack range were performed free from support interference. Observations regarding the structure of the trailing vortices during these tests were in agreement with published data from conventional tests of a similar model. Blockage of the test section was very high, reducing confidence in the absolute values of lift, drag and pitching moment obtained. A method for optimising the use of the electromagnet array for resisting the action of aerodynamic forces was demonstrated.

13.3 MSBS CONTROL SYSTEM

Two software calibration methods for eliminating the observed DC non-linearity in power supply output were implemented. Both performed well, with the selection of one method over the other representing a trade-off between processing overhead and the use of computer memory. The calibration gave an improvement in the quality of suspension under some conditions, and could be applied to any MSBS facility. Future dynamic testing and dynamic calibration at Southampton may benefit from the power supply calibration.

Magnetisation of iron models over a large angle of attack range was achieved, using a task distribution strategy similar to that used for the generation of force components. Conflict was observed between the use of the electromagnet array for the generation of control forces and magnetising fields. A process for achieving a combined optimisation of these two tasks was suggested.

The control system was transferred to a PC and implemented in a higher level language. A number of benefits resulted from this transfer, including increased system memory for software and data storage, faster processing, portability of the software, accessibility of the software to non-computing specialists, and the availability of hardware upgrades.

Improved suspension stiffness was observed during trials of multiple-phase advance control algorithms. This improvement was of benefit during the wind tunnel test series described. State space control of a single degree of freedom was demonstrated, but further research in this area is required before a fair comparison with phase advance control can be made.

14. CONCLUSIONS

14.1 PROPULSION SIMULATION

- Propulsion simulation experiments are feasible in an MSBS wind tunnel.
- Solid rockets out-performed compressed gas thrusters at a small scale.
- At larger scales, objections to compressed gas thrusters remain.
- Thrust profile must be compatible with the MSBS *hardware* capabilities.
- The control *software* was less critical than expected.
- Pressure telemetry was used to indicate instantaneous thrust.

14.2 FORCE MEASUREMENT WITH AN EXTERNAL BALANCE

- A rapid assessment of aerodynamic loads was demonstrated.
- Generation of force components by the control system was improved.
- Pre-calibration of model cores could be simplified by this technique.
- Interference-free, high α wind tunnel tests were performed.

14.3 MSBS CONTROL SYSTEM

- The new PC-based controller offers improved power and portability.
- A novel technique for magnetising iron models was developed.
- Software calibration improved the power supply characteristics.
- The benefits of improved control algorithms were demonstrated.

15. REFERENCES

1. Tournier, M; and Laurenceau, P: Suspension Magnetique d'une Maquette en Soufflerie. La Recherche Aeronautique, no. 59, July-August 1957, pp. 21-27.

2. Tuttle, MH; Moore, DL; and Kilgore, RA: Magnetic Suspension and Balance Systems: A Comprehensive, Annotated Bibliography. NASA TM-4318, August 1991.

3. Kilgore, RA (Ed): Magnetic Suspension and Balance Systems Newsletter.

4. Bloom, HL: Design Concepts and Cost Studies for Magnetic Suspension and Balance Systems, Final Report, November 1980-March 1981. NASA CR-165917, July 1982.

5. Boom, RW; Abdelsalam, MK; Eyssa, YM and McIntosh, GE: Magnetic Suspension and Balance System, Advanced Study-Phase II, Final Report, July 1986-May 1990. NASA CR-4327, November 1990.

6. Britcher, CP: Some Aspects of Wind Tunnel Magnetic Suspension Systems with Particular Application to Large Physical Scales. University of Southampton PhD Thesis, July 1982. Also NASA CR-172154, September 1983.

7. Britcher, CP; Ghofrani, M; Britton, TC; and Groom, NJ: The Large-Angle Magnetic Suspension Test Fixture. Presented at the International Symposium on Magnetic Suspension Technology, August 19-23, 1991, NASA Langley Research Centre, Hampton VA.

8. Britcher, CP: Large-Gap Magnetic Suspension Systems. Presented at the International Symposium on Magnetic Suspension Technology, August 19-23, 1991, NASA Langley Research Centre, Hampton VA.

9. Britcher, CP; Goodyer, MJ; Scurlock, RG; and Wu, YY: A Flying Superconducting Magnet and Cryostat for Magnetic Suspension of Wind-Tunnel Models. Cryogenics, vol. 24, April 1984, pp. 185-189.

10. Stephens, T: Design, Construction and Evaluation of a Magnetic Suspension and Balance System for Wind Tunnels. MIT-TR-136, NASA CR-66903, November 1969.

11. Towler, WR: Electromagnetic Position Sensor for a Magnetically Suspended Model in a Wind Tunnel. 2nd Int. Symposium on Electro-Magnetic Suspension, Proceedings. July 12-14, 1971, pp. Q4-Q7; Discussion, p. Q8.

12. Matthews, RK; Brown, MD; and Langford, JM: Description and Initial Operation of the AEDC Magnetic Model Suspension Facility: Hypersonic Wind Tunnel (E). Final Report, September 1967-January 1970. AEDC TR-70-80, May 1970.

13. Parker, DH; and Britcher, CP: Progress Towards Extreme Attitude Testing With Magnetic Suspension and Balance Systems. Presented at AIAA 15th Aerodynamic Testing Conference, San Diego, CA, May 18-20, 1988.

14. Tuttle, MH; and Gloss, BB: Support Interference of Wind Tunnel Models - A Selective Annotated Bibliography. NASA TM-81909, March 1981.

15. Tuttle, MH; and Lawing, PL: Support Interference of Wind Tunnel Models - A Selective Annotated Bibliography. NASA TM-81909, Supplement, May 1984.

16. Martindale, WR; Butler, RW; and Starr, RF, Jr: Study on Needs for a Magnetic Suspension System Operating With a Transonic Wind Tunnel. Presented at AIAA 15th Aerodynamic Testing Conference, San Diego, CA, May 18-20, 1988.

17. Stephens, T; and Adams, R: Wind Tunnel Simulation of Store Jettison With the Aid of Magnetic Artificial Gravity. MIT TR-174, March 1971, also NASA CR-1955.

18. Schott, TD; Jordan, T; Daniels, TS; and Alcorn, CW: Present Status of the MIT/NASA Langley 6-Inch MSBS. Presented at the International Symposium on Magnetic Suspension Technology, August 19-23, 1991, NASA Langley Research Centre, Hampton VA.

19. Tcheng, P; Schott, TD; and Bryant, EL: A Miniature, Infrared Pressure Telemetry System. Presented at the 34th International Instrumentation Symposium, Albuquerque, New Mex. May 2-6, 1988.

20. Parker, DH: Techniques For Extreme Attitude Suspension of a Wind Tunnel Model in a Magnetic Suspension and Balance System. University of Southampton PhD Thesis, April 1989. Also NASA CR-181895, October 1989.

21. Judd, M; and Goodyer, MJ: Some Factors in the Design of Magnetic Suspension Systems for Dynamic Testing. Sum. of ARL Symposium on Magnetic Wind Tunnel Model Suspension and Balance Systems, April 13-14, 1966, pp. 349-385.

22. Goodyer, MJ: The Magnetic Suspension of Wind Tunnel Models for Dynamic Testing. University of Southampton PhD Thesis, April 1968.

23. Goodyer, MJ: The Roll Control of Magnetically Suspended Wind Tunnel Models by Transverse Magnets. University of Southampton Rep No. AASU-291, 1969.

24. Goodyer, MJ; Henderson, RI; and Judd, M: The Measurement of Magnus Force and Moment Using a Magnetically Suspended Wind Tunnel Model. 13th Int. Magnetics Conference, London, April 14-17, 1975.

25. Britcher, CP: The Magnetic Suspension and Balance System in the Cryogenic Wind Tunnel. University of Southampton BSc Honours Project Report, April 1978.

26. Eskins, J: Further Investigation Into Calibration Techniques for a Magnetic Suspension and Balance System, Contractor Report, January-September 1985. NASA CR-178056, February 1986.

27. CSR Contraves, Contraves Goertz Corporation: Operating and Service Manual, NC400 Series Servo Controller.

28. Newcomb, AW: The Effect of Sting Interference at Low Speeds on the Drag Coefficient of an Ellipsoidal Body Using a Magnetic Suspension and Balance System. University of Southampton BSc Honours Project Report, May 1987.

29. Peters, WL; and Kennedy, TL: Jet Simulation Techniques - Simulation of Aerodynamic Effects of Jet Temperatures by Altering Gas Composition. AIAA 17th Aerospace Sciences Meeting, New Orleans, January 15-17, 1979.

30. Ferri, A: Review of the Conclusions of the AGARD Ad-Hoc Committee on Engine Airplane Interference and Wall Corrections in Transonic Wind Tunnel Tests. 38th Meeting, AGARD Propulsion and Energetics Panel, Sandefjord, Norway, September 13-17, 1971, AGARD-CP-91-71.

31. Edmunds, H; and Riedel, H: Contribution of the Institut Für Angewandte Gasdynamik of the DFVLR, Porz-Wahn. 35th Meeting, AGARD Fluid Dynamics Panel, Rome, September 4-10, 1974, AGARD-AG-208.

32. Joshi, PB; Beerman, HP; Chen, J; Krech, RH; Lintz, AL; and Rosen, DI: Propulsion Simulator for Magnetically-Suspended Wind Tunnel Models, Phase I Final Report. Physical Sciences Inc, Andover MA, August 1988.

33. Fuhs, AE: Nozzles and Inlet Testing in Transonic Flight Regime. 38th Meeting, AGARD Propulsion and Energetics Panel, Sandefjord, Norway, September 13-17, 1971, AGARD-CP-91-71.

34. Asai, K: Hot-Jet Simulation in Cryogenic Wind Tunnels. NASA RP-1220, July 1989.

35. Jaarmsa, F: Inlets-Airplane Testing in Transonic Wind Tunnels. 38th Meeting, AGARD Propulsion and Energetics Panel, Sandefjord, Norway, September 13-17, 1971, AGARD-CP-91-71.

36. Compton, WB III: Effect of Jet Exhaust Gas Properties on Exhaust Simulation and Afterbody Drag. NASA TR R-444, 1975.

37. Pindzola, M: Jet Exhaust Simulation in Ground Test Facilities. AGARD-AG 79, November 1963.

38. Goodyer, MJ: A Preliminary Investigation of the Dynamic Force Calibration of a Magnetic Suspension and Balance System. NASA CR-172580, May 1985.

39. Eskins, J: An Investigation Into Force/Moment Calibration Techniques Applicable to a Magnetic Suspension and Balance System. University of Southampton M.Phil Thesis, NASA CR-181695, August 1988.

40. Krauss, JD: Electromagnetics. McGraw-Hill, New York, 1984.

41. Scurlock, RG: Magnetic Suspension Using High Temperature Superconducting Cores. Presented at the International Symposium on Magnetic Suspension Technology, August 19-23, 1991, NASA Langley Research Centre, Hampton VA.

42. Joshi, PB; Malonson, MR; Sacco, GP; Goldey, CL; Garbutt, KS; Goodyer, MJ: Propulsion Simulator for Magnetically-Suspended Wind Tunnel Models. NASA CR-189560, January 1992.

43. Brown, ED: Model Rocket Engine Performance. Estes TN-2, Estes Industries, Penrose CO, 1971.

44. Squire, HB; and Trouncer, J: Round Jets in a General Stream. Ministry of Aircraft Production, Aeronautical Research Council, R&M no. 1974, 1944.

45. Roberts, PW; and Tcheng, P: Strain-Gage Balance Calibration of a Magnetic Suspension and Balance System. Presented at the 12th International Congress on Instrumentation in Aerospace Simulation Facilities, Williamsburg, VA, June 22-25, 1987.

46. Vlajinac, M: A Pneumatic Calibration Rig for use with a Magnetic Suspension and Balance System. MIT-TR-159, January 1970.

47. Schewe, GA: A Multicomponent Balance Consisting of Piezoelectric Force Transducers for a High-Pressure Windtunnel. Presented at the Conference on Sensors and Systems, Pasadena, CA, May 18-20, 1982.

48. Manufacturers Notes: ELF-500 Series Ultra-Miniature Load Cells. Entran Ltd, Garston, Herts, UK.

49. Pankhurst, RC; and Holder, DW: Wind Tunnel Technique. Pitman, 1952.

50. Modi, VJ; and Stewart, AC: Approach to Side Force Alleviation Through Modification of the Pointed Forebody Geometry. J. Aircraft, vol. 29, no. 1, January-February 1992, pp. 123-130.

51. Moir, IRM: An Experimental Investigation of the Effect of Fineness Ratio on Lateral Force on a Pointed Slender Body of Revolution. DRA TM-AERO-2225, October 1991.

52. Degani, D: Instabilities of Flows over Bodies at Large Incidence. AIAA Journal, vol. 30, no. 1, January 1991, pp. 94-100.

53. Canning, TN; and Nielsen, JN: Experimental Study of the Influence of Supports on the Aerodynamic Loads on an Ogive Cylinder at High Angles of Attack. AIAA 19th Aerospace Sciences Meeting, St Louis MO, January 12-15, 1981.

54. Degani, D; and Zilliac, GG: Experimental Study of Nonsteady Asymmetric Flow Around an Ogive-Cylinder at Incidence. AIAA Journal, vol. 28, no. 4, April 1990, pp. 642-649.

55. Degani, D; Tobak, M; and Zilliac, GG: Surface Flow Patterns on an Ogive-Cylinder at Incidence. AIAA Journal, vol. 30, no. 1, January 1991, pp. 272-274.

56. Champigny, P: Effect of the Reynolds Number on the Aerodynamic Characteristics of an Ogive-Cylinder at High Angle of Attack. AIAA 2nd Applied Aerodynamics Conference, Seattle WA, August 21-3, 1984.

57. Sarpkaya, T: Separated Flow About Lifting Bodies and Impulsive Flow About Cylinders. AIAA Journal, vol. 4, no. 6, March 1966, pp. 414-420.

58. Dietz, WE Jr; and Altstatt, MC: Experimental Investigation of Support Interference on an Ogive Cylinder at High Incidence. J. Spacecraft, vol. 16, no. 2, March-April 1979, pp. 67-68.

59. Gowen, FE; and Perkins, EW: Drag of a Circular Cylinder for a Wide Range of Reynolds Numbers and Mach Numbers. NACA TN-2960, June 1953.

60. Apelt, CJ; West, GS; and Szewczyk, AA: The Effect of Wake Splitter Plates on the Flow Past a Circular Cylinder in the Range $10^4 < R < 5 \times 10^4$. J. of Fluid Mechanics, vol. 61, no. 1, January 1973, pp. 187-198.

61. Futter, DH: Improvements to the Control Scheme of the Magnetic Suspension and Balance System. University of Southampton BEng Honours Project Report, May 1992.

62. Britcher, CP: The Southampton University Magnetic Suspension and Balance System - A Partial User Guide. University of Southampton Rep No. AASU-TM-83/8, April 1984.

63. Thomas, MJ: An Optimal Controller for the Vertical Heave Channel of a Magnetic Suspension System. University of Southampton BSc Honours Project Report, May 1988.

64. Kernighan, BW; and Ritchie, DM: The C Programming Language. Prentice-Hall, New Jersey, 1978.

65. Vig III Personal Computer Users Guide. Viglen Ltd, Hanwell, London, UK.

66. University of Southampton, Department of Aeronautics and Astronautics, Electronics Workshop. The MSBS Hardware Interface.

67. Fortescue, PW; and Bouchalis, C: Digital Controllers for the Vertical Channels of a Magnetic Suspension System. NASA CR-165684, May 1981.

16. LIST OF FIGURES

17. LIST OF PLATES

18. FIGURES

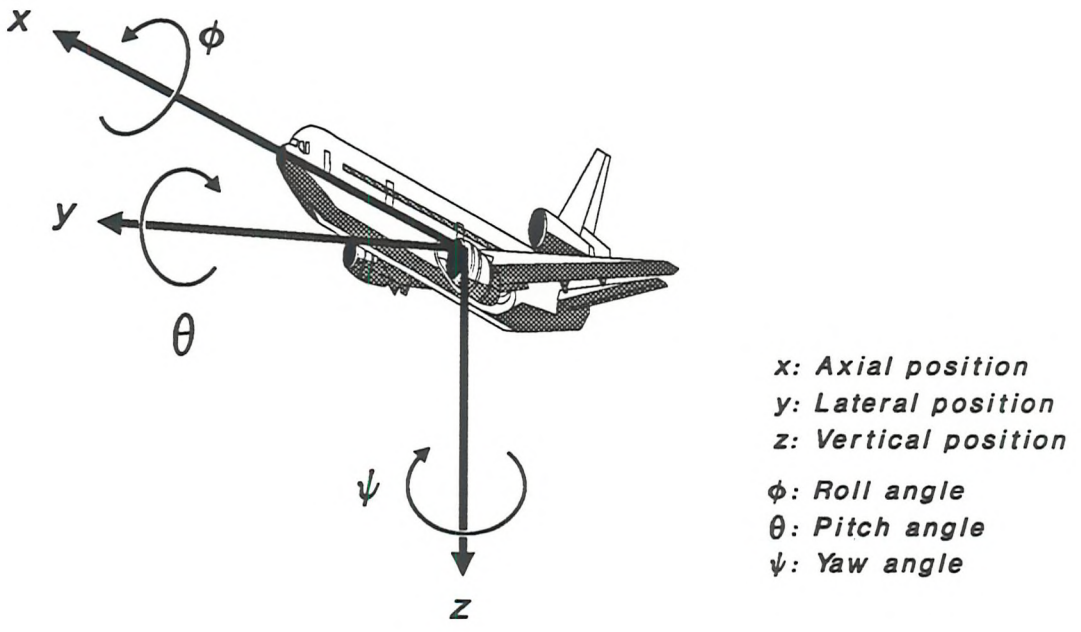

Figure 2.1a: Conventional axis system for a flight vehicle

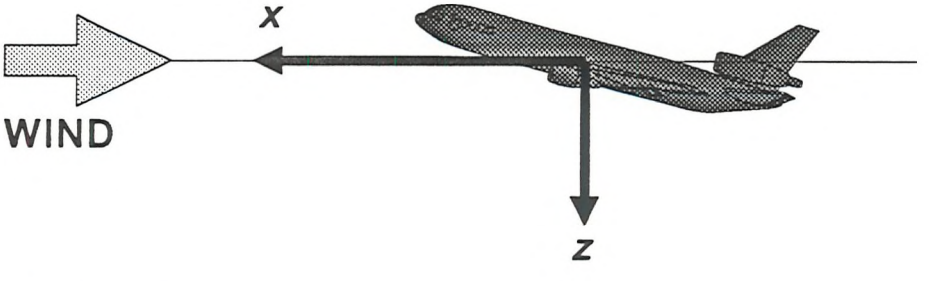

Figure 2.1b: Wind tunnel axes

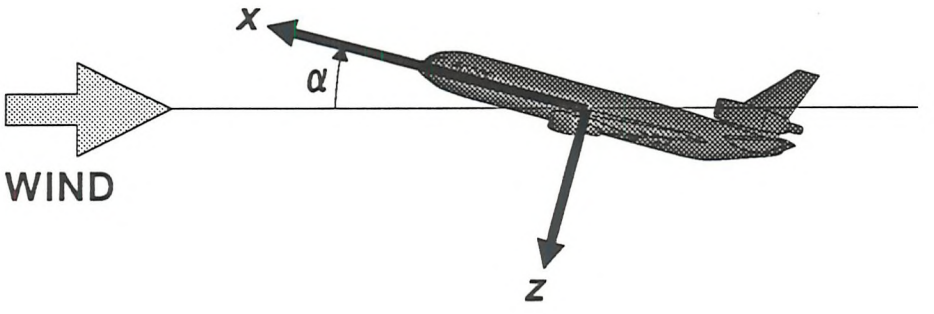

Figure 2.1c: Model axes

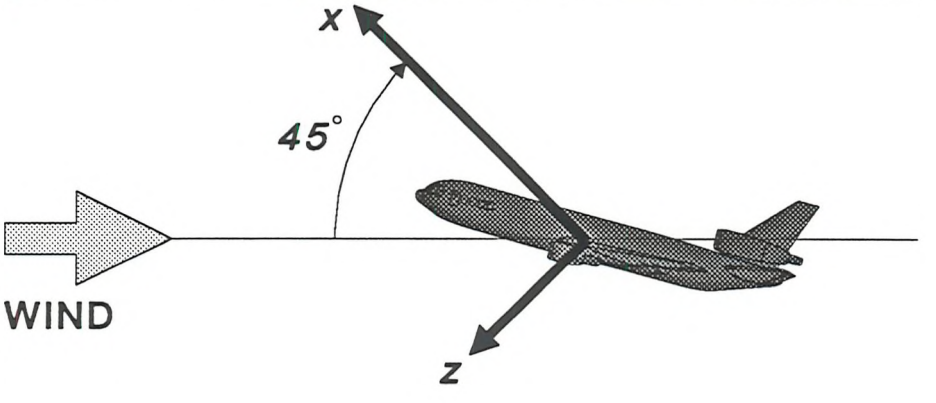

Figure 2.1d: Sensing system axes

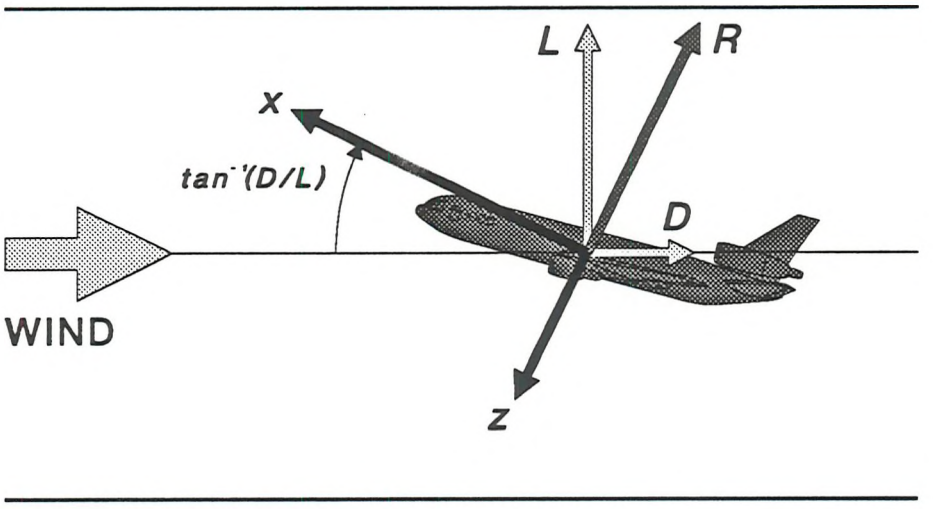

Figure 2.1e: Axes based on resultant of aerodynamic forces

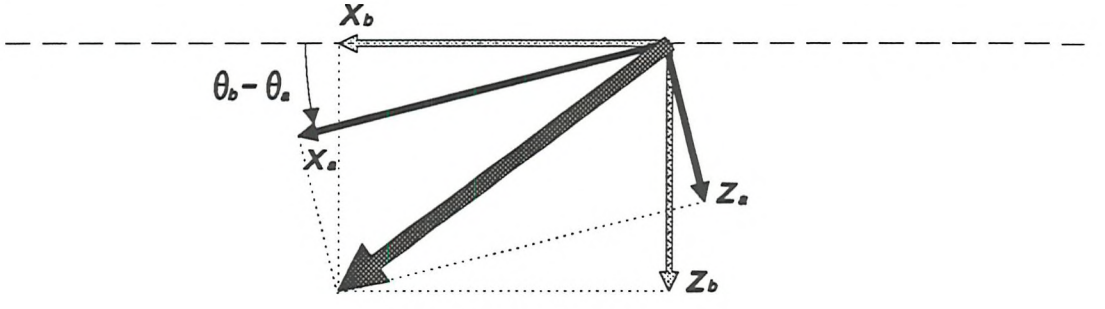

Figure 2.2: Typical axis transformation

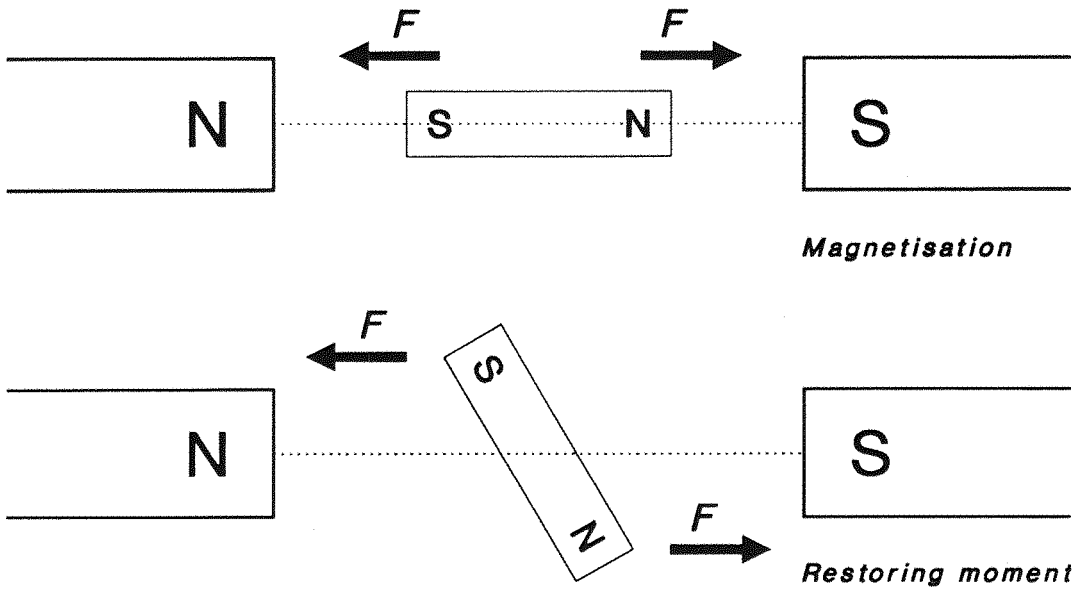

Figure 2.3: Action of uniform magnetic field

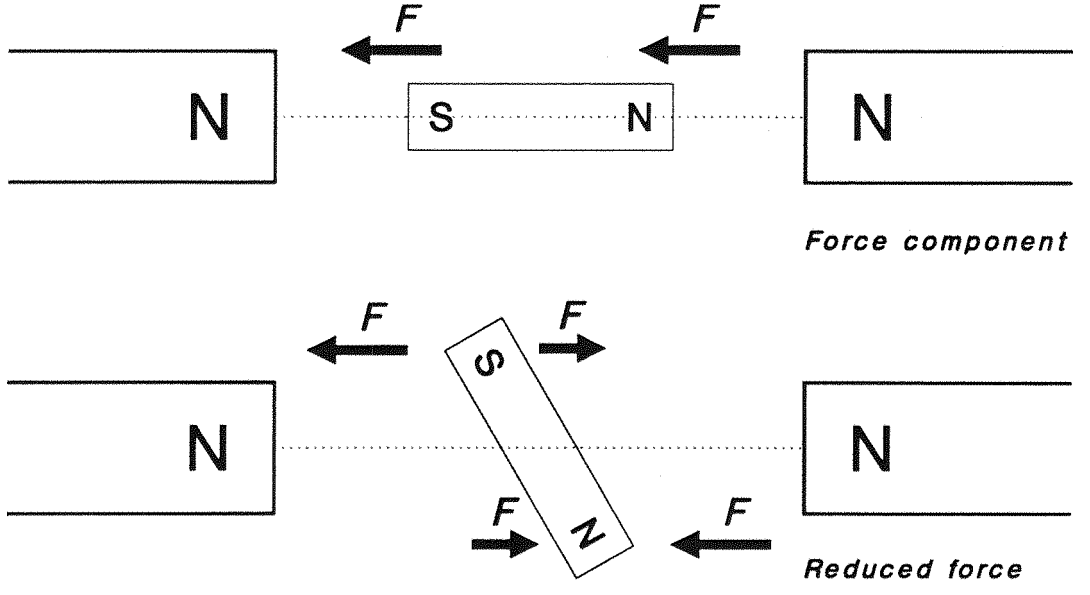

Figure 2.4: Action of magnetic field gradient

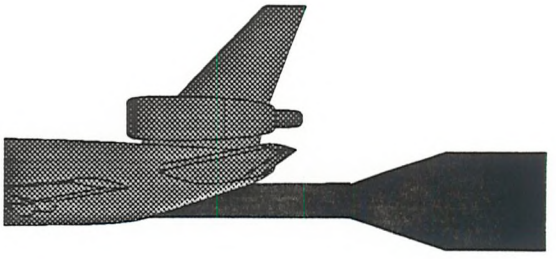

Distortion of model geometry, interference with flow over tailplane

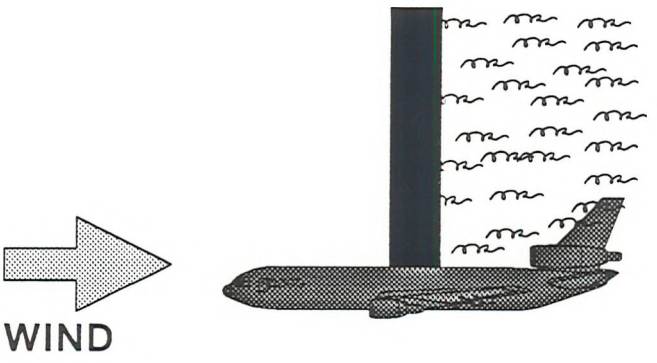

Disturbed airflow over model

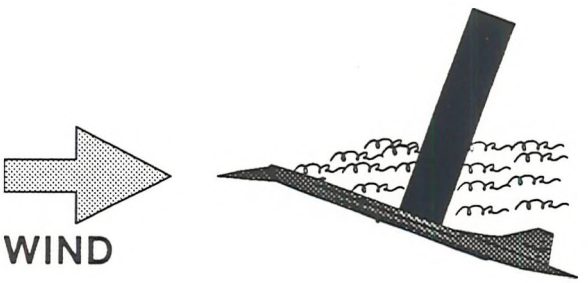

Interference with wake

Figure 2.5: Examples of support interference

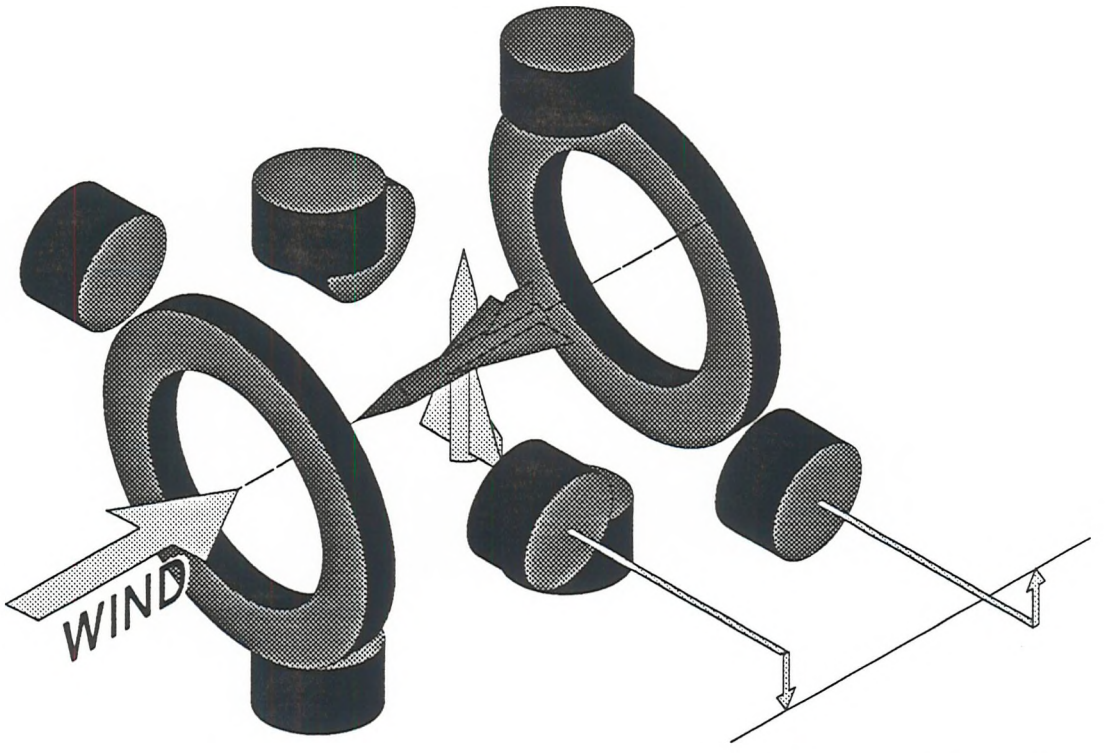

Figure 2.6: Layout of electromagnet array

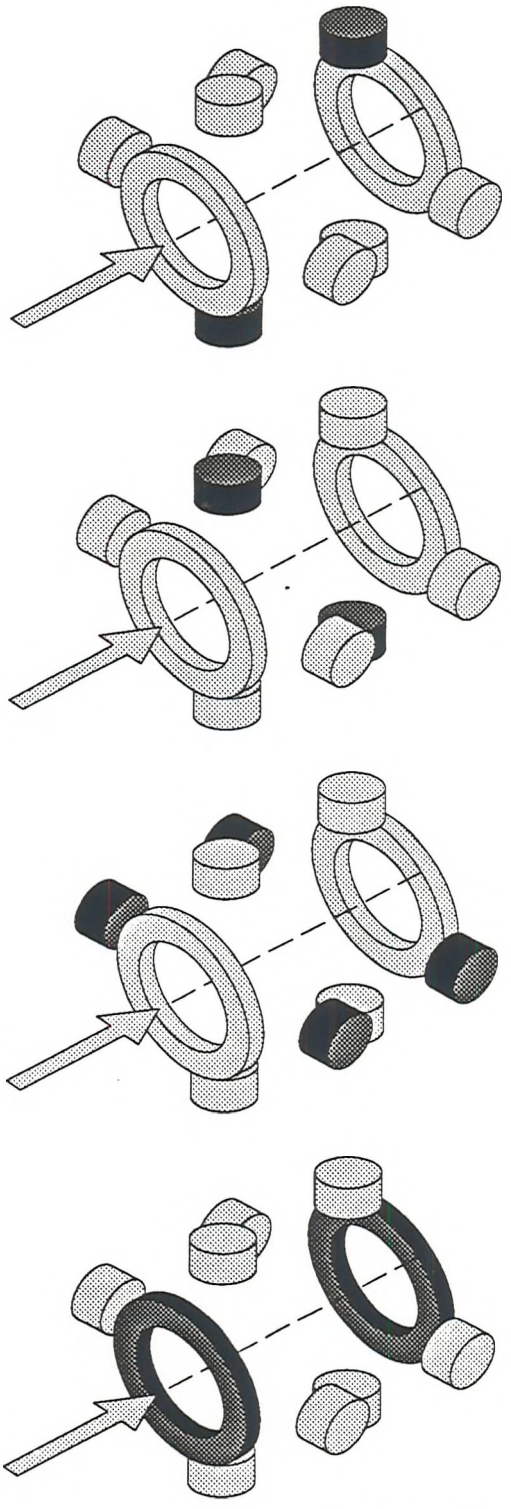

Group I: Vertical magnets

Group II: Vertical magnets

Group III: Lateral magnets

Group IV: Axial magnets

Figure 2.7: Electromagnet groups

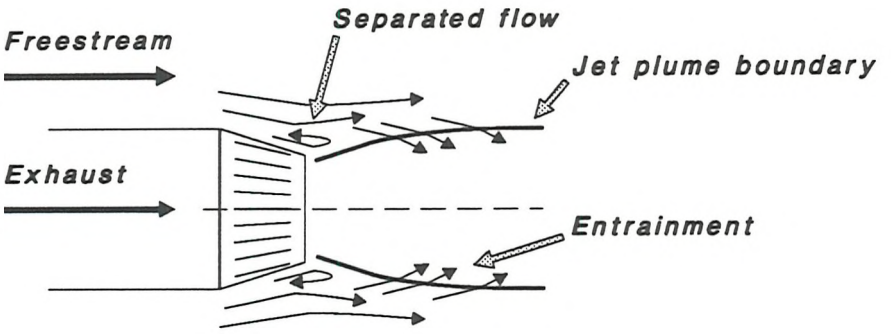

(a) Exhaust flow at a boattail

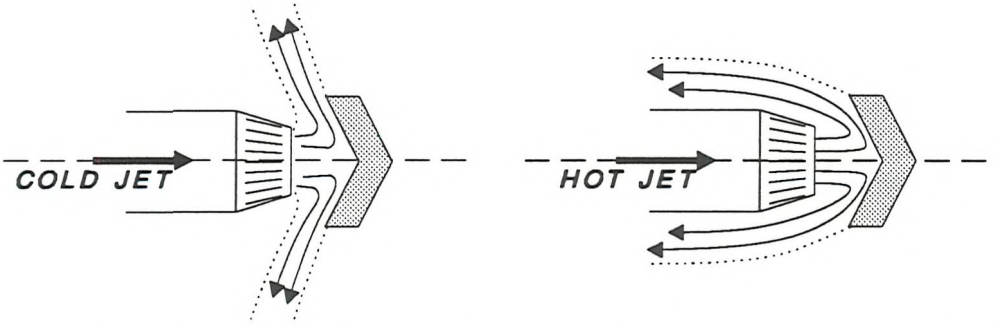

(b) Effect of jet temperature on thrust reverser performance

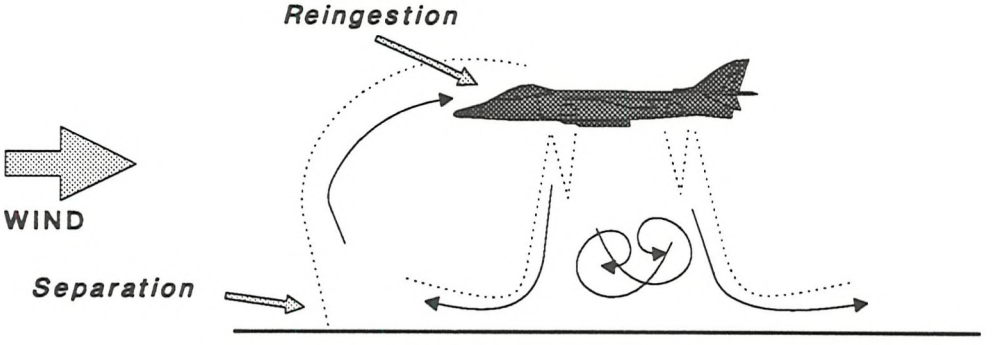

(c) VTOL jet interaction with ground (from ref 36)

Figure 3.1: Examples of propulsion aerodynamics

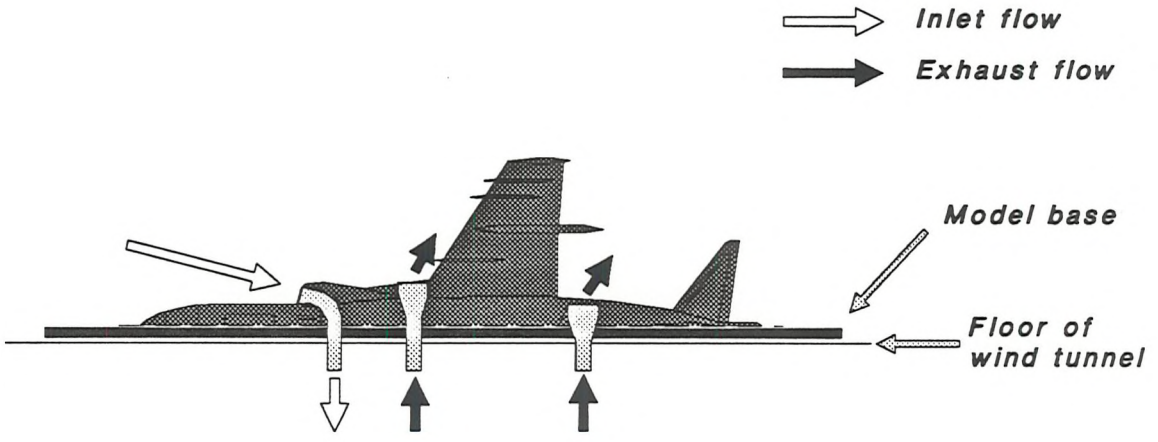

Figure 3.2: Half-span model for propulsion system tests

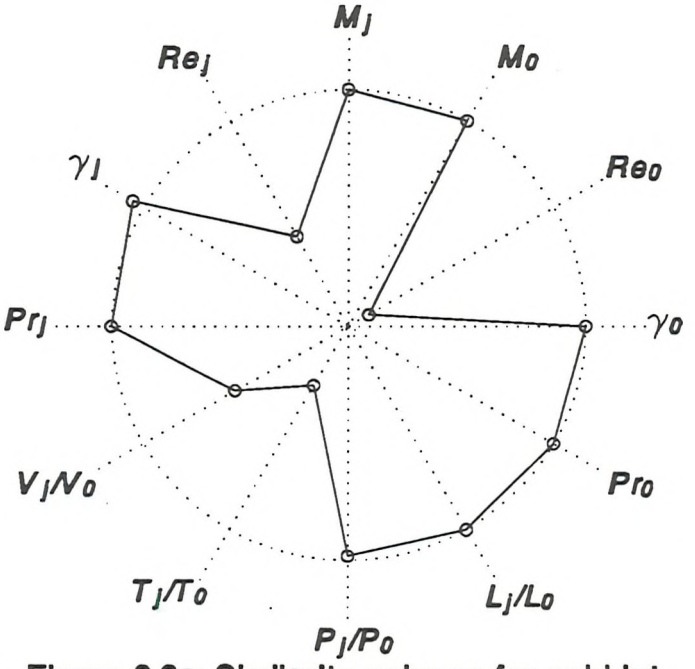

Figure 3.3a: Similarity polygon for cold jet

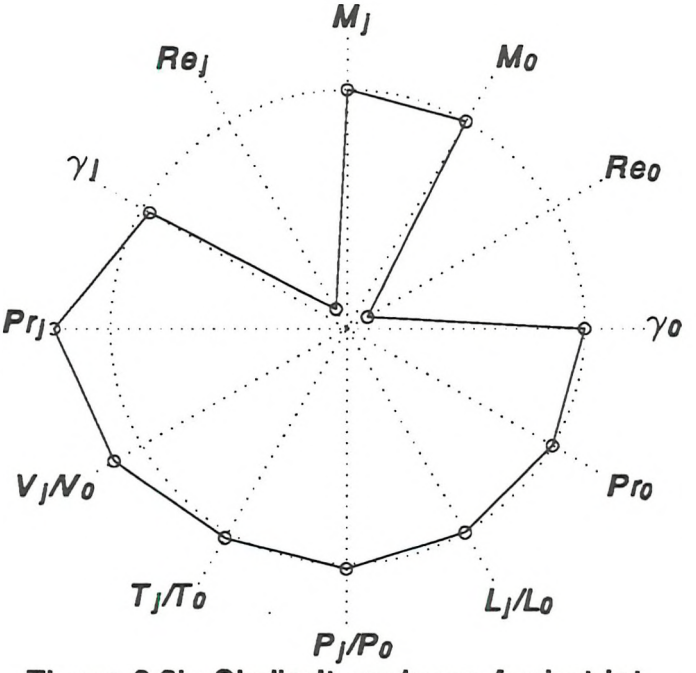

Figure 3.3b: Similarity polygon for hot jet

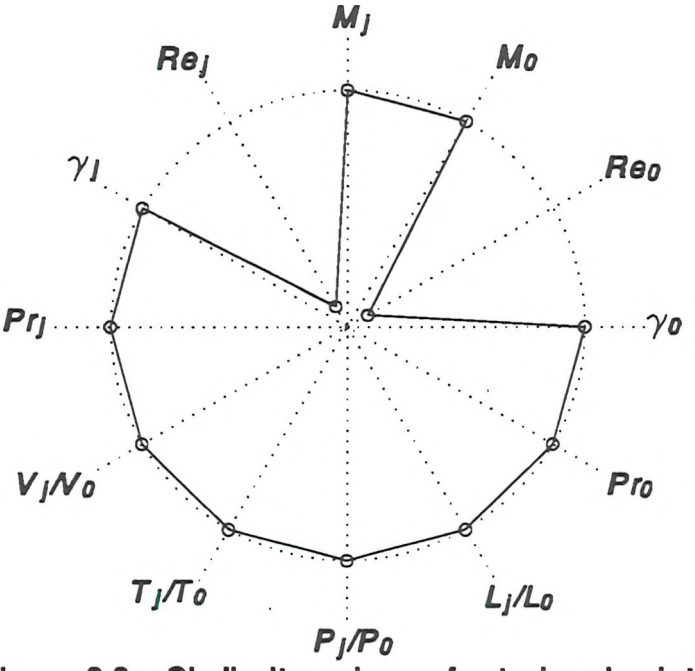

Figure 3.3c: Similarity polygon for turbo simulator

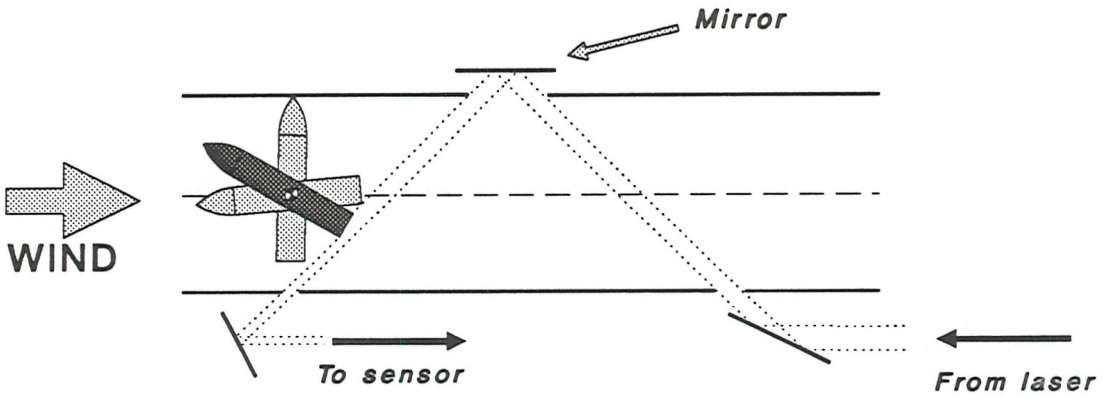

Figure 4.1: Initial axial position sensing geometry

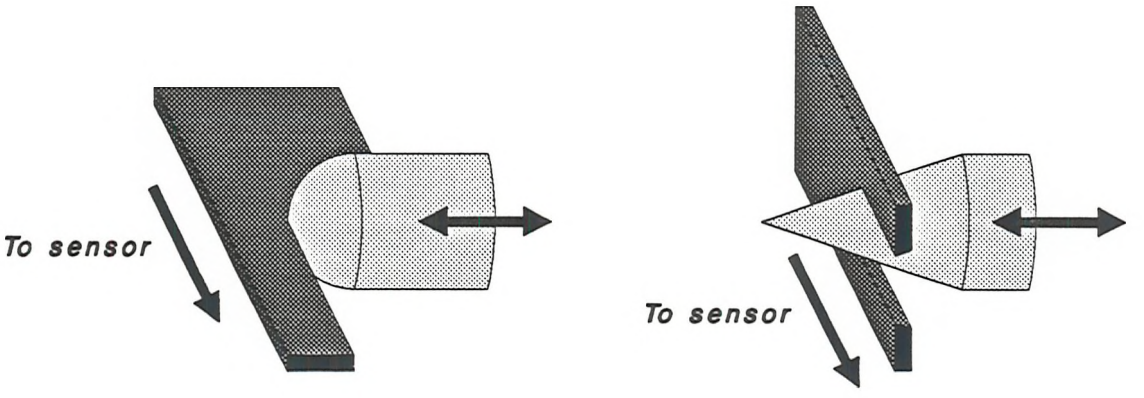

Figure 4.2: Axial position sensing for different nose geometries

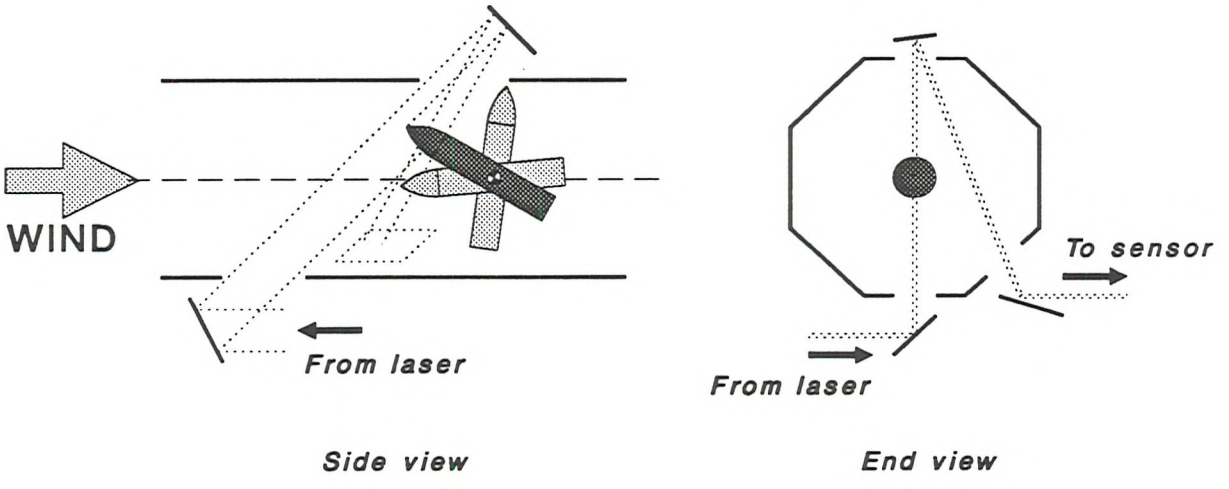

Figure 4.3: Modified axial position sensing geometry

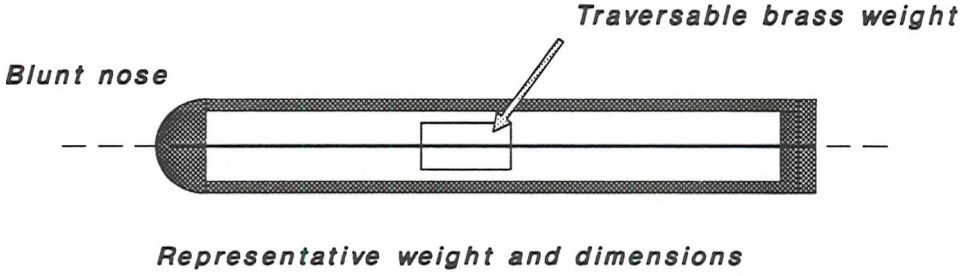

Figure 4.4: Representative propulsion simulator

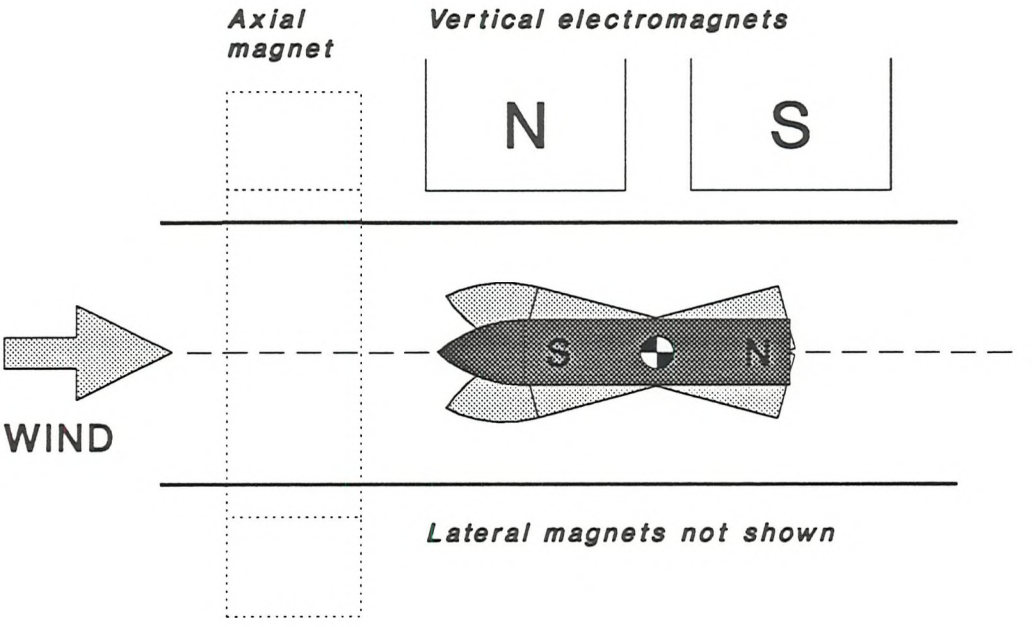

Figure 5.1: 'Automatic' magnetisation due to an asymmetric electromagnet array

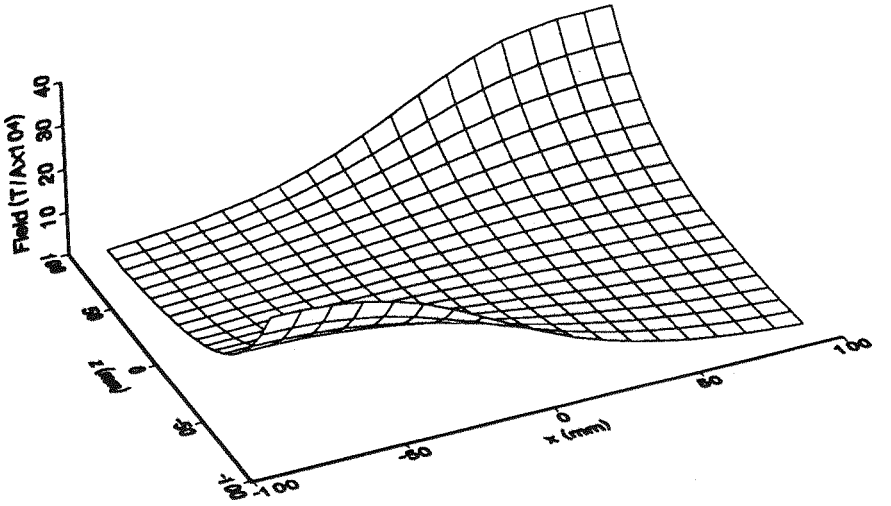

Figure 5.2a: Magnetic field produced by the group I electromagnets

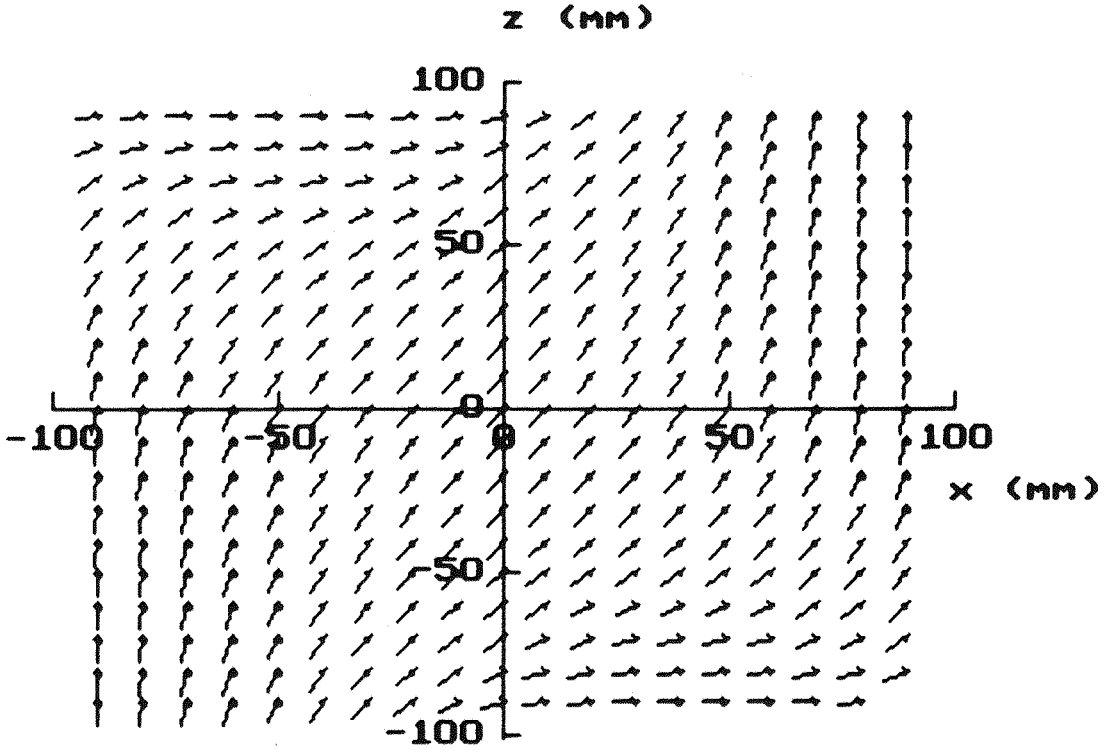

Figure 5.2b: Direction of group I magnetic field gradients

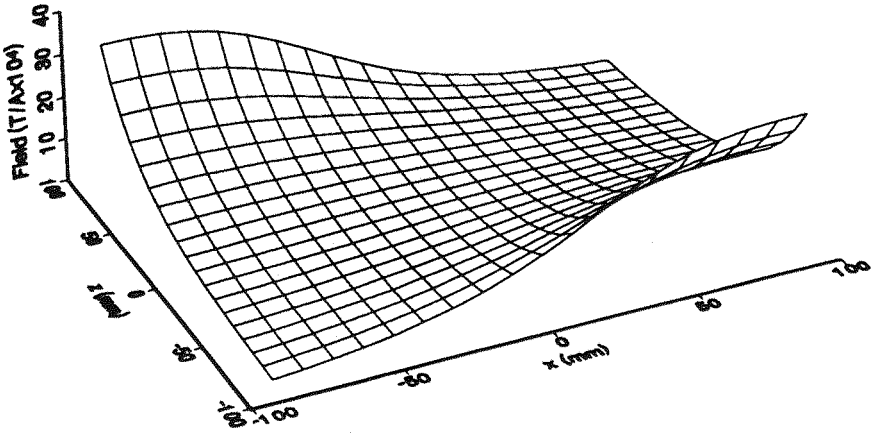

Figure 5.3a: Magnetic field produced by the group II electromagnets

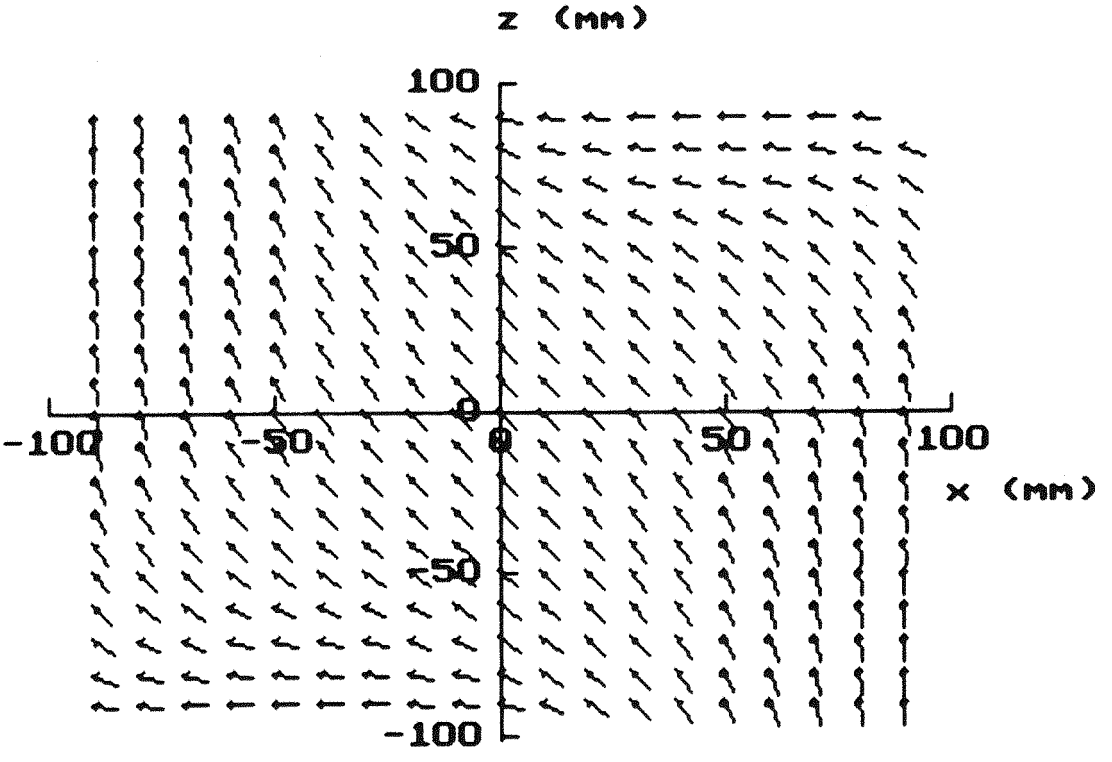

Figure 5.3b: Direction of group II magnetic field gradients

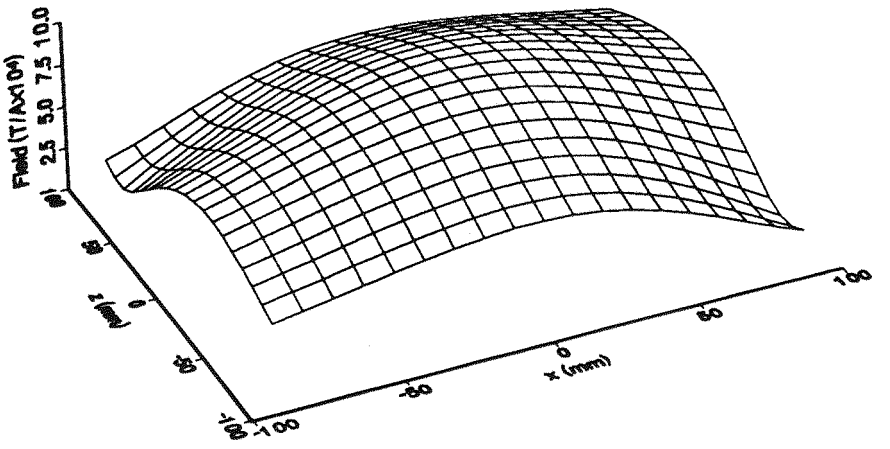

Figure 5.4a: Magnetic field produced by the group III electromagnets

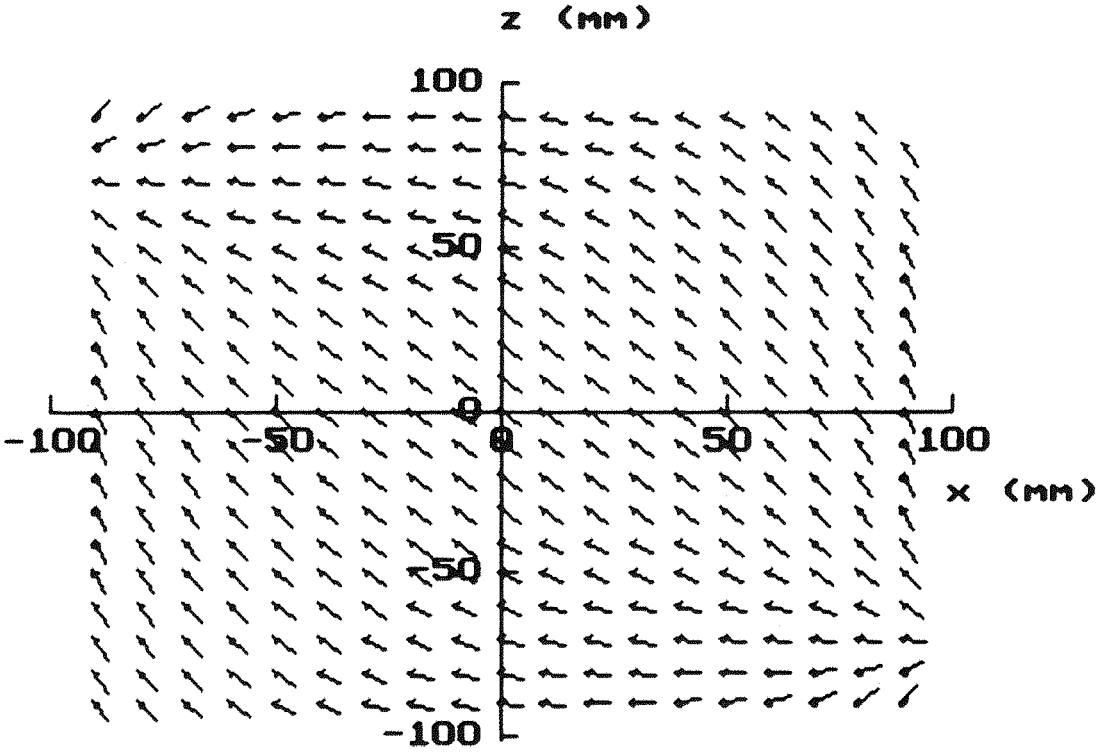

Figure 5.4b: Direction of group III magnetic field gradients

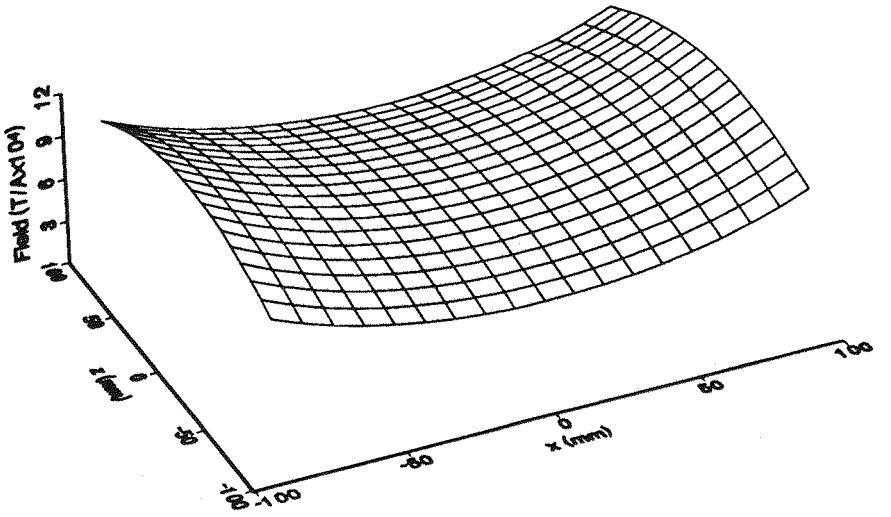

Figure 5.5a: Magnetic field produced by the group IV electromagnets

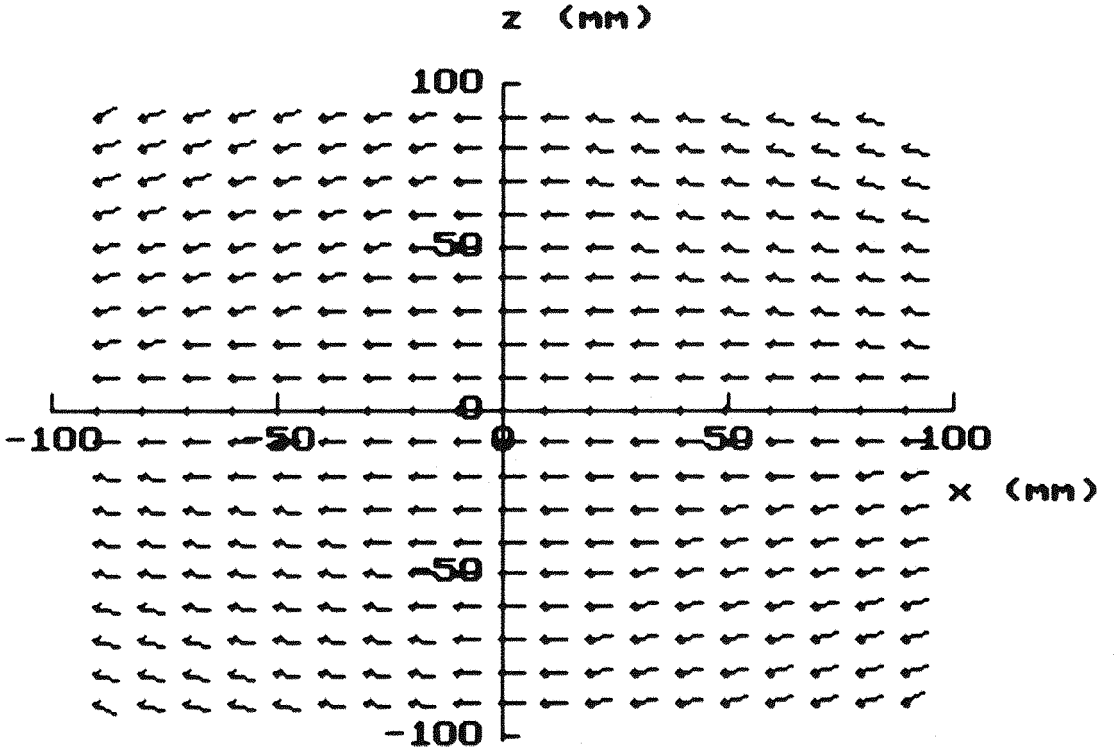

Figure 5.5b: Direction of group IV magnetic field gradients

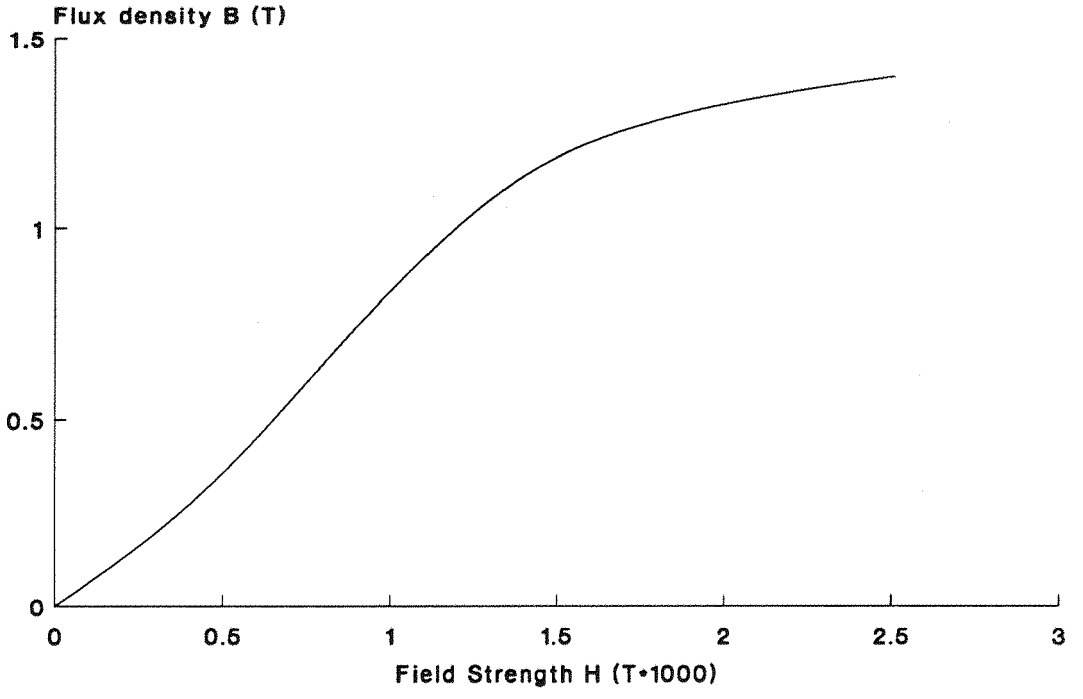

Figure 5.6: Magnetisation characteristic of cast steel

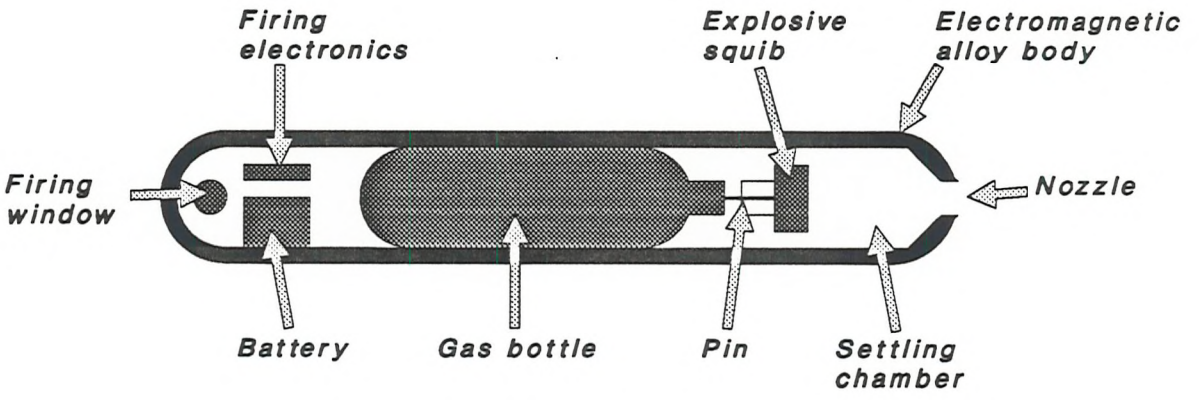

Figure 6.1: Schematic of compressed gas exhaust simulator

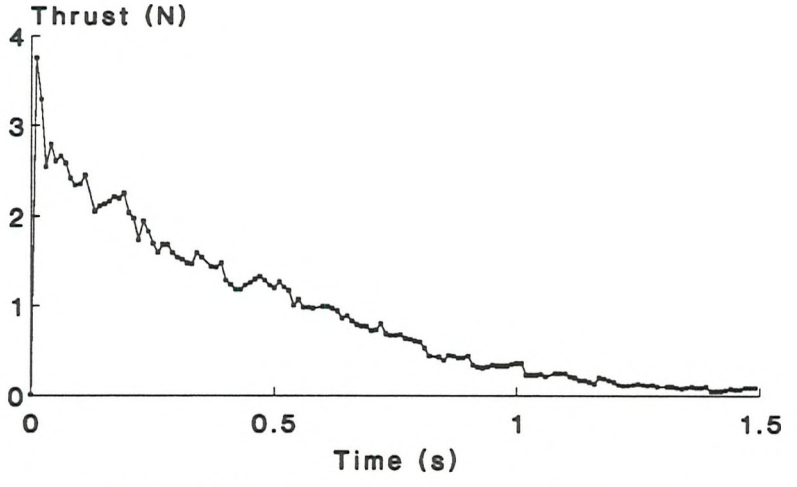

Figure 6.2: Thrust profile produced by the compressed gas propulsion simulator

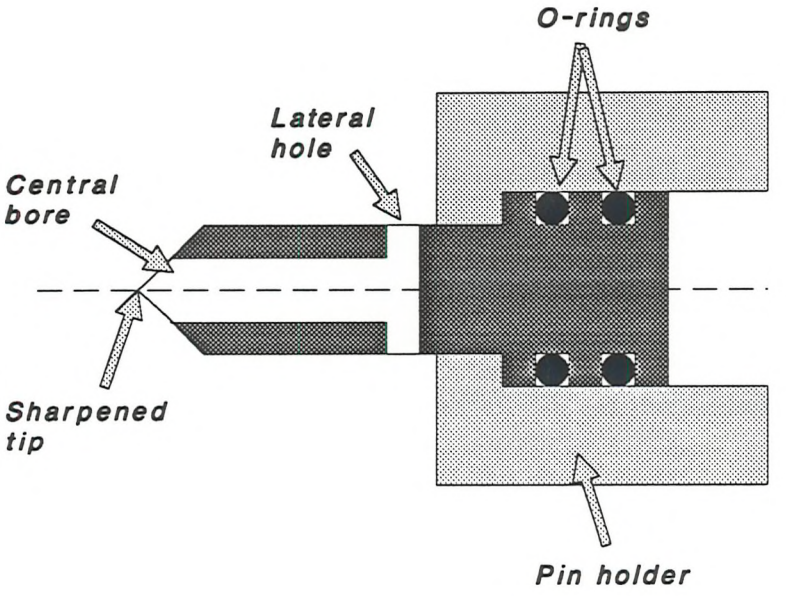

Figure 6.3: Design of firing pin for compressed gas thruster

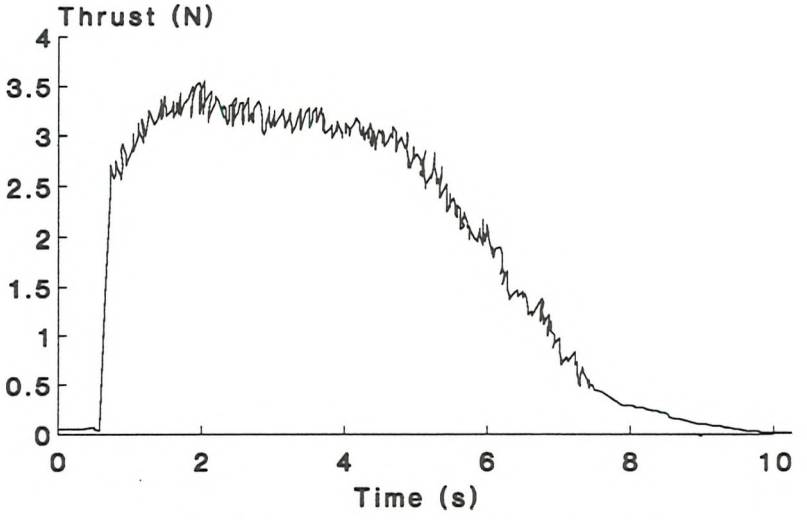

Figure 6.4: Performance of large compressed gas thruster (from ref 42)

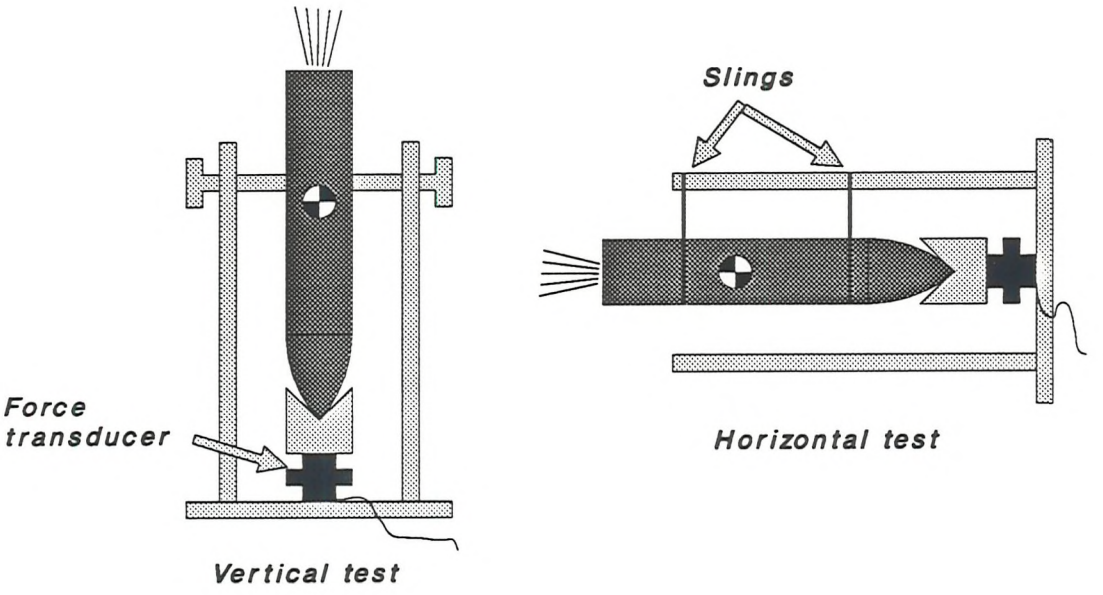

Figure 6.5: Thruster test stand

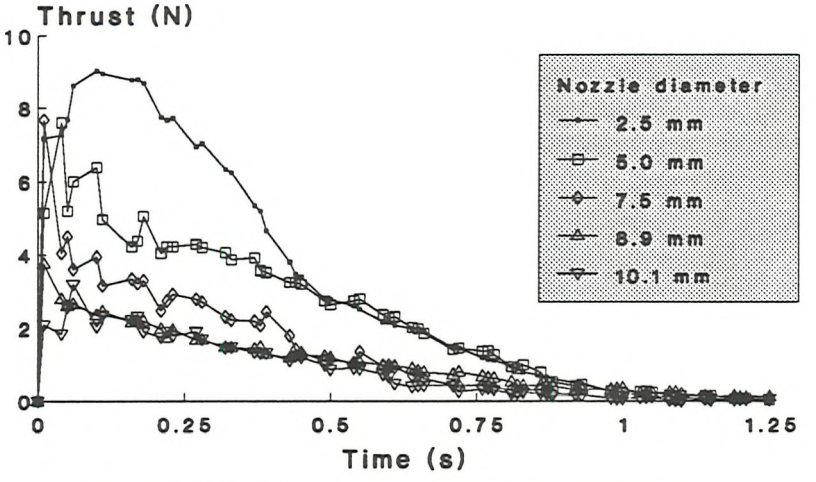

Figure 6.6: Effect of nozzle enlargement
on compressed gas thruster performance

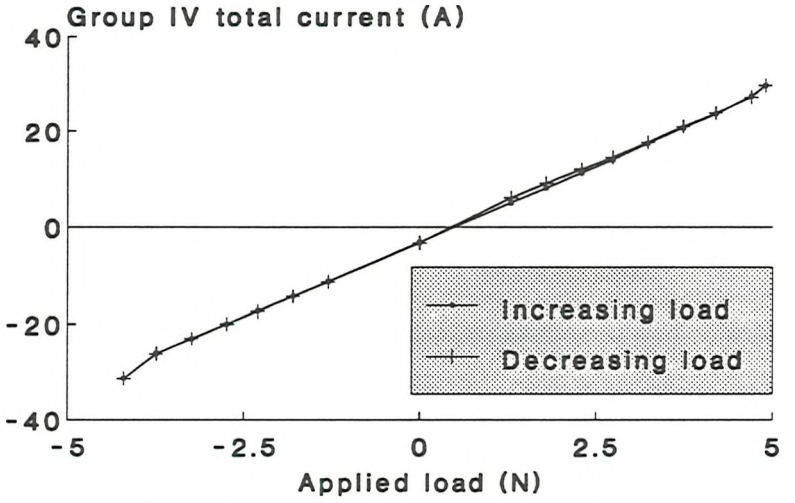

Figure 6.7: Axial force calibration for compressed gas thruster

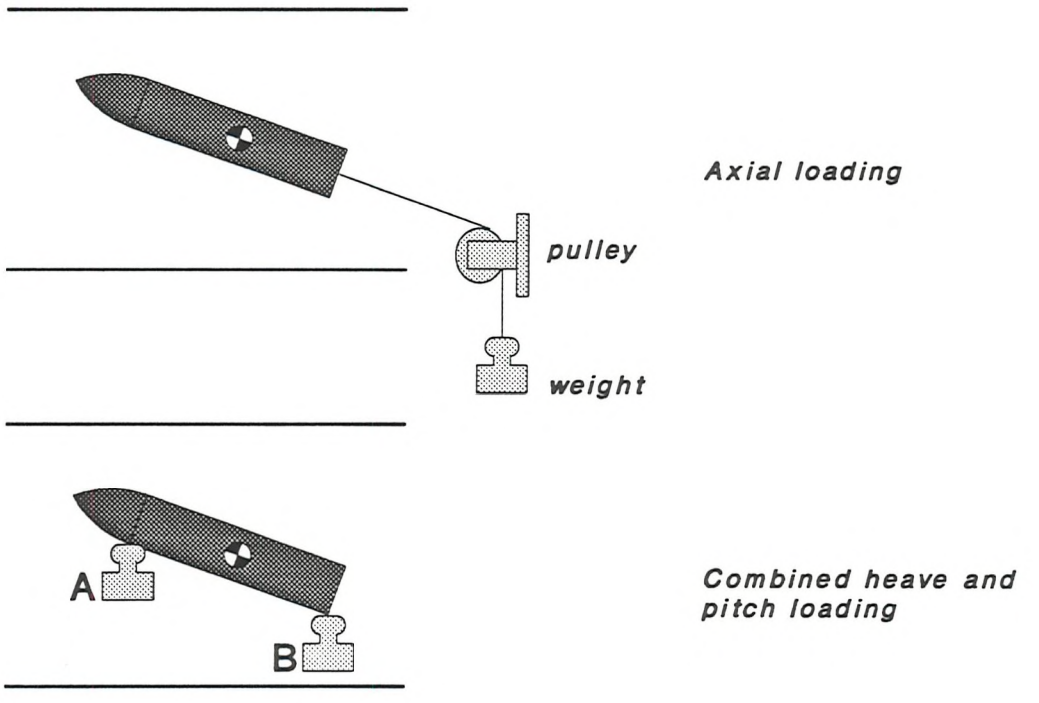

Figure 6.8: Static calibration loading geometries

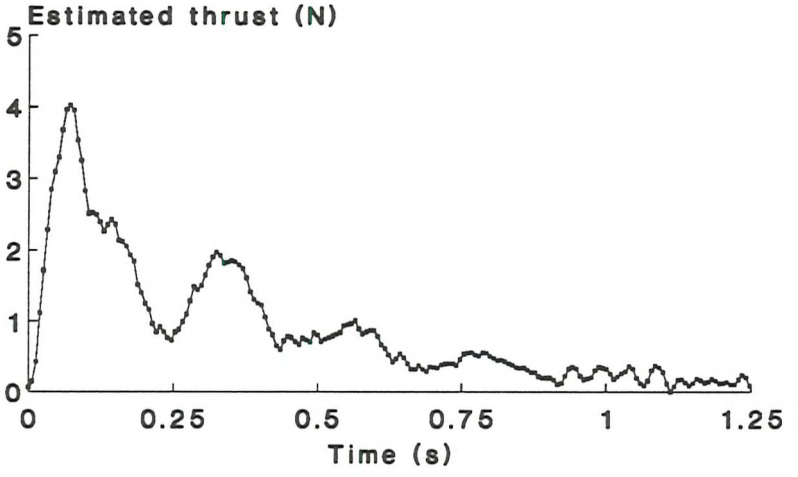

Figure 6.9: Thrust calculated from position and current data

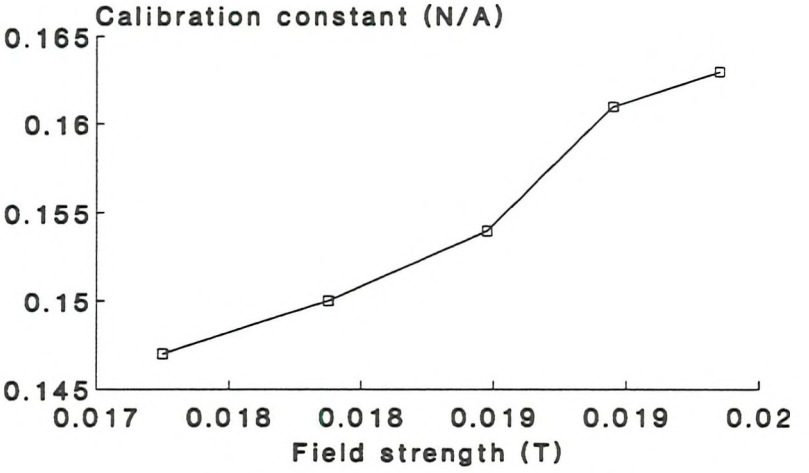

Figure 6.10: Variation of axial calibration constant with magnetising field strength

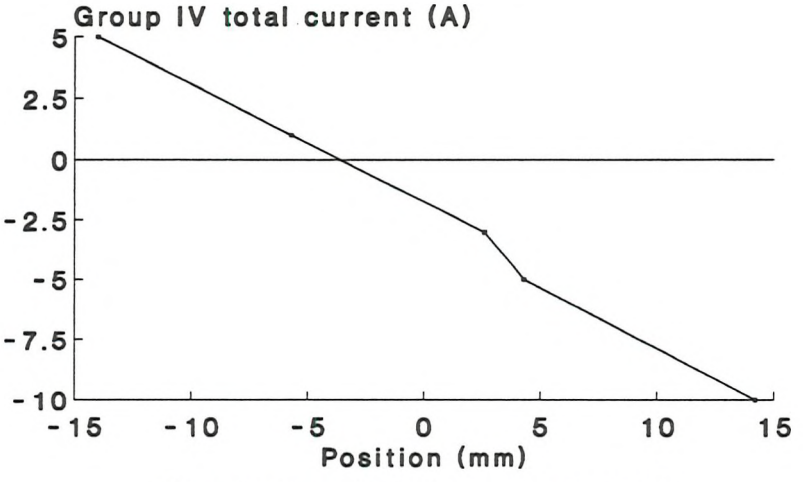

Figure 6.11: Variation of current in group IV magnets with axial position

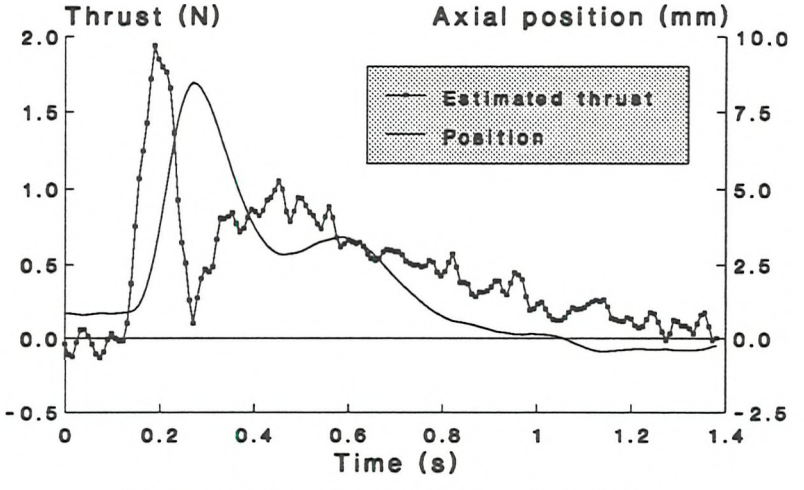

Figure 6.12: Improved thrust profile calculated from current and position

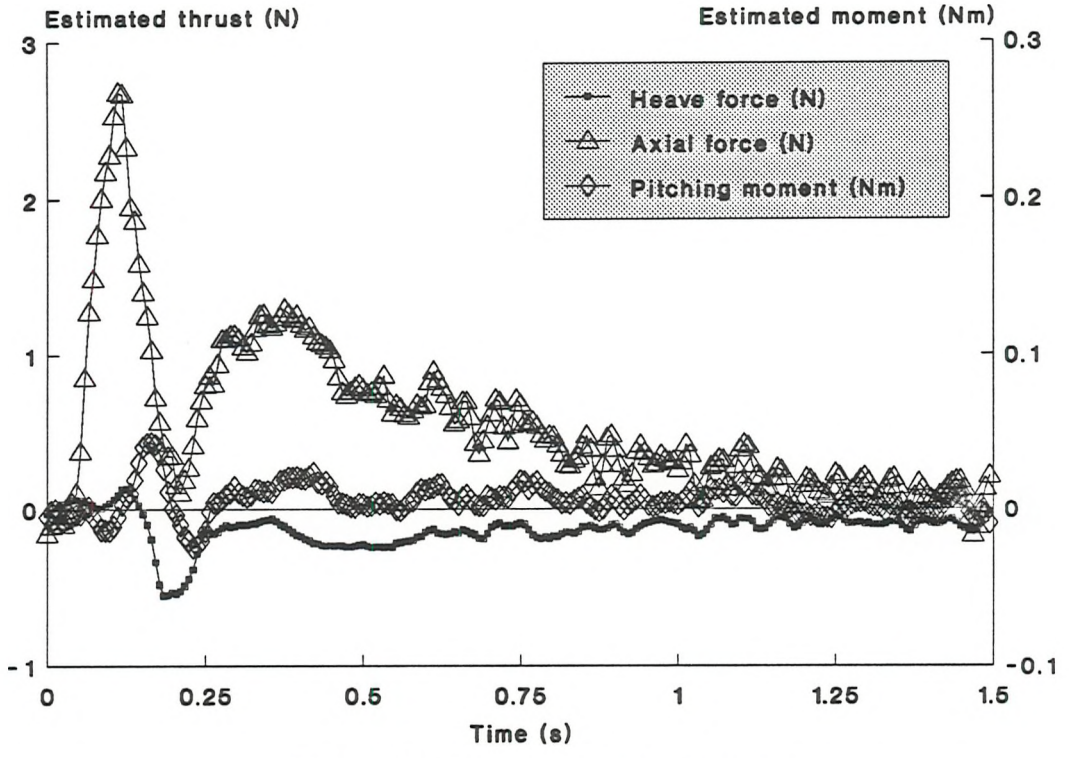

Figure 6.13: Force and moment results
for 10 degree test at Mach 0.1

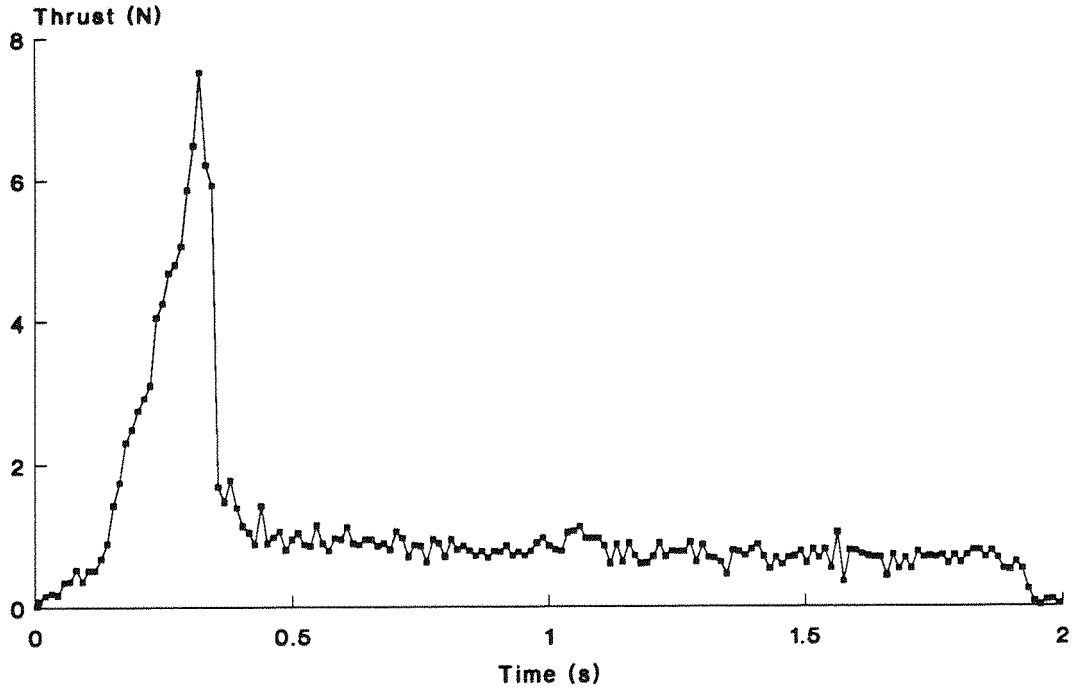

Figure 7.1: Thrust profile for Estes solid propellant rocket motor

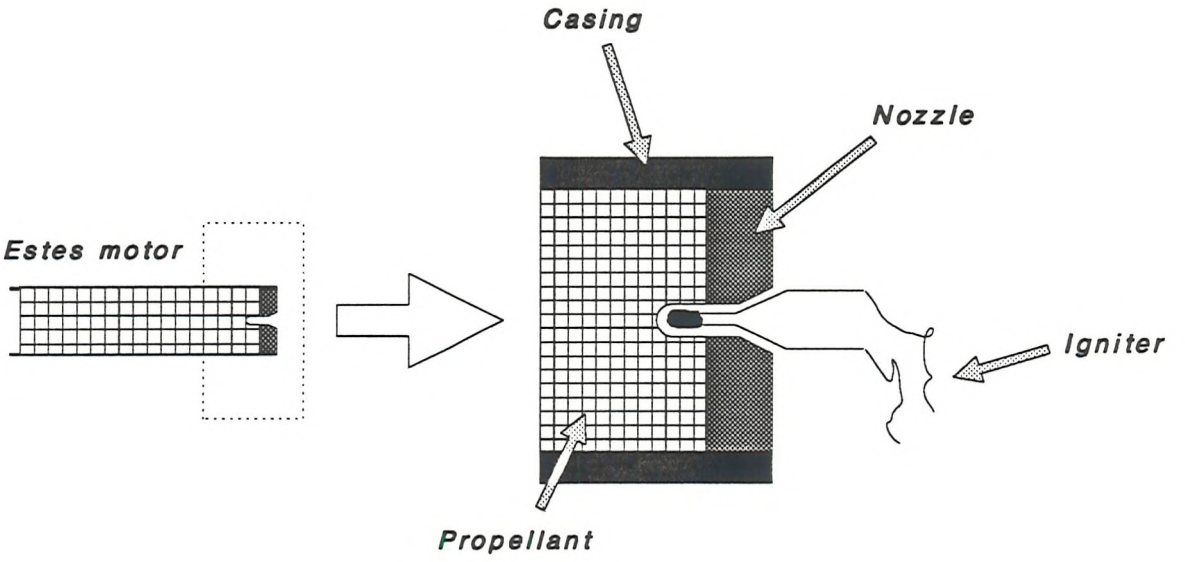

Figure 7.2: Ignition of Estes rockets

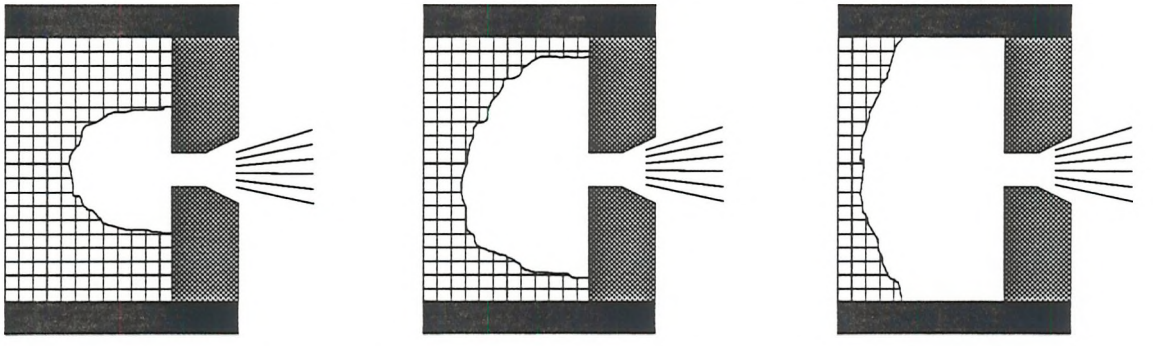

Figure 7.3: Transition from *Core* to *End* burning

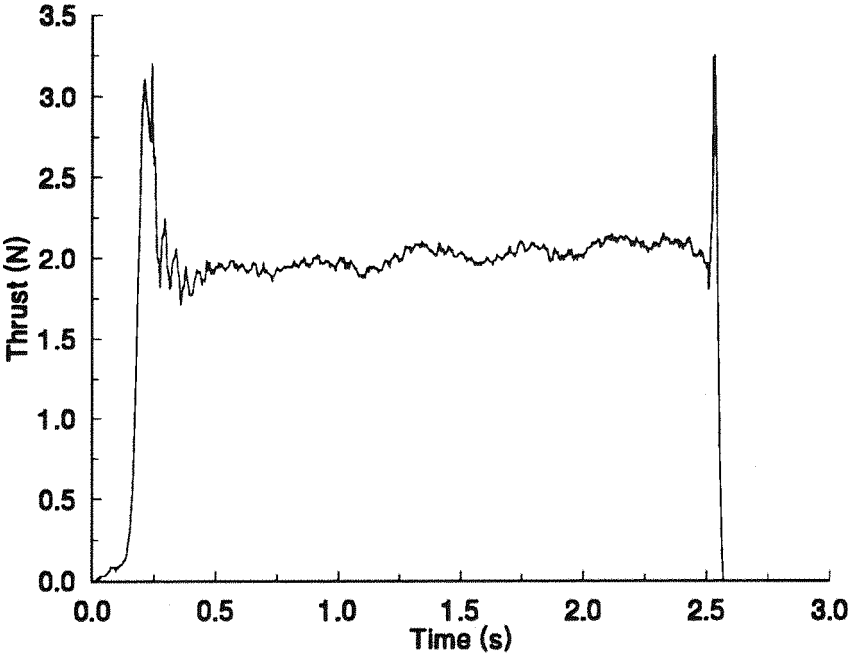

Figure 7.4: New solid propellant rocket motor thrust profile

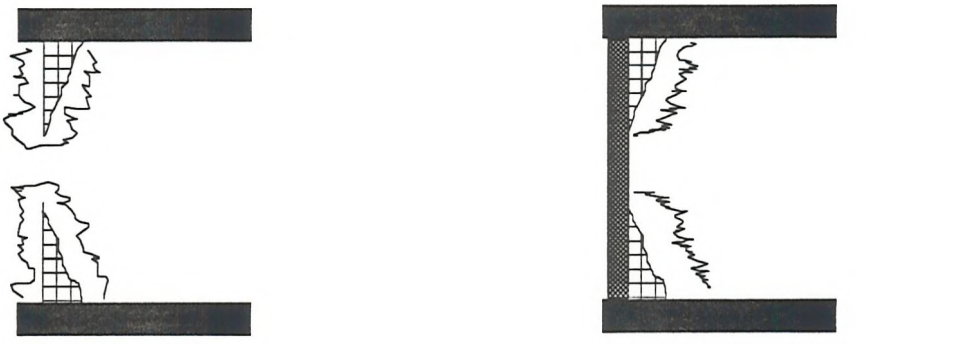

Figure 7.5a: Use of an epoxy layer
to control end of thrust profile

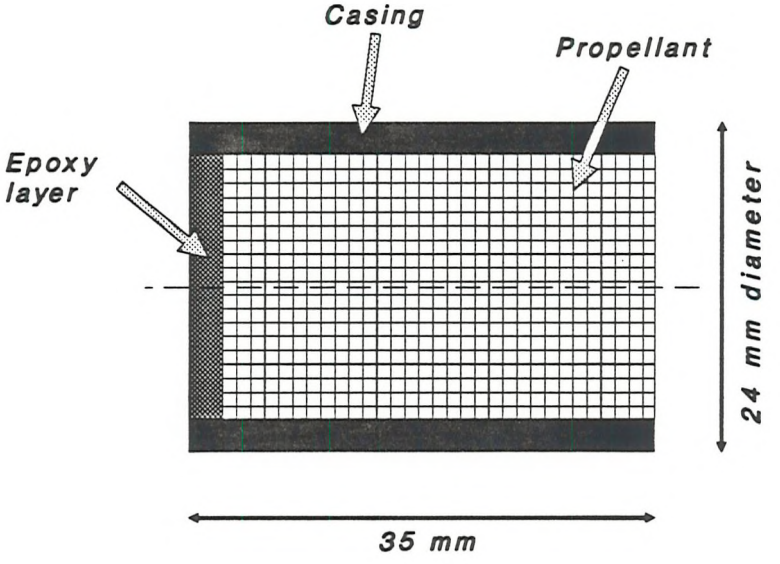

Figure 7.5b: New rocket motor design

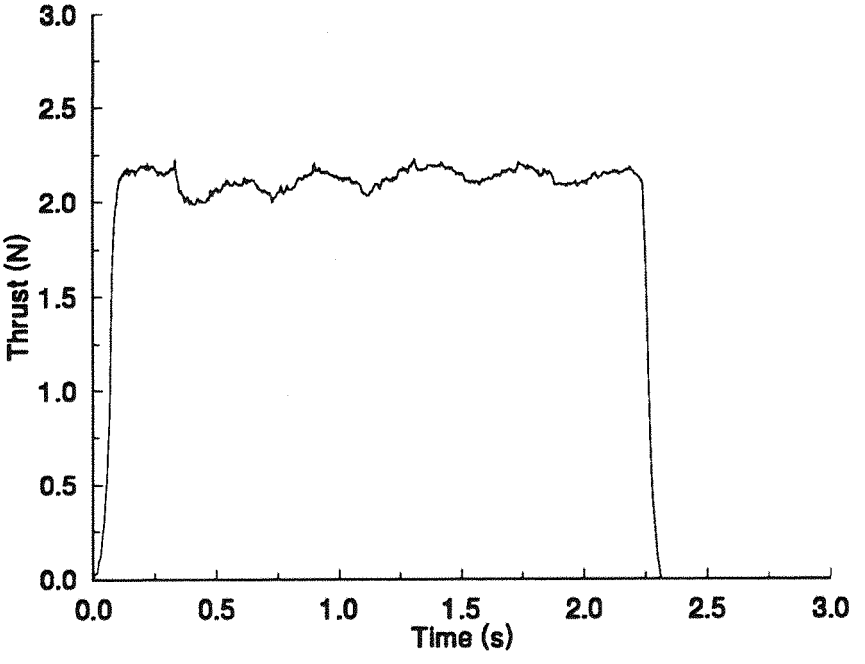

Figure 7.6: Thrust profile for improved solid rocket motor

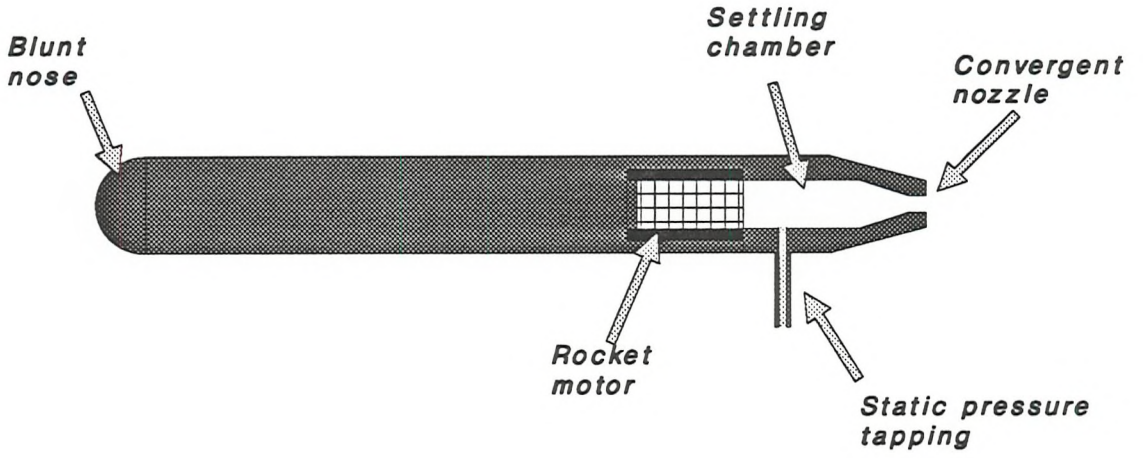

Figure 7.7: Schematic of solid rocket exhaust simulator

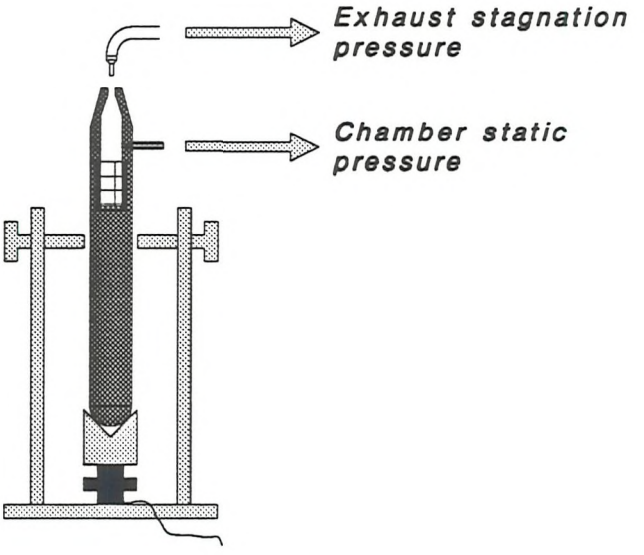

Figure 7.8: Pressure measurement with solid rockets

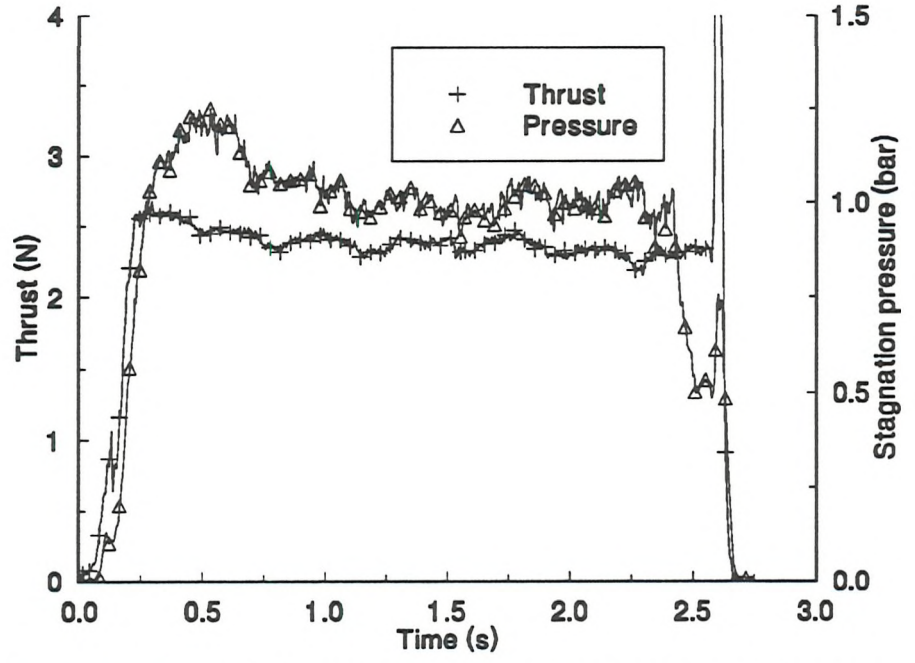

Figure 7.9: Thrust and exhaust stagnation pressure for a solid rocket

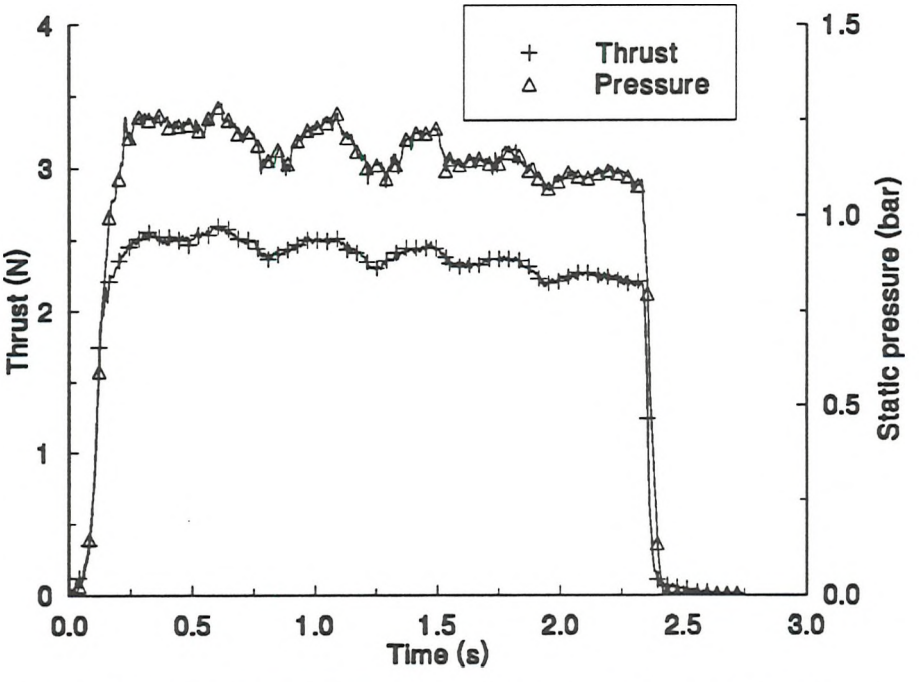

Figure 7.10: Thrust and chamber static pressure for a solid rocket

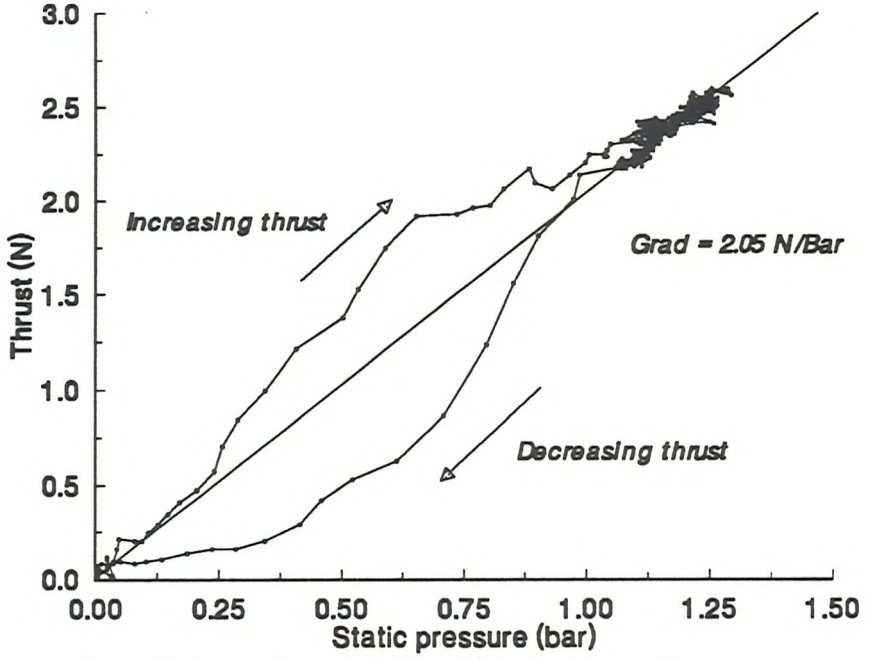

Figure 7.11: Solid rocket chamber static pressure and thrust

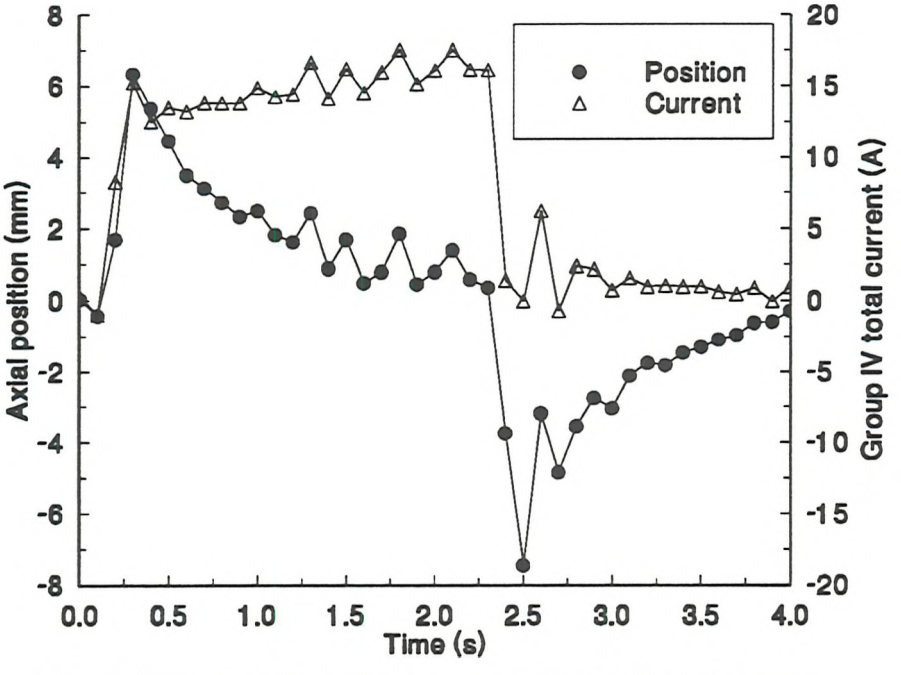

Figure 7.12: Control system response to a solid rocket firing

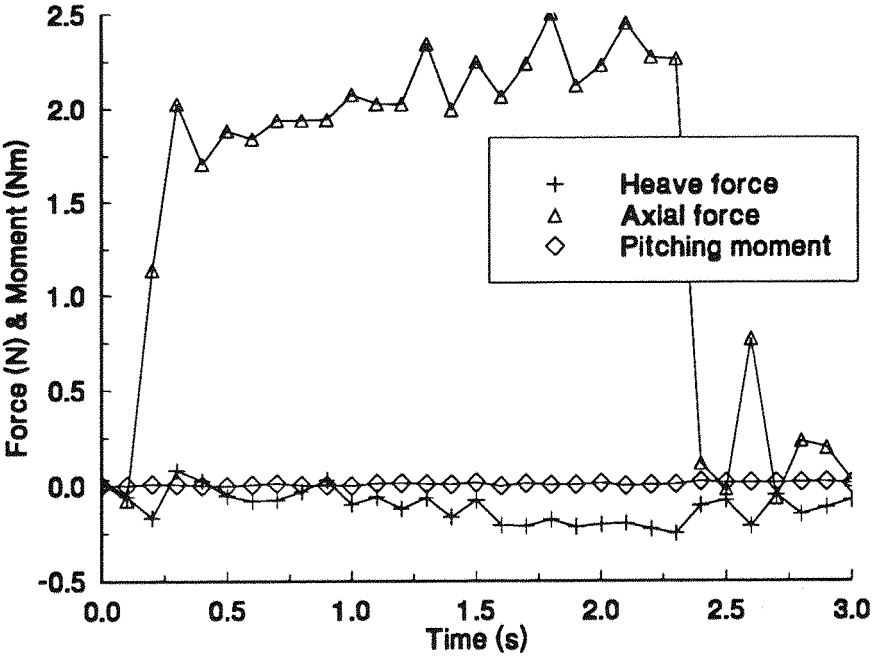

Figure 7.13: Measured loads on solid rocket thruster in suspension

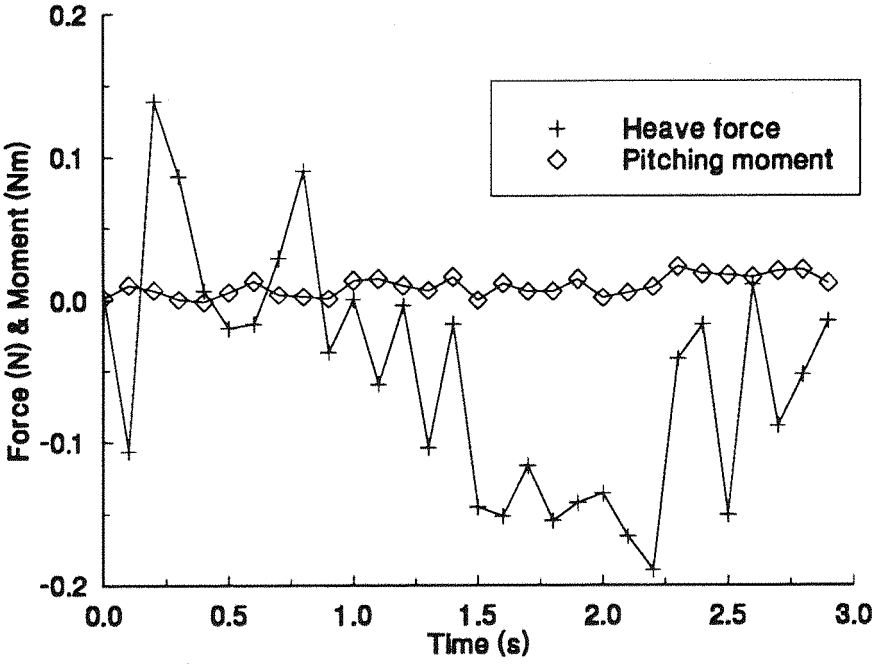

Figure 7.14: Observed heave force due to consumption of propellant

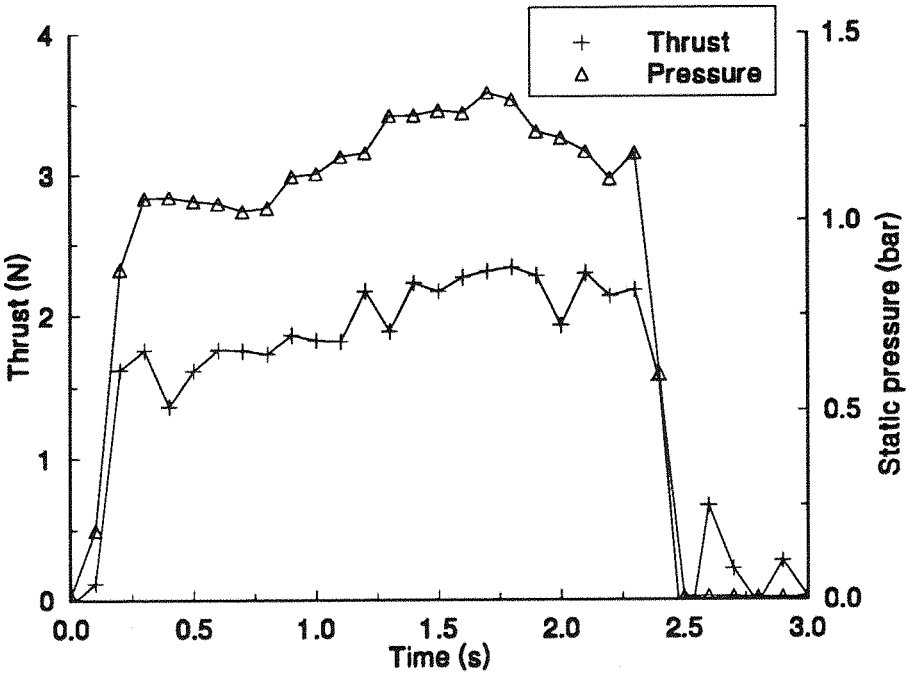

Figure 7.1 5: Thrust and chamber pressure for a suspended rocket

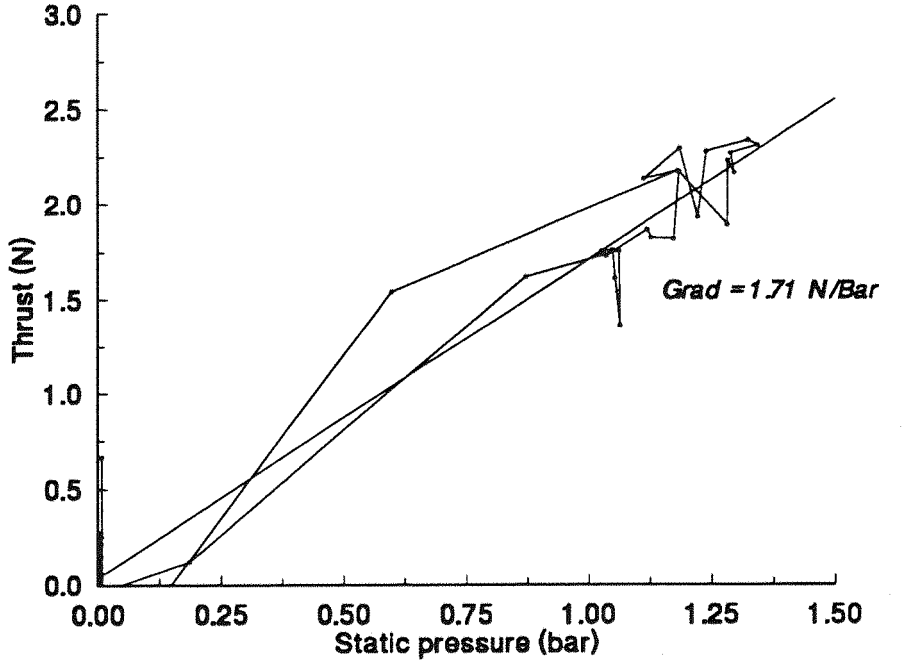

Figure 7.1 6: Static pressure and thrust from suspended solid rocket

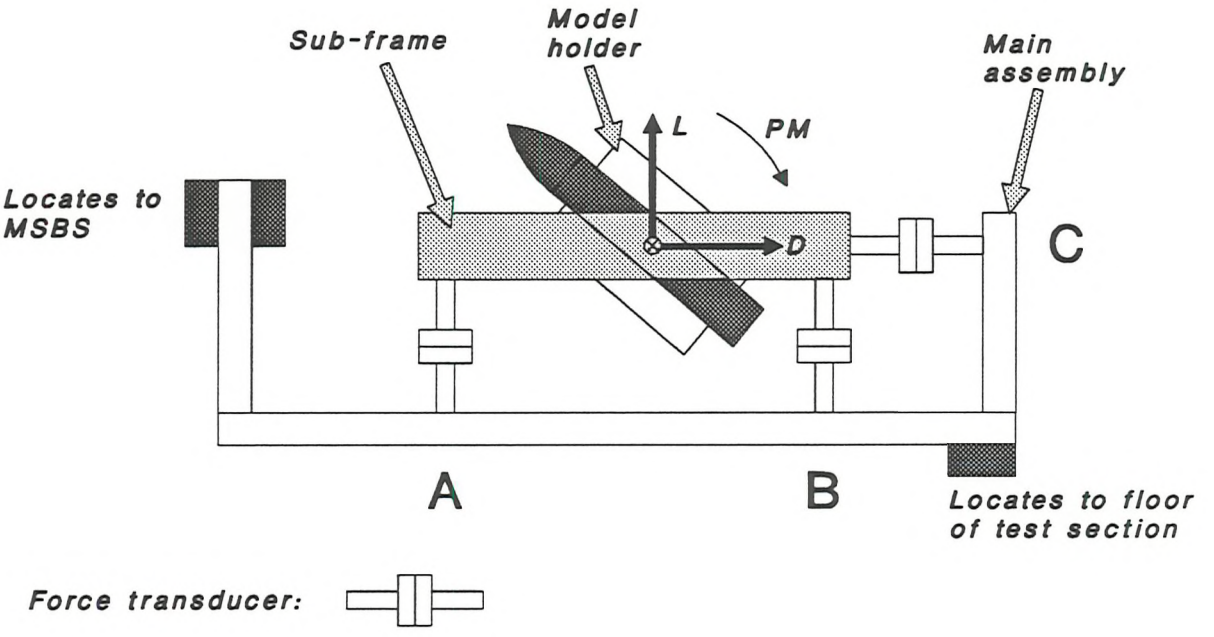

Figure 8.1: DFM rig schematic

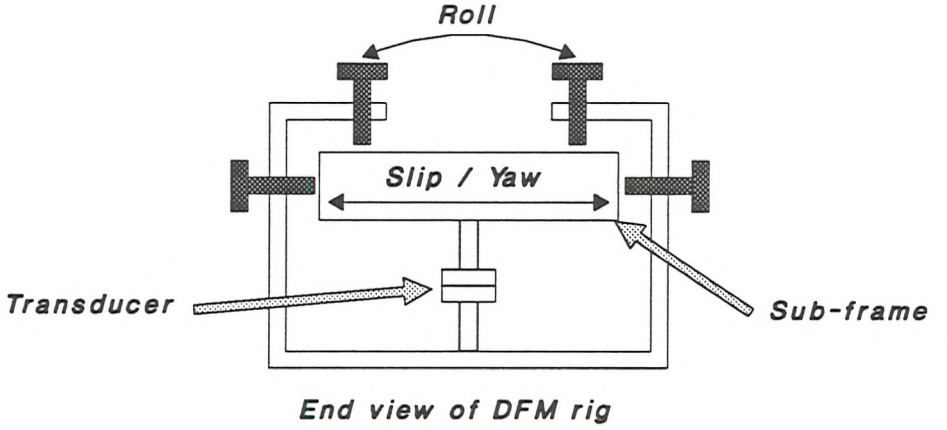

Figure 8.2: Use of stops to restrict lateral motion of DFM rig sub-frame

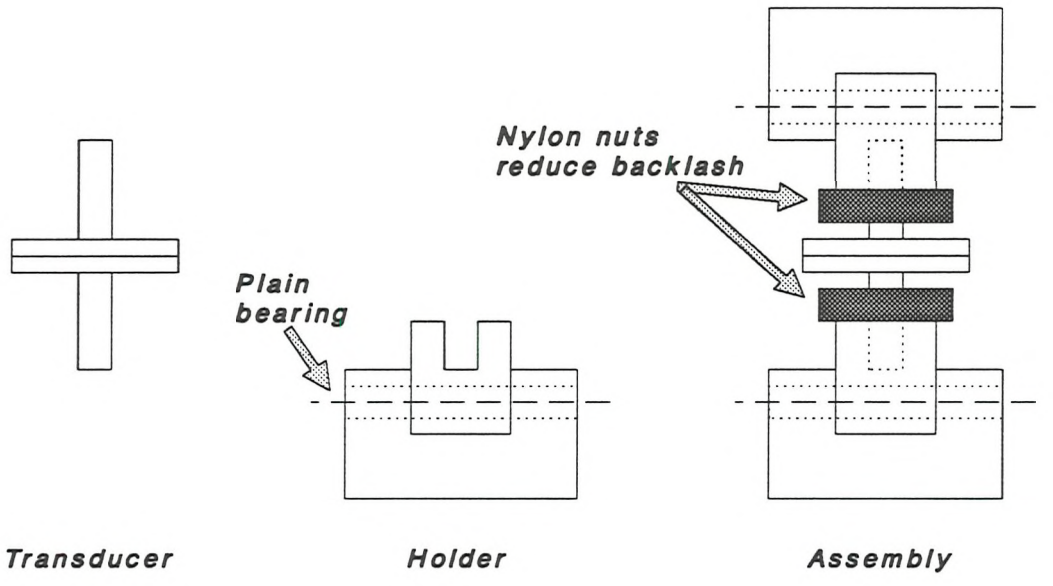

Figure 8.3: Force transducer installation

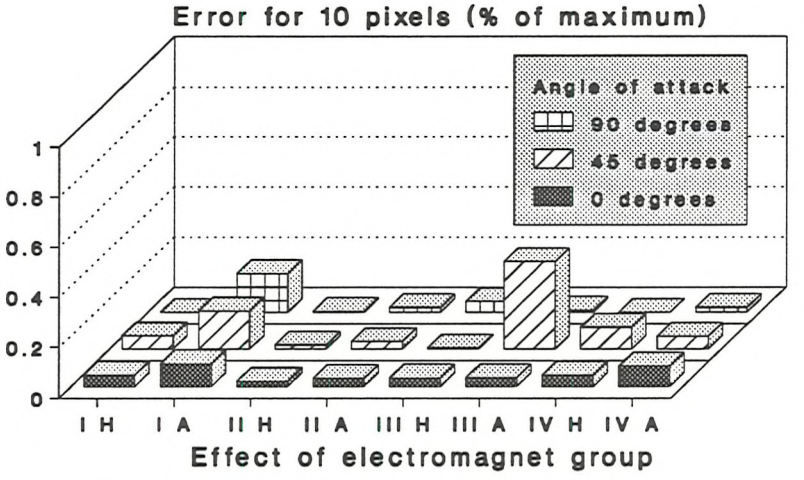

Figure 9.1a: Influence of heave position error on magnet group effectiveness

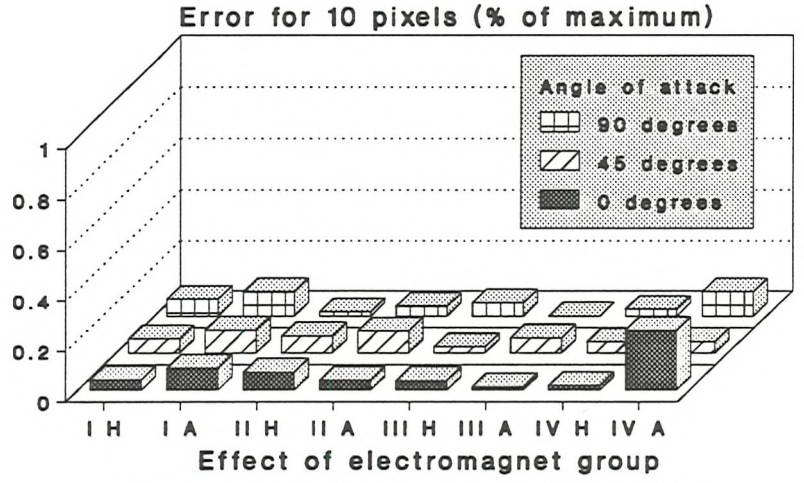

Figure 9.1b: Influence of axial position error on magnet group effectiveness

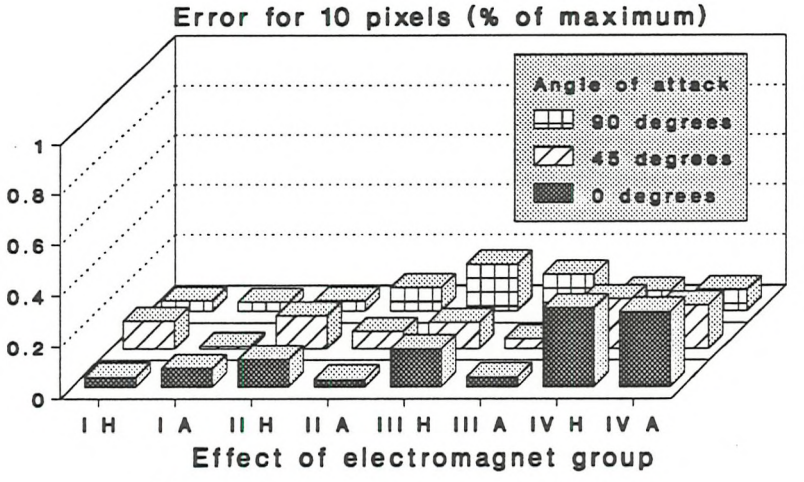

Figure 9.1c: Influence of sideslip error on magnet group effectiveness

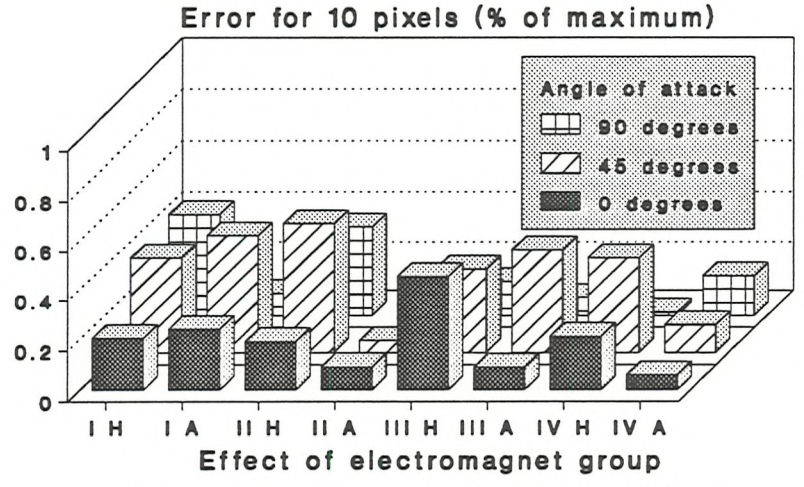

Figure 9.1d: Influence of pitch position error on magnet group effectiveness

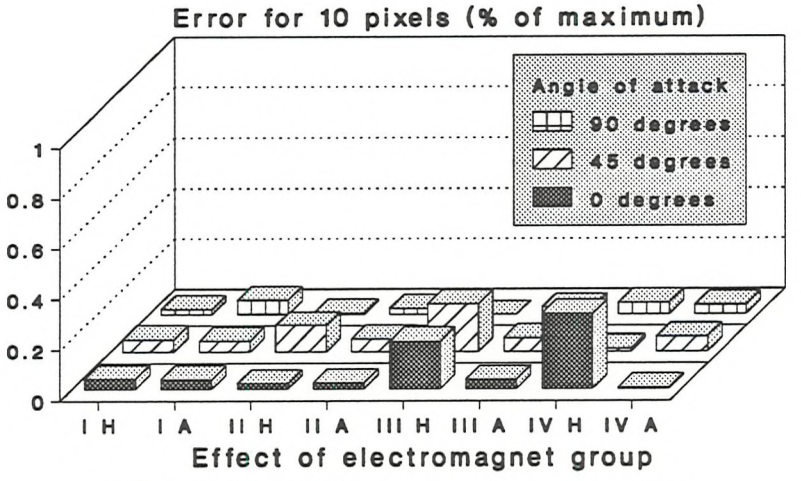

Figure 9.1e: Influence of yaw position error on magnet group effectiveness

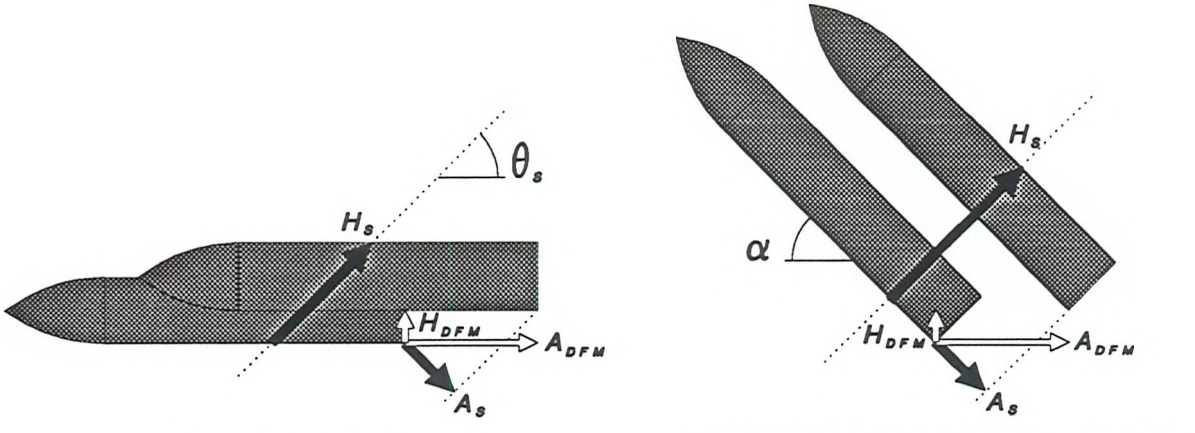

Low incidence

Larger heave motion in sensing axes at higher incidence

Figure 9.2: Effect of change in incidence on coupling of position measures

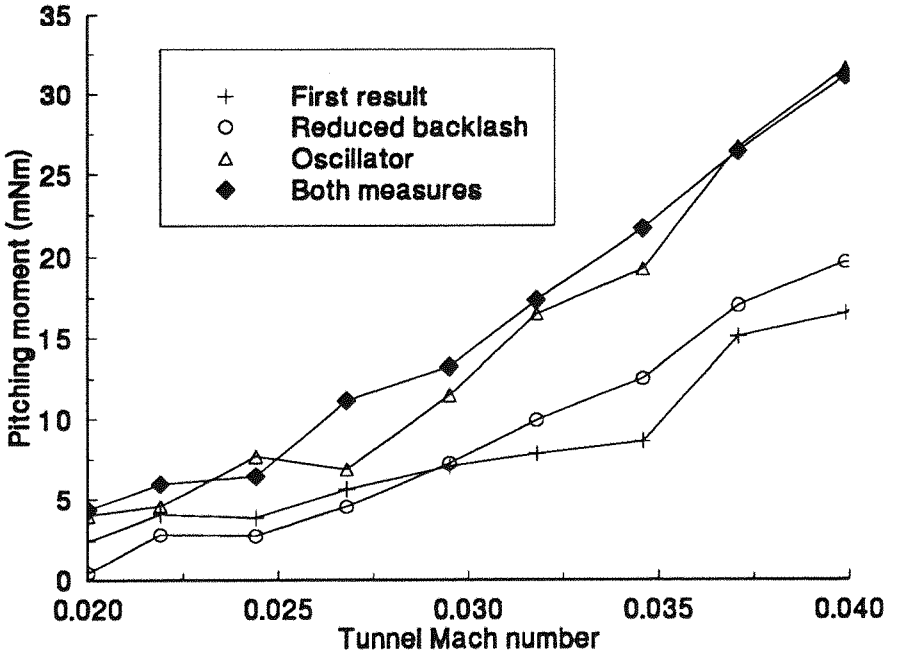

Figure 9.3: Change in measured moment with reduced rig friction for the ogive cylinder at 30 degrees of incidence

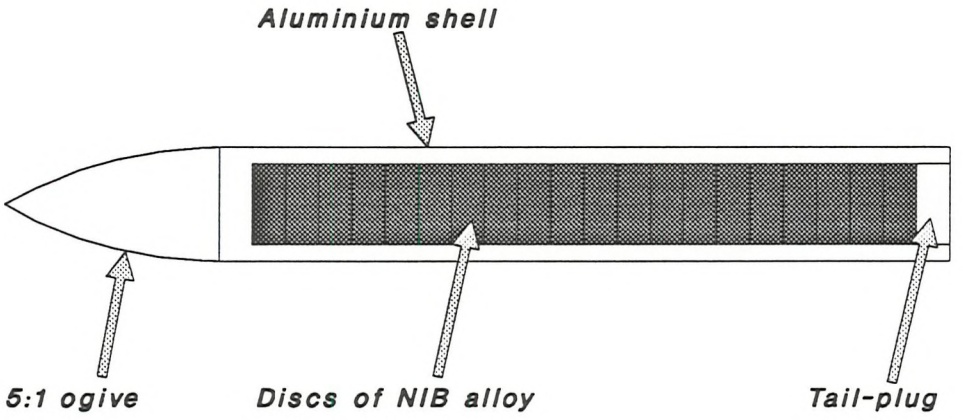

Figure 10.1: Ogive cylinder model

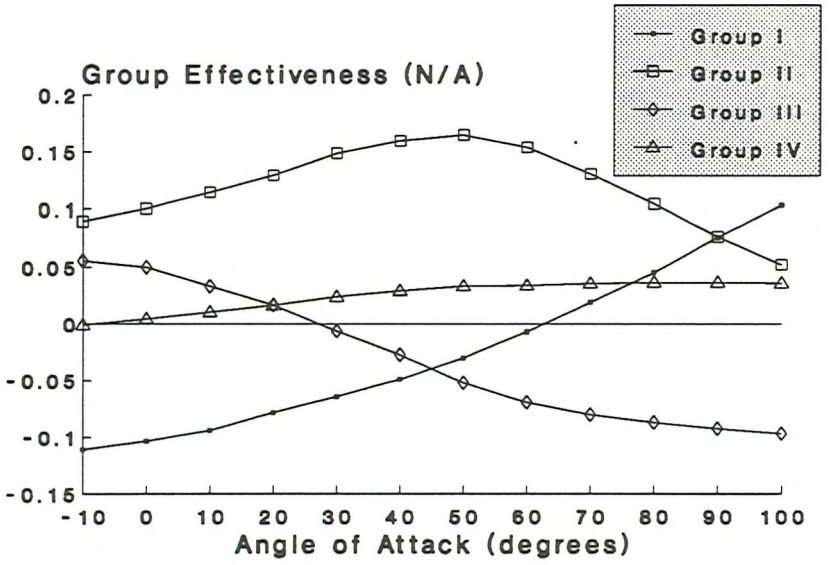

Figure 10.2: Effectiveness of magnet groups in producing lift force

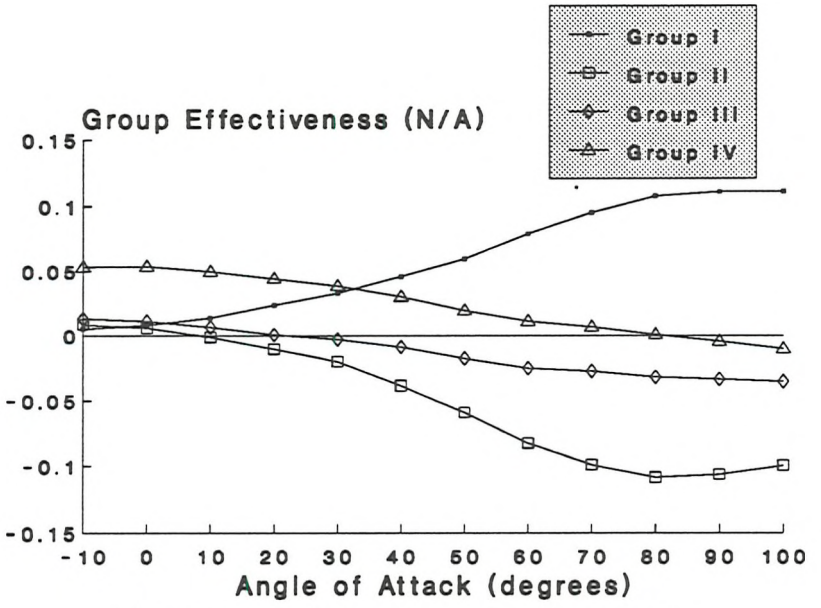

Figure 10.3: Effectiveness of magnet groups in producing drag force

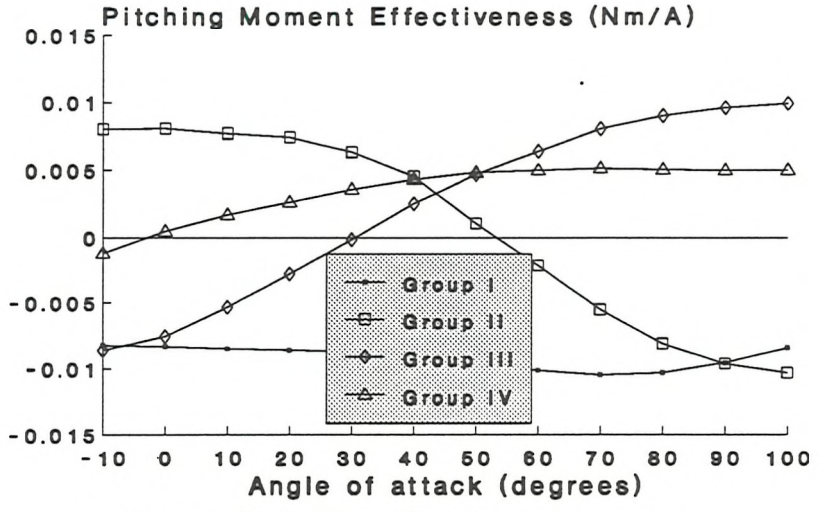

Figure 10.4: Effectiveness of magnet groups in producing pitching moment

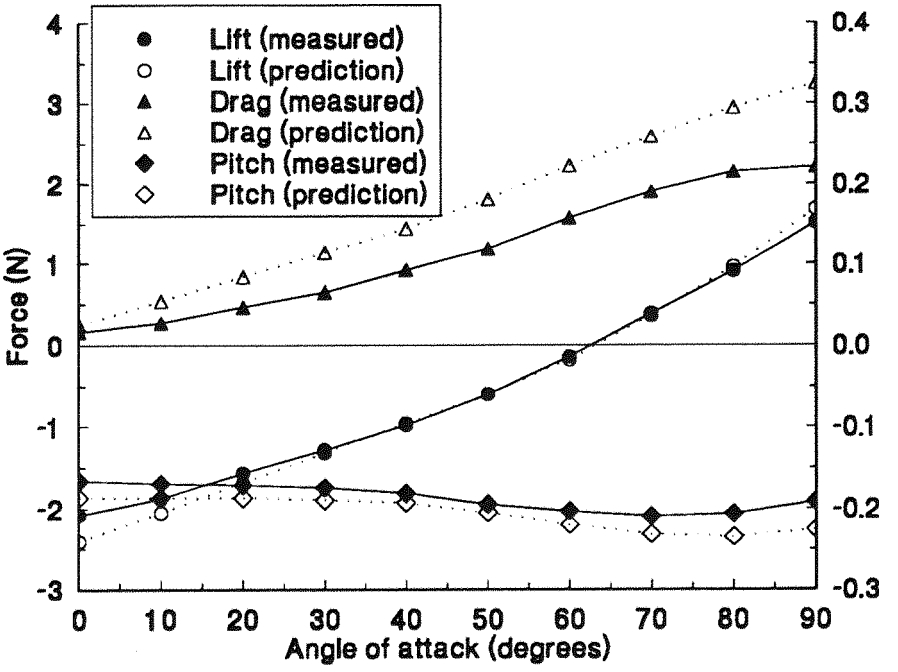

Figure 10.5: Measured group I effectiveness vs prediction

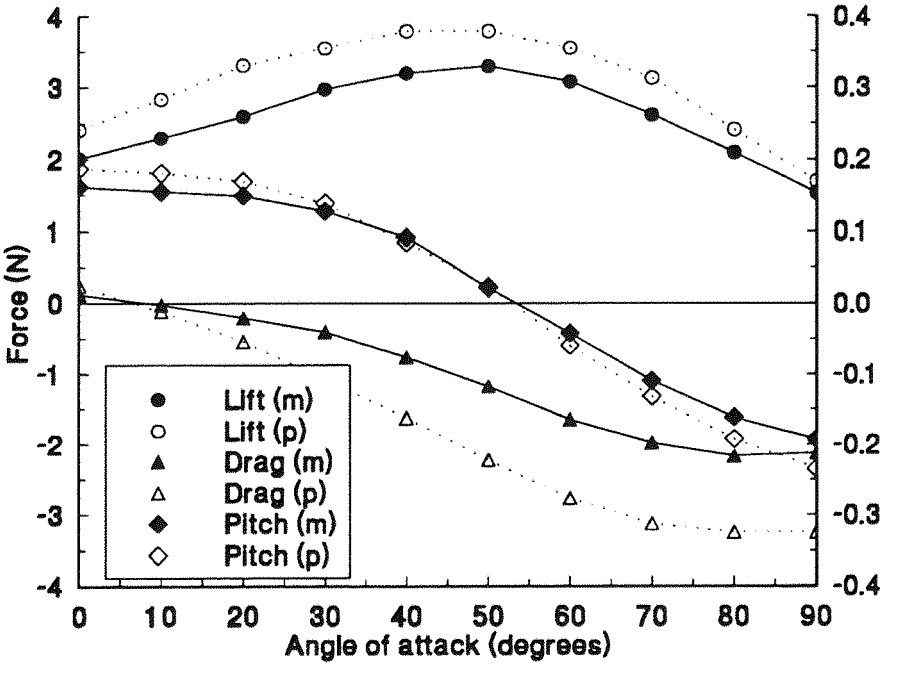

Figure 10.6: Measured group II effectiveness vs prediction

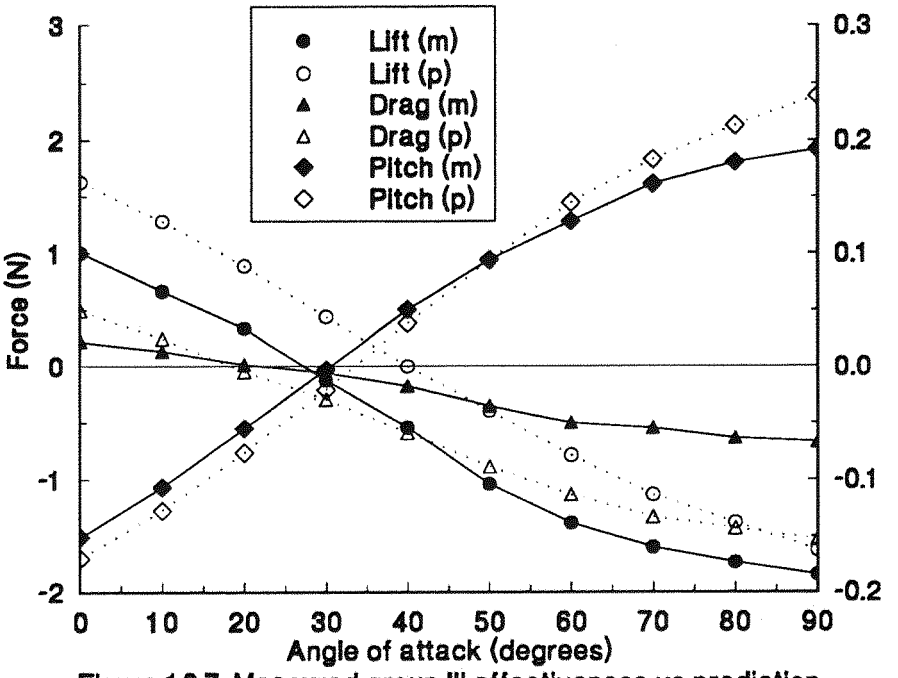

Figure 10.7: Measured group III effectiveness vs prediction

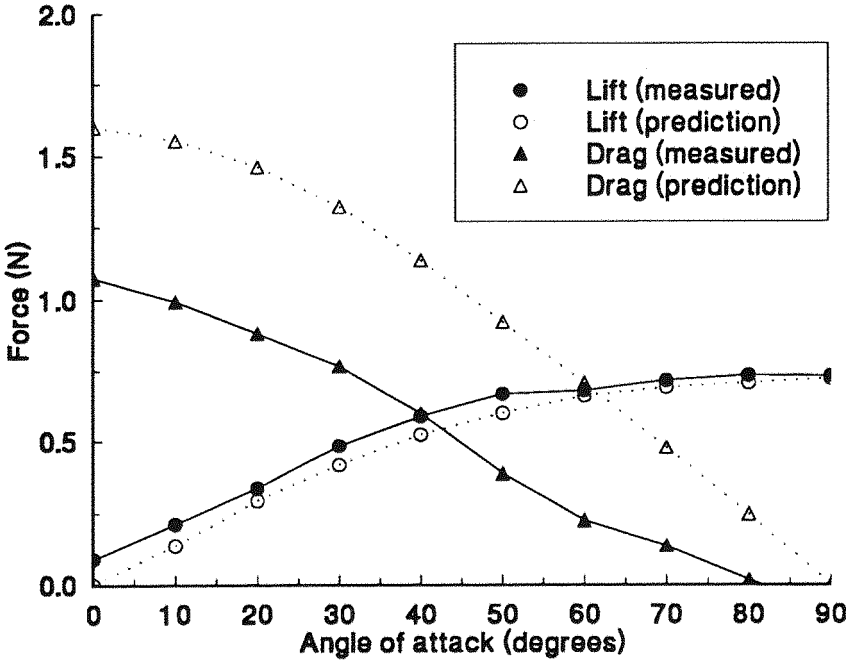

Figure 10.8: Measured group IV effectiveness vs prediction

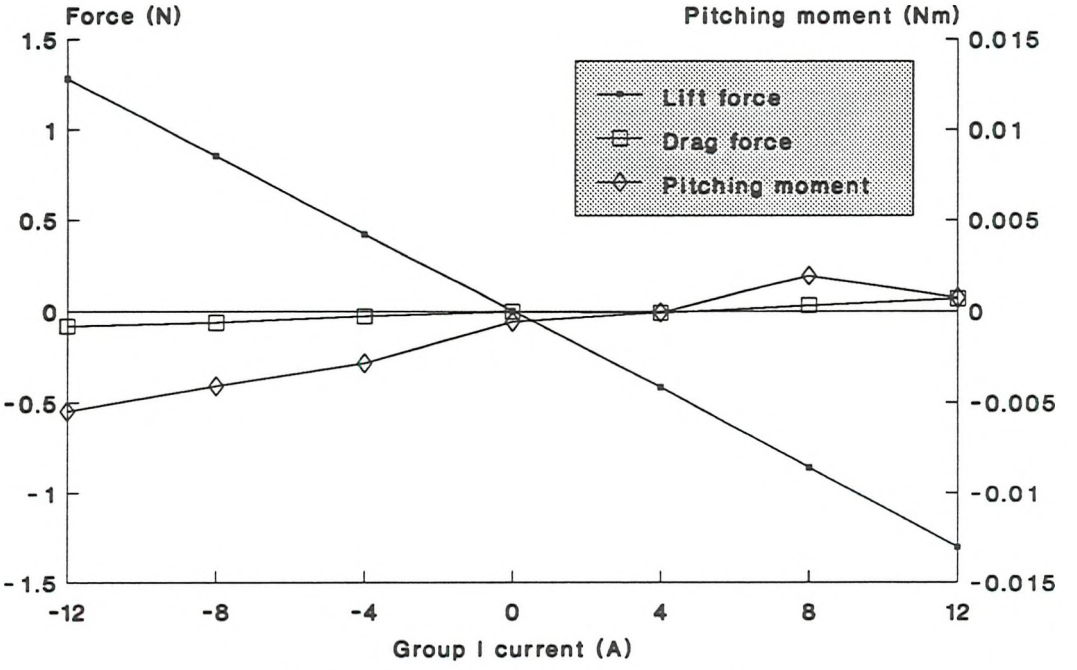

Figure 10.9: Pitching moment generation detected during force effectiveness test at zero incidence

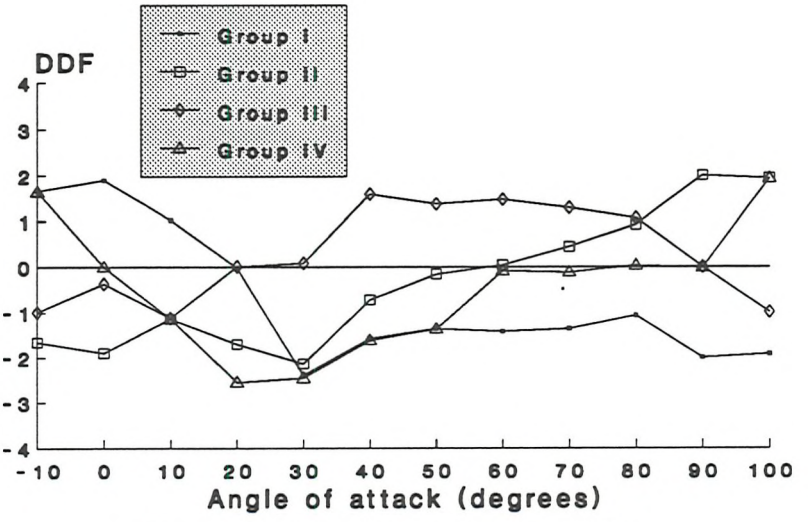

Figure 10.10a: Heave force DDFs producing a variable force in response to a unit control system demand

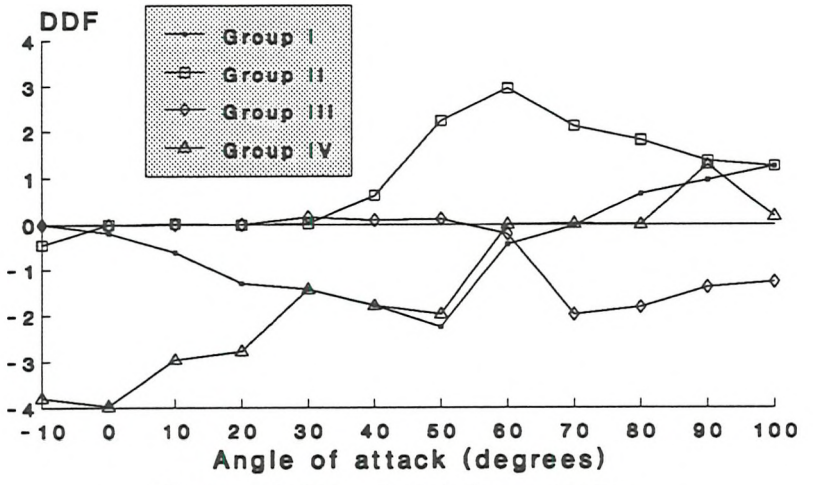

Figure 10.10b: Axial force DDFs producing a variable force in response to a unit control system demand

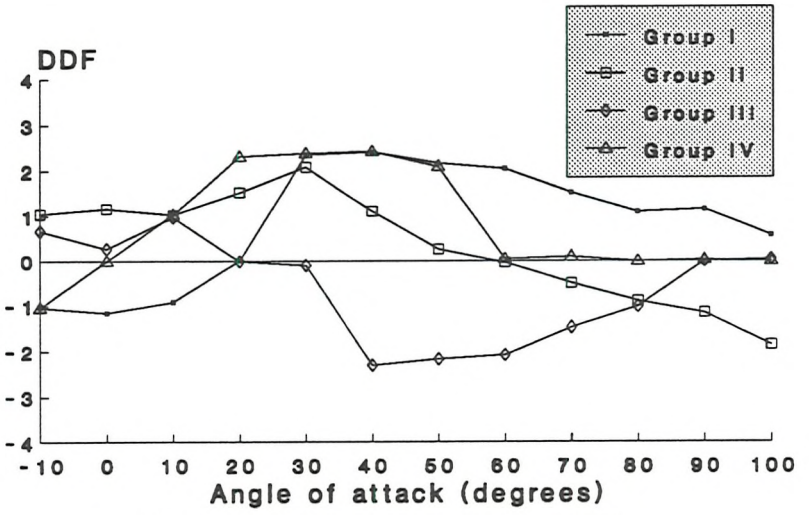

Figure 10.10c: Heave force DDFs producing a constant force in response to a unit control system demand

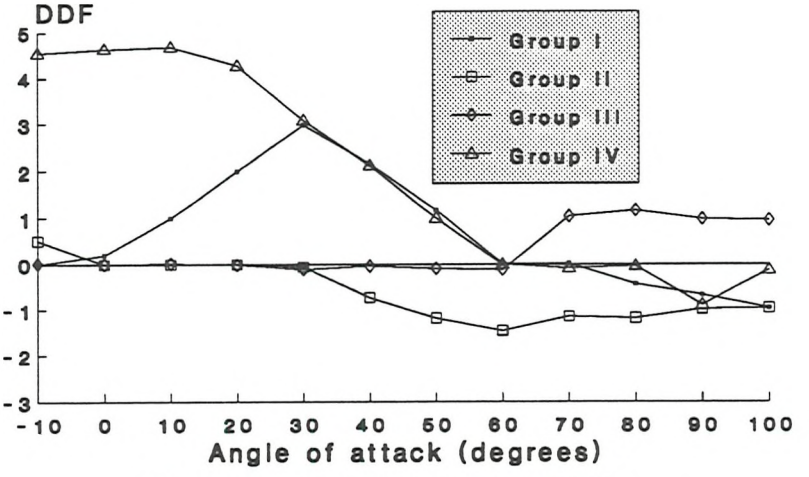

Figure 10.10d: Axial force DDFs producing a constant force in response to a unit control system demand

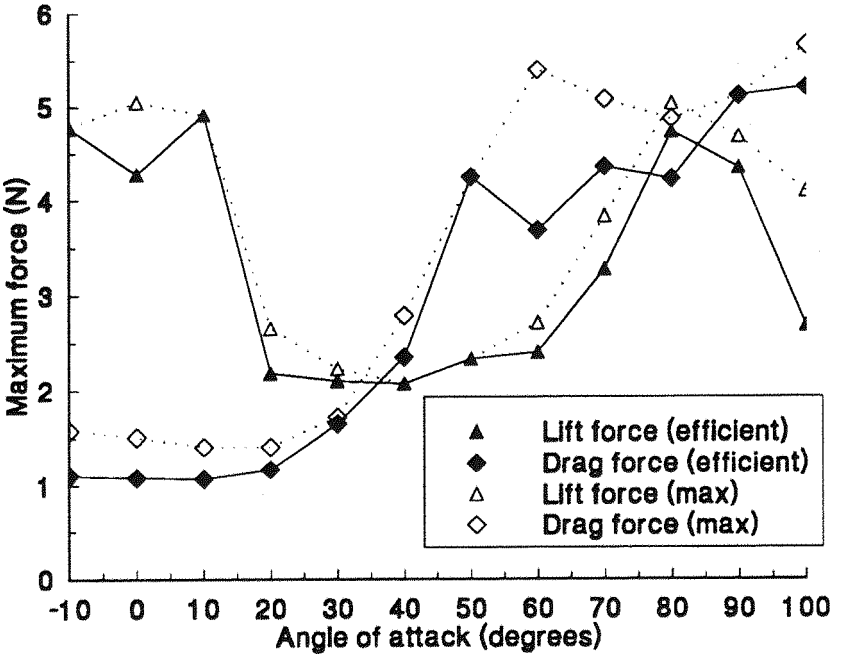

Figure 10.11a: Force capabilities of two DDF selection procedures

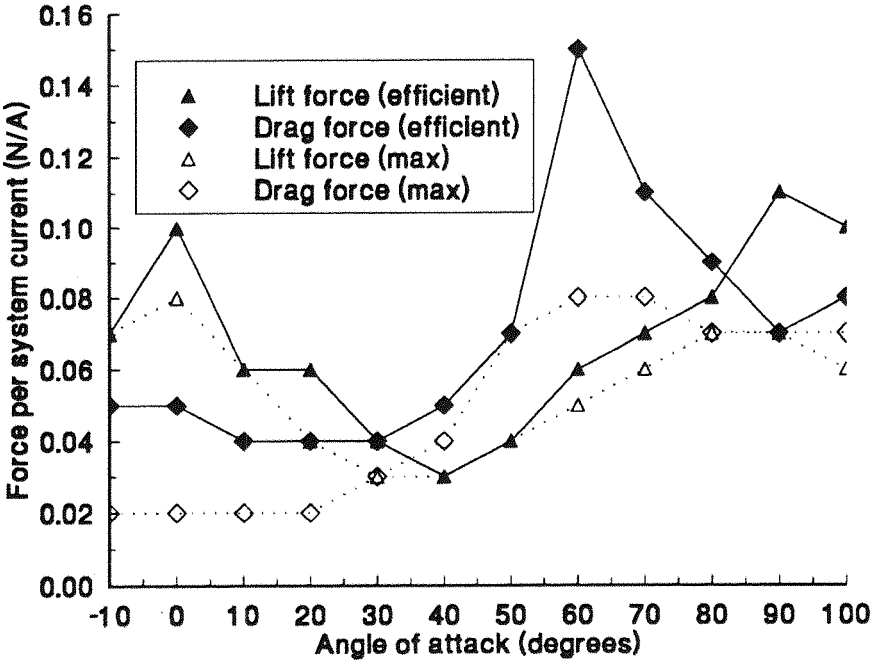

Figure 10.11b: Force generation efficiency of two DDF selection procedures

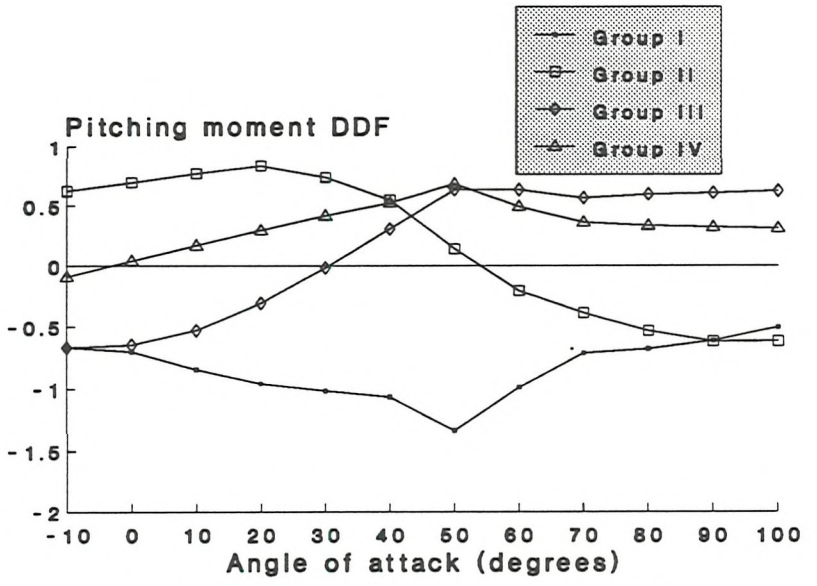

Figure 10.12: Proportional assignment of demand distribution factors for pitching moment

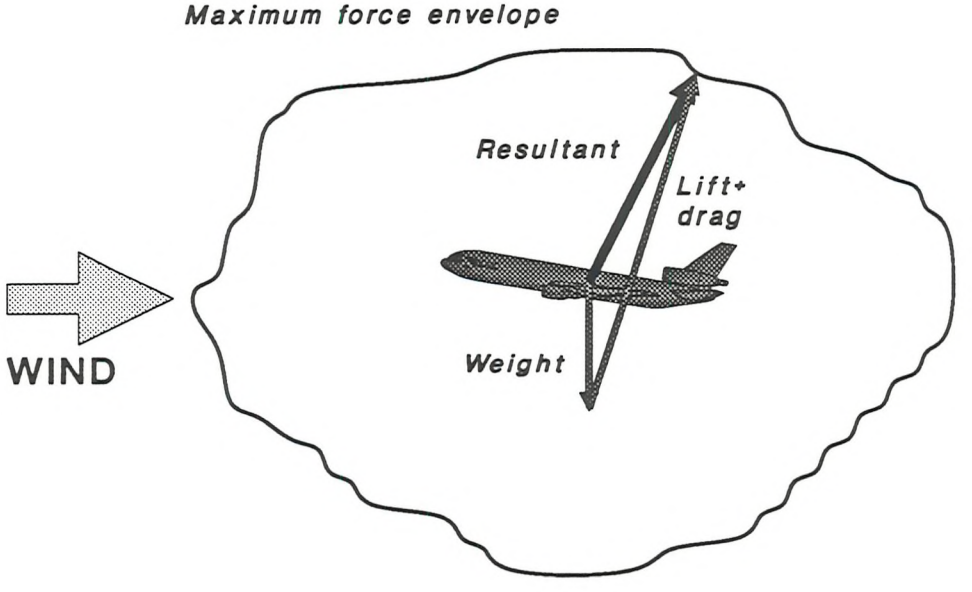

Figure 10.13: Envelope of MSBS Force capability

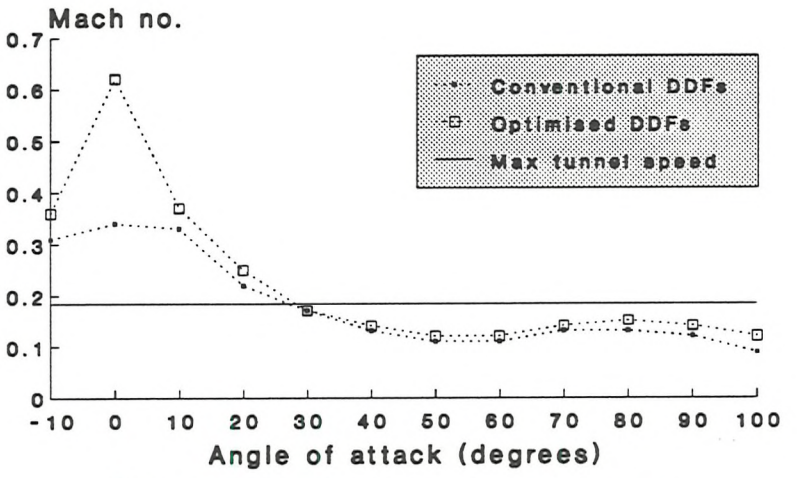

Figure 10.14: Predicted tunnel speed range for the ogive cylinder

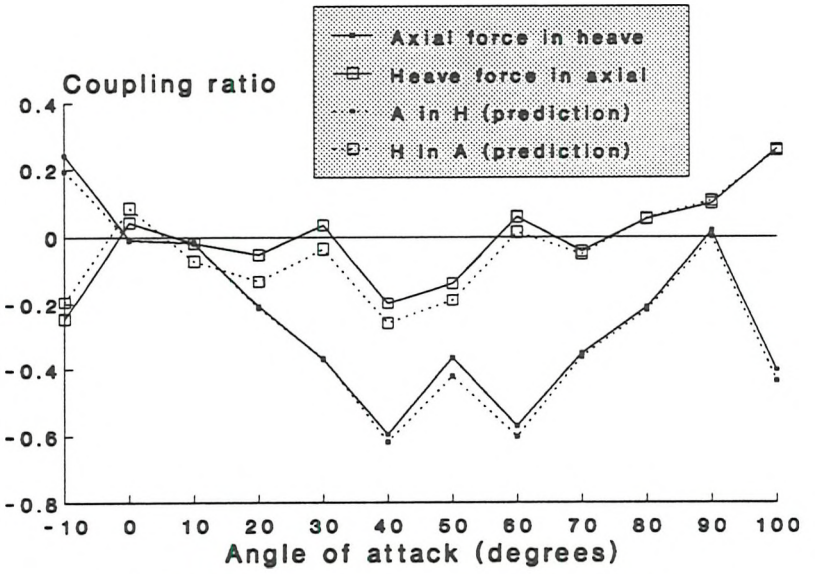

Figure 10.15a: Coupling between force components: Old DDFs

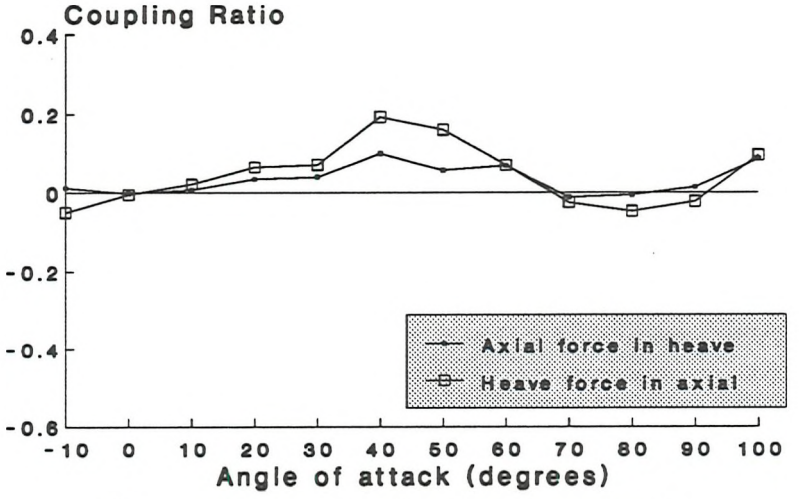

Figure 10.15b: coupling between force components: New DDFs

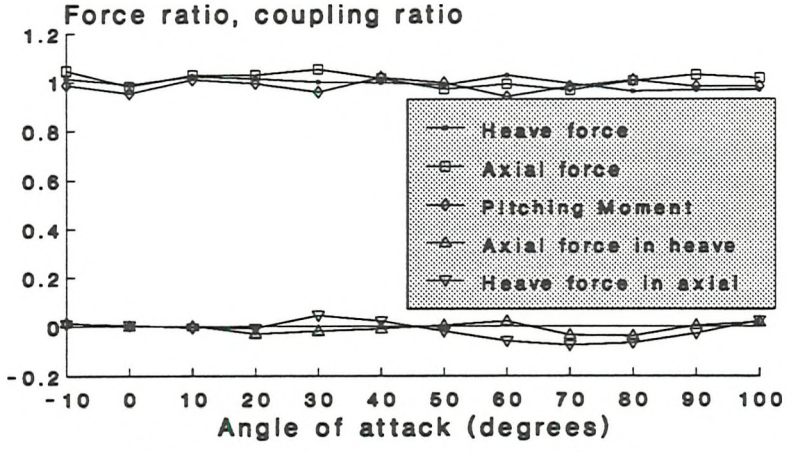

Figure 10.15c: Generation of force components compared to coupling: New DDFs

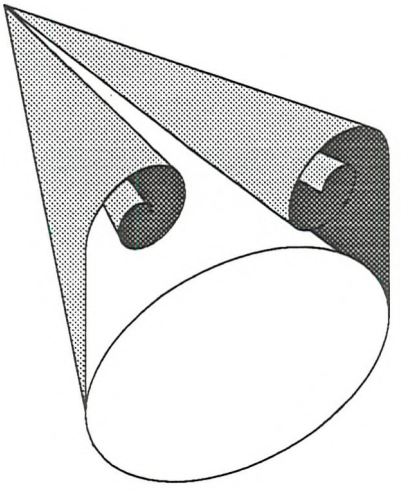

Figure 11.1a: Vortex configuration for a pointed nose at low incidence (after ref 51)

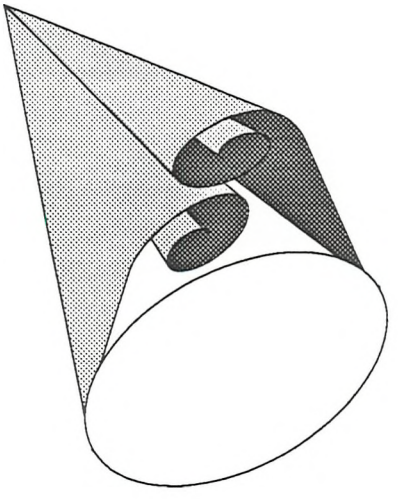

Figure 11.1b; Vortex configuration for a pointed nose at high incidence (after ref 51)

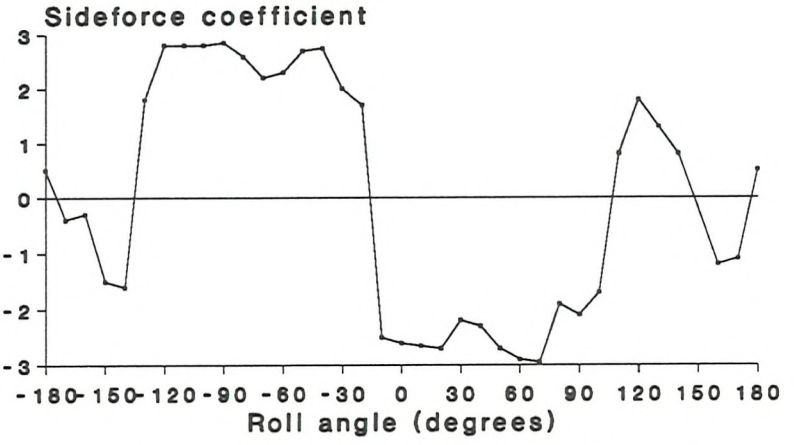

Figure 11.2: Example of variation of sideforce coefficient with roll angle for an ogive cylinder (from ref 51)

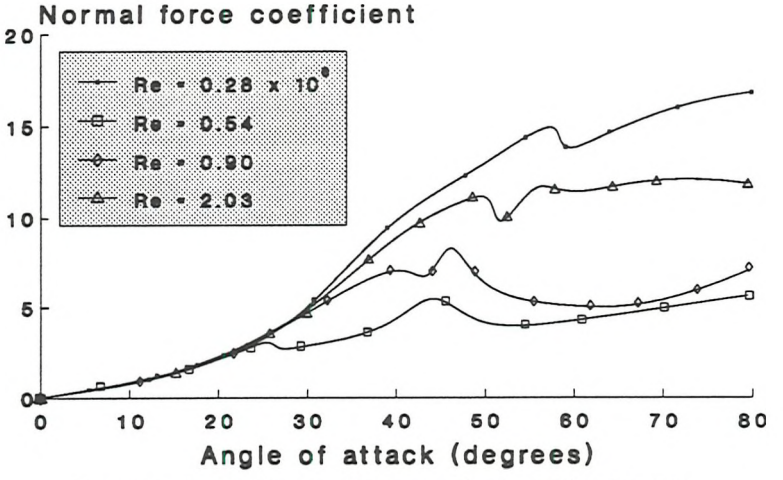

Figure 11.3: Reynolds number effects on normal force coefficient (from ref 56)

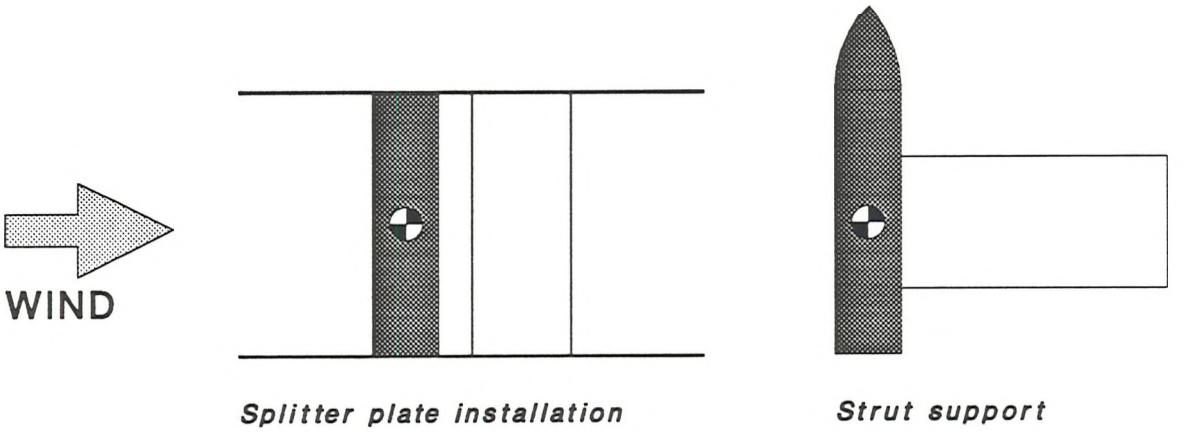

Figure 11.4a: Similarity between strut support and 'splitter' plate downstream of cylinder in crossflow

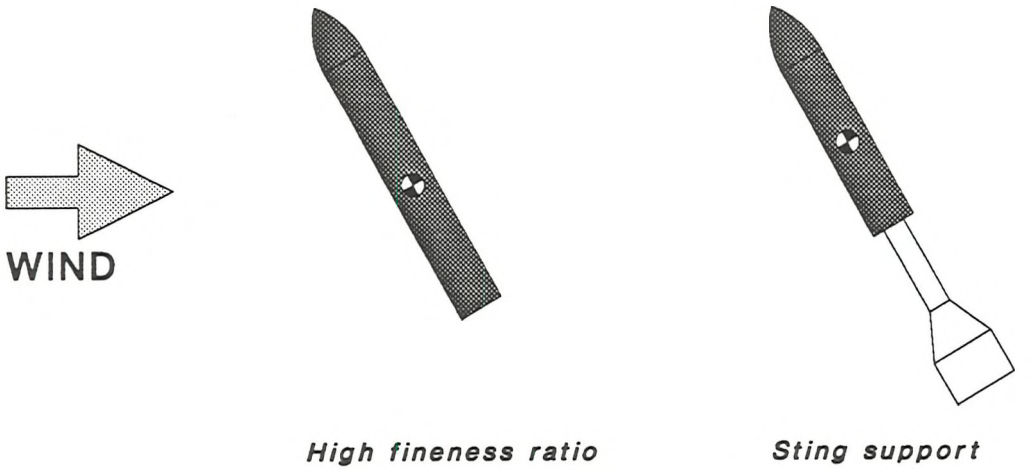

Figure 11.4b: Similarity between sting support and increased fineness ratio of ogive cylinder

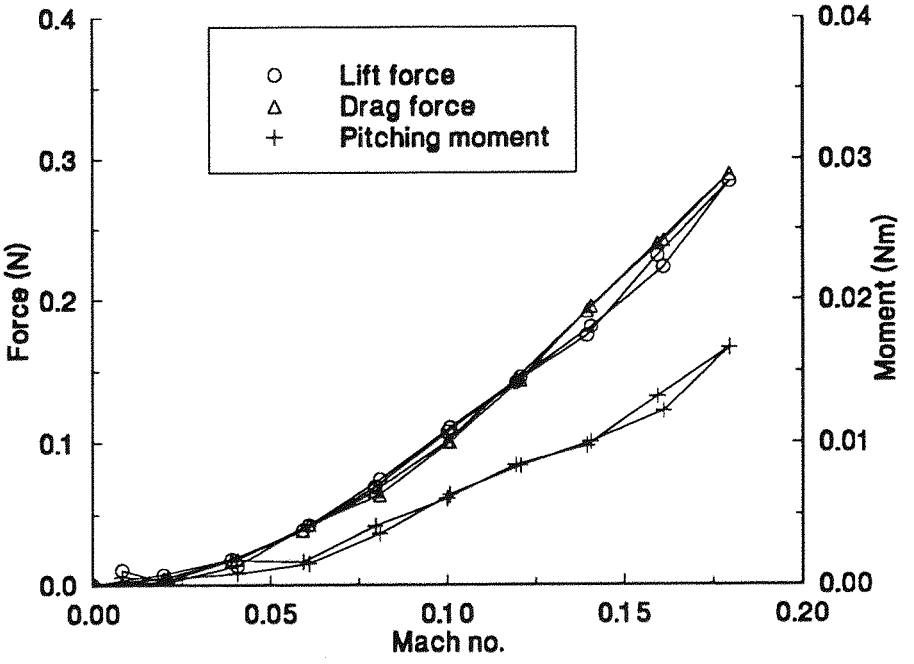

Figure 11.5a: Forces and moments at 10 degrees of incidence

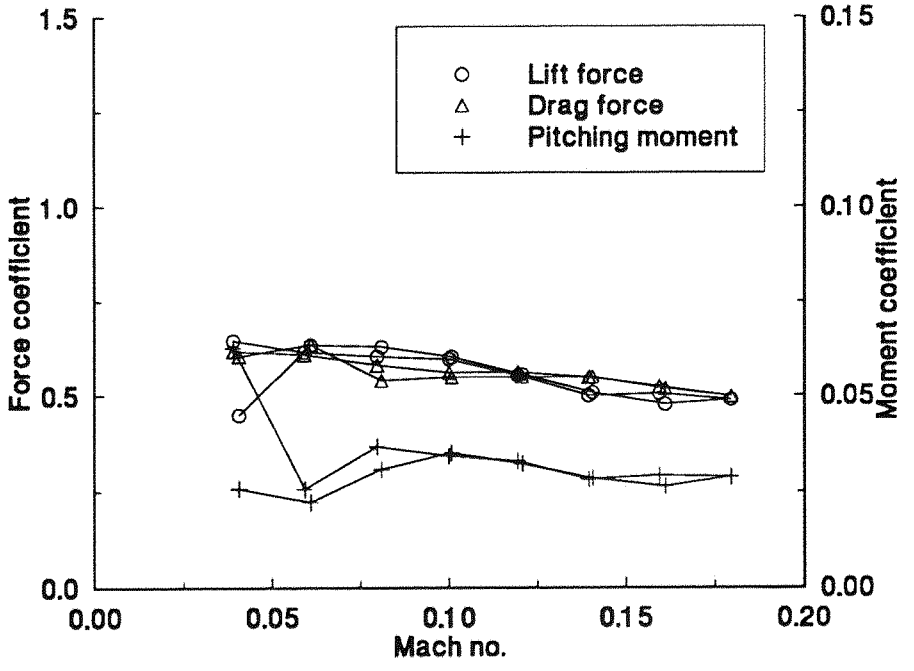

Figure 11.5b: Aerodynamic coefficients at 10 degrees of incidence

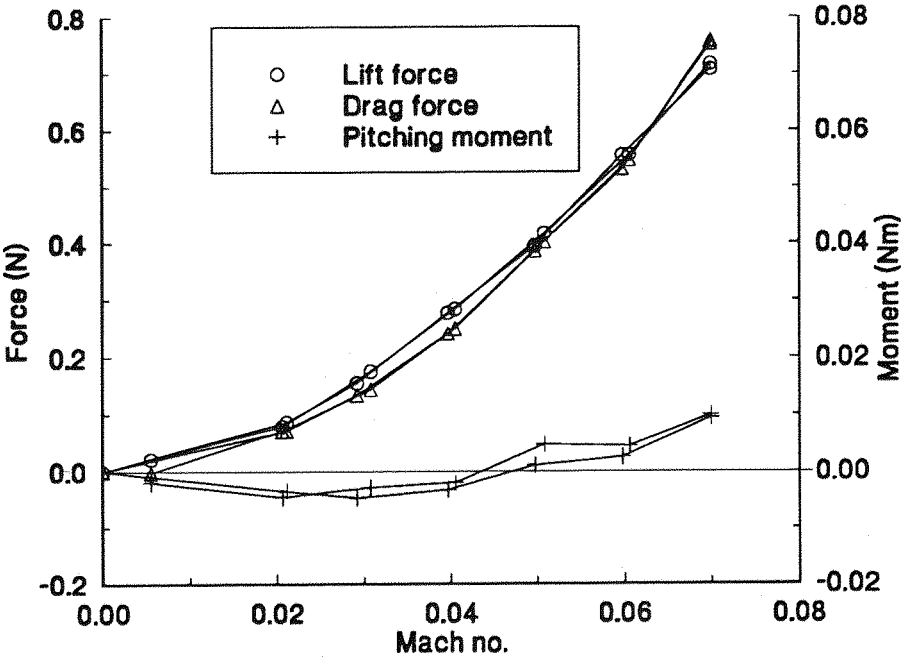

Figure 11.6a: Forces and moments at 50 degrees of incidence

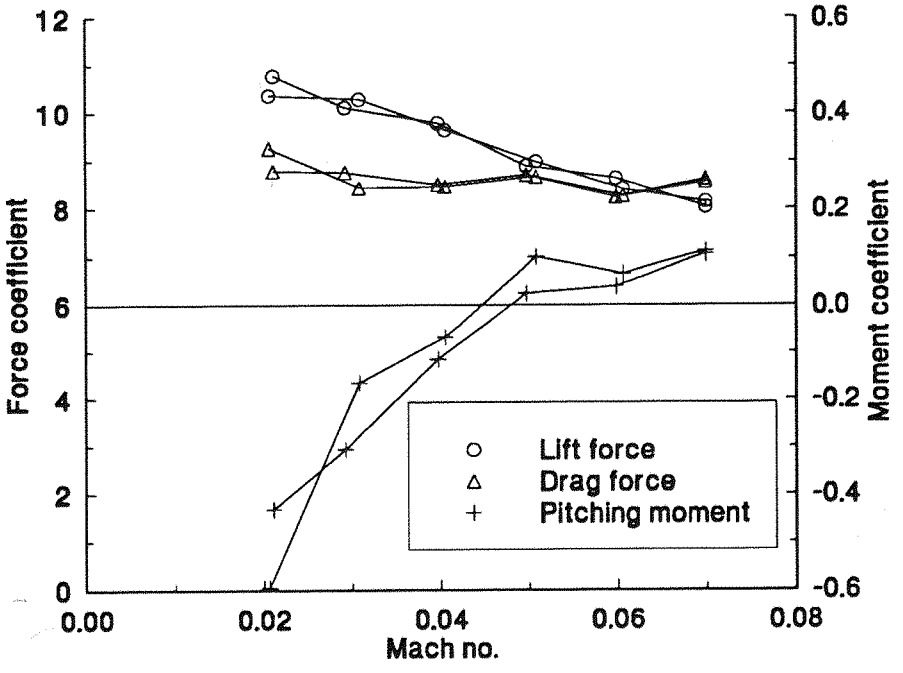

Figure 11.6b: Aerodynamic coefficients at 50 degrees of incidence

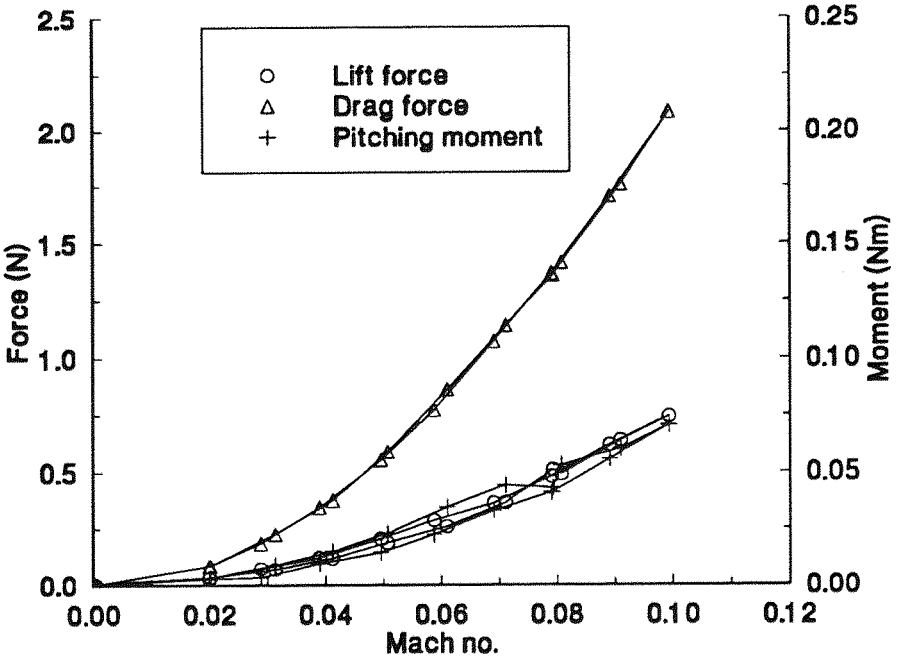

Figure 11.7a: Forces and moments at 70 degrees of incidence

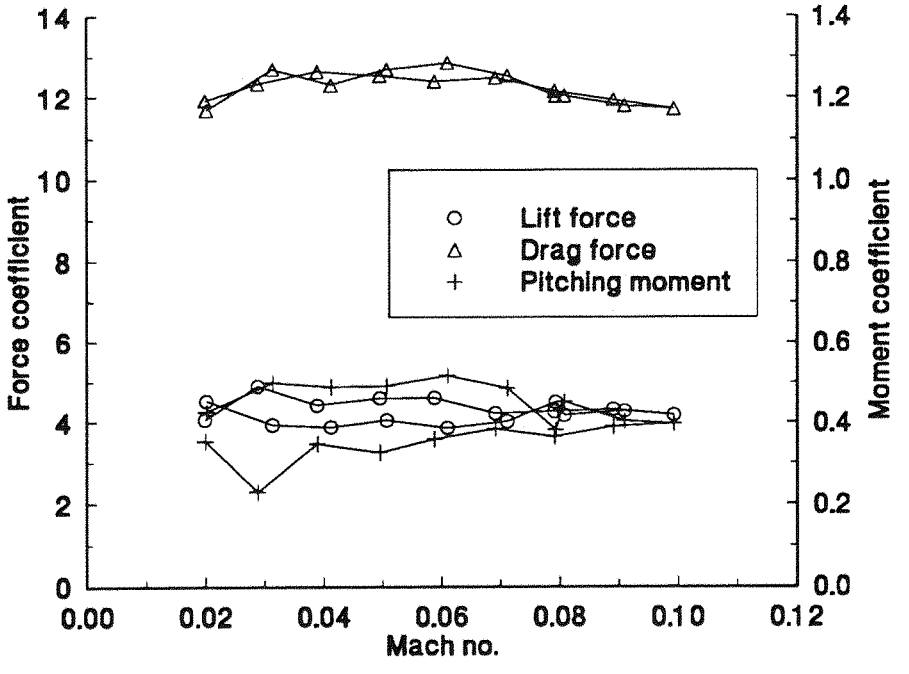

Figure 11.7b: Aerodynamic coefficients at 70 degrees of incidence

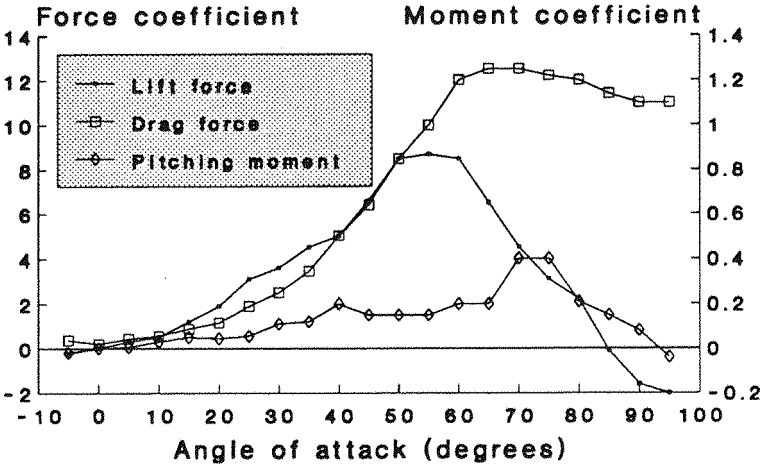

Figure 11.8: Variation of force and moment coefficients with incidence for an ogive cylinder at M = 0.1

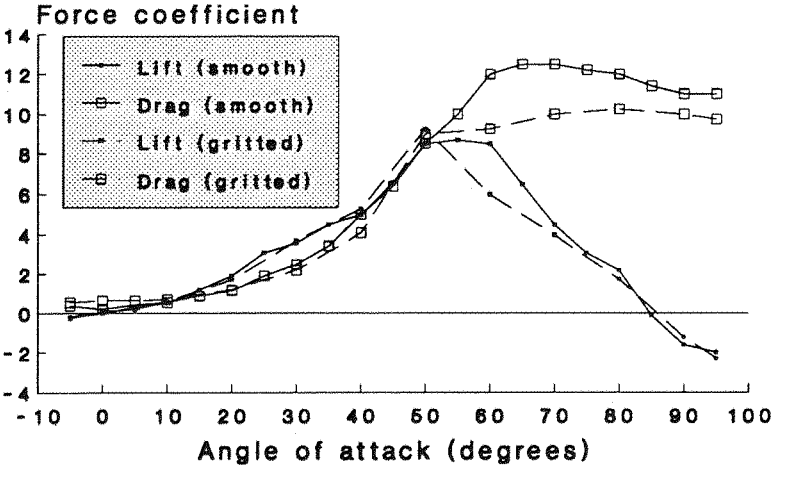

Figure 11.9: Results of simulating a higher Reynolds no. by gritting the surface of the ogive cylinder

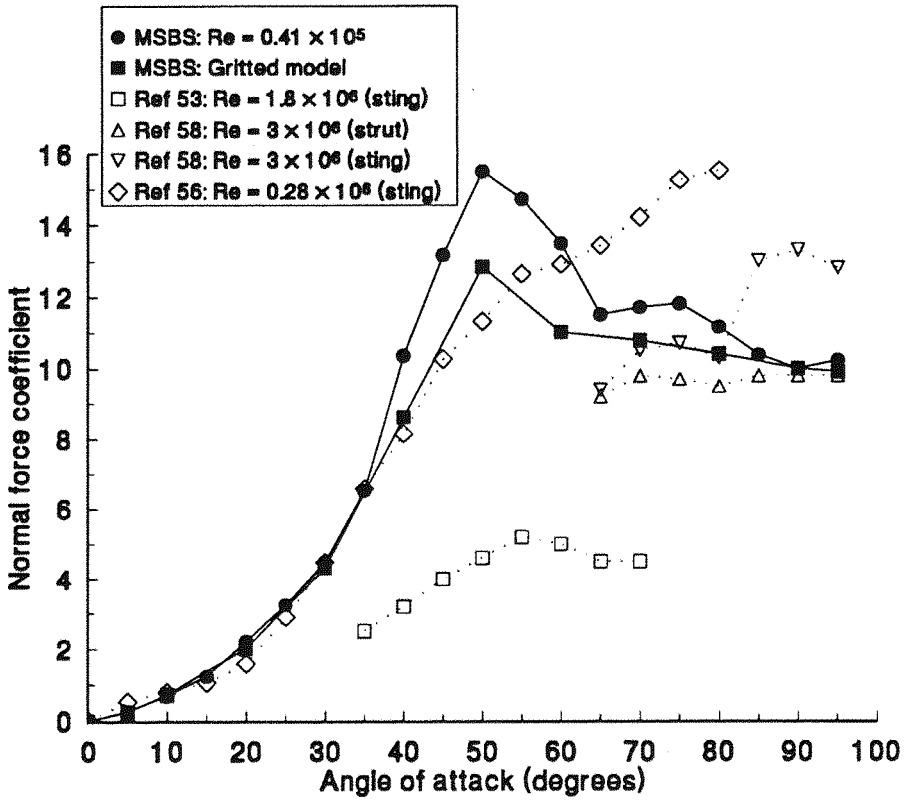

Figure 11.10: Comparison of normal force variation with published data

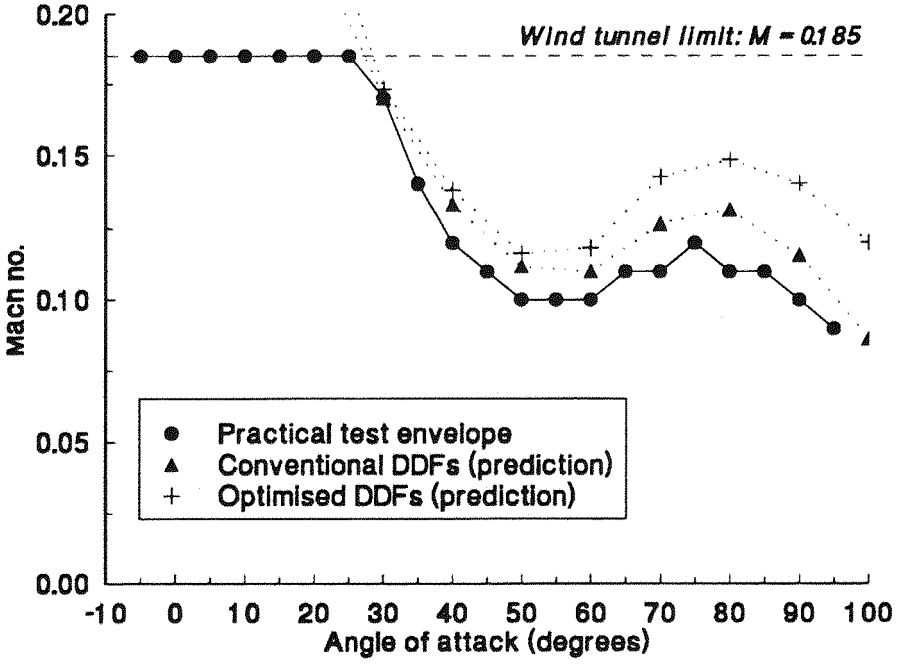

Figure 11.11: Test envelope for ogive cylinder vs predictions

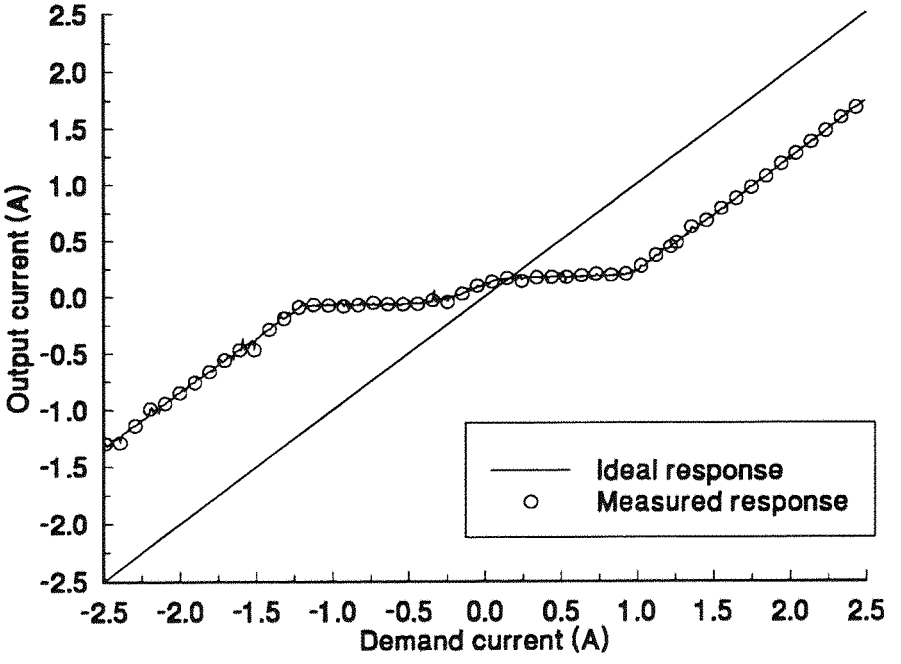

Figure 12.1: Line segment structure of electromagnet response

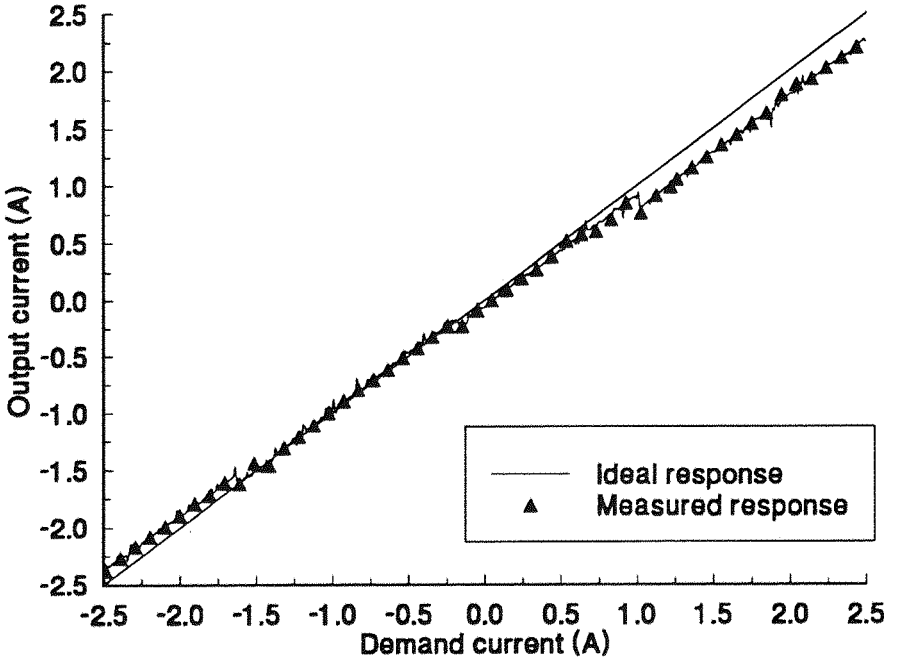

Figure 12.2: Electromagnet response with software calibration

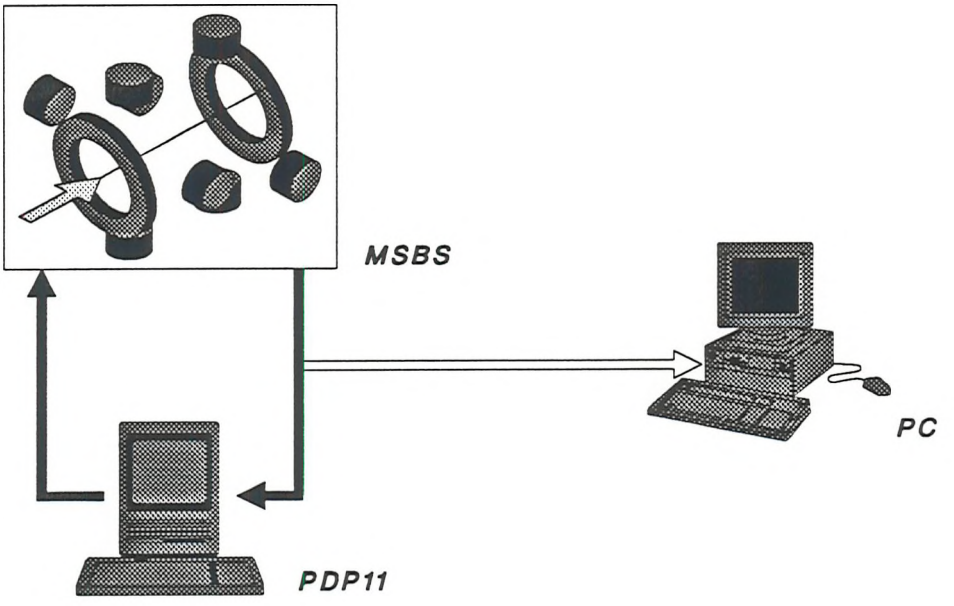

Figure 12.3: MSBS communications with PC as data-logger

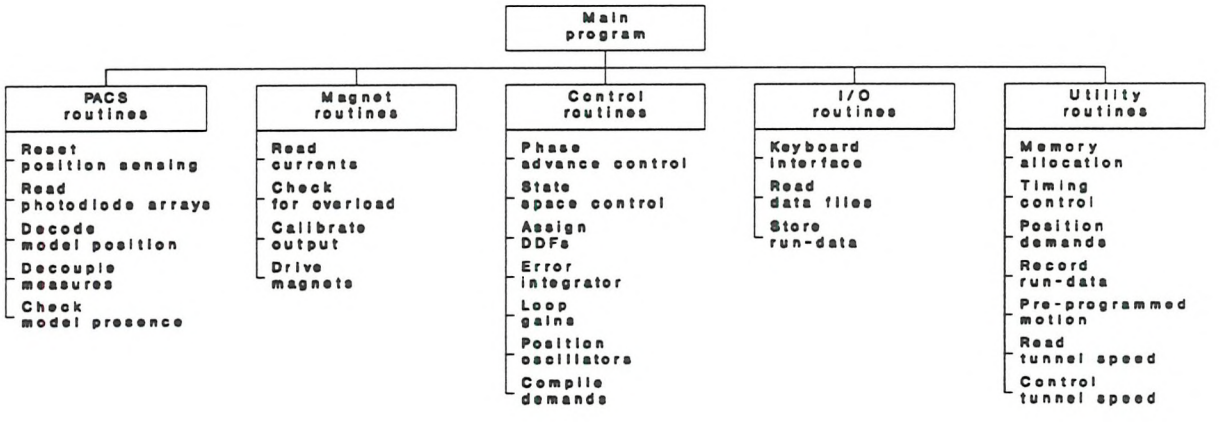

Figure 12.4: PC-based control system

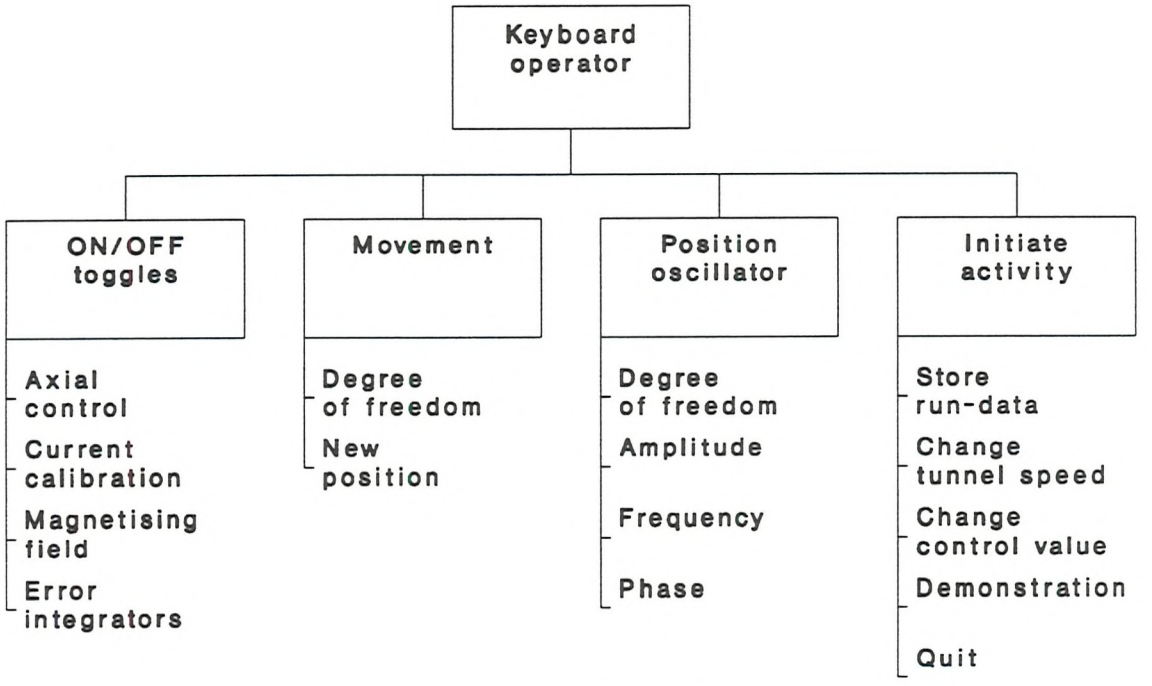

Figure 12.5: Structure of command menu

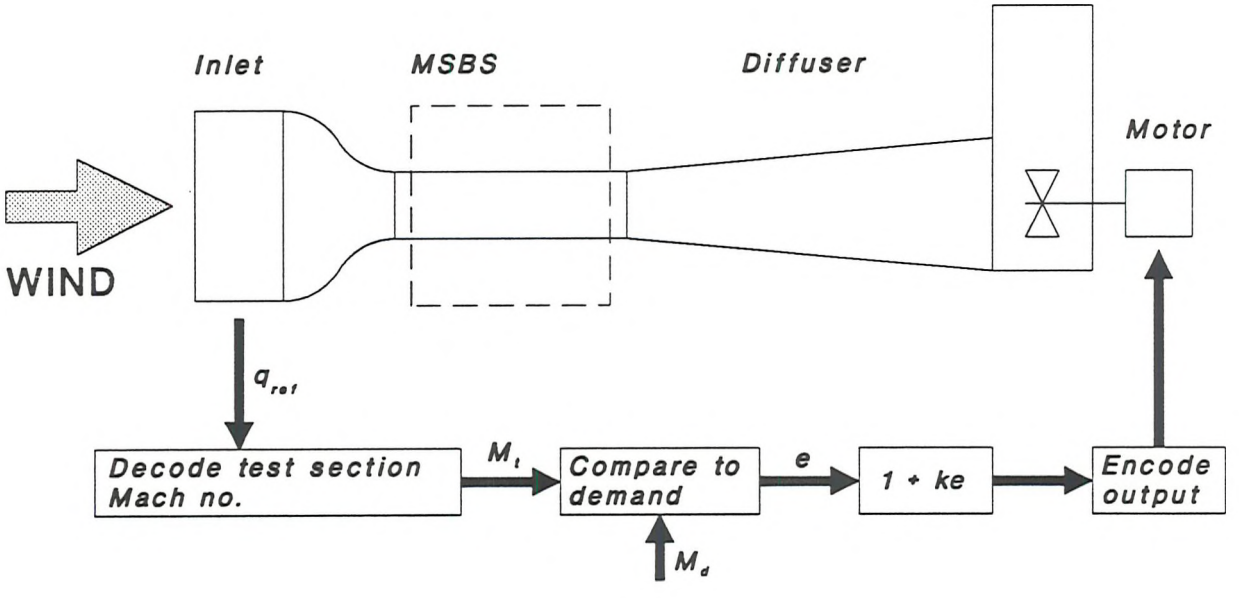

Figure 12.6: Tunnel speed control block diagram

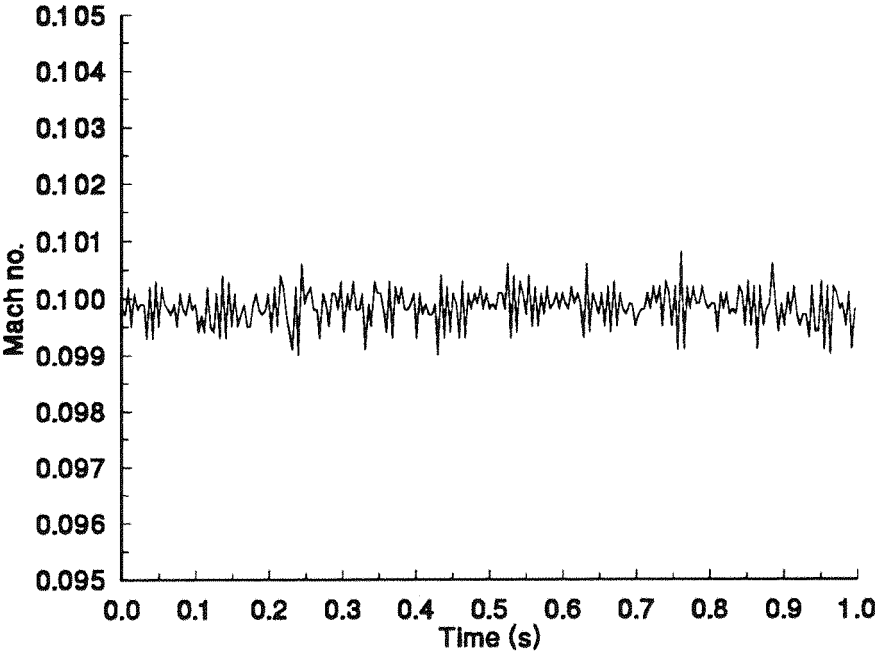

Figure 12.7: Example of tunnel speed control at M = 0.1

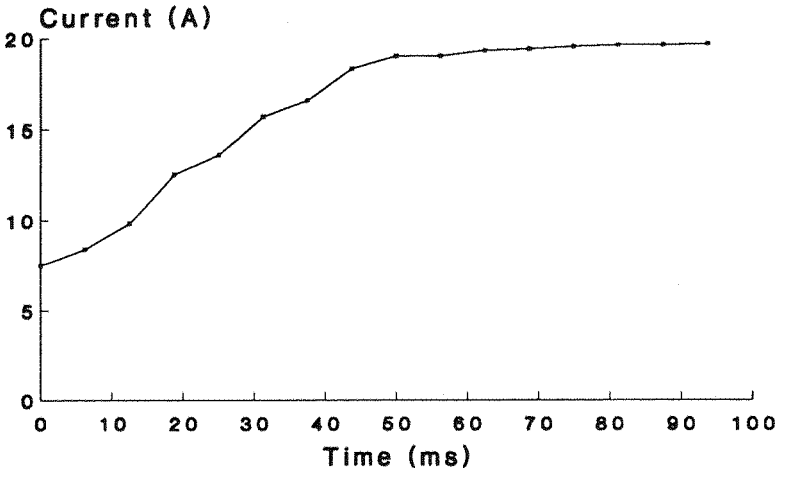

Figure 12.8a: Axial magnet current response during propulsion simulation

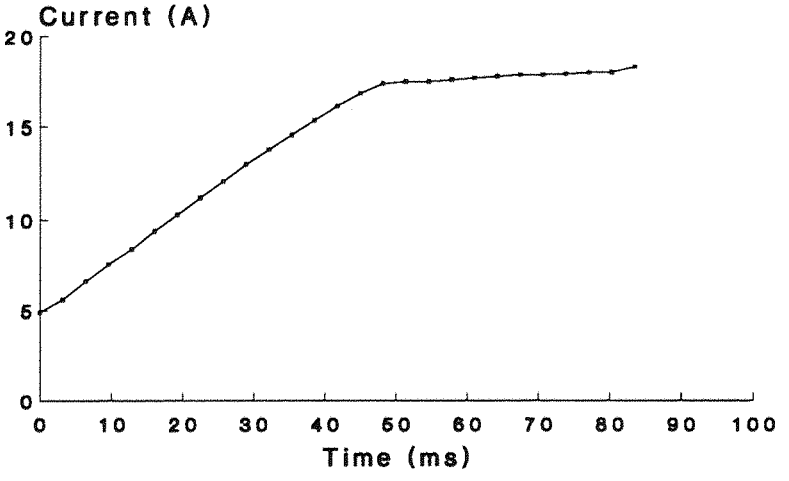

Figure 12.8b: Axial magnet current response to a step change in demand

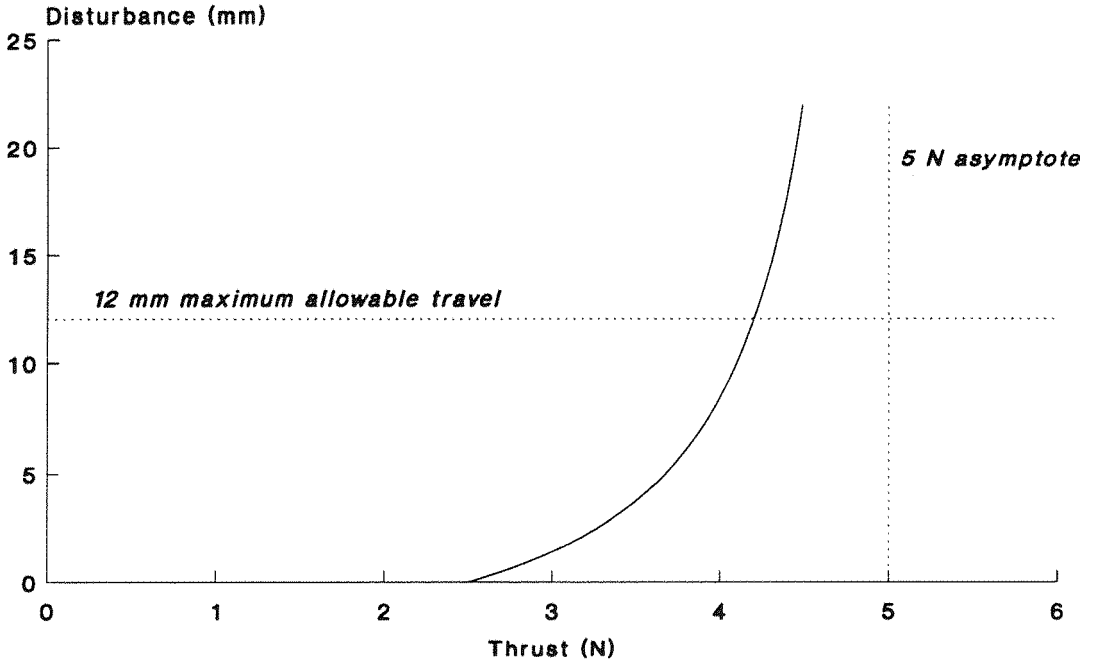

Figure 12.9: Prediction of axial motion response to different step thrust impulses

19. PLATES

Plate 1: Compressed gas and solid rocket exhaust simulators and representative model

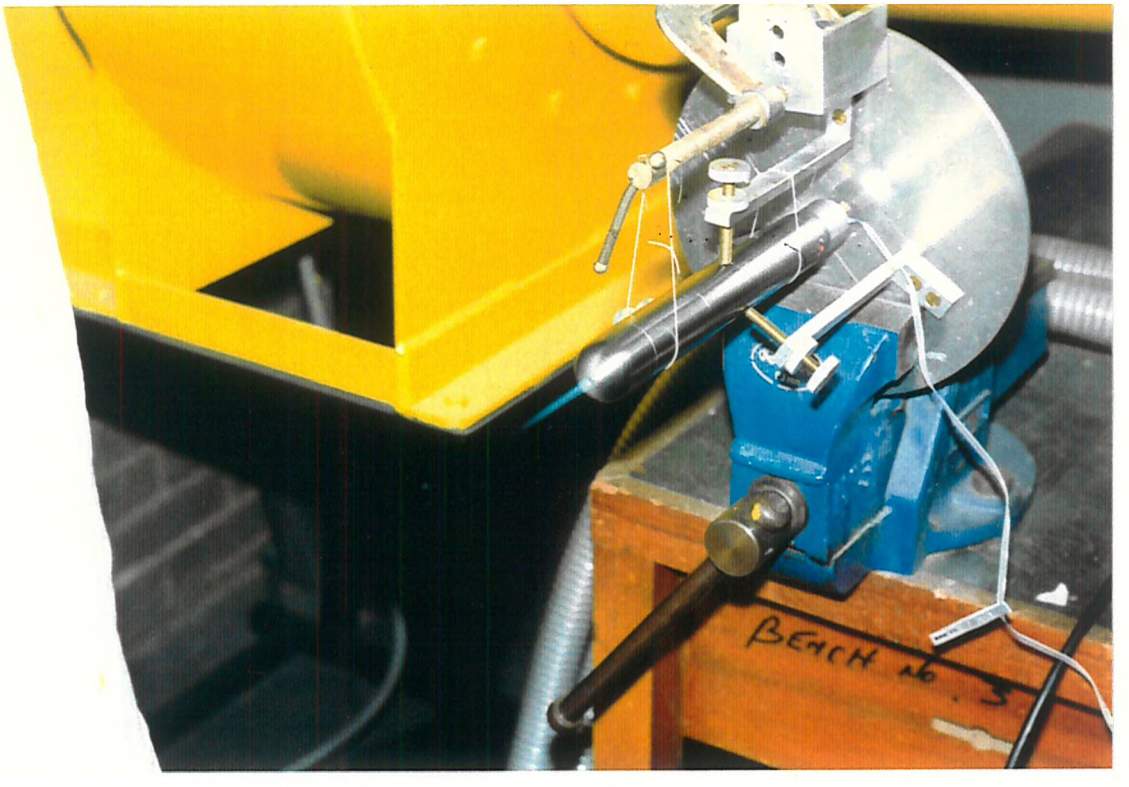

Plate 2: Horizontal bench test of the compressed gas exhaust simulator

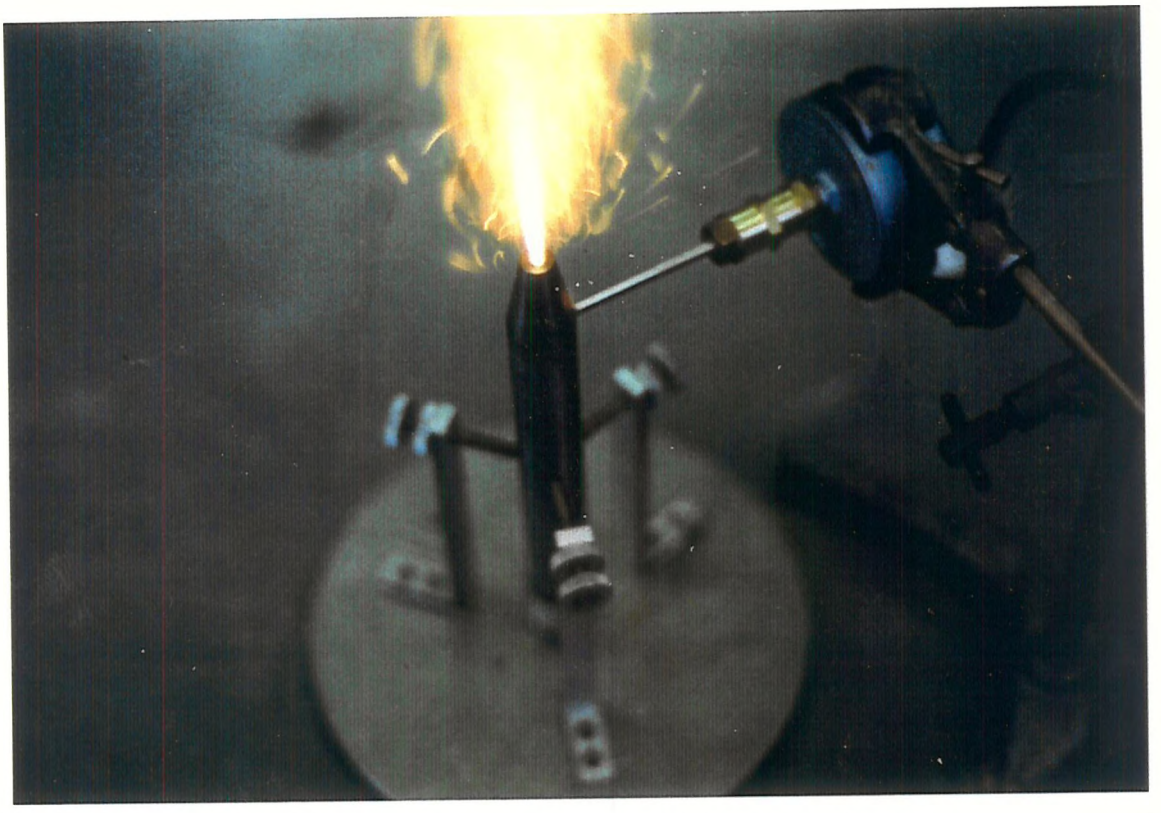

Plate 3: Bench test of the solid rocket thruster with measurement of chamber static pressure

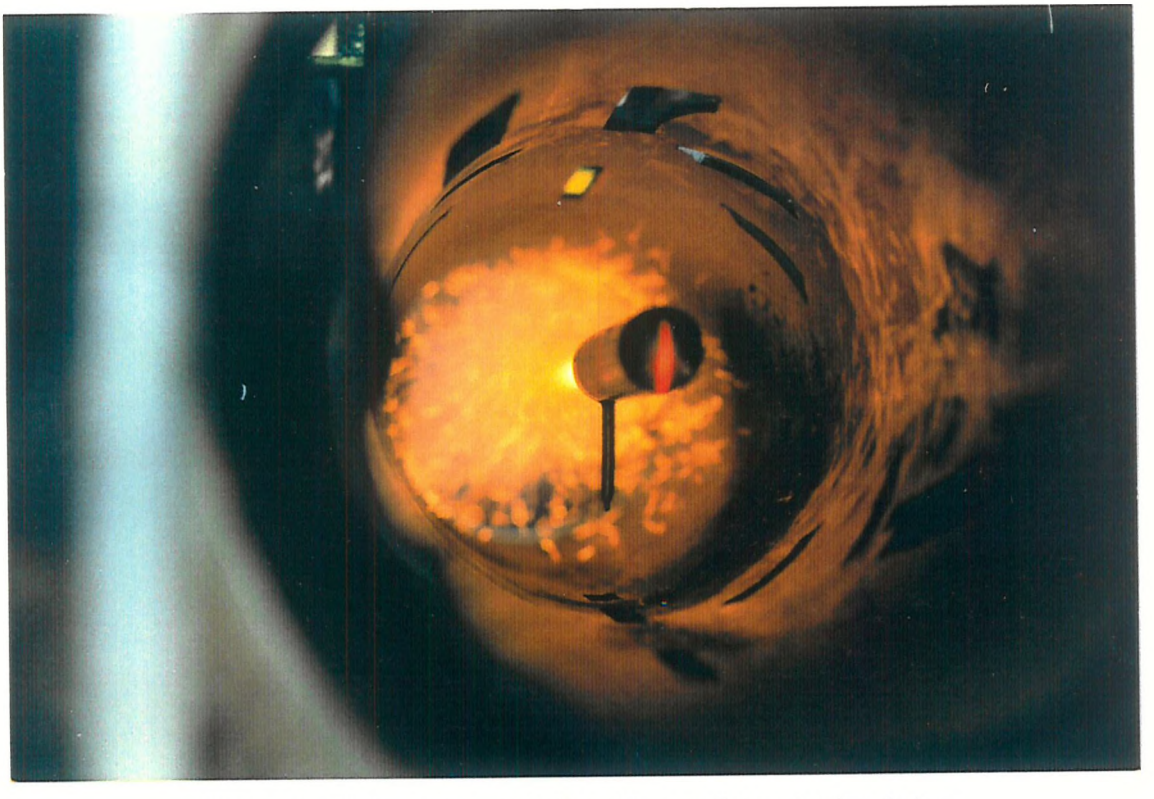

Plate 4: Firing the solid rocket exhaust simulator suspended in the MSBS

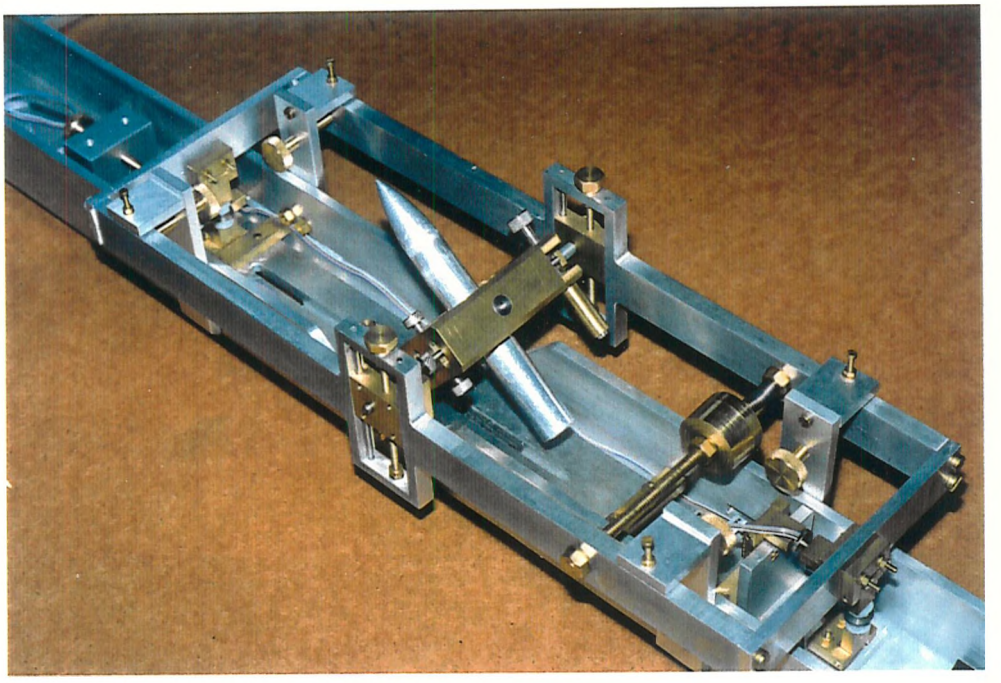

Plate 5: Direct Force Measurement (DFM) rig
and ogive cylinder model

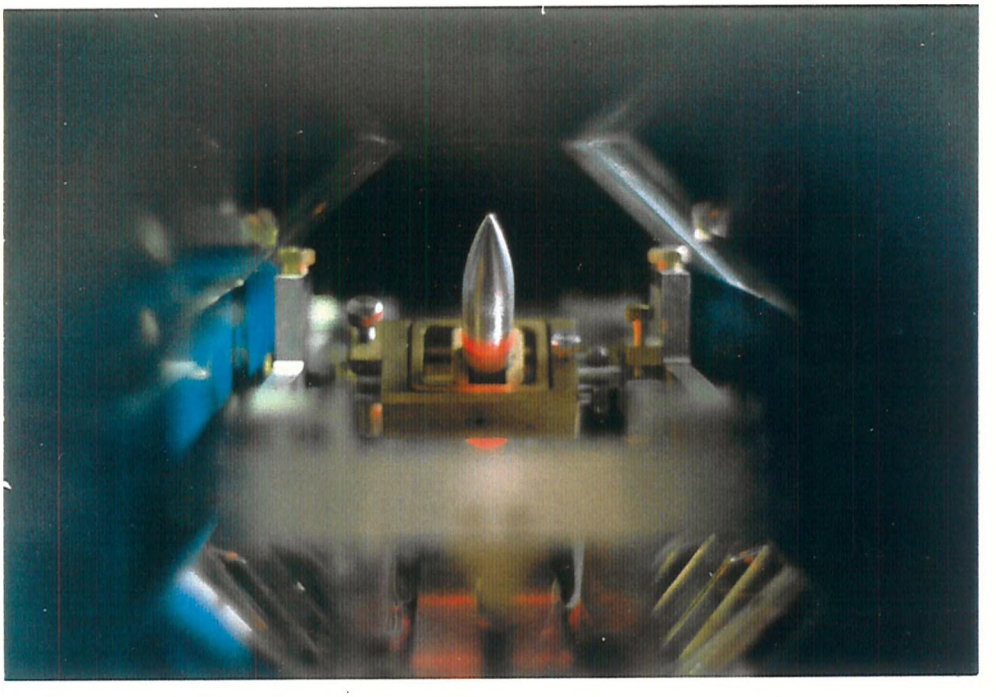

Plate 6: DFM rig and ogive cylinder model
installed in the MSBS wind tunnel

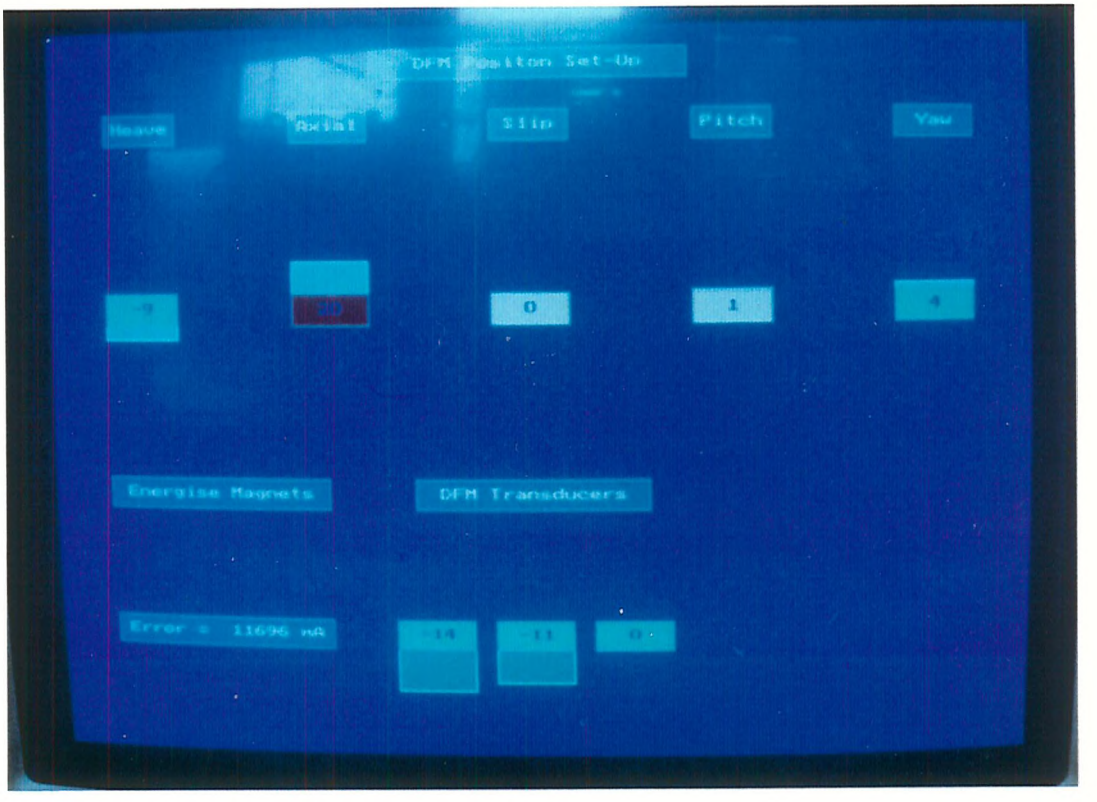

Plate 7: Graphical VDU display during DFM analysis of suspension data

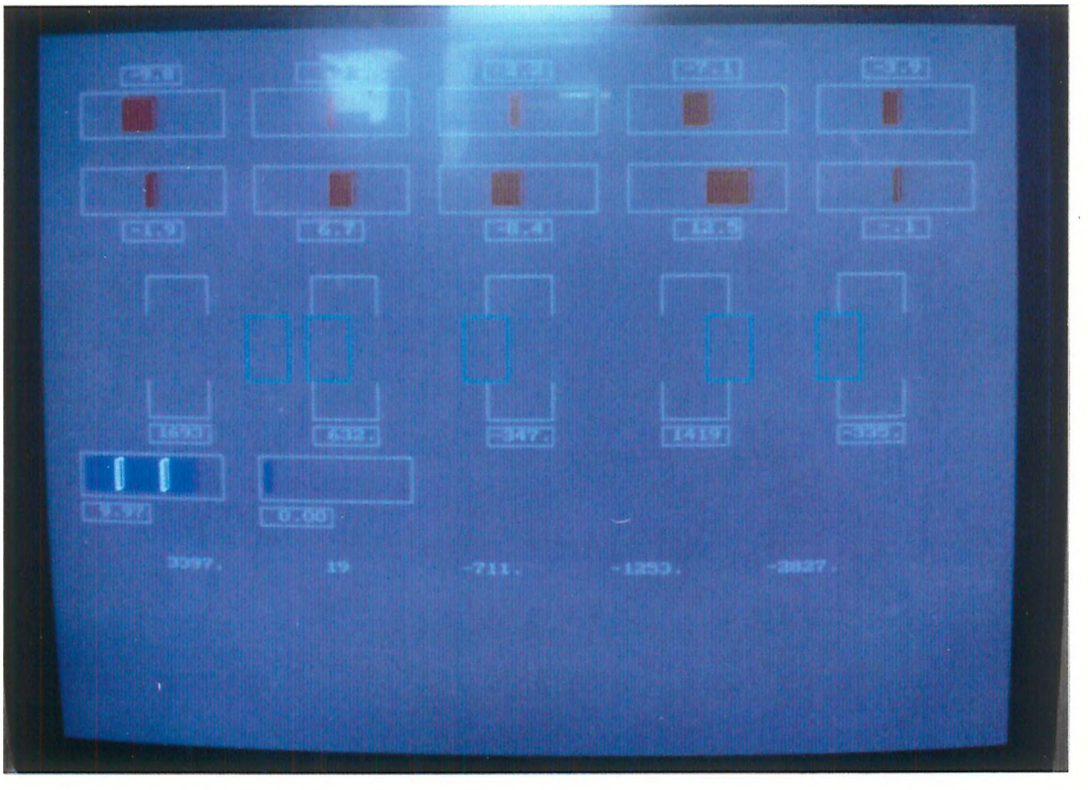

Plate 8: Graphical VDU display during replay of suspension data